Autotaxin and Tumor-Promoting Inflammation

by

Matthew Gary Kenneth Benesch

A thesis submitted in partial fulfillment of the requirements for the degree of

Doctor of Philosophy

Department of Biochemistry
University of Alberta

ABSTRACT

Autotaxin is a secreted enzyme that produces most of the extracellular lysophosphatidate from lysophosphatidylcholine, the most abundant phospholipid in plasma. Lysophosphatidate mediates many physiological and pathological processes by signaling through six G-protein-coupled receptors to promote cell survival, proliferation and migration. Knocking out autotaxin in mice is embryonically lethal as a result of impaired vasculogenesis and improper neural-crest folding. In the post-natal organism, autotaxin/ lysophosphatidate signaling mediates wound healing and tissue remodeling through acute inflammatory processes. However, in chronic inflammation, this signaling drives many diseases including rheumatoid arthritis, hepatitis, colitis, asthma and cancer. In cancer, lysophosphatidate promotes cell proliferation and migration, angiogenesis, metastasis and chemotherapy and radiotherapy resistance. Currently, there are no therapies targeting lysophosphatidiate signaling and this provides an opportunity for introducing new cancer treatments. Because most lysophosphatidate is produced by autotaxin activity, an inhibitor of the autotaxin catalytic site would block subsequent lysophosphatidate signaling. Therefore, it is important to understand how autotaxin activity is regulated by lysophosphatidate. It has been proposed that autotaxin is product-inhibited by lysophosphatidate or a related lipid called sphingosine-1-phosphate. This has led to the design of several lipid-mimetic autotaxin inhibitors. We now show that this competitive

inhibition is ineffective at high concentrations of lysophosphatidylcholine that occur *in vivo*. Instead, lysophosphatidate and sphingosine-1-phosphate inhibit autotaxin expression through phosphatidylinositol-3-kinase activation. However, this physiological inhibition is overcome by inflammatory-mediated signaling. We propose that inflammation is vital for pathological autotaxin and lysophosphatidate production, and lysophosphatidate signaling in turn further drives an inflammatory environment. Consequently, an autotaxin inhibitor should be able to break this vicious cycle. However, this hypothesis has not been tested as historical autotaxin inhibitors have poor bioavailability profiles. We tested a novel non-lipid-mimetic ATX inhibitor (ONO-8430506) in mice which decreases plasma autotaxin activity by >80% and concentrations of unsaturated lysophosphatidates by >75% for 24 h. We also showed for the first time that inhibiting autotaxin decreases initial tumor growth and subsequent lung metastasis in a 4T1/Balb/c syngeneic orthotopic breast cancer mouse model by 60% compared to vehicle-treatment. When combined with doxorubicin, ONO-8430506 synergistically decreases tumor growth and lung and liver metastases by >70%, whereas doxorubicin alone had marginal effects. Significantly, 4T1 breast cancer cells express neglible autotaxin compared to the mammary fat pad. Autotaxin activity in the fat pad of non-treated mice is increased 2-fold by tumor growth. This increase correlates with increases in inflammatory chemokine and cytokine production that is suppressed by ATX inhibition. We also extended our studies of autotaxin-

mediated cancer growth and inhibition to papillary thyroid cancer. The diagnosis of thyroid cancer by fine needle biopsies is imprecise in ≥25% of cases resulting in unnecessary surgery. Many thyroid cancer patients also become resistant to radiotherapy and chemotherapy. Our work addresses both of these problems. We demonstrate that high expression of inflammatory chemokines and cytokines and increased secretion of autotaxin by thyroid cancer cells provides a definitive identification of human papillary thyroid cancer from benign nodules. Autotaxin secretion is hijacked in thyroid cancer in a vicious inflammatory cycle in which lysophosphatidate stimulates autocrine chemokine and cytokine secretion. This in turn increases autocrine autotaxin production. We show that treating mice daily with ONO-8430506 decreases thyroid tumor growth in xenograft models by >50%. There were also decreases in multiple inflammatory chemokines and cytokines, platelet-derived growth factor and vascular endothelial growth factor in the tumors. This results in decreased cancer cell division and angiogenesis. Therefore, regardless of whether autotaxin is produced in an autocrine fashion like in thyroid cancer or in a paracrine manner like in breast cancer, this work describes a new paradigm where autotaxin secretion is inflammatory-mediated and an autotaxin inhibitor is therapeutically effective. Autotaxin inhibitors have great potential to improve cancer patient outcomes and we propose that they also could have utility in other chronic inflammatory-mediated conditions.

PREFACE

This thesis is an original work by Matthew Benesch. Animal studies complied with the Canadian Council of Animal Care as approved by the University of Alberta Animal Welfare Committee (Animal User Protocol 226). De-identified patient data was obtained with approval from the Health Research Ethics Board of Alberta – Cancer Committee ("Lysophosphatidate Signaling as a Promoter of Breast Cancer Therapy Resistance and Metastasis", ID 26195, 01/16/2014). Human specimens were obtained with approval of the University of Alberta Health Research Ethics Board ("Mechanisms of Lymph Node Metastases", ID Pro00018758, 01/15/2011).

Components of Chapters 1 and 6 have been published as:

Benesch, M.G.K., Ko, D., Tang, X., McMullen, T.P.W., and Brindley, D.N. (2014) Autotaxin in the crosshairs: Taking aim at cancer and other inflammatory conditions. (Review) *FEBS Letters* 588 (16*),* 2712-2727.

Brindley, D.N., **Benesch, M.G.K.,** and Murph, M.M. Autotaxin: An Enzymatic Augmenter of Malignant Progression Linked to Inflammation. (Review). In "Melanoma", InTech. (Accepted August 25, 2014).

Components of Chapters 3 and 4 have been published as:

Benesch, M.G.K., Tang, X., Maeda, T., Ohhata, A., Zhao, Y., Kok, B.P.C., Dewald, J., Hitt, M., Curtis, J.M., McMullen, T.P.W., and Brindley, D.N. (2014) Inhibition of autotaxin delays breast tumor growth and lung metastasis in mice. *FASEB Journal* 28 (6)*,* 2655-2666.

Venkatraman, G., **Benesch, M.G.K.,** Tang, X., Dewald, J., McMullen, T.P.W., and Brindley, D.N. (2015) Lysophosphatidate signaling stabilizes Nrf2 and increases the expression of genes involved in drug resistance and oxidative stress responses: implications for cancer treatment. *FASEB Journal* 29 (3), 772-785.

To my father and mother, Bruce and Linda, and brother John.

"There is no medicine like hope, no incentive so great, and no tonic so powerful as expectation of something better tomorrow."

Orison Swett Marden

ACKNOWLEDGEMENTS

I would like to thank my primary supervisor Dr. Dave Brindley for all of his support, guidance and encouragement through this project. I am also indebted to my co-supervisor Dr. Todd McMullen for his invaluable mentorship during these early days as a future clinician scientist. Thank you also to Dr. Shairaz Baksh for his advice on my supervisory committee.

I would also like to thank and acknowledge former and present members of the Brindley Lab for their assistance and contributions to an enriching environment: Jay Dewald, Xiaoyun Tang, Bernard Kok, Nancy Ling, Ganesh Venkatraman, Raie Bekele, Dora Captos, Betty Chang, Morgan Belsek and Jenny Campbell (in order of seniority). Similarly, thank you to the McMullen Lab members: Ana Lopez-Campistrous, Larissa Vos, Jingdong Zhang, David Ko and Esther Ekpe Adewuyi.

Much of this project would not have been possible without the generous supply of the autotaxin inhibitor ONO-8430506 from Ono Pharmaceuticals Ltd. in Japan. I thank especially Mr. Tatsuo Meaeda and Dr. Tetsuya Sugiyama for many valuable discussions. I hope our combined efforts will provide new treatments for cancer patients. Thank you to Dr. Yuan Zhao and Dr. Jonathan Curtis in the Faculty of Agriculture, Food and Nutritional Science for assistance with mass spectrometry measurements.

The MD/PhD program is a very long and arduous training process, but it has been made significantly easier through some very key people. First

thank you to Ms. Janis Davis for taking care of all funding and registration headaches! Thank you also to the MD/PhD program directors during my time in the program: Dr. Alan Underhill, Dr. Ken Butcher and Dr. Kathryn Todd. I am also grateful to Dr. Charles Holmes and Ms. Kimberly Arndt for their support particularly in my Vanier CGS application.

I am indebted to my undergraduate research supervisor Dr. Ronald McElhaney for all aspects of my research career. First, his supervision and guidance instilled in me a deep curiosity about science. Further, he was responsible for suggesting my PhD project with Dr. Brindley and Dr. McMullen. He convinced Dr. Brindley to take on one final graduate student and Dr. McMullen to get involved in autotaxin through my co-supervision.

Thank you also to Dr. Alan Underhill and Dr. Sujata Pesad for serving on my candidacy committee. I would also like to extend my gratitude and appreciation to Dr. Frank Wuest and Dr. Sylvain Bourgoin for agreeing to participate in my thesis defense. I would also like to acknowledge numerous friends both in and outside the university setting, and in particular friends and future colleagues from both my original MD Class of 2014 (Para14zers) and my adoptive MD Class of 2017 (Lobotim17ers).

Finally, and most importantly, I acknowledge the ongoing love and support of my parents and brother, which have enabled me to succeed in my academic studies.

TABLE OF CONTENTS

LIST OF TABLES

LIST OF FIGURES

List of Abbreviations

AC	adenylate cyclase
Akt	protein kinase B
ATX	autotaxin
BALF	bronchoalveolar lavage fluid
BSA	bovine serum albumin
C18:0	indicates the numbers of carbon atoms in a fatty acid and the number of double bonds
cAMP	cyclic adenosine monophosphate
CCL	chemokine (C-C motif) ligand
CD	cluster of differentiation
CHO	Chinese hamster ovary
COX-2	cyclooxygenase-2
CXCL	chemokine (C-X-C motif) ligand
DMSO	dimethyl sulfoxide
Edg	endothelial differentiation gene (LPA/S1P receptor family)
ELISA	enzyme-linked immunosorbent assay
ENPP	ecto-nucleotide pyrophosphatase/phosphodiesterase family member
EGF	epidermal growth factor
ERK	extracellular signal-regulated kinase
FA	follicular adenoma

FNB	fine needle biopsy
FBS	fetal bovine serum
FBSC	charcoal-treated FBS (to remove lipids from FBS)
FS-3	Fluorescent Substrate-3
HBS	HEPES-buffered saline
HCC	hepatocellular carcinoma
IC_{50}	inhibitory concentration of 50%
G-CSF	granulocyte colony-stimulating factor
GDP	guanosine diphosphate
GAPDH	glyceraldehyde-3-phosphate dehydrogenase
GM-CSF	granulocyte-macrophage colony-stimulating factor
GPAT	glycerol acyltransferase
GPCR	G-protein-coupled receptor
GTP	guanosine triphosphate
Gy	Gray (unit of radiation)
HPRT	hypoxanthine-guanine phosphoribosyltransferase
IL	interleukin
IP3	inositol triphosphate
$iPLA_2\beta$	Ca^{2+}-independent phospholipase
IPF	idiopathic pulmonary fibrosis
K_i	binding affinity
LDL	low density lipoprotein

LIF	leukemia inhibitory factor
LCAT	lectin:cholesterol acyltransferase
LPA	lysophosphatidate/lysophosphatidic acid
LPC	lysophosphatidylcholine
lysoPLD	lysophospholipase D
LPA_{1-6}	LPA receptors 1-6
LPAR	LPA receptors (in general)
LPPs	lipid phosphate phosphatases
kDa	kilodaltons
KO	knockout
MAG	monoacylglycerol
MAPK	mitogen-activated protein kinase
mRNA	messenger ribonucleic acid
NFAT	nuclear factor of activated T-cells
NF-κB	nuclear factor κ-B
NSAID	nonsteroidal anti-inflammatory drug
NUC	carboxy-terminal nuclease-like domain (of autotaxin)
PA	phosphatidate
PBS	phosphate-buffered saline
PBST	PBS with 0.1% Tween-20
PDE	phosphodiesterase domain (of autotaxin)
PI3K	phosphatidylinositol-3-kinase

PKC	protein kinase C
PLA	phospholipase A
PLC	phospholipase C
PLD	phospholipase D
PTC	papillary thyroid carcinoma
qRT-PCR	quantitative real-time polymerase chain reaction
Th1 or 2	T helper cell type 1 or 2
PDGF	platelet-derived growth factor
RBC	red blood cells (erythrocytes)
Rho	Rho GTPase
RIPA	radioimmunoprecipitation (buffer)
ROCK	Rho-associated protein kinase
$sPLA_2$	secretory phospholipase A_2
SCID	severe combined immunodeficiency
SD	standard deviation
SEM	standard error of mean
S1P	sphingosine-1-phosphate
$S1P_{1-5}$	S1P receptors type 1-5
SA1P	sphinganine-1-phosphate
sCD40L	soluble cluster of differentiation antigen 40 ligand
SDS-PAGE	sodium dodecyl sulphate-polyacrylamide gel electrophoresis
SMB	somatomedin-B like domain (of autotaxin)

SRF	serum response factor
TMA	tissue microarrays
TNF-α	tumor necrosis factor alpha
U	units (enzymatic units of activity)
VEGF	vascular endothelial growth factor
WBC	white blood cells (leukocytes)

CHAPTER 1

INTRODUCTION

1.1 LPA generation, signaling and turnover

1.1.1 Generation of extracellular LPA and LPC

Lysophosphatidate (LPA) is the simplest phospholipid comprising a glycerol backbone, one fatty acid and a phosphate head group. LPA has an ester-linked fatty acid at the *sn*-1 or *sn-2* position of the glycerol backbone and a hydroxyl group at the other position, and a phosphate head group at the *sn*-3 position (Figure 1.1). This modest structure belies the multitude of physiological and pathophysiological processes it mediates. Normally, LPA levels in plasma are about 100 nM and LPA is bound to albumin. LPA can rise to about 1 μM in serum as a result of thrombin-mediated activation of platelets (1-3). The predominant LPA species in human plasma are C20:4 (39%), C18:2 (30%), and C18:1 (9%) (3, 4). The majority of extracellular LPA is generated from lysophosphatidylcholine (LPC) (Figures 1.1 and 1.2), by the lysophospholipase D activity (lysoPLD) of autotaxin (ATX) that hydrolyzes choline from the phosphate head group. Levels of circulating LPA are decreased by about 50% in mice carrying a heterozygous null-mutation for ATX (5, 6). Further, the contribution of ATX to maintaining circulating LPA is demonstrated since ATX inhibition causes a rapid decrease in plasma LPA of >95% (7, 8).

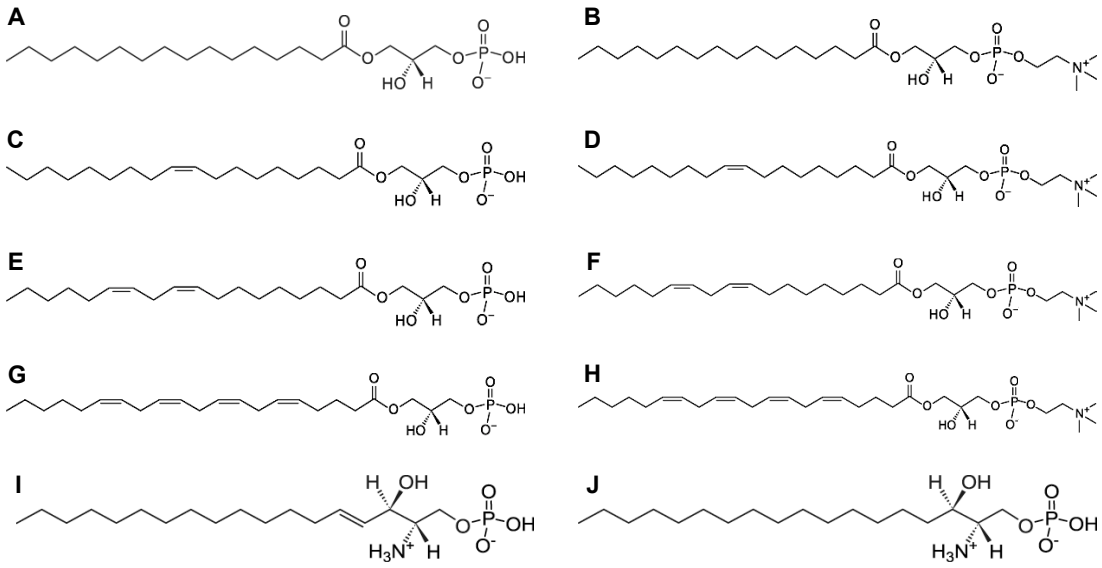

Figure 1.1. Structures of lysophospholipids. A & B: C16:0 lysophosphatidate (LPA) and lysophosphatidylcholine (LPC). C & D: C18:1 LPA and LPC. E & F: C18:2 LPA and LPC. G & H: C20:4 LPA and LPC. I: sphingosine-1-phosphate (S1P). J: sphinganine-1-phosphate (SA1P).

LPC is the most abundant phospholipid in plasma where it reaches concentrations of greater than 200 μM in humans (9, 10). LPA is mostly associated with albumin and lipoproteins such as low-density lipoprotein (LDL) (11, 12). The liver secretes the majority of unsaturated LPC, and this is presumed to be dependent on the activity of a phospholipase A_1 (PLA_1) since much of this LPC is unsaturated (13). However, LPC exists in the plasma as a composite of different molecular species such as C16:0 (40%), C18:2 (20%), C18:1 (15%), C18:0 (10%) and C20:4 (10%) (14). Saturated LPC species (C16:0 and C18:0) make up 25-40% of the total LPC produced by cultured hepatocytes and perfused liver, indicative of the activity of PLA_2 on membrane phosphatidylcholine (PC) (13, 15). In circulation, saturated LPC is

produced mainly by lecithin:cholesterol acyltransferase (LCAT) acting on PC in high density lipoproteins (HDL) and transferring the unsaturated fatty acid to cholesterol (16). Historically, LPC was believed to be a bioactive molecule. However, more recent work has shown that ATX inhibition blocks the effects of LPC on cell migration and survival (17, 18). Therefore, LPC biological properties are mediated through LPA via ATX activity. Interestingly, the proportions of the molecular species of plasma LPC are not reflected in the proportions of LPA molecular species despite ATX producing most plasma LPA from LPC. Instead, this increased proportion of unsaturated LPA species is reflective of the specificity of ATX for unsaturated LPC species (19) (see Section 1.2.2).

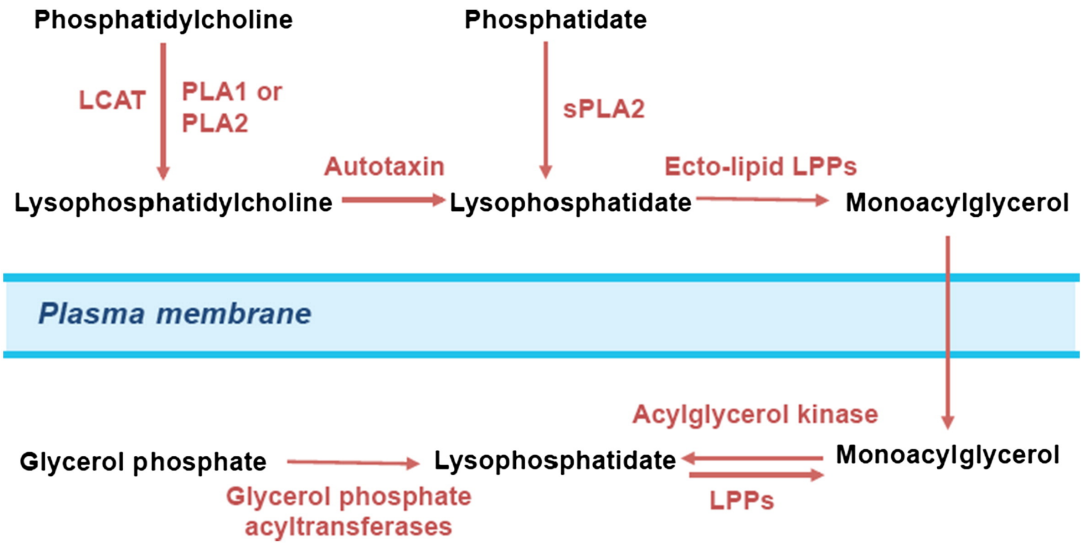

Figure 1.2. Regulation of LPA production and turnover. Most of the extracellular LPA is produced from autotaxin (ATX) from LPC in plasma and extracellular fluids. LPA can also be produced from phosphatidate by secreted phospholipase A2 and iPLA2β. Extracellular LPA is degraded by the ecto-activities of the lipid phosphate phosphatases (LPPs) that reside on the plasma membrane. Intracellular LPA is generated from glycerol phosphate. LCAT, lectin:cholesterol acyltransferase; PLA, phospholipase A; $sPLA_2$, soluble phospholipase A2. Adapted from (10).

Extracellular LPA is also generated in small quantities by the actions of secretory phospholipase A_2 ($sPLA_2$) or Ca^{2+}-independent phospholipase A_2 ($iPLA_2\beta$) on phosphatidate (PA) (Figure 1.2) (20-22). Intracellular LPA is largely generated from glycerol phosphate by glycerol phosphate acyltransferases (GPATs) (Figure 1.2) (23). There is no evidence though that this pool of LPA communicates directly with the extracellular LPA population.

1.1.2 LPA receptor diversity and signaling

To date, there are at least six known LPA receptors, all of which are G-protein-coupled receptors (GPCRs) (Figure 1.3) (24). GPCRs are integral membrane proteins composed of a single polypeptide with seven transmembrane domains. They control many physiological processes initiated by extracellular ligands ranging from photons to hormones, neurotransmitters, odors, peptides and large proteins (25). GPCRs are also the target of nearly 50-60% of all modern pharmaceuticals (26). The importance of GPCRs to biology is reflected in at least eight Nobel Prizes that have been awarded for GPCR research, including most recently the 2012 Nobel Prize in Chemistry (27). GPCRs transmit the signals from extracellular stimuli to intracellular signals through activation of a heterotrimeric guanosine triphosphate-binding protein (G-protein) by the receptor. This activation involves dissociation of the α subunit from the βγ subunits by exchange of a guanosine diphosphate

(GDP) for a guanosine triphosphate (GTP). These subunits, particularly the α subunit, interact with a host of downstream effectors to elicit an intracellular response.

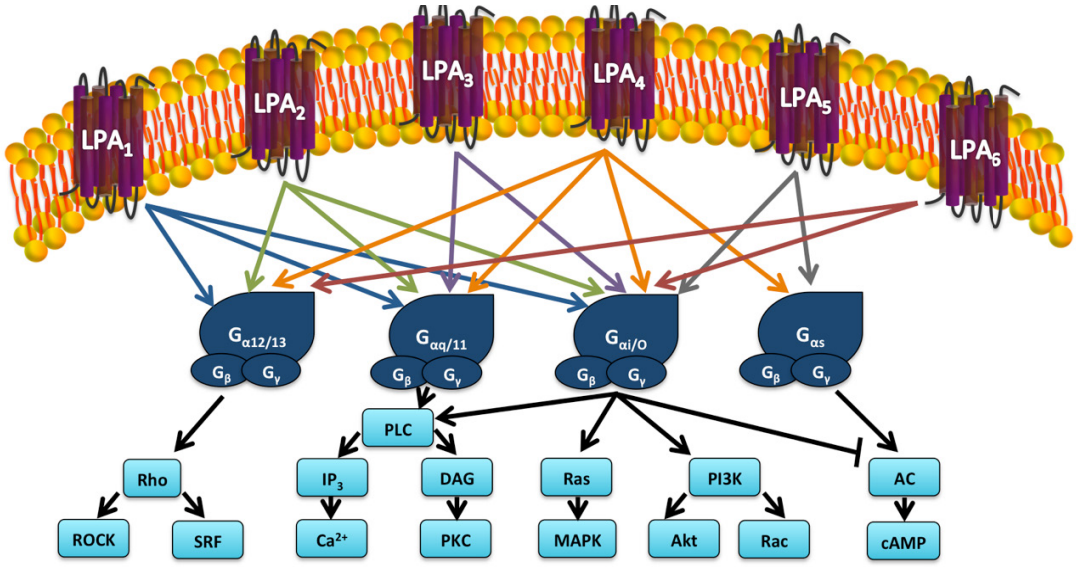

Figure 1.3. Overview of LPA signaling. LPA signals through at least six G-protein coupled receptors to elicit a wide range of cellular responses. Signaling through some of these receptors may be redundant and/or antagonistic, depending on which heterotrimeric G-protein is coupled to the LPA receptor. Gα/β/γ, G-protein alpha/beta/gamma subunits; Rho; Rho GTPase; ROCK, Rho-associated protein kinase; SRF, serum response factor; IP3, inositol triphosphate; PLC, phospholipase C; DAG, diacylglycerol; PKC, protein kinase C; MAPK, mitogen-activated protein kinase; PI3K, phsophoinositide 3-kinase; Akt, protein kinase B; AC, adenylate cyclase; cAMP, cyclic adenosine monophosphate.

The first three of the LPA receptors, $LPA_{1\text{-}3}$, belong to the Edg (endothelial differentiation gene) family (24). These are the best understood of the LPA receptors and most studied in terms of LPA-mediated signaling. LPA_1/EDG2 was the first to be discovered in 1996, followed soon after by LPA_2/EDG4 and LPA_3/EDG7 (28-31). These receptors have a ubiquitous distribution, and the other five GPCRs in the Edg-subfamily are receptors for sphingosine-1-phosphate (S1P) ($S1P_{1\text{-}5}$), a lipid of similar structure to LPA

(24). Knockout (KO) mice have been generated for all the known LPA receptors, as well as double KOs for combinations of LPA_{1-3} and the triple KO of LPA_{1-3}, all of which are viable (9, 32, 33). LPA_1 deletion shows craniofacial deformity while LPA_3 deletion leads to delayed implantation of embryos and impaired embryo spacing (34, 35). No obvious phenotype defect has been found in LPA_2 KO mice (36). These findings underscore the incredible redundancy of LPA-receptor signaling pathways (Figure 1.3) and also suggest there may be other receptors that can mediate LPA signaling.

LPA_{4-6} belong to the P2Y purinergic receptor family and have specific tissue distributions unlike LPA_{1-3} (24, 37). LPA4/GPR23/p3y9 is found in the embryonically-developing brain and in adults largely in the ovaries (38, 39). LPA_5/GPR92 is highly expressed in the spleen, small intestine and dorsal root ganglion cells (40). In mast cells, LPA_5 is the main LPA receptor responsible for LPA-induced release of chemokine (C-C motif) ligand 4 (CCL4/MIP-1β) (41). Genetic ablation of either LPA_4 or LPA_5 does not result in obvious phenotypic defects (42, 43). LPA_6/p2y5 appears to be important for hair growth as genetic truncations of the receptor leads to hypotrichosis simplex, a set of diseases involving familial hair loss (44). *In vitro*, this receptor only responds to μM concentrations of LPA while LPA_{1-5} will activate in response to nM concentrations (45). Finally, there are at least three more proposed LPA receptors (GPR87, P2Y10 and GPR35), but further experimental validation is required (24).

1.1.3 Turnover of LPA

LPA is hydrolyzed to inorganic phosphate and monoacylglycerol (MAG) by catalytic activity of three related proteins called the lipid phosphate phosphatases (LPP1-3) (46). All three LPPs are integral membrane proteins containing six transmembrane helices with the C- and N-terminus facing the cytosolic side of the plasma membrane (47). At the plasma membrane, the catalytic site of the LPPs faces the extracellular environment, enabling access to extracellular LPA and related substrates (46, 47). The importance of this ecto-activity has been demonstrated *in vivo* where the half-life of circulating LPA increases from 3 min to 12 min in LPP1 hypomorph mice compared to normal control littermates (48). LPA can also be degraded to glycerol phosphate by the action of lysophospholipase A activities, however the importance of this pathway is unknown (49). In mice, exogenously-added LPA is rapidly taken up by the liver without enzymatic degradation (50). It is proposed that this could be a mechanism for regulating the concentrations of circulating lysophospholipids, as well as means of entry into hepatic pathways of lipid metabolism (50).

1.2 Overview of ATX structure and production

1.2.1 History of ATX

Enzymatic generation of LPA in plasma by lysoPLD activity was first described in 1986 (51). ATX is a 125-kDa secreted glycoprotein that was first

isolated in 1992 from A2058 melanoma cells and described as an “autocrine motility factor” (52). At the time, its enzymatic activity and homology to other growth or motility factors were unknown. Two years later, sequencing the cDNA clone of ATX was found to have significant homology the plasma cell glycoprotein-1 (PC-1) (53), which was known to have nucleotide pyrophosphatase and phosphodiesterase (NPP) activity (54, 55). PC-1 was later named NPP1 and ATX as NPP2, the first two members of a family of seven enzymes that hydrolyze phosphodiester and pyrophosphate bonds to remove phosphates from ADP and ATP (9). As a secreted enzyme, NPP2 was later referred to as ecto-NPP2 (ENPP2), which has since become the gene symbol for ATX (56). However, is was not clear how this extracellular nucleotide activity could explain the motility-stimulating capability of ATX described in melanoma cell culture. This mystery remained until 2002, when the plasma lysoPLD activity described in 1986 was purified and found to be identical to ATX (57-59). Subsequent work showed that ATX/ENPP2 was unique among the NPPs/ENPPs because of its lysoPLD activity that converts LPC to LPA (57). The affinity of ATX for LPC was shown to be higher than for nucleotides, suggesting that LPC is the preferred physiological substrate for ATX (57). The motility-stimulating function of ATX was also shown to be significantly enhanced by addition of LPC to cell culture experiments, and could be mimicked by direct addition of LPA (17, 57). Further, deletion of

LPA_1 in fibroblasts abolished the effects of ATX on cell migration (60). Thus, LPA, the product of ATX, is the actual “motility factor” initially described.

1.2.2 Structural features of ATX

Consisting of a single polypeptide, ATX has two amino-terminal somatomedin B-like (SMB) domains (Figure 1.4A), which mediate protein-protein interactions (61). The SMB1 domain interacts with the adjacent phosphodiesterase (PDE) domain and may mediate LPA exit from the catalytic site (61, 62). The SMB2 domain is positioned to engage with other proteins, and is known to interact with activated platelets though β1 and β3 integrins (63) (see Section 1.2.3). The PDE domain contains the catalytic site. Thr210 is the key catalytic residue and is surrounded by two zinc ions (64). Compared to other members of the ENPP family, ATX has an 18-residue deletion, which establishes a pocket for the accommodation of lysophospholipids and explains why ATX is unique for its lysoPLD activity (64). Insertion of this 18-residue sequence into ATX significantly impairs LPC hydrolysis but not nucleotide hydrolysis (19). The PDE domain and carboxy-terminal nuclease-like (NUC) domain are tethered together by seven hydrogen bonds, nine salt bridges and an intramolecular cysteine bridge (63). There is also a 50-residue lasso domain that starts at the end of the PDE domains and wraps tightly around the NUC domain, which maintains the structural rigidity of the ATX catalytic domain (63, 64). The NUC domain

tightly binds Ca^{2+} via an EF hand-like motif, however, the precise function of this domain is unclear (62, 64).

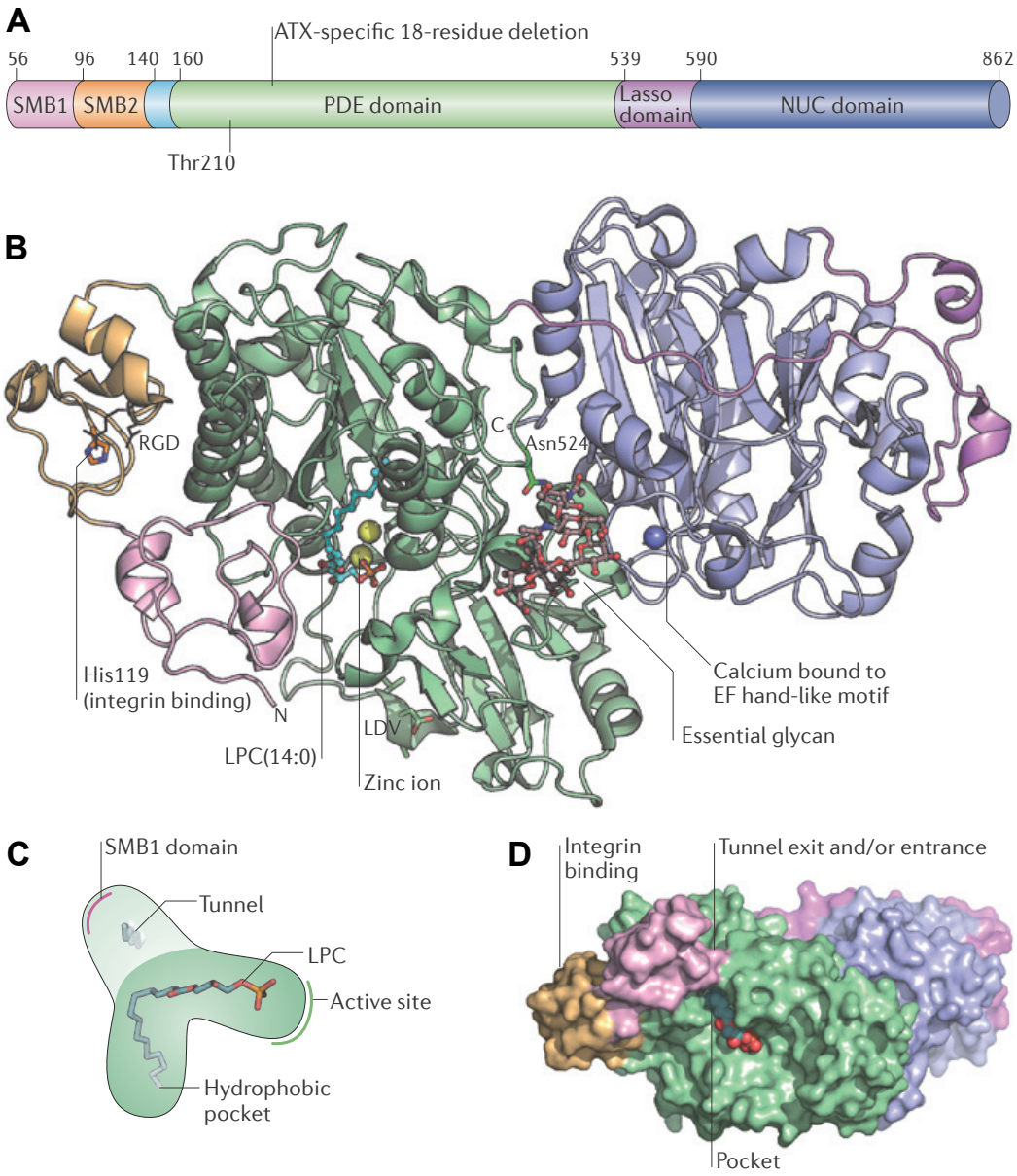

Figure 1.4. Overview of the structure of ATX. A: The domain organization of ATX (ENPP2). The amino terminus somatomedin B-like (SMB) domains are involved in integrin binding and other protein-protein interaction. The phosphodiesterase (PDE) domain contains the catalytic site and the key residue Thr210. The PDE domain also contains an 18-residue specific deletion compared to other ENPP enzymes, which confers lysophospholipid specificity. The “lasso” domain and carboxy-terminal

nuclease-like (NUC) domain, which are catalytically inactive confer structural stability on the PDE domain. B: The crystal structure of ATX bound to C14:0 LPC. C: Schematic diagram of the relationship between the active site, tunnel and U-shaped hydrophobic pocket. D: Surface representation of ATX with a space-filling model of LPC, highlighting the tunnel as either an entrance or exit from the catalytic site. Figure adapted from (64).

Overall, this 3D arrangement establishes several key features that give ATX specificity for lysophospholipids (Figure 1.4B-D). First, forming between the SMB1 and PDE domains is a tunnel forming a T-junction with the substrate-binding pocket (62). This tunnel is capable of accommodating the hydrophobic tail of lysophospholipids. However, it is not clear if this tunnel serves as an entrance for LPC to the catalytic site, or an exit for LPA in which case ATX may be able to deliver its product to an adjacent LPA receptor (62). Within the catalytic site is a U-shaped hydrophobic pocket (19). This configuration is better able to accommodate the kinked acyl chains of unsaturated fatty acids compared to the extended linear conformations of saturated fatty acids, explaining why ATX has a preference for unsaturated and polyunsaturated substrates (19) (Section 1.1.1).

1.2.3 Integrin binding of ATX

As a secreted enzyme, an attractive idea has been that ATX can localize to the surface of specific cells, which provides for direct production and delivery of LPA to adjacent LPA receptors. The first report of ATX binding to cell surfaces came in 2008 showing ATX binding to the $\alpha 4\beta 1$ integrin in leukocytes, and that this interaction could be blocked with

antibodies to either the α4- or β1-subunits (65). This study concluded that LPA from ATX promoted the entry of lymphocytes into secondary lymphoid organs (65). Later, ATX binding to β1- or β3-integrins by its SMB2 domain (Section 1.2.2) was demonstrated on platelets and Chinese hamster ovary (CHO) cells (66, 67). These findings were also verified with antibodies that blocked ATX binding to integrins. Likewise, integrin-binding antibodies could block binding of SMB2 domain fragments to β3 integrins on CHO cells in an identical manner to that of wild-type ATX (67). This was further verified through experimental mutations of key residues in the SMB2 domain that impeded interactions with platelet β3 integrins (63). However, integrin-binding is not required for ATX activity since integrin-binding deficient mutants have virtually the same activity as wild-type ATX (68). Nevertheless, this same study did report that integrin-mediated cell surface recruitment of ATX promoted persistent directional cell migration of MDA-MB-231 human breast cancer cells (68). Overall, ATX interaction with the cell surface may lead to more efficient LPA production and signaling, but this does appear to be absolutely necessary.

1.2.4 ATX isoforms

To date, five alternatively-spliced isoforms of ATX have been described in man. All ATX isoforms display similar lysoPLD activities and substrate preferences (62, 69, 70). The original ATX described in melanoma

cell culture is termed ATXα, whereas the most abundant isoform is ATXβ and this is the same isoform responsible for the majority of plasma lysoPLD activity (61). ATXα is the longest isoform with a 52-residue polybasic insertion within the catalytic domain (62) (Figure 1.5). This insertion confers specific binding to heparin sulfate proteoglycans on the plasma membrane (71), representing an integrin-independent means of protein interaction (Section 1.2.3). ATXε, which was identified during the cloning of ATXα from A2058 melanoma cells, also contains this insertion, but has a 4-residue deletion in the "lasso loop" or L2 linker region between the PDE and NUC domains (69) (Figure 1.5). The importance of this deletion is unclear. This deletion is uniquely shared with ATXδ, the second most abundant isoform (69). ATXδ and ATXε comprise about 30% of the total ATX in most tissues and they are enriched in the spleen and intestine (69). Interestingly, the 52-residue polybasic insertion results in ATXα and ATXε having significantly lower thermal stabilities than the other three isoforms (69). ATXγ is a brain-specific form of ATX with a 25-residue insertion in the NUC domain (56, 72). The significance of this insertion is not known. Finally, ATXβ, the most abundant and ubiquitous isoform, is equivalent to the ATXα isoform, but without the 52-residue PDE domain insertion (62, 69) (Figure 1.5). Virtually all studies on ATX have made use of this isoform (62). In most tissues and cell lines, the ratio of ATXβ to ATXδ is 7:3 (69). Overall, it is unclear if any of the ATX isoforms have unique physiological or pathophysiological roles (62).

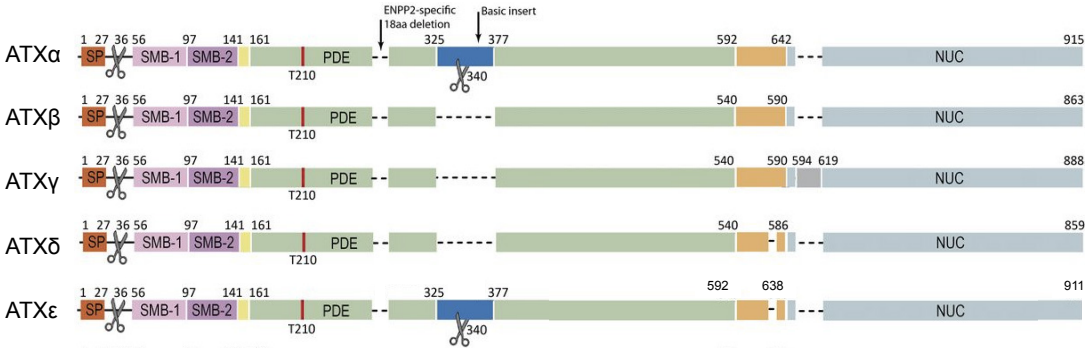

Figure 1.5. Scheme for the different alternatively-spliced isoforms of ATX. ATXα and ATXε have a 52-residue polybasic insert within the catalytic PDE domain compared to ATXβ, the most abundant ATX form. ATXγ has an extra 25-residue insertion in the NUC domain, while ATXδ and ATXε have a 4-residue deletion in the lasso domain (orange) between the PDE and NUC domain. SP, signal peptide. Adapted from (62).

1.2.5 ATX secretion, maturation and turnover

Full-length ATX is synthesized as a pre-proenzyme and is secreted by the classical secretory pathway (73, 74). ATX is cleaved at two N-terminal sites, first by signal peptidase that removes the N-terminal signal sequence of 27 residues and second by furin at residue 35 as ATX is co-translationally translocated (74). A later study looking at ATX secretion from mouse 3T3-F442A adipocytes showed that signal peptidase activity is critical for the secretion of ATX, whereas the furin cleavage site does not contribute to secretion, nor ATX lysoPLD activity (75). ATX is also an N-glycosylated enzyme, which increases the mass of the enzyme from 100 to 125 kDa (76). N-glycosidase treatment significantly reduces ATX lysoPLD activity and inhibition of N-glycosylation by tunicamycin blocks ATX secretion (75). Further, mutagenesis and deglycosylation experiments revealed that only the

glycosylation of Asn524, a residue within the catalytic domain, is essential for ATX lysoPLD activity (77). Later, the crystal structure of ATX demonstrated that this glycosylation assists in the forming of the interface between the PDE and NUC domains (63).

Like its product LPA, the liver also clears ATX. Mouse studies using ^{125}I-labeled ATX showed that scavenger receptors on liver sinusoidal endothelial cells bound ATX within 5 min of injection, and cleared most labeled ATX within 24 h (78). More recent work in the liver fibrosis field has corroborated this work. In fibrosis, hepatic stellate cells are activated and produce abundant extracellular matrices, blocking endothelial fenestrae and impairing ATX uptake (79). This decrease in ATX clearance leads to increases in plasma ATX levels, which in turn fuels disease progression (79). The significance of this will be discussed in Section 1.5.

1.3 Embryological and physiological roles of ATX

1.3.1 ATX knockout studies

ATX is a vital enzyme that is needed for proper early embryological development. ATX knockout (KO) (ENPP2 -/-) embryos die *in utero* on average at day 9.5 with vascular and neural tube defects (5, 80-82). In these mice, malformations in the allantois, neural tube and headfold are detected by day 8.5, and by day 10.5 embryos become necrotic and are reabsorbed (83). Normally, extra-embryonic endothelial cells remodel from day 8.5 to 9.5 to

create a vascular network that connects with the embryo, allowing the yolk sac to function as the main nutrient source. ENPP2 -/- embryos have increased expression of VEGF mRNA, consistent with hypoxic conditions in the absence of a functional vascular system (5, 6). This illustrates the importance of LPA in vascular development.

Neural tube closure begins at day 8.5 and closure defects in ENPP2 -/- embryos have been attributed to a local deficiency in ATX expression (5). In ENPP2 -/- embryo explants, these folding abnormalities are abrogated by exogenous addition of LPA (84). The role of ATX in vascular and neural development has also been confirmed in zebrafish (83, 85). ATX regulates oligodendrocyte differentiation in the developing zebrafish hindbrain (86) and the correct left-right asymmetry for normal organ morphogenesis through Wnt-dependent pathways (87). ENPP2 +/- mice are viable, and express half the levels of both ATX and LPA compared to normal mice (88). However, they are hyper-responsive to hypoxia-induced vasoconstriction and remodeling, and they develop pulmonary hypertension (88).

1.3.2 ATX expression and its role as a mediator of wound healing and tissue remodeling

The importance of ATX to proper neuronal development and function is also reflected by high ATX mRNA in adult neuronal tissues (89) (Figure 1.6). ATX mRNA levels are also high in adipose tissues (Figure 1.6) and this will be discussed further in Section 1.5.3 (90). Physiologically, the most important

role of ATX after birth is probably in wound healing and tissue remodeling. LPA is a potent activator of platelet aggregation and it stimulates the growth and migration of fibroblasts, vascular smooth muscle cells, endothelial cells and keratinocytes (91). In fact, fibroblasts are second only to brain/spinal cord tissue as the highest expressers of ATX mRNA (Figure 1.6). Increased ATX activity is found in blister fluid where local production of LPA promotes re-epithelialization (92). ATX expression and LPA production are also increased in rabbit aqueous humor following corneal freeze wounds (93).

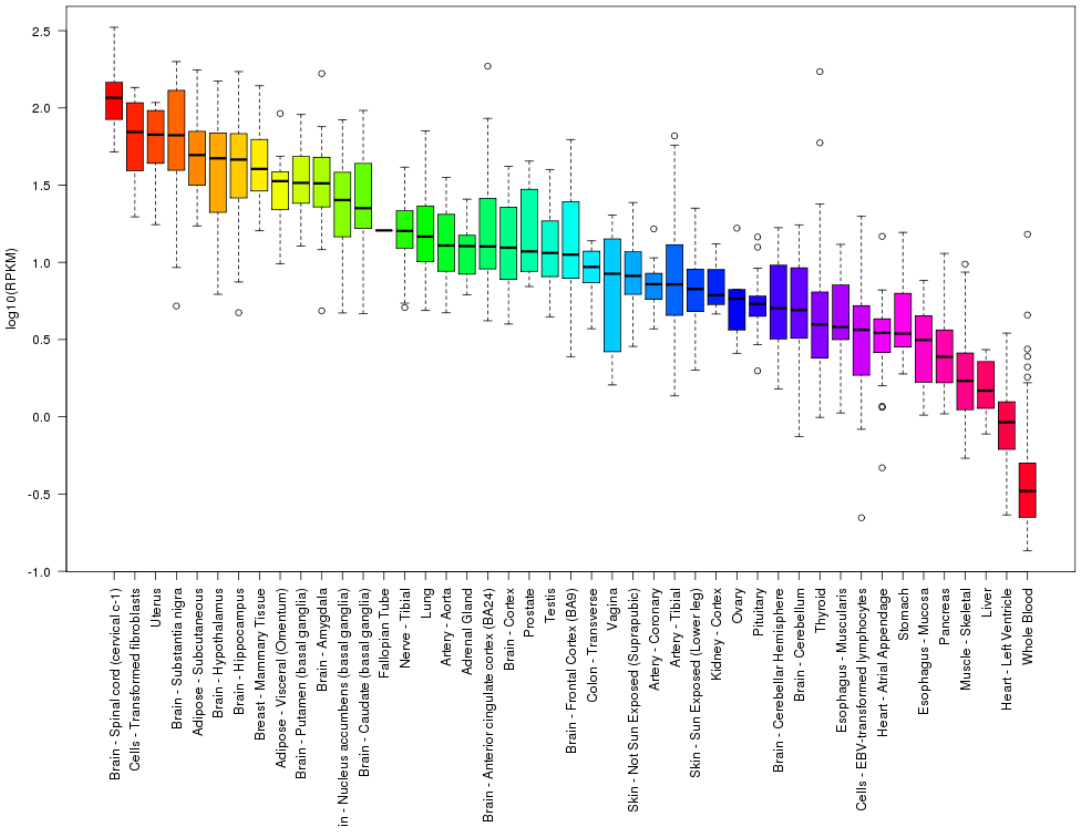

Figure 1.6. ATX mRNA expression in normal human tissues. Data retrieved from the Genotype-Tissue Expression Portal from the Broad Institute (89) (www.gtexportal.org). Pilot Data 2013-01-31. ATX expression varies greatly throughout the body, but it is very high in nervous and adipose tissue. RPKM, reads per kilobases per million (y-axis).

Recently discovered physiological roles for ATX include hair follicle morphogenesis (94), bone mineralization (95) and myeloid differentiation in human bone marrow (96). ATX/LPA signaling also remodels luteal tissue in regressing corpora lutea of cycling rats by recruiting phagocytes and proliferating fibroblasts (97). ATX expression is also upregulated in microglia in response to oxidative stress. This protects microglia cells against damage from H_2O_2, an effect which is partially reversed in the presence of the mixed $LPA_{1/3}$ antagonist Ki16425 (98). A follow-up study showed that ATX overexpression in microglia limited the pro-inflammatory response to lipopolysaccharide exposure, mimicking gram-negative infection (99). ATX is expressed in high endothelial venules (HEVs) in lymph nodes and other secondary lymphoid tissues (100) and mediates lymphocyte extravasation, which is crucial for maintaining immune homeostasis (101-103). However, in chronically inflamed tissues, ATX mediates lymphocyte trafficking and upregulates cytokine production in response to repeated microinjuries and incomplete tissue repair (104-106).

1.4 Acute physiological inflammation versus chronic pathological inflammation

1.4.1 Overview of acute and chronic inflammation

Inflammation is a protective host response designed to rid the organism of damaged and/or necrotic tissues and microbes. In the absence of

inflammation, injured tissues would not be repaired and infections would go unchecked (107). However, cellular mechanisms designed to eliminate foreign material as well as necrotic cells also have the tendency to cause collateral damage to nearby normal cells. Consequently, inflammation can be harmful in situations where it is inappropriately activated or poorly controlled. In fact, in clinical medicine, much attention is given to the damaging consequences of inflammation since they underlie many common chronic diseases, such as rheumatoid and osteoarthritis, atherosclerosis, organ fibrosis, diabetes and obesity (108). For this reason, pharmacies abound with anti-inflammatory drugs, which ideally would control the harmful sequelae of inflammation and not interfere with its beneficial effects.

The insult driving inflammation may be acute or chronic (Figure 1.7). Acute inflammation has a rapid onset of action and lasts for hours or days. This rapid host response serves to deliver leukocytes and plasma protein to the site of tissue injury and/or infection. The redness (rubor), warmth (calor), swelling (tumor) and pain (dolor) of acute inflammatory reactions are caused by increases in blood flow and vascular permeability (109). Circulating leukocytes (primarily neutrophils) then migrate to the site of injury under the influence of chemotactic signals (110). To eliminate the offending agents, activated leukocytes can release toxic metabolites and proteases resulting in tissue damage causing pain (dolor). In contrast, chronic inflammation can last from weeks to years (Figure 1.7). It may follow acute inflammation or it may

begin as a low-grade response without any initial manifestations of an acute reaction. Tissue destruction and attempts at repair often coexist in varying combinations throughout its clinical course (111, 112).

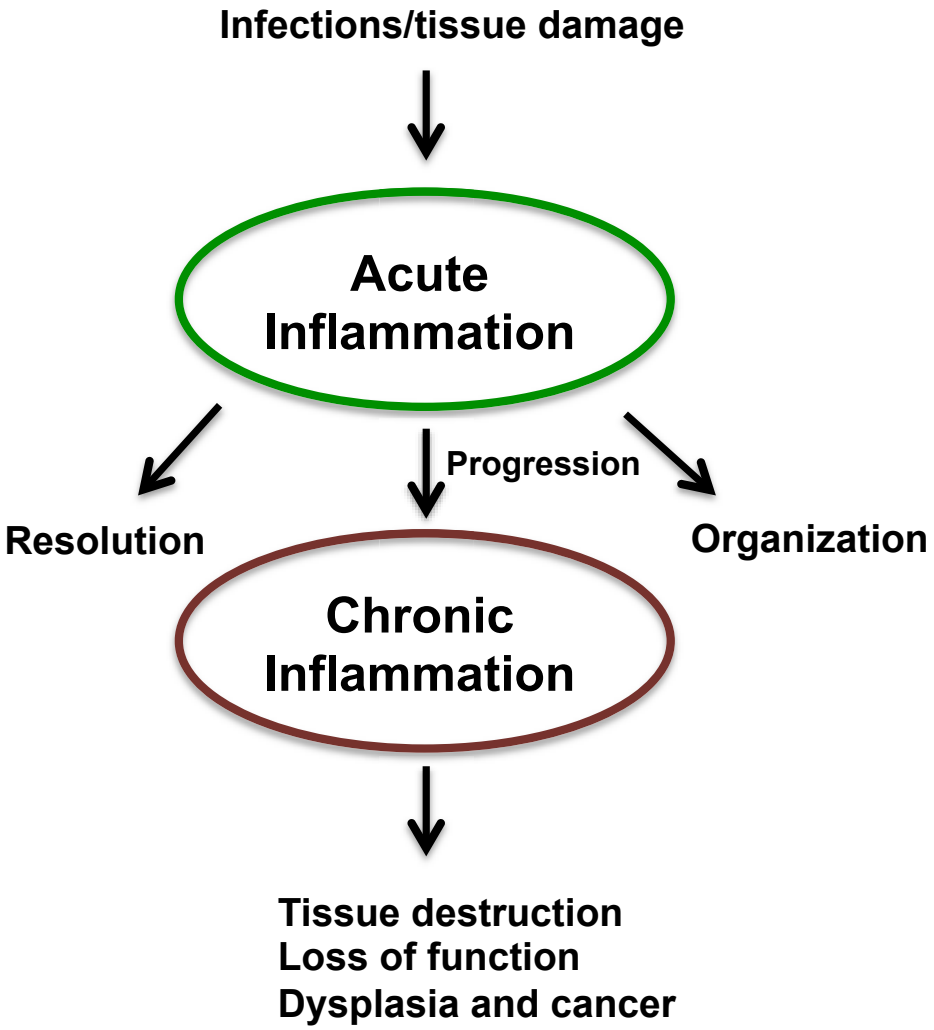

Figure 1.7. Overview of acute and chronic inflammation. In response to infections or tissue damage, acute inflammatory processes attempt to restore homeostasis. If successful, the inflammation will cause the tissue to recover completely (resolution), or undergo fibrotic and/or other tissue remodeling processes that will overcome the insult (organization). However, in the case of repeated microinjuries or incomplete repair, acute inflammation can progress to chronic inflammation, which can worsen the original pathogenesis. In the process, tissue is usually destroyed and functionality is lost. In worst cases, cells of the tissue can become morphologically abnormal (dysplasia) and eventually cancerous.

1.4.2 Termination of acute inflammation

Once the injurious stimulus has been successfully neutralized, the inflammatory reaction normally subsides partly because the inflammatory mediators are produced only as long as the stimulus persists (Figure 1.7). More importantly, towards the end of acute inflammation, there is a switch from pro-inflammatory to anti-inflammatory mediators. Bioactive lipids such as lipoxin, resolvins and protectins, which are derived from omega-3 polyunsaturated fatty acids, contribute to the resolution of inflammation. The principal action of these molecules is to inhibit leukocyte recruitment to the area of inflammation and reduce vascular permeability. In short, the activation of these anti-inflammatory lipid mediators limits the progression of inflammation (108, 113, 114). Under ideal circumstances, the site of acute inflammation should be restored to normal upon complete resolution, both functionally and structurally. In tissues lacking regenerative potential, the site of injury is replaced by fibrous tissue through a process known as organization (114). When the process of acute inflammation is unable to eliminate the offending agents, there is a transition from acute to chronic inflammation, ultimately leading towards tissue destruction, loss of function, potential dysplasia and even cancer (Figure 1.7).

1.4.3 Cytokines in inflammation

Cytokines are a very diverse group of small proteins typically under 20 kDa in size that orchestrate inflammatory cells such as lymphocytes, macrophages and neutrophils to generate a proper immune response. The term “cytokine” was proposed in 1974 to replace the misleading term “lymphokine” since these signaling molecules were quickly discovered to be produced by many cell types besides lymphocytes (115). A decision was made in 1979 to adopt the interleukin (IL) nomenclature to encompass the ever-growing list of identified cytokines (116), but since then, the cytokine family has expanded to also include interferons, colony stimulating factors (CSFs), tumor necrosis factors (TNFs) and chemokines (117). Inteferons are involved primarily in antiviral responses (118). CSFs are glycoproteins that were initially found to stimulate hemopoietic stem cells macrophage [macrophage-CSF (M-CSF/CSF1), granulocyte macrophage-CSF (GM-CSF), and granulocyte-CSF (G-CSF)]. Both recombinant G-CSF and GM-CSF are used to stimulate bone marrow regeneration in cancer patients following treatment with radiotherapy and/or cytotoxic chemotherapy (119). TNFs are a family of 19 proteins initially characterized as inducers of apoptosis under some circumstances (117). The most well-recognized member of this family, TNF-α, is a very potent inflammatory mediator and is central to the inflammatory response of the innate immune system (120). TNF-α also stimulates the production of many other cytokines. Chemokines (short for

"**chemo**tactic cyto**kines**") are a diverse group of very small (8-15 kDa) signaling proteins that mediate chemo-attraction between cells (117). Generally speaking, in response to damage or following the initiation of pro-inflammatory signaling by ligands such as TNF-α or IL-1, tissues secrete chemokines to recruit macrophages, T-lymphocytes, mast cells, neutrophils and eosinophils into the affected site to mediate repair (121). In the human genome, 44 chemokines and 23 chemokine receptors have been identified, and these are further classified into subfamilies based on the location of three or four conserved cysteine residues (117). Chemokines are historically classified as being either homostatic or inflammatory. However, this is overly simplistic since the significant redundancy in ligand/receptor pairings results in chemokines having diverse situational roles (122).

Functionally, cytokines can be divided into two groups, namely pro-inflammatory and anti-inflammatory. Pro-inflammatory cytokines are produced predominately by activated macrophages. Anti-inflammatory cytokines belong to the T cell-derived cytokines.

1.4.3.1 Pro-inflammatory cytokines

Prototypical pro-inflammatory cytokines include TNF-α, IL-1, IL-6 and IL-8. TNF-α was originally described as a tumor-cell killer and it is produced by activated macrophages and natural killer cells following lipopolysaccharide (LPS) exposure. Most cell types express TNF-α receptors with the exception

of erythrocytes (123). In acute inflammation, TNF-α is important in endothelial activation. TNF-α is a direct pyrogen and potent inducer of systemic acute-phase responses associated with infection or tissue injury (124). IL-1α and IL-1β are the most studied members of the IL-1 family and they are produced mainly by mononuclear and epithelial cells as precursor proteins, which are activated by the multiprotein oligomer inflammasome (125). IL-1α and IL-1β function similarly to TNF-α in that they also trigger fever and acute-phase responses. IL-6 is a small glycoprotein that is produced by a variety of immune and non-immune cells such as the endothelial cells, macrophages, fibroblasts and lymphocytes. It is also a potent inducer of fever and acute-phase responses. (126, 127). Like IL-6, IL-8 is produced by macrophages, epithelial, endothelial and airway smooth muscle cells. IL-8 was originally known as neutrophil chemotactic factor since it induces neutrophil migration to target tissues and induces phagocytosis (128). IL-8 is also a potent mediator of angiogenesis and its secretion is increased by oxidative stress, which further drives the recruitment of other pro-inflammatory cells to the site of inflammation (129).

1.4.3.2 Anti-inflammatory cytokines

Pro-inflammatory responses are typically mitigated by anti-inflammatory cytokines like IL-4, IL-10 and IL-13. IL-4 and IL-13 utilize a common subunit in their receptors and consequently share many biological

functions. Activated T cells, mast cells and natural killer cells produce both of these cytokines. IL-4 plays a fundamental role in the production of B cell-mediated IgE antibodies, which mediate allergic reaction and defend against helminth infections. More importantly, IL-4 inhibits macrophage activation and supports the differentiation of T helper type 2 (Th2) cells, which decrease pro-inflammatory responses. Similarly, IL-13 also induces IgE production and inhibits inflammatory cytokine synthesis (130-132). IL-10, previously known as human cytokine synthesis inhibitory factor (CSIF), is mainly produced by Th2 cells and monocytes. The most important biological effect of IL-10 with respect to immune modulation is to support the development of Th2 cells, while limiting Th1 pro-inflammatory responses (120).

1.5 The role of ATX in inflammatory diseases

The ATX/LPA signaling is implicated in fueling many inflammatory diseases. As discussed previously, ATX is a part of the physiological wound healing response. When the inflammation in these acute processes become chronic in the context of repeated micro-injury and incomplete repair, ATX/LPA signaling fuels additional cytokine production and recruitment into the local tissue environment, which can aggravate the original disease.

1.5.1 Asthma and pulmonary fibrosis

Asthma is a chronic inflammatory disease of the airways characterized by bronchospasm and reversible airflow obstruction. Acute symptoms are treated with inhaled β2-agonists like salbutamol, and asthma is typically managed with inhaled corticosteroids (133). IL-4, IL-5, IL-9 and IL-13, which are derived from Th2 cells, play a critical role in the asthmatic inflammatory response (134). LPA increases chemotaxis of Th2 cells, and it augments both IL-13 gene expression and secretion and transcriptional activity of the IL-13 promoter (135, 136). More recently, increased ATX protein was found in bronchoalveolar lavage fluid (BALF) of asthmatic patients after allergen challenge (137). Similar findings were also found in mice when subjected to a triple-allergen model of asthma (house dust mite, ragweed, and *Aspergillus* allergen). This increase in ATX protein was correlated with increases in C22:5 and C22:6 species of LPA. Mice that were transgenic for ATX had a more severe asthmatic phenotype and a significant increase in BALF IL-4 and IL-5 levels. This ATX-induced phenotype was partly diminished after treatment with the ATX inhibitor GWJ-A-23 (half-life of 50 min) (137).

ATX has been implicated in other lung diseases. The most researched is idiopathic pulmonary fibrosis (IPF), a chronic and progressive fibrotic diffuse lung disease occurring mainly in older adults. LPA concentrations are increased in BALF of IPF patients and bleomycin-treated mice, a murine model for IPF (138, 139). Conditional genetic deletion of ATX from

bronchiolar epithelial cells and macrophages diminished the severity of bleomycin-induced IPF (140). Like in the murine asthmatic model, the ATX inhibitor GWJ-A-23 attenuated disease progression in bleomycin-treated mice, implicating the potential value of ATX inhibitors in treating IPF (137, 140).

1.5.2 Rheumatoid arthritis and osteoarthritis

Rheumatoid arthritis is an autoimmune disorder characterized by synovial inflammation and subsequent joint destruction. Hypertrophy and inflammation of the soft tissues around the synovial joint are common findings. Macrophages are critically involved in the pathogenesis of rheumatoid arthritis by producing a wide range of pro-inflammatory cytokines and growth factors such as IL-1, IL-6, IL-8, TNF-α and GM-CSF (141, 142). LPA in synovial fluid of rheumatoid arthritis patients stimulates cyclooxygenase-2 (COX-2) expression. It synergizes with IL-1α and IL-1β to promote pathogenesis (143), and upregulates IL-6 and IL-8 production (144). Further, TNF-α increases LPA_3 mRNA expression in synoviocytes from rheumatoid arthritis patients, which in turn modulates cytokine production (144). TNF-α drives increased ATX production from synovial fibroblasts in both mouse and human arthritic joints, and anti-TNF-α treatment with infliximab injections attenuated this ATX expression in mice (145). Increased ATX levels were also detected in the serum of rheumatoid arthritis patients (4,

145). Also, conditional genetic ablation of ATX in mesenchymal cells in mice slowed disease development through decreases in inflammation and synovial hyperplasia as indicated by histopathological analysis (145). Thus, rheumatoid arthritis is an ideal model for studying the interconnectivity of classical inflammation to ATX/LPA signaling (146). Osteoarthritis is a degenerative joint disease characterized by damaged articular cartilage and subchondral bone that is not sufficiently self-repaired. One very recent study has positively correlated both plasma and synovial fluid ATX levels with the severity (functionally and radiographically) of knee osteoarthritis (147).

1.5.3 Obesity, atherosclerosis and acute coronary syndrome

Obesity, which is strongly associated with type 2 diabetes, is considered to be a low-grade, chronic inflammatory state. This is orchestrated by adipocytes in response to excess nutrients and energy through low-level induction of cytokines such as TNF-α, IL-1β and chemokine C-C motif ligand 2 (CCL2) in the adipose tissue environment (148). In the presence of excess nutrients, a modified milieu with an altered composition of immune cells favors an unresolving pro-inflammatory situation in adipose tissue and surrounding organs (148). The roles that ATX/LPA signaling play in obesity-mediated health manifestations are beginning to be elucidated. ATX from white adipose tissue produces a significant proportion of extracellular LPA (Figure 1.6). Mice carrying a null ATX allele specifically in adipose tissue

show a 38% reduction in plasma ATX levels and an improvement in glucose tolerance levels (90). Conversely, ATX expression is increased in adipose tissue of obese and insulin-resistant mice and human beings (90, 149, 150). Transgenic mice that overexpress ATX have reduced expression of brown adipose tissue-related genes in peripheral white adipose tissue when fed a high-fat diet, and they accumulate more fat than wild-type controls (151). Furthermore, treatment of mice on a high-fat diet with the $LPA_{1/3}$ inhibitor Ki16425 improved glucose tolerance compared to controls. Intraperitoneal injection of LPA acutely impaired both glucose tolerance and insulin secretion (152). It is not entirely clear from these studies if increases in ATX expression promote or are a consequence of obesity, but there is evidence that ATX inhibition could play a part in the management of obesity-induced hyperglycemia.

Like obesity, atherosclerosis is another manifestation often associated with a sedentary lifestyle. Historically, atherosclerosis was believed to be a disease involving the accumulation of lipids in the vessel walls of arteries. However, recent research suggests that inflammation plays an active role in all stages of atherosclerosis (153). These inflammatory processes are initiated in endothelial cells in response to retained low-density lipoprotein (LDL). As this LDL oxidizes, tissue macrophages derived from circulating monocytes engulf these particles, but only partially process them. This leads to deposition of oxidized cholesterol and phospholipids in plaques in the

arterial walls. These plaques promote the deterioration of the arterial wall resulting in the recruitment of even more white blood cells to the affected area, which reinforces the cycle (153). Oxidation of LDL leads to local production of LPC, which is subsequently converted into LPA by ATX (154). Plasma LPA levels are significant higher in patients suffering from acute coronary syndrome (myocardial infarction from either partial or complete blockage of coronary arteries) compared to patients with normal coronary arteries (155). In these patients, LPA levels were significantly higher in blood obtained from the affected coronary artery(ies) compared to patient-matched peripheral blood samples (156). Overall, these findings suggest that ATX/LPA signaling may be involved in all stages of atherosclerosis from silent plaque formation to myocardial infarction (155-157).

1.5.4 Liver and colonic disorders

The importance of ATX/LPA signaling in liver and colonic diseases is rapidly becoming appreciated. Both plasma LPA and serum ATX levels are increased in patients with chronic hepatitis C and there is a positive correlation between ATX/LPA levels and the histologic stage of fibrosis (158). These findings were complemented with rat studies of liver injuries, which concluded that plasma LPA and serum ATX levels are increased in chronic carbon tetrachloride-induced liver fibrosis models, and acutely following dimethylnitrosamine-induced injury or 70% hepatectomy (159). Chronic

hepatitis is a major risk factor for hepatocellular carcinoma, and the relationship between hepatitis, hepatocellular carcinoma and ATX will be discussed in greater detail in Section 1.6.

Other studies have validated serum ATX levels as being among the best three biomarkers for the diagnosis of liver cirrhosis as evaluated against definitive physical examination and diagnostic imaging (160). A mechanism for this increased serum ATX was proposed by Ikeda and Yatomi (79). They demonstrate that in normal liver, ATX is taken up from the hepatic sinusoid, a unique vasculature, for degradation in liver sinusoidal endothelial cells. However, in fibrosis, hepatic stellate cells are activated and produce abundant extracellular matrices, blocking endothelial fenestrae and impairing ATX intake. Therefore, the reduced clearance of ATX from the circulation may contribute to the increase in serum ATX in patients with liver fibrosis (79).

Cholestatic pruritus is the sensation of itch due to liver diseases. Interestingly, only ATX activity, but not histamine, tryptase, substance P, serum bile salts or μ-opioid activity in serum correlated with itch intensity of patients with cholestatic itch (161). Pruritus can be induced in a dose-dependent manner in mice by intradermal injections of LPA through transient increases in Ca^{2+} concentrations in neuronal cells (161). This can be reversed by administration of the $LPA_{1/3}$ antagonist Ki16425 (162).

Besides liver disorders, increased ATX expression has been found in biopsies from patients with Crohn's disease and ulcerative colitis (163). ATX

mRNA levels are increased by at least five-fold in inflammation progression from redness to ulceration. ATX expression in both the vascular endothelium and lymphocyte infiltration were increased with successive treatments of dextran sodium sulphate (DSS) in mice, a common colitis model. When treated with the non-specific ATX inhibitor bithionol, these mice had significantly abrogated colitis activity and decreased numbers of infiltrating lymphocytes (163). Bithionol treatment attenuated the thickening of the intestinal wall and shortening of the colon relative to vehicle-treated mice, signs of both deceased inflammation and tissue remodeling (163). This work illustrated that ATX inhibition could be a novel treatment option for inflammatory bowel diseases (163).

1.6 The role of the ATX-LPA-LPP axis in cancer

Ultimately, pathological ATX/LPA signaling is more complicated than simply upregulated ATX production, and this has been best studied in cancer. LPA signaling can be roughly divided into three distinct domains: ATX activity, LPA receptors, and extracellular LPA degradation by the ecto-activity of lipid phosphate phosphatases (LPPs) (10, 46, 164). ATX protein is increased leading to higher LPA levels in the tumors of many cancers. Cancer cells also have increased expression of LPA receptors on their cell surface compared to normal and benign cells, and downregulated expression of LPPs (10, 164). Thus, a triad of increased LPA production by ATX, increased response to

LPA by increased LPA receptor expression and decreased LPP activity to degrade LPA on the cell surface creates the perfect storm for cancer cell proliferation, migration, metastasis and therapy resistance (10, 46, 164, 165). It is not known if other ATX-mediated inflammatory diseases follow the cancer model by increasing LPA receptor expression and decreasing LPP activity, in addition to increasing ATX production. However, the importance of studying LPA signaling in terms of the whole-picture of the ATX-LPA-LPP axis is becoming better appreciated (166, 167).

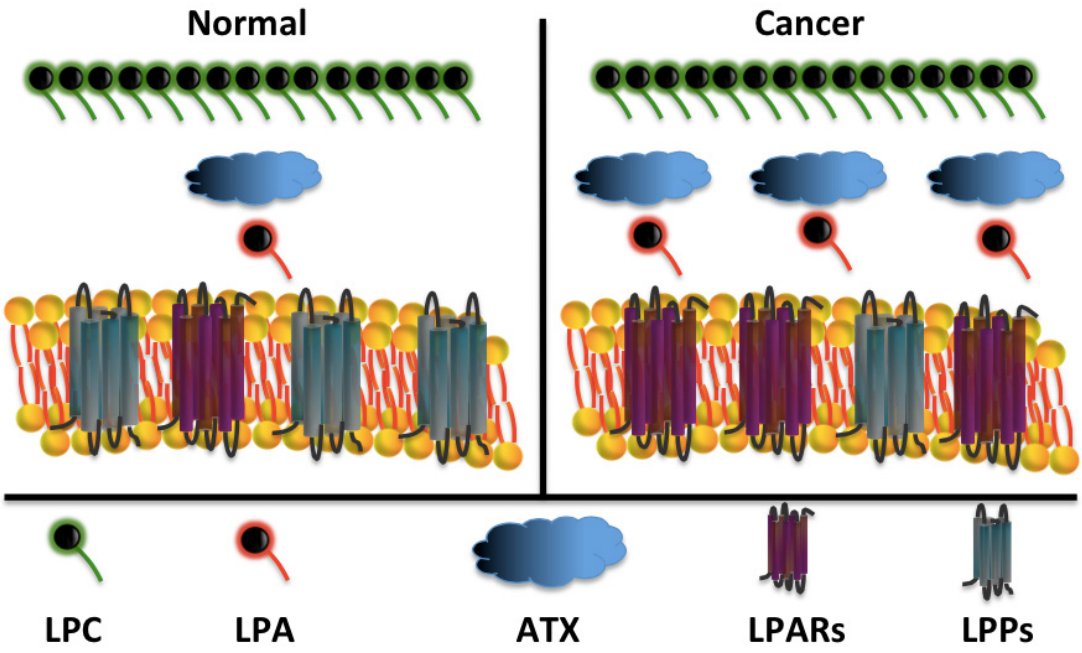

Figure 1.8. Overview of the ATX-LPA-LPP axis in cancer. Compared to normal tissues, in many cancers, ATX is overexpressed. Increased ATX leads to increased LPA production for signaling through LPA receptors, which are also overexpressed in many cancers. Simultaneously, LPPs, which can degrade LPA, are downregulated. The overall effect is increased LPA signaling, which drives the cancer phenotype.

1.6.1 Overview of ATX in tumor biology

The initial relation of ATX/LPA signaling with melanoma cells resulted in much of the early research into ATX being concentrated in the cancer field (91, 168-176). LPA increases vascular endothelial growth factor (VEGF) production, which stimulates angiogenesis (177), a process necessary for tumor progression. LPA decreases the expression of the tumor suppressor p53 (178), thus increasing cancer cell survival and division. LPA levels as high as 10 μM have been found in ascites fluid of advanced ovarian cancer patients (3). Mice that overexpress ATX in mammary epithelium develop spontaneous metastatic mammary tumors (179). Further, ATX is among the top 40 most up-regulated genes in metastatic cancers (180). ATX/LPA signaling is positively correlated with the invasive and metastatic potential of several cancers including melanoma, breast cancer, ovarian cancer, thyroid cancer, renal cell cancer, lung cancer, neuroblastoma, hepatocellular carcinoma and glioblastoma multiforme (165, 181).

However, the tumor is a heterogeneous environment composed of many different cell types including fibroblasts, endothelial cells and leukocytes in addition to cancer cells. There are also a host of soluble molecules in the tumor and this heterogeneity adds another layer of complexity to ATX/LPA signaling. Popnikolov *et al.* showed that ATX and LPA_3 immunohistochemical staining correlate positively with cancer aggressiveness (182). This work is particular novel because the authors showed that ATX staining is

predominantly stromal, whereas cancer epithelial cells stain heaviest for LPA_3 (182). More recent work has shown that metastasis of breast cancer cells to bone depends on the interaction of platelet-derived ATX with cancer-cell integrin $\alpha_V\beta_3$ (183). Hence, in tumors like neuroblastoma and melanoma, the cancer cells may be abundant producers of ATX whereas in other cancers like breast, the cancer cells may instead rely on ATX produced from other tissues like adjacent adipose tissue or in platelets for metastatic cells. An overview of the wide distribution of ATX mRNA levels in cancer cells is shown in Figure 1.9.

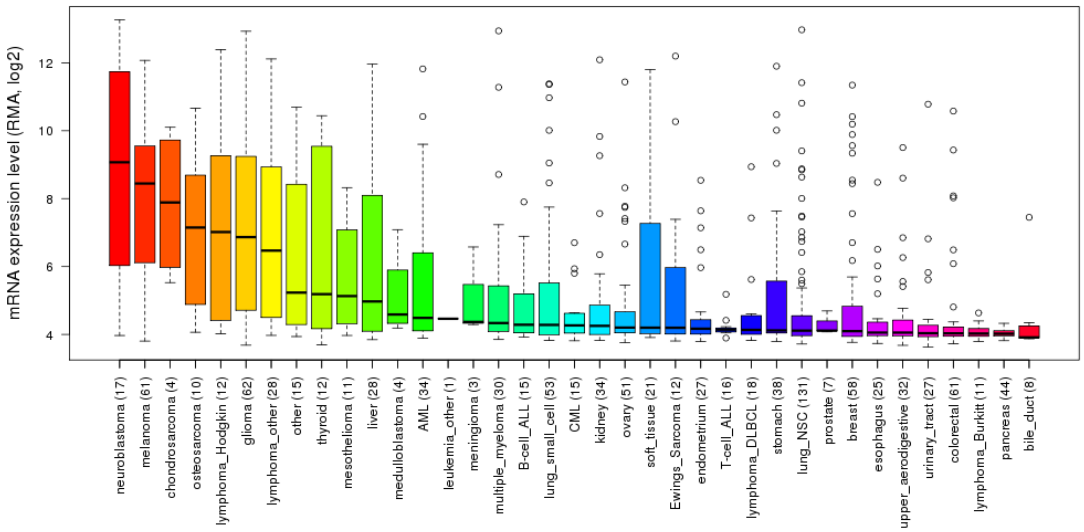

Figure 1.9. ATX mRNA levels in different cancer cell lines as retrieved from the Cancer Cell Line Encyclopedia (184) from the Broad Institute, ID # 5168. At the time of writing, the Cancer Cell Line Encyclopedia contains gene expression data for 1046 cancer cell lines. The number of cell lines per cancer type assayed is indicated in the x-axis. RMA, robust multi-array average (y-axis); AML, acute myeloid leukemia; ALL, acute lymphoblastic leukemia; CML, chronic myeloid leukemia; DLBCL, diffuse large B-cell lymphoma; NSC, non-small cell.

Despite all of the literature on the mechanisms of LPA-mediated signaling in cancer (91, 168-176), the regulation of ATX expression is poorly understood, although some progress has been made. Galectin-3, a β-galactoside binding protein known to increase the invasive potential of cancer cells, increases ATX expression at the transcriptional level by modulating the expression of the transcription factor Nuclear Factor of Activated T-cell 1 (NFAT1) (185). Silencing galectin-3 suppresses NFAT1 protein expression, which in turn reduces ATX expression. Re-expression of ATX in galectin-3-silenced cells rescues angiogenesis, tumor growth and metastasis *in vivo* (185). Similar work has been done in mantle cell lymphoma, where knock-down of the transcription factor SOX11 suppresses ATX production (186). In breast cancer specimens, there is a positive correlation between nuclear tyrosine-phosphorylated signal transducer and activator of transcription factor 3 (pStat3) and ATX. In primary cultures of breast cancer specimens from patients, inhibition of pStat3 or reduced Stat3 expression deceases both ATX levels and cell migration (187).

1.6.2 Overexpression of LPA receptors in cancer

Overall, LPA signaling through at least six known G-protein-coupled receptors (LPA_{1-6}) stimulates cell survival and migration through the relative activations of phosphatidylinositol 3-kinase (PI3K), $ERK_{1/2}$, mTOR, Ca^{2+}-transients, Rac, Rho and Ras, and these receptors are often overexpressed

in cancer cells (165) (Figure 1.3). Like for ATX, mice that overexpress LPA_1, LPA_2 or LPA_3 in mammary epithelium develop spontaneous metastatic mammary tumors (179). LPA_1 and/or LPA_2 receptors are overexpressed in many cancers, particularly gastric, ovarian, breast, colorectal and thyroid cancers compared to healthy tissues (188-193). In melanoma, LPA_3 is the dominant receptor subtype, and LPA_3 overexpression in rat hepatoma cells enhances tumor growth and cell migration (10, 194). Little cancer research has focused on LPA_{4-6}, however one study showed an increase in the unmethylated state of LPA_5-encoding DNA in lung and hepatic cancer cell lines compared to normal tissues (195). KO mice for LPA_1 and LPA_5 have fewer lung metastatic nodules compared to wild-type mice following tail vein injection of cancer cells (196). This finding suggests that LPA signaling in the host tissue is important for establishing a permissible microenvironment for metastatic cancer cells to form new tumors.

1.6.3 LPPs in cancer

The LPPs and their role in cancer biology is an emerging field of study. Significantly, LPP1 expression is decreased in many different cancers including ovarian, renal, leukemia, colorectal, melanoma, and lung cancers compared to normal tissues (197). Increasing LPP1 expression in ovarian cancer cells increases LPA hydrolysis, and in turn deceases cell proliferation and colony-forming activity, and increases apoptosis (198). Virtually identical

results in ovarian cancer cell lines have been obtained through overexpression of LPP3 (199). However, there is one report that LPP3 overexpression actually increases tumor growth in glioblastoma models by increasing β-catenin stability and cyclin D1 synthesis, and LPP3 was found to be highly expressed in human glioblastoma primary tumors (200). In our laboratory, we have shown that overexpression of LPP1 in breast and thyroid cancer cell lines decreases tumor growth and metastasis by up to 80% compared with the expression of catalytically inactive LPP1 in both syngeneic and xenograft mouse models (197). We also demonstrated that these effects cannot be explained by the increased ecto-activity, which degrades exogenous LPA or S1P. Instead, this effect is mediated downstream of receptor activation since LPP1 overexpression also decreased the stimulation of Ca^{2+}-transients by the non-dephosphorylatable $LPA_{1/2}$ receptor agonist wls-31 (197). LPP1 expression also decreased Ca^{2+}-transients that resulted from activation by a protease-activated receptor-1 peptide, which acts independently of LPA signaling. At present, we do not know what substrate LPP1 acts on intracellularly to modify cell signaling and slow tumor progression.

Thus far, the relationship between LPP2 expression and cancer is unclear. Work also in our laboratory showed that overexpression of LPP2 in fibroblasts causes premature entry into S-phase of the cell cycle, whereas knockdown of LPP2 delays entry by 1.5 h (201). Similar effects could not be

reproduced with either overexpression or knockdown of LPP1/3, suggesting that LPP2 might have a unique role among the LPPs in cell cycle regulation (201). Genomic screens have shown LPP2 (*PPAP2C*) to be upregulated in transformed human adult mesenchymal stem cells, and in the same study knockdown of LPP2 impaired anchorage-dependent of cancers cells and mesenchymal stem cells but not differentiated fibroblasts (202). Their work replicated our S-phase cell cycle findings, and further showed LPP2 to be negatively regulated by p53, a major tumor suppressor (202). We are currently studying whether knockdown of LPP2, or increasing the ratio of LPP1/3 to LPP2, might slow cancer growth rates and tumor progression in mouse models.

1.6.4 ATX/LPA and inflammation in cancer

As stated above, insights into ATX/LPA signaling learned from cancer studies have been applied to other disease models where inflammation is a common factor (4, 9, 79, 146, 203-209). The ATX/LPA signaling pathway is involved in chronic inflammatory conditions, and for some patients, inflammation could underlie the development and progression of their cancers. This is best understood in colon cancer models where chronic inflammation of colonic mucosa leads to dysplasia and eventual cancer (163, 210, 211) (Figure 1.7). Chronic inflammation is associated with both initiation and progression of many neoplastic conditions (212), and ATX may be a

player in the process. Hepatocellular carcinoma is particularly interesting because it often develops in patients with chronic disease as a complication of liver cirrhosis (213). This is especially true for hepatitis C, which accounts for 25% of all hepatocellular carcinoma cases and is the most significant risk factor for hepatocellular carcinoma (214). Microarray analysis of liver samples from hepatitis C and hepatocellular carcinoma patients showed an increase in ATX mRNA levels compared to normal patients (215). This work was followed with ATX immunohistochemical analysis of hepatocellular carcinoma biopsies derived from different etiologies. ATX staining was heaviest in patients with histories of either hepatitis C, hepatitis B or nonalcoholic steatohepatitis (NASH) compared to hepatocellular carcinoma patients with otherwise normal livers and without identified risk factors (216). ATX staining was most positively correlated to both the degree of liver inflammation and cirrhosis regardless of etiology (216). *In vitro*, ATX expression was elevated in poorly-differentiated hepatocellular carcinoma lines Hep3B and Huh7 compared to the well-differentiated HepG2 hepatocellular carcinoma cell line, normal embryonic CL-48 liver cells and primary hepatocyte cultures (216). ATX expression could be further increased in Hep3B and Huh7 cell lines upon treatment with TNF-α through a nuclear factor-kappa B (NF-κB)-dependent mechanism, but not for HepG2 or CL-48 cell lines (216). Further discussion on inflammation as an enabling hallmark of cancer will be presented in Section 5.6.

1.6.5 ATX/LPA and cancer therapy resistance

ATX/LPA signaling in cancer is also well known to promote chemotherapy and radiotherapy resistance (10). Our laboratory discovered that LPA produces resistance to the cytotoxic effects of paclitaxel, a first line treatment for breast cancer (18, 217). This was confirmed (218) and extended to carboplatin resistance (219). ATX and LPA also protect against radiation-induced cell death (10, 220). Specifically, LPA signaling through LPA_2 leads to binding of Siva-1 to the C-terminus of LPA_2 (221). Siva-1 is an immediate early response gene product regulated by p53, and its presence in the cytoplasm promotes apoptosis by binding to and depleting the anti-apoptotic protein Bcl-X_L (10). However, LPA_2 binding of Siva-1 leads to polyubiquitination and degradation of Silva-1, which blocks apoptosis in response to chemotherapy and radiotherapy-induced cell damage (221, 222). Furthermore, others have recently shown that endothelial-derived ATX activity in renal cell carcinoma promotes renal tumorgenesis and acquired resistance to sunitinib through an IL-8-mediated mechanism (223). ATX/LPA signaling is a physiological response to promote wound-healing following injury. Significantly, cytotoxic cancer therapy and ionizing radiation essentially produce an injury to the tumor and adjacent tissues. In the process of self-repair, affected tissues use ATX/LPA signaling to increase the expression of survival pathways, which reduces the subsequent effectiveness of the therapy. Hence, inhibiting ATX production of LPA should block this vicious

cycle of injury and tissue repair and therefore have great utility in abrogating cancer therapy resistance (10, 164, 165, 224-229).

1.7 Targeting ATX/LPA signaling *in vivo*

ATX/LPA signaling can in principle be targeted at multiple levels: by antibody therapy against LPA, antagonizing LPA receptor signaling, blocking LPA production through potent ATX activity inhibition, and attenuating LPA signaling by increasing LPP1 or LPP3 activities. To date little is known how to pharmacologically increase LPP production. One early study showed gonadotropin-releasing hormone increased LPP activity in ovarian cancer cells expressing the gonadotropin-releasing hormone receptor (230). There has been much more success in inhibiting ATX activity or blocking LPA receptor activation, and this work is summarized in this section.

1.7.1 LPA antibodies

Antibody-mediated therapy is advantageous over traditional therapeutics in that it is extremely selective in its targeting and is very stable once delivered intravenously (231). Normal immunological processes clear antibodies once they bind to their targets. For LPA as a target, all published work thus far comes from Lpath Inc. in San Diego. Their first work determined the X-ray crystal structure of LPA bound to the humanized monoclonal anti-LPA antibody LT3015 (232). They found that both heavy and light chain

loops of the antibody create eight hydrogen bonds with the glycerophosphate headgroup of LPA (232). Further, the antibody had no binding affinity to S1P, LPC, PA or PC (232). Blocking LPA signaling with another monoclonal antibody called B3 improved spinal cord injury outcomes in both zebrafish and mouse models (233). When treated with B3, there was reduced glial inflammation and neuronal cell death, leading to increased neuronal survival upstream of the injury and consequently some improvement in function (233). B3 was later renamed Lpathomab™, and in a followup study, treatment with Lpathomab™ reduced both expression of IL-6 and lesion volume, and improved functional outcomes is a mouse model of traumatic brain injury (234). The authors also quantified increases in LPA in the cerebrospinal fluid of both human patients and mice with traumatic brain injuries relative to controls. This led the authors to conclude that anti-LPA antibody therapy could have neuroprotective effects following injury (234).

1.7.2 LPA receptor antagonists

Thus far, there are dozens of known LPA receptor antagonists, but few are effective *in vivo* (106). Virtually all research into LPA receptor antagonist therapy come from studies of fibrotic models (106, 235, 236). LPA accelerates lung fibrosis by differentiating mesenchymal stem cells into myofibroblasts through LPA_1 signaling in idiopathic pulmonary fibrosis (IPF). This is a disease of interstitial infiltrates in lung bases, progressive shortness

of breath and worsening pulmonary function (237, 238) (discussed also in Section 1.5.1). This process is slowed in bleomycin-induced IPF mouse models with the LPA_1 antagonist AM966 (139). To date, there are at least three LPA_1 antagonists in phase I/II clinical trials for IPF (235).

Scleroderma is also a fibrotic disease characterized by hardening of the skin and is a chronic system systemic autoimmune disease (239). Significantly, C20:4-LPA levels are two-fold higher in the serum of scleroderma patients compared to healthy controls (240). Studies with LPA_1 KO mice shown protection against scleroderma (241), and phase II clinical trials of the $LPA_{1/3}$ inhibitor SAR100842 are underway for systemic sclerosis (235).

Most efforts from the pharmaceutical industry have been on the development of LPA_1-selective, LPA_2-selective, and $LPA_{1/3}$ dual antagonists, since LPA_1 and LPA_3-mediated signaling is extremely overlapping (106) (Figure 1.3). However, to address the issue of signaling redundancy among the LPA receptors, there is a debate as to whether a more effective approach would be to develop pan-LPA receptor antagonists (106). Ultimately, drug design approaches need to balance efficacy with safety, and a hypothetical pan-antagonist is more likely to have cross-reactivity with other unintended G-protein-coupled receptors than an antagonist designed specifically to interact with one or two receptors. Such antagonists would likely have to be delivered directly to the organ of treatment to limit otherwise increased systemic side

effects compared to simpler oral, subcutaneous and/or intravenous administration options (106). Instead, a safer approach may be to use an ATX inhibitor to prevent production of LPA altogether. So far, there are no published studies using ATX inhibitors in models of fibrosis (242).

1.7.3 Inhibiting ATX production of LPA

As an extracellular enzyme, ATX is a very attractive drug target. Considerable attention has been given towards designing potent inhibitors of ATX (225, 243, 244). Discussed below are only those inhibitors that have been used primarily *in vivo*, beginning with a summary of ATX targeting strategies through indirect means, the development of both lipid- and non-lipid competitive ATX inhibitors and ending with the current methods being employed to develop more effective ATX inhibitors.

1.7.3.1 Indirect approaches to targeting ATX

Among the first inhibitors of ATX activity was L-histidine, reported to have an ATX binding affinity (K_i) of about 1 mM *in vitro*, with 10 mM concentrations required to block ATX-stimulated migration in melanoma cells by 90% (245). L-histidine inhibits ATX activity in a non-competitive manner in part by chelating divalent (Ca^{2+}, Co^{2+} and Zn^{2+}) cations required for optimum catalytic rates, since L-histidine inhibition can be overcome by addition of Zn^{2+}

to culture media (245). Later work showed L-histidine administered intraperitoneally to rats limits thioacetamide-induced liver fibrosis (246).

Few studies have focused on inhibiting ATX production at the level of transcription. One such study showed that cholera toxin inhibits human hepatocellular carcinoma cell proliferation *in vitro* by suppressing ATX production through a TNF-α-dependent mechanism (247). Cholera toxin treatment increases the expression of the anti-inflammatory cytokines IL-4 and IL-10, which were previously known to suppress ATX mRNA levels (248). Another study showed that oral administration of prednisolone, the bioactive form of the anti-inflammatory corticosteroid prednisone, significantly decreased serum ATX levels in a dose-dependent manner in patients being treated for autoimmune skin diseases (249). In these patients, it is unclear if ATX suppression contributed to symptom relief since tapering of the prednisolone dosage led to a rebound in serum ATX levels independently of disease severity. However, the authors proposed that serum ATX levels could be used as a marker of compliance and/or efficacy of steroid therapy (249). Finally, rifampicin, an inhibitor of DNA-dependent RNA polymerase, lowers transcription of ATX mRNA in the treatment of cholestatic pruritus. In these patients, removal of rifampicin treatment led to both reoccurrence of pruritus and a return of ATX levels to pretreatment levels (250). However, all of these treatment options that decrease ATX protein expression appear to be effective only in specific diseases. Instead, most ATX-targeting therapies are

designed to inhibit ATX activity and LPA production so as to have utility in multiple conditions.

1.7.3.2 Lipid-mimetics as ATX inhibitors

To be effective as a therapy, drugs needs to have good bioavailability, potency and have a sufficient safety profile. For ATX, finding an inhibitor that meets these criteria began around 2006, when the very first synthetic competitive ATX inhibitors were reported. These were analogs of cyclic phosphatidate (cPA) with a K_i of approximately 100 nM (Figure 1.10). These compounds significantly inhibited melanoma cell metastasis in tail vein-injection mouse models (251) and inhibited C-fiber stimulation caused by chronic inflammation in rat neuropathic pain models (252). However, cPA analogs are also weak agonists of LPA receptors, which limit their utility (225).

The next group of lipid-mimetic ATX inhibitors developed in 2009 were α-bromophosphonates (BrP-LPA). The *anti*-BrP-LPA isomer had IC_{50} of 22 nM in plasma, which was more potent than for *syn*-BrP-LPA (253) (Figure 1.10). BrP-LPA is also a pan-antagonist of $LPA_{1\text{-}3,}$ and has been used to decrease MDA-MB-231 breast tumor growth in orthotopic xenograft models (253) and A549 lung cancer metastasis in nude mice (254). BrP-LPA treatment of heterotopic murine glioma models using GL-261 cells had radiosensitizing effects on tumor vasculature and delayed tumor growth by 7

days compared to mice treated with irradiation alone (255). This study was one of the first to demonstrate that ATX inhibitors have potential as an adjuvant therapy for cancer. A later report using a collagen-induced arthritis mouse model showed that BrP-LPA attenuated disease symptoms by diminishing synovial LPA signaling. Histopathological analysis of joints of the mice indicated marked decreases in both inflammation and synovial hyperplasia (256).

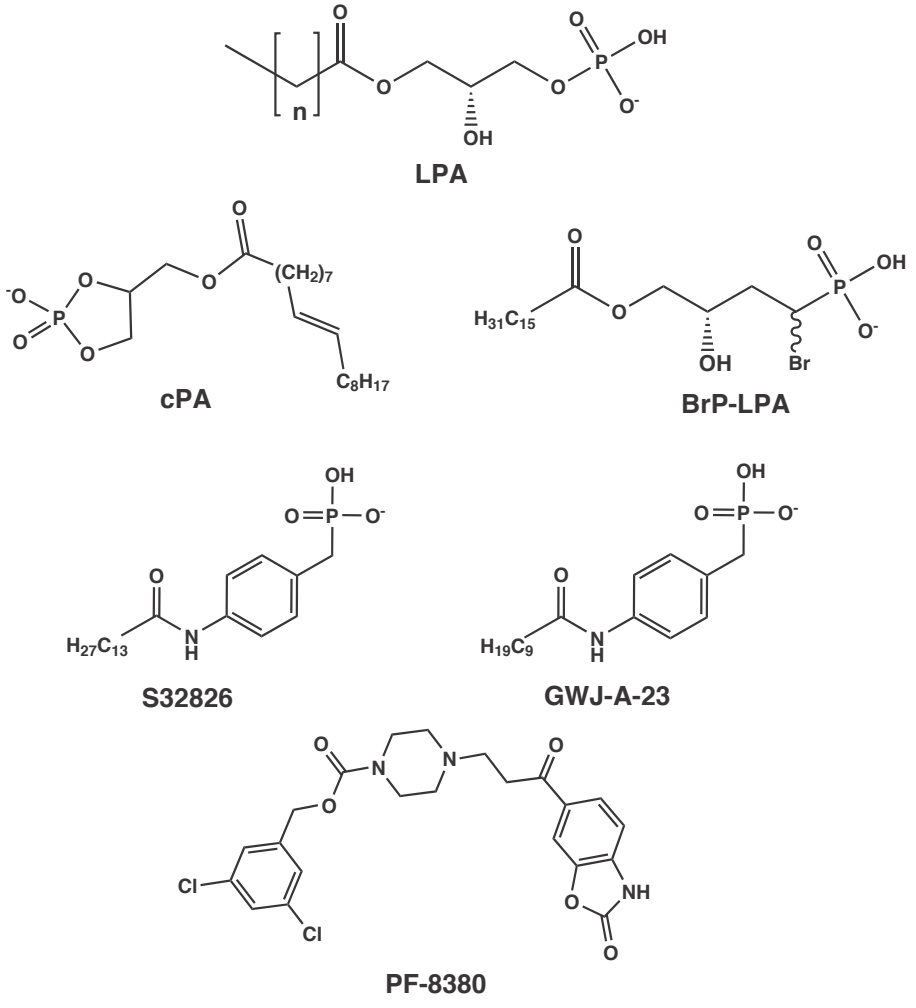

Figure 1.10. Structures of major ATX inhibitors used experimentally *in vivo* compared to the structure of LPA.

Nevertheless, lipid-analog ATX inhibitors tend to have poor bioavailability largely because of the hydrophobic acyl tail (244). The inhibitor S32826, a benzyl phosphonic acid derivative, best demonstrates this effect (Figure 1.10). Despite having a very low nM IC_{50} *in vitro*, the presence of a long chain means the drug has a very high lipophilicity and cannot suppress circulating ATX activity for more than a few minutes (7). Analogs of S32826 have been developed such as GWJ-A-23 by shortening the lipophilic chain and adding α-halo- or α-hydroxy-substituents to increase solubility (Figure 1.10). However, most of these compounds are less potent as ATX inhibitors compared to S32826 (257). Hence, efforts have shifted over the last couple of years to finding and developing ATX inhibitors that are more soluble and non-lipid based.

1.7.3.3 Small non-lipid molecules as ATX inhibitors

There are numerous small non-lipid molecules that have been discovered and modified to inhibit ATX activity through screening large libraries of compounds (243, 244). Unlike lipid analogs, these inhibitors tend to have better oral bioavailability due to their decreased hydrophobicity and they are unlikely to be degraded rapidly by endogenous hydrolytic pathways (258). PF-8380, a piperazinylbenzoxazolone derivative, was developed by Pfizer from screening a compound library followed by optimization (Figure 1.10). It has an IC_{50} of 2.8 nM against recombinant human ATX and 101 nM

for human whole blood. It was the first reported ATX inhibitor to reduce plasma LPA levels *in vivo* for an extended period (8). In rat air-pouch models, 30 mg/kg PF-8380 inhibited inflammatory hyperalgesia with the same efficacy as 30 mg/kg naproxen, a routinely used nonsteroidal anti-inflammatory drug (NSAID) (8). At this concentration, PF-8380 maximally reduced LPA levels in both plasma and at the site of inflammation. Like BrP-LPA, PF-8380 had radio-sensitizing effects in glioblastoma multiforme heterotopic mouse models, delaying tumor growth by at least 20 days (255, 259). In this study, inhibition of ATX by PF-8380 abrogated radiation-induced activation of Akt and subsequently decreased tumor vascularity and tumor growth (259). Another potent ATX inhibitor, ONO-8430506 (Patent WO20120052227), currently in development by Ono Pharmaceuticals Ltd. (Osaka, Japan), is a tetrahydrocarboline derivative with an IC_{50} of 5 nM for plasma ATX activity (260). Dosing rats orally with 30 mg/kg of this compound potently suppressed ATX plasma activity and LPA concentrations for 24 h and decreased intraurethral pressure in benign prostatic hyperplasia models (260). We have extended these inhibition studies to breast and thyroid cancer mouse models (Chapters 4 and 5).

1.7.3.4 Strategies for ATX inhibitor design

To date the most common technique for ATX inhibitor discovery and design is to screen huge libraries of compounds by using ATX substrates

such as Fluorescent Substrate-3 (FS-3), and then modify hits to further increase potency. FS-3 is a fluorgenic substrate that is a doubly-labeled analog of LPC. The fluorophore is quenched through intramolecular energy transfer, and hydrolysis of the substrate by ATX produces an increase in fluorescence (261). The first studies employing this technique in the search for non-lipid ATX inhibitors appeared in 2008 and identified several inhibitors with an IC_{50} in the μM range (262, 263). Later work using compounds from these studies developed nine pharmacophores for ATX inhibition and the results of these analyses were used to screen the National Cancer Institute's (NCI) open chemical repository database to prioritize screening efforts (258). This led to the identification of several novel compounds with an IC_{50} in the low to high μM range (258, 264).

Since these initial reports, the crystal structure of ATX has been solved enabling for structure-activity relationship studies and more rational-design approaches towards optimizing inhibitors. The interpretation of this structural data and its application to inhibitor design has been previously reviewed (61, 64, 244, 265, 266), but briefly the most significant finding has been that ATX has a hydrophobic tunnel formed from the interactions between its SMB1 and the central PDE domains. This tunnel connects the hydrophobic pocket, which accommodates the tail of a bound lipid substrate, and the catalytic site (Section 1.2.2). It is believed that the tunnel may function as both a binding site for substrates as well as a release site for products, and hence

represents an ideal target for inhibitor design and/or optimization. The first study to use this approach was by Kawaguchi *et al.* to identify a thiazolone derivative, which had an IC_{50} for ATX activity of 180 nM, from a 81,600-compound library (265). The authors were able to design from the crystal structure of ATX complexed with this inhibitor a series of side-chain modifications that led to a derivative compound named 3BoA with an IC_{50} of 13 nM (265). More recent studies by Fells *et al.* have combined large library screening results using the crystal structure of ATX with virtual screening tools to discover additional novel ATX inhibitors (267, 268). This approach has identified a common aromatic sulfonamide structural motif among potent inhibitors that targets the hydrophobic pocket of ATX, which accommodates the hydrocarbon tail of LPC/LPA (267, 268). Similar techniques are expected to lead to the rapid development of ATX inhibitors for subsequent testing and development *in vivo*.

1.8 Thesis objectives

ATX/LPA signaling is increasingly appreciated for its roles in driving many pathological conditions, and in particular cancer progression and therapy resistance (9, 10). From a therapeutic standpoint, targeting this pathway could be achieved on three main levels. One means is to increase the rate of LPA degradation, particularly in cancer by increasing the low expression of LPP1 and LPP3 (46). However, activation of LPP expression is

very poorly understood and this technique as a cancer treatment may ultimately require a gene therapy approach. The second possibility is to antagonize signaling through the LPA receptors (106, 269). The technique though may lead to unintentional agonist stimulation through non-targeted receptors (106). With at least six known LPA receptors, there is incredible redundancy such that one antagonist cannot be expected to target all receptors and not without certain side effects. Further, the inhibitory effects of receptor-specific antagonists could be circumvented through other receptors. The final main approach would be to shut off LPA production at this source, effectively starving the LPA axis of its initiating signal. Fortunately, greater than 95% of all circulating LPA is generated by ATX (8, 50), and the importance of ATX is reflected in that ATX KO mice are not viable (5, 82) (Section 1.3.1). Therefore, pharmacologically inhibiting ATX is an attractive means to both target pathological LPA-mediated signaling as well as to study ATX biology *in vivo*.

Designing inhibitors of ATX catalytic activity has been ongoing for over 10 years (243, 244, 251, 270). Most historical inhibitors are LPA and S1P analogs, inspired in part by early reports showing that LPA and S1P are potent competitive inhibitors of ATX activity in assays using low μM concentrations of fluorescent LPC analogs (261, 271-273). However, most of the inhibitors have little potency *in vivo*, calling into question the validity of these competitive inhibitor assays as physiological concentrations of LPC are

>200 μM (64). Therefore, our first objective was to definitively characterize the effect of LPA and S1P on the catalytic activity of ATX and to determine if this level of feedback inhibition has physiological relevance. In light of our results, we also extended these studies to the transcriptional regulation of ATX. ATX is often studied in pathological conditions, however, understanding the physiological relationship between LPA and ATX is vital to appreciating maladaptive changes in the context of disease.

In recent years, numerous ATX inhibitors have been discovered through compound library screens and the recently solved crystal structure of ATX is now enabling rational drug design (244, 265) (Section 1.7.3.4). We examined and established the potency and bioavailability of one of these novel inhibitors, ONO-8430506, on plasma ATX activity and molecular species of LPA. We next evaluated the effect of ATX inhibition on breast tumor growth in an orthotropic and syngeneic mouse model of breast cancer. Breast cancer is the most common malignancy amoung women and as many as one-third of these patients die from metastases because their cancers become resistant to their therapy regimens (10, 274, 275). Further, LPA signaling is known to promote chemotherapy and radiotherapy treatment resistance (10, 165). We therefore assessed the use of an ATX inhibitor in combination with doxorubicin, a common first-line breast cancer therapy for a synergistic therapeutic response.

ATX research has always been closely tied to cancer biology studies since ATX expression is often elevated in tumors and it promotes metastasis (180). LPA is a potent proliferative and migratory signaling factor (203). Therefore, we examined whether ATX could be used a biomarker to distinguish benign from malignant neoplasms. We studied papillary thyroid cancer, an increasingly common disease that is usually diagnosed by fine needle biopsy (276-278), and compared ATX levels to those in benign follicular adenomas and normal thyroid tissue. Up to 25% of fine needle biopsy results are indeterminate resulting in the need for a diagnostic hemi-thyroidectomy (276, 279, 280). Hence, the validation of biomarkers for malignant pathology could decrease the incidence of these diagnostic dilemmas.

Throughout our investigations, we kept in mind that pathology is usually an aberrant manifestation of a physiological phenomenon. ATX/LPA signaling is a well-recognized mediator of wound healing and tissue remodeling responses, both of which are mediated by acute inflammatory processes (172). Most chronic inflammatory diseases arise from unresolved inflammatory conditions, and cancer is often likened to a wound that does not heal (281, 282). Therefore, in all our studies, we assessed the relationship between ATX/LPA signaling and inflammation as we predicted these two processes to be both re-enforcing and interdependent.

CHAPTER 2

MATERIALS AND METHODS

2.1 Reagents

Common chemicals and reagents were obtained from Sigma-Aldrich (Oakville, ON), Thermo Fisher Scientific (Waltham, MA, USA) or EMD Chemicals (Darmstadt, Germany) and were the highest grade available. Fetal bovine serum (FBS), penicillin/streptomycin and Roswell Park Memorial Institute (RPMI) 1640 medium were from Gibco/Life Technologies (Burlington, ON). Serum was charcoal-stripped to remove lipids (FBSC) by adding activated charcoal washed twice with phosphate-buffed saline to FBS (2 g per 50 mL of FBS) and then rotated overnight at 4°C. The mixture was then centrifuged and the supernatant was filtered twice through 0.22-μm sterile filters. Lipids and lipid standards were purchased from Avanti Polar Lipids (Alabaster, AL, USA). FS-3 fluorogenic ATX substrate (L-2000) was purchased from Echelon (Salt Lake City, UT, USA). Human recombinant ATX, Ki16425 and SEW2871 were from Cayman Chemical (Ann Arbor, MI, USA). LY294002, wortmannin, PD98059 and Gö6983 were purchased from Calbiochem/EMD Millipore (Etobicoke, ON). Wls-31 was a gift from Dr. W. Santos and Mr. N. Patwardhan (Department of Chemistry, Virginia Tech, VA, USA) (283, 284). All protein-based signaling ligands were from PeproTech (Rocky Hill, NJ, USA). ONO-8430506 was obtained from Ono Pharmaceuticals (Osaka, Japan; patient number WO2012005227) (285) under a materials transfer agreement. S32826 was from Institut de Recherches SERVIER (Croissy-sur-Seine, France) (7). All primers were

obtained from Integrated DNA Technologies Inc. (Coralville, IA, USA). Other reagents and their sources are mentioned within the text.

2.2 Tissue culture

2.2.1 Mammalian cell lines

MDA-MB-435S melanoma cells (HTB-129™), Hs578T breast cancer cells (HTB-126™), Hs578Bst breast stromal cells (HTB-125™), SW-579 thyroid cancer cells (HTB-107™) and Balb/c mouse 4T1 breast cancer cells (CRL-2539™) were all purchased from the American Type Culture Collection (ATCC) (Manassas, VA, USA). 8305C (ACC-133™) were from Deutsche Sammlung von Mikroorganismen und Zellkulturen (DSMZ) (Braunschweig, Germany). 4T1-luc2 (286) and 4T1-12B (287) cells, which express firefly luciferase for imaging, were purchased from Caliper Biosciences (Hopkinton, MA, USA) and Dr. Sahagian (Department of Physiology, Tufts University School of Medicine, Boston, MA, USA) (287), respectively. All cells were used at low passage number. Cells were cultured in 10% RPMI 1640 medium with 10% FBS and 1% penicillin/streptomycin at 37°C, 5% CO_2 and 95% humidity. Cell lines were proven to be mycoplasma free using the MycoAlert™ Mycoplasma Detection Kit (Lonza, Allendale, NJ, USA). Cells were routinely treated with a prophylactic dose of Plasmocin™ (2.5 μg/ml) (InvivoGen, San Diego, CA, USA) for one week to prevent mycoplasma infection (288).

2.2.2 Patient thyroid specimens and primary thyroid cell culture

Patients provided written informed consent prior to collection of samples. Tissue collection inclusion criteria include all patients with papillary thyroid cancer that were identified on initial fine needle aspiration cytology and ultimately confirmed histologically on the final pathologic specimens. Patients with other concurrent malignancies, anaplastic or other poorly differentiated follicular carcinomas of the thyroid, and previous radiation exposure were excluded from the study. Two separate pathologists confirmed the diagnosis on core sections for analysis and validated all histologic specimens prepared for the tissue arrays. Specimens prepared for primary culture or tissue banking were placed in culture medium, or Optimal Cutting Temperature (OCT) Compound or flash frozen, respectively, within 10 min of devascularization. At the time of tumor banking a representative frozen section determination was used to ensure that >90% of the cells in the banked specimens represented the thyroid neoplasm, benign or malignant, or histologically normal thyroid tissue.

Primary culture specimens were prepared and purified using the Cancer Cell Isolation Kit (CI0010, Affymetrix, Santa Clara, CA, USA). Briefly, about 100-250 mg of tissue was diced into 1-2 mm^3 pieces and suspended in 10 mL of Tumor Cell Digestion Solution in a T25 flask, and lightly agitated on a shaker at 37°C for 1-2 h. Next, 10 mL of Tumor Cell Suspension Solution was added and mixed by pipetting. The suspension was then passed through

a 100-μm and then a 40-μm strainer into a 50 mL conical tube. The flow through was centrifuged at 1200 rpm for 8 min and the supernatant removed. The pellet was resuspended in 20 mL of Tumor Cell Suspension Solution (Tube A). In another 50 mL tube (Tube B), 20 mL of Tumor Cell Purification Solution was centrifuged at 1200 rpm for 2 min. The contents of Tube A were carefully layered onto Tube B by pipetting the solution slowly down the wall of the conical tube. Tube B was held in a vertical position for 6 min at room temperature, and the bottom 6 mL was then carefully transferred to a fresh tube, centrifuged, and resuspended and plated in culture medium.

Primary cells were cultured in high-glucose (4.5 g/L) DMEM containing 10% FBS, 1% penicillin/streptomycin, and 6-hormone cocktail (10 mU/mL thyroid stimulation hormone (TSH), 10 μg/mL insulin, 5 μg/mL transferrin, 10 nM hydrocortisone, 10 ng/mL somatostatin and 10 ng/mL glycyl-L-histidyl-L-lysine acetate) (289) and incubated at 37°C, 5% CO_2 and 95% humidity. All experiments were performed within 3-5 passages from establishment.

2.2.3 Mammary adipose tissue culture

Sacrificed mice were secured supine and the exterior fur was wiped down with 95% ethanol under a tissue culture hood. All instruments were cleaned in ethanol, and mammary adipose tissue from the inguinal region was diced finely into 1-2 mm^3 pieces using two scalpel blades in opposite directions. Each fat pad produces 20-30 pieces of tissue. Five or six pieces

would be placed into a 24-well plate and incubated in 1 mL of RPMI 1640 phenol-free serum-free medium (290). Adipose tissue pieces were weighed at the end of the experiment, averaging about 20-30 mg per well. Adipose tissue was homogenized (see section 2.4.2) in 200 μL of radioimmunoprecipitation (RIPA) buffer (50 mM Tris base, pH 8, 150 mM NaCl, 0.1% SDS, 0.5% sodium deoxycholate, 1% NP-40, Sigma Protease Cocktail) (291) and protein content was measured using the bicinchoninic acid (BCA) protein assay (Thermo Scientific) to normalize results (292).

2.2.4 Incubation of signaling molecules and inhibitors

For all experiments, cells were seeded in 6-well plates and grown until 80% confluent. Cells were then washed with HEPES-buffered saline (HBS) and pre-treated a minimum of 6-8 h in the experimental medium without the addition of signaling ligands or inhibitors in 10% FBS. Cells were then washed again in HBS prior to the start of the experiment. In some experiments, cells were pre-treated in 10% FBS with 1 μM wortmannin, 10 μM LY294002, 10 μM Gö6983 or 20 μM PD98059 for 6-8 h before the start of the experiment with fresh medium. In experiments with 100 μM LPC, LPC was dried down from a chloroform suspension and suspended in medium additionally supplemented with 1% BSA to ensure sufficient albumin to bind all lysophospholipids 1:1. LPA was diluted into medium (final concentration from 1 to 5 μM) containing serum or minimum 0.1% BSA from a stock of 20 mM in water, and S1P from

a stock of 10 mM in ethanol. Protein chemokine, cytokine and growth factor stocks were prepared at minimum 1000x concentration in water containing 0.1% BSA, and used at final concentrations from 1 to 100 ng/mL in medium containing serum or minimum 0.1% BSA.

2.2.5 Gamma irradiation of cells

Cells prepared in media suitable for ATX activity measurements (Section 2.5) were exposed to increasing dosages of gamma irradiation up to 5 Gray (Gy) at a rate of 1 Gy/min using a ^{60}Co Gammacell Irradiator (Atomic Energy of Canada Limited) (293), and then incubated for 48 h.

2.3 Animal Models

2.3.1 Animal housing and care

Mice were maintained at 21 ± 2°C, 55 ± 5% humidity and a standard 12 h light/dark cycle. Mice were housed at a maximum of 5 per cage, and cages and water bottles were changed weekly. The mice had free access to standard laboratory (4% fat) diet and water. Mice used for luminescence imaging were fed 2014S Telkad Global 14% Rodent Maintenance Diet, Sterilizable (Harlan Laboratories, Mississauga, ON) starting from 10 days prior to experiment to decrease background luminescence. Mice were allowed to acclimatize to their new environment following arrival for at least seven days prior to the start of experiments. During experiments, mice were

weighed and pain and distress were assessed daily according to Table 2.1. Any mouse with a total score of 2 in more than one category was observed closely, and any mouse with a score of 3 or more was immediately euthanized or sacrificed for tissues. All procedures were performed in accordance with the Canadian Council of Animal Care as approved by the University of Alberta Animal Welfare Committee.

Assessment Criteria/Score	Score = 0	Score = 1	Score = 2	Score = 3
Attitude	Investigates whole cage. Same as pre-experimental assessment.	Slow to move around cage, sleeping most of the time.	Stays in corner of cage. Does not explore cage on own without stimuli.	Not responsive physically when stimulated. Lying on side.
Injection Site	No discharge, redness or swelling.	Slight redness and/or swelling. Animal may be licking or starting to chew at site.	Injection site is open, red, and/or swollen. Animal is chewing vigorously.	Injection site is open, very red, swollen and purulent discharge is present.
Appearance	Same as pre-experimental assessment.	Huddled, with mild piloerection.	Dull, huddled and ungroomed.	Huddled, severe piloerection, no movement or moribund.
Body Weight	Same or increased from pre-experimental assessment.	< 0-5% decrease	6-20% decrease	>20% decrease
Elimination	Urination and defecation appears normal.			Bloody diarrhea or no urination or defecation in previous 24 hours.

Table 2.1. Pain and distress assessment chart for mice.

2.3.2 Orthotopic and syngeneic 4T1 breast cancer/Balb/c mouse model

Female Balb/c mice 8-10 weeks old (BALB/cAnNCrl, Stain Code 028) were purchased from Charles River (Kingston, ON). All experiments were started on mice under 14 weeks of age.

2.3.2.1 Preparation and injection of cancer cells

Cells were trypsinized and suspended in phenol red-free serum-free RPMI 1640 medium and washed twice with medium before being suspended at a concentration of 20 times the final number of cells injected into the mouse (for example, for an injection of 20,000 cells per mouse, cells were prepared at a concentration of 400,000 cells/mL). Cancer cells were mixed with an equal volume of Matrigel (BD Biosciences, Mississauga, ON) on ice and 100 µL of this mixture was injected using a 27 or 31-gauge needle into the fourth inguinal mammary fat pad of mice that were anesthetized with 5% isoflurane and maintained at 2% isoflurane. The area around the nipple was wiped with 70% ethanol and the injection was made into the mammary fat pad using the exposed nipple as a landmark (Figure 2.1). When necessary to facilitate identification of the nipple, the hair around the injection site was removed with battery-operated cat grooming clippers. For experimental metastasis studies, 150,000 4T1 cells in 100 µL of phosphate buffered saline (PBS) were injected through the tail vein of conscious mice, which were restrained under a heat lamp to dilate the tail vein (294).

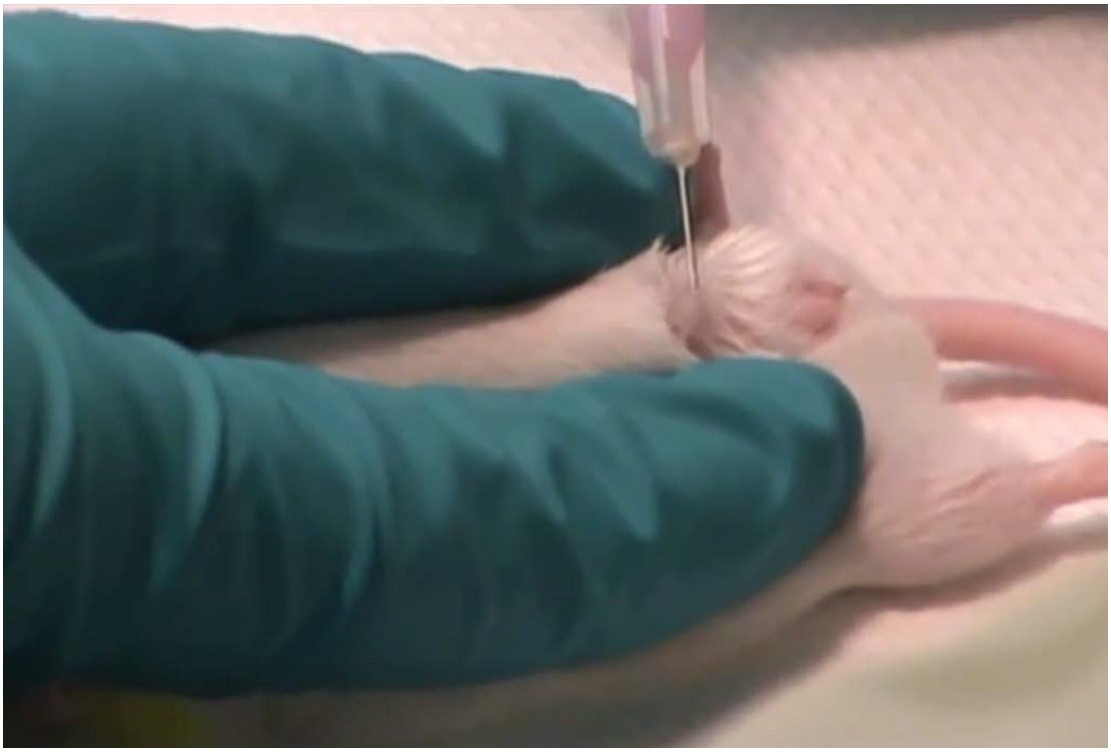

Figure 2.1. Illustration of cancer cell injection in the mammary fat pad. The anesthetized mouse rests supine with its nose inside a nose code. An inguinal mammary nipple is exposed with an ethanol wipe. Cancer cells suspended in Matrigel are injected perpendicular to and just under the nipple, ensuring that the cancer cells are implanted directly into the mammary adipose tissue.

2.3.2.2 4T1 tumor growth rate monitoring

Following palpation of a solid mass in the mammary fat pad, two orthogonal caliper measurements were taken and tumor volume was estimated from width^2 x length/2, where width is the smaller of the two measurements (295). We assessed tumor growth rates for tumors from 2500, 5000, 20,000, and 1,000,000 4T1 cells (Figure 2.2). We found tumors of 20,000 cells had the least variance in size among individual mice, and tumors from 1,000,000 cells grew too quickly to be experimentally useful.

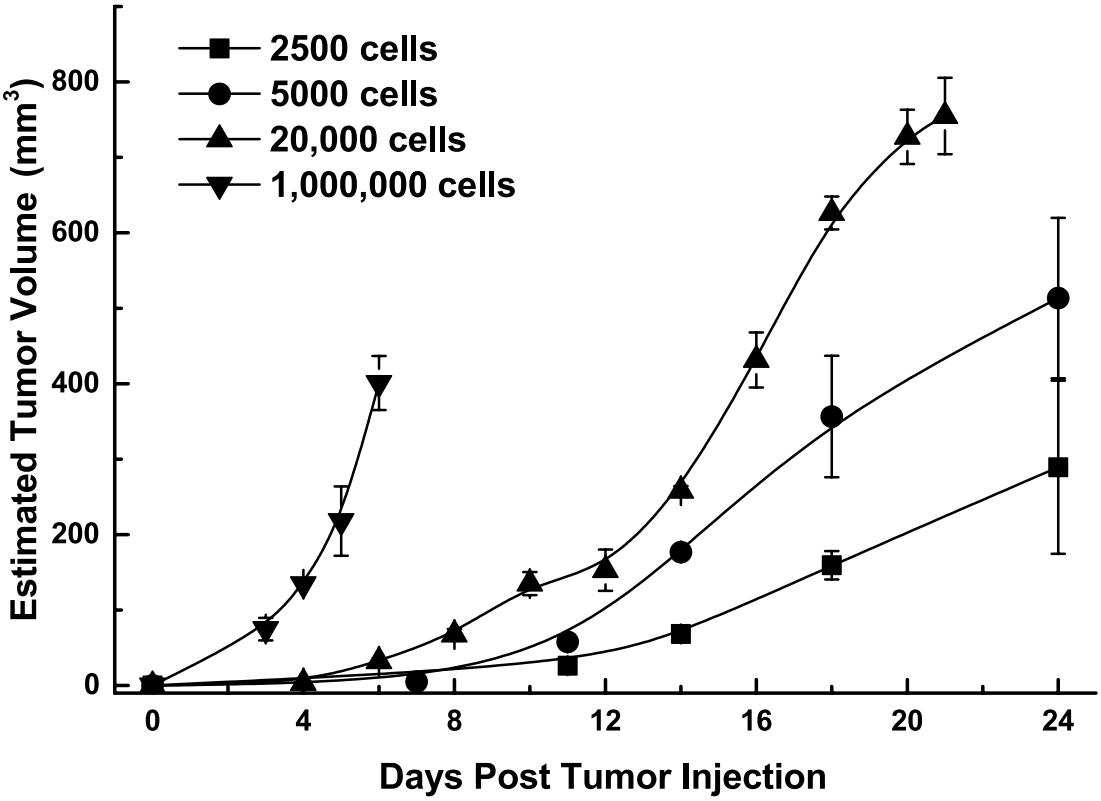

Figure 2.2. 4T1 tumor growth curves for differing numbers of injected cells. Results are means ± SEM for 3-4 mice per group.

2.3.2.3 *In vivo* luciferase imaging

For luminescent imaging, mice were anesthetized with isoflurane and were then injected intraperitoneally in the upper left quadrant with 100 μl of 30 mg/ml D-luciferin (Caliper Biosciences) (final dose of 150 mg/kg). Eye lubricant was dabbed on the eyes of the mice and they were then immediately imaged with a Xenogen IVIS imaging system (PerkinElmer, Waltham, MA, USA) with the following settings: luminescent mode, medium binning and F/Stop of 1 (296). Images were taken every minute until at least three images were collected after luminescent signal intensity peaked (typically 10-15 min).

While being imaged, mice were maintained on 2-3% isoflurane at an oxygen flow rate of 0.5-1 L/min.

2.3.2.4 Effects of luciferase expression on tumor growth and metastasis

In our initial metastatic studies, we used mouse 4T1-12B cells, which express luciferase for luminescence imaging. This allowed us to track the development of metastasis rather than depending on a final assessment once the animal was sacrificed. We injected 20,000 4T1-12B into the orthotopic fat pad and the initial phase of tumor growth with the 4T1-12B cells lasted for about 11 days. The tumors then regressed (Figure 2.3) and there were no detectable metastasis, either visually or by luminescence, at day 21. We then tested parental 4T1 cells and another luciferase expressing clone, 4T1-luc2, for more sustained tumor growth and metastasis. 4T1 tumors grew until about 21 days when the primary tumor rapidly invaded the abdominal wall making it difficult to estimate tumor volume accurately. The experiment was terminated at day 25. Tumors from the 4T1-luc2 cells regressed slightly from day 11 to day 16 and then grew again. However, the tumor size from the injected 4T1 cells was nearly 2.5-times larger than those from 4T1-luc2 cells at day 25. 4T1-12B tumors had completely disappeared by this time (Figure 2.3).

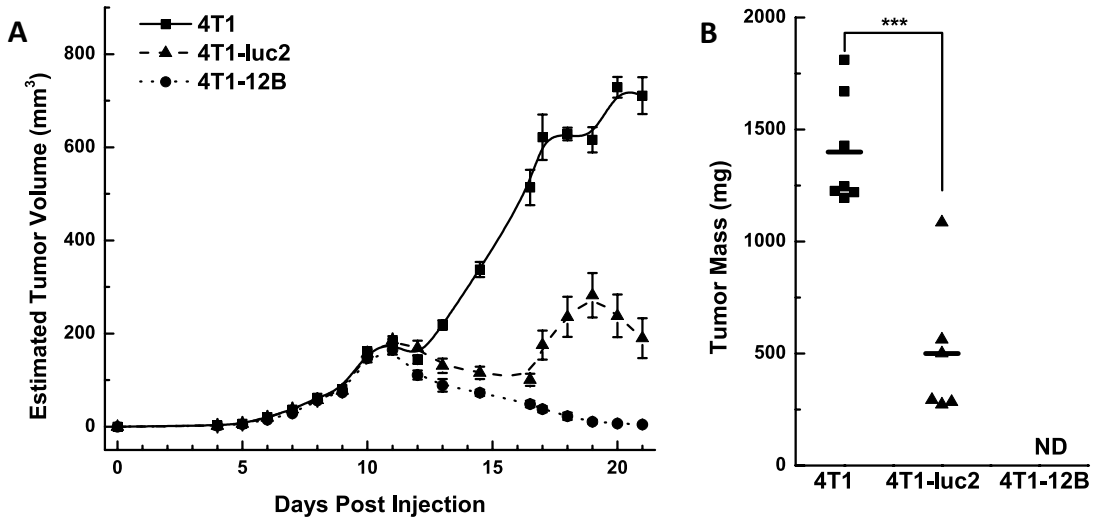

Figure 2.3. Effects of luciferase expression on 4T1 tumor growth. A) Tumor volumes were calculated from caliper measurements using width^2 x length/2. Tumor growth for the first 11 days was identical for all three 4T1 clones. Results are expressed as means ± SEM for 6-7 mice per group. B) Masses of tumors excised on day 25. Means indicated by horizontal bars. ***, indicates a significant difference ($p < 0.0005$). ND = not detectable.

Mice injected with the 4T1 cells had numerous visible metastatic nodules in the lungs unlike the 4T1-luc2 mice, which had only micro-metastases that were detected weakly by D-luciferin scanning (Figure 2.4). Injection of firefly luciferase DNA into mice is known to induce a T-helper-cell type 1 response in Balb/c mice, and CT-26 Balb/c colon cancer tumors regress after 10 days if they are transfected with the firefly luciferase gene compared to tumors of mock-transfected cells (297). Hence, despite firefly luciferase being very useful for luminescence imaging, its utility to follow metastasis in an immuno-competent model is limited. However, as expected this rejection is not seen in immuno-compromised mice (287).

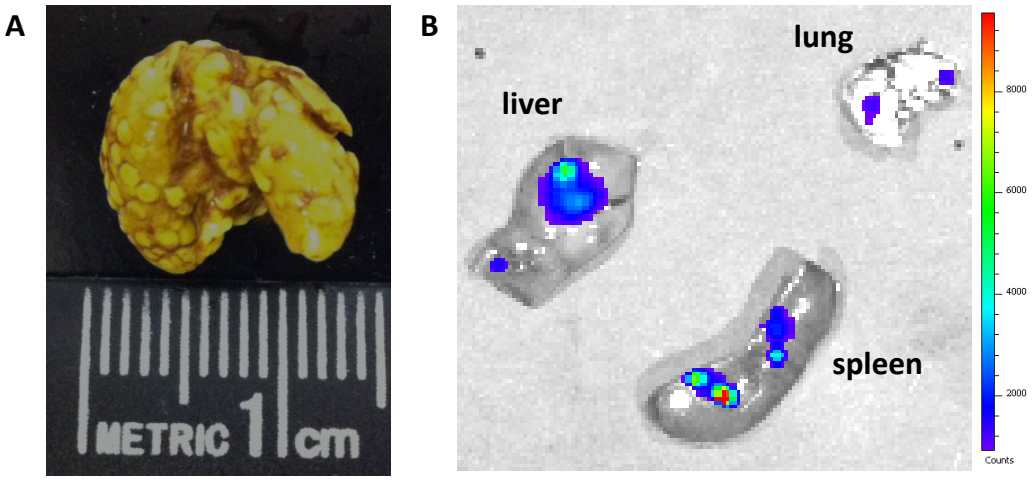

Figure 2.4. Comparison of lung metastasis in mice with 4T1 (A) or 4T1-luc2 tumors (B). A) Lungs from a mouse at 25 days after injection with 20,000 parental 4T1 cells into the mammary fat pad with overt macrometastasis stained with Bouin solution. B) D-Luciferin imaging of micrometastasis in lungs, liver, and spleen of a mouse with a 4T1-luc2 tumor. No macrometastasis was visualized. No micro- or macrometastasis were detected in mice that carried a 4T1-12B tumor (not shown).

2.3.2.5 Collection of plasma, tumors and mammary adipose tissue

Mice were euthanized with 50 µL of Euthanyl (sodium pentobarbital, 240 mg/mL) (Bimeda MTC Animal Health Inc., Cambridge, ON) and blood was collected from the inferior vena cava or cardiac puncture using heparinized syringes with 23-gauge needles immediately following loss of response to foot-pinch stimuli. The needle was then removed from the syringe and the blood was added immediately to tubes that contained 200 pmol of prostaglandin I_2 (Cayman Chemical) in 2 µL of 200 mM Tris base, pH 9, to prevent platelet activation. Blood was then centrifuged at 13,000 rpm for 5 min, plasma collected, aliquoted and frozen immediately at -80°C. To determine the effects of drug treatment on white blood cell (WBC) counts, 10

μL of the packed cell pellet was added to 190 μL of red blood cell (RBC) lysis buffer 400 mM NH_4Cl, 30 mM $NaHCO_3$, 25 μM EDTA pH 7.2). The lysis buffer is a hypotonic solution that lyses RBCs selectively by osmosis and leaves the WBCs intact by taking advantage of the disproportionate solubility of RBCs in NH_4Cl (298). WBCs were counted using a hemocytometer as triplicates. Tumors and samples of mammary adipose tissue were collected and either placed in 10% buffered formalin for paraffin imbedding, flash frozen in liquid nitrogen, or otherwise used immediately in experiments.

2.3.2.6 Micrometastasis and macrometastasis quantification

Quantification of micrometastases in lungs and livers from paraffin-embedded sections (prepared as described in Section 2.8.2) was achieved by staining with hematoxylin and eosin followed by photographing at 5X magnification. The number of metastatic colonies was averaged from at least five random fields of view.

For macrometastasis quantification, lungs were fixed and stained by immersion in standard Bouin solution (saturated picric acid aqueous solution: formalin 37% aqueous solution: glacial acetic acid 75:25:5, by volume) and the numbers of metastatic nodules were counted after at least one day in the solution. The softer tissue of the lung parenchyma absorbs picric acid more readily than harder metastatic nodules, increasing contrast between the two tissue types.

2.3.2.7 Tumor digestion and fluorescence-activated cell sorting (FACS) into different tumor cell populations

4T1 tumors were diced into 1-2 mm^3 pieces and added to a T25 flask in DMEM/F12 medium with 100 U/mL collagenase IV (Worthington, Lakewood, NJ, USA) for 1 h on a shaker at 37°C (299). Normally, 30 mL of medium was used for 500 mg of tumor. The flask was shaken vigorously every 15 min to disperse clumps of tissue. After incubation, the mixture was pipeted several times with a 10-mL serological pipet to complete the release of cells, and an equal volume of DMEM/F12 medium with 10% FBS was then added to neutralize collagenase activity. Cells were passed through a 70-μm strainer into a 50-mL conical tube, and centrifuged. Cells were resuspended in 4 mL of HBSS (Hank's balanced salt solution) with 150 mM NH_4Cl to lyse red blood cells. Cells were then centrifuged again and resuspended in 4 mL HBSS and counted. On average, 7-10 million cells were obtained from 500 mg of tumor. Cells were then centrifuged and resuspended in 100 μL of FACS buffer (PBS Ca^{2+}/Mg^{2+} free, 2 mM EDTA, 25 mM HEPES pH 7.0, 1% heat inactivated (30 min at 65°C) FBS, which was filtered through a 0.2-μm membrane). Two μL of Fc block (TruStain fcX™ (anti-mouse CD16/32, clone 93, 0.5 mg/mL, Biolegend, San Diego, CA, USA) per 1 million cells was added and the mixture incubated on ice for 10 min. The mixture was then aliquoted into FACS tubes as needed and the volume brought up to 100 μL in FACS buffer (one tube for each antibody used), with 5% of the total mixture

set aside as an unstained fraction. The following antibodies (Affymetrix) were then added to each separate aliquot for 30 min at room temperature to isolate individual tumor cell populations:

- Cancer (epithelial) cells – 0.625 μL/test; rat anti-mouse CD326 (EPCAM – epithelial cell adhesion molecule) APC-tagged antibody (catalog # 17-5791, clone G8.8, 0.2 mg/mL) (299)
- Fibroblasts – 12.5 μL/test; rat anti-mouse CD-140a (PDGFa – platelet derived growth factor receptor a) PE-tagged antibody (catalog # 12-1401, clone APA5, 0.2 mg/mL) (300, 301)
- Endothelial cells – 12.5 μL/test; rat anti-mouse CD-31 PE-Cy7-tagged antibody (catalog # 25-0311, clone 390, 0.2 mg/mL) (299)
- Leukocytes – 0.5 μL/test; rat anti-mouse CD-45 FITC-tagged antibody (catalog # 11-0451, clone 30-F11, 0.2 mg/mL) (299)

Next, cells were centrifuged and washed in 1 mL of FACS buffer. Cells were resuspended in FACS buffer at 2 million cells/mL or 500 μL (whichever volume was greater), and passed through a 40-μm strainer cap into a 5 mL 12x75 mm round-bottomed polystyrene tube (BD Biosciences). Cells were sorted into FACS buffer with a BD FACS Canto II sorter (BD Biosciences). Dead cells were identified by positive propidium iodine staining (5 μL of 0.5 μg/μL solution per sort). Sorted cells were then centrifuged and 1 mL Trizol® was added for subsequent mRNA isolation (Section 2.6.1).

2.3.3 Thyroid cancer xenograft models

Female 8-10 week-old Fox Chase-SCID® (severe combined immunodeficiency) beige mice (CB17.Cg-*Prkdc*^{scid}*Lyst*$^{bg-J}$/Crl) were from Charles River. 5x10^5 8305C or 1x10^6 SW-579 cells were prepared as described in Section 2.3.2.1 and injected subcutaneously into the shaved lower flank with a 27-gauge needle. Tumors became palpable 7 days after injection.

2.3.4 Drug preparation and administration

2.3.4.1 ONO-8430506

ONO-8430506 was prepared at 10 mg/mL in 25 mM sodium hydroxide and heated to 60°C for 5 min to dissolve. Mice were gavaged daily (disposable silicon-tip mouse feeding needle, 38 mm long, 0.92 mm external diameter, catalog # 4202, Fuchigami Kikai, Japan) with this solution at 10 µL/gram body weight for a dose of 100 mg/kg. ONO-8430506 at 10 mg/mL was diluted 1/5 or 1/10 with water to prepare solutions for dosing at 20 mg/kg or 10 mg/kg, respectively. Control mice were gavaged with water.

Balb/c mice with 4T1 tumors were gavaged daily starting one day after tumor injection. SCID mice injected with thyroid cancer cells were gavaged daily starting 7 days after cancer cell injection once the tumor became palpable. All solutions were passed through a 0.22-µm filter prior to administration and kept at 4°C.

2.3.4.2 Doxorubicin

Doxorubicin hydrochloride (Cayman Chemical) was prepared freshly prior to each injection in warmed PBS at a concentration of 1.6 mg/mL and filtered through a 0.22-μm filter. Mice received 4 mg/kg (50 μL) doxorubicin by intraperitoneal injection in the upper left quadrant with a 31-gauge needle. Control mice were injected with PBS. Balb/c mice were treated every 3 days starting 3 days after cancer cell injection.

2.4 Choline-release ATX assay

2.4.1 Introduction

In the choline-release assay, LPC, the natural substrate for ATX, is typically used in mM quantities to ensure that ATX is completed saturated during the course of the incubation. At the end of the incubation, the choline that is cleaved from LPC by the lysoPLD activity of ATX is treated with choline oxidase, an enzyme that catalyzes the reaction to completion: choline + O_2 → (glycine)betaine aldehyde + H_2O_2.

The hydrogen peroxide (the limiting reagent) is then detected using horseradish peroxidase, which catalyzes an oxidation reaction to condense TOOS (N-Ethyl-N-(2-hydroxy-3-sulfopropyl)-3-methylaniline, sodium salt, dehydrate) and 4-aminoantipyrine to form a purple-colored product that is quantified using a spectrophotometer (Figure 2.5) (302, 303).

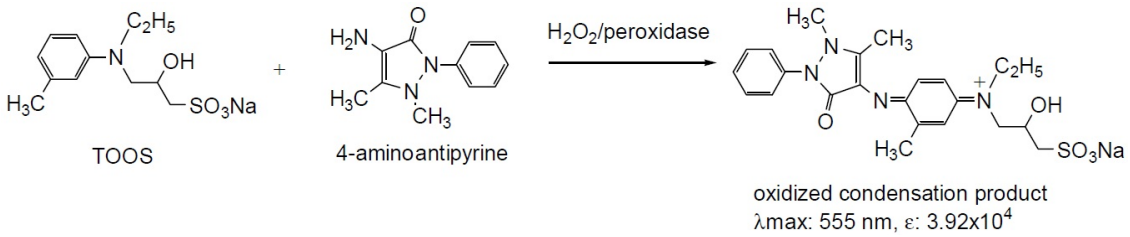

Figure 2.5. Schematic of the oxidized condensation product formed in the final step of the choline-release ATX assay. Image from www.dojindo.com/store/p/284-TOOS.html.

The H_2O_2 produced is directly proportional in a 1:1 ratio to the amount of colored oxidized condensation product produced. This measurement can then be normalized to the amount of sample used and the total incubation time to determine the rate of the reaction.

2.4.2 Sample preparation for the choline-release ATX assay

Tissue samples (20-40 mg) were homogenized in 500 µL of Buffer A (100 mM Tris-HCl pH 9.0, 500 mM NaCl, 5 mM $MgCl_2$, 0.05% (v/v) Triton X-100) using 2 mL safe-lock microcentrifuge tubes with 5-mm stainless steel beads in the Qiagen TissueLyser II system (24-sample plates, 25 Hz, 5 min) (Qiagen, Toronto, ON). Samples were then centrifuged for 5 min at 13,000 rpm and the supranatant (or infranatant in the case of mammary adipose tissue) was collected into a fresh tube. Lysates of cultured cells were scraped directly in Buffer A. Plasma samples were used directly in the assay without any additional preparation.

2.4.3 Measurement of ATX activity by and validation of the choline-release ATX assay

For plasma, 10 µL of plasma was mixed with 10 µL of Buffer A and 5 µL of Buffer A with 10% DMSO or 10% DMSO containing 1 mM ONO-8430506, and pre-incubated at 37°C for 30 min. Samples were then mixed with 25 µL of 6 mM C14:0-LPC in Buffer A and incubated for 6 h at 37°C when 20 µL samples were pipetted in duplicate into a 96-well plate and incubated at 37°C for 20 min with 90 µL/well of Buffer C [9.65 mL Buffer B (100 mM Tris-HCl, pH 8.5, 5 mM $CaCl_2$), 110 µL of 30 mM TOOS (Dojindo Molecular Technologies, Rockville, MD, USA), 110 µL of 50 mM 4-aminoantipyine, 6.6 µL 1000 units/mL horseradish peroxidase, and 110 µL of 300 units/mL choline oxidase]. Choline formation was measured at 550 nm.

For homogenized tissues or cell lysates, protein lysates as prepared in Section 2.4.2, were assayed as for plasma, except the incubation time with LPC was 24 h. These activity measurements were then normalized to protein content by the BCA protein assay (Thermo Scientific) (292).

For experiments on recombinant ATX, 10 µL of ATX protein was incubated with 25 µL of 400 µM C18:1-LPC and 15 µL of C18:1-LPA or S1P or choline assay buffer for a total volume of 50 µL for 4 h at 37°C. Final ATX concentrations of 750, 1000, and 1250 ng/mL were used to demonstrate that the activity results were directly proportional to protein.

To ensure that the measured choline formed during the incubation is from the enzymatic action of ATX, we also treated an aliquot of the sample

with an excess of ONO-8430506 (final concentration of 100 μM, enough to completely block all activity using recombinant ATX) (Figure 2.6A). Choline produced by ATX is then considered to be the difference between the total measured choline after incubation with LPC and the measured choline in the sample when incubated with both LPC and ONO-8430506 (Figure 2.6B). We also verified that for a given incubation time, the amount of choline produced by ATX was directly proportional to the amount of enzymatic activity present. This typically meant using a substrate amount that would consume less than 10% of the total LPC added (Figure 2.6C).

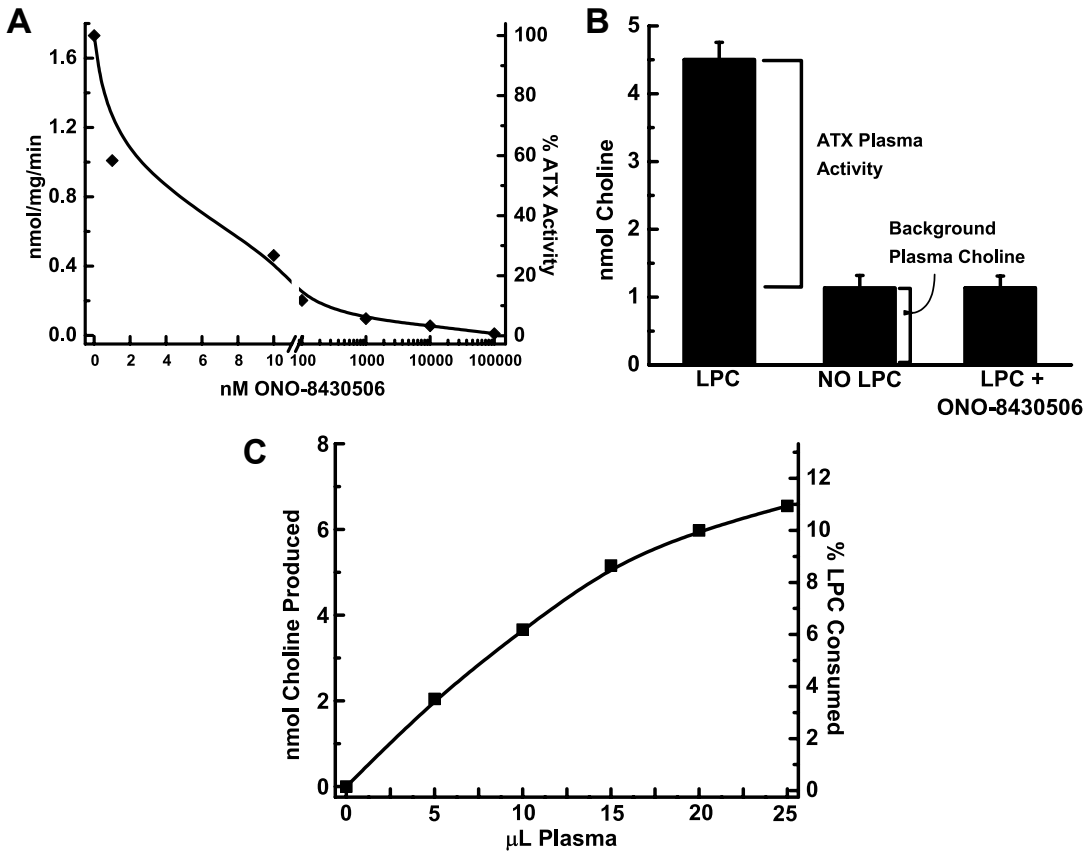

Figure 2.6. Validation of the choline-release ATX assay for measuring ATX activity. A) Effects of ONO-8430506 addition on the activity of recombinant human ATX. ONO-8430506 completely abolished ATX activity by 100 µM. B) Representative choline measurements in 10 µL plasma incubated with 3 mM LPC, without 3 mM LPC, and with both 3 mM LPC and 100 µM ONO-8430506. ONO-8430506 at 100 µM completely suppresses the measured choline production in the presence of 3 mM LPC to levels measured in the absence of added LPC. Hence, we define ATX activity in plasma and tissues as the activity that is suppressed by ONO-8430506. Results are given as means ± SEM for plasma from four mice. C) The 6-h ATX assay on plasma gives a linear response with the quantity of plasma assayed up to about 15 µL plasma. Under these conditions, all plasma ATX measurements were performed on 10 µL plasma.

2.5 Fluorescent Substrate-3 (FS-3) ATX assay

2.5.1 Introduction

FS-3 (Echelon) is a doubly-labeled analog of LPC such that the fluorophore is quenched through intramolecular energy transfer (261) (Figure 2.7). Hydrolysis of the substrate produces an increase in fluorescence, and the initial rate of increase in fluorescence is proportional to amount of ATX activity in the reaction mixture. Typically, final FS-3 concentrations in activity assays are 0.5 to 5 μM (261). The FS-3 assay was used to measure ATX secretion in concentrated conditioned media from cell cultures. Ideally, cell culture medium should be serum-free or serum-reduced (for example to 1%) to reduce the background activity from serum-derived ATX. Phenol-red free medium should also be used to reduce the background emission from phenol red. Lysophospholipids are potent competitive inhibitors of the FS-3 reaction (Chapter 3), hence the assay is unsuitable for measuring plasma ATX activity. Consequently, if serum is required in cell culture medium, it should be dilapidated (FBSC).

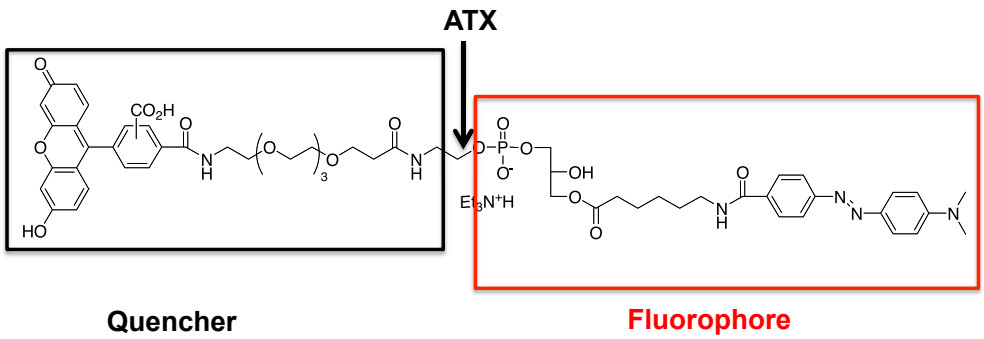

Figure 2.7. Structure of Fluorescent Substrate-3 (FS-3). LysoPLD activity of ATX releases the quencher from the fluorophore to increase fluorescence upon excitation.

2.5.2 Conditioned media preparation for the FS-3 ATX assay

Cells were cultured in 6-well plates with 2 mL of serum-free RPMI 1640 phenol-red free medium, usually for 48 h following a 6-h preincubation in basal medium. If cell viability was adversely affected by these conditions, particularly with fibroblasts, medium was supplemented with 1% FBSC. As a control, ATX activity was also measured in medium that was not exposed to cells. At the end of the experiment, medium was collected, centrifuged to remove any debris and weighed. Medium was concentrated between 5-30 fold by weight using Amicon Ultra-0.5 Centrifugal Filter Units with Ultracel-10 membranes (10 kDa nominal molecular weight limit) (UFC501096) (EMD Millipore; Billerica, MA, USA). Filters were rinsed with distilled water prior to use to remove trace glycerol (used as a humectant for long-term storage) from the membranes.

2.5.3 Measurement of ATX activity by and validation of the FS-3 ATX assay

For FS-3 assay measurements on conditioned medium, FS-3 substrate was prepared at 1.25X the final working concentration (typically 3 μM) in FS-3 assay buffer (140 mM NaCl, 5 mM KCl, 1 mM $CaCl_2$, 1 mM $MgCl_2$, 50 mM Tris-HCl, pH 8.0 and 1 mg/ml BSA). Eighty μL of FS-3 substrate was added to 20 μL of concentrated conditioned medium in a black-well plate (Corning, Corning, NY, USA) and covered with iCycler IQ® Optical Tape (Biorad).

For experiments on recombinant ATX, LPA, S1P and recombinant ATX were prepared at 10X the final working concentration in FS-3 assay buffer. FS-3 substrate (80 µL) was added to 10 µL of ATX (1000 ng/mL) and 10 µL of either C18:1-LPA, S1P or FS-3 assay buffer for a final volume of 100 µL. Final ATX protein concentrations of 75, 100, and 125 ng/mL were used to demonstrate that the activity results were directly proportional to enzyme quantity present.

Fluorescence measurements were taken at 5 or 10 min intervals for 4-12 h at 37°C using a Fluoroskan Ascent fluorometer (Thermo Lab Systems, Gormley, ON) at an excitation wavelength of 485 nm and an emission wavelength of 527 nm (17). The initial rate of the reaction was determined using the linear curve-fitting algorithm in Origin Pro 8.5 (OriginLab Corporation, Northampton, MA, USA) (Figure 2.8A) and subtracted from the initial rate of the reaction from control medium. The results were then normalized to cell protein content.

ATX activity measurements were taken using at least three different fold concentrations of conditioned medium per cell line to demonstrate that the initial rate measured (Figure 2.8A) was directly proportional to the amount of conditioned medium assayed (Figure 2.8B). The specificity of the initial rate for ATX activity was demonstrated in that the autotaxin inhibitor ONO-8430506 at 1 µM final concentration completely blocked the measure activity

(Figure 2.8A). Background fluorescence in this reaction comes from the auto-hydrolysis of the FS-3 substrate.

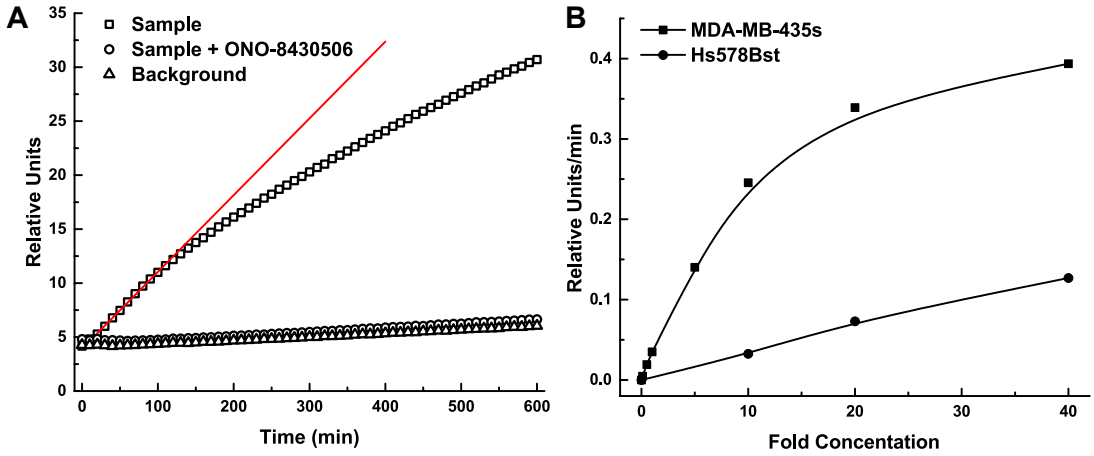

Figure 2.8. Determination of the linear response range for the FS-3 ATX assay using cell culture conditioned medium. A) Plot of raw fluorescent data over time for a particular sample. The slope of the red line represents the initial rate of the reaction. Addition of 1 μM ONO-8430506 completely blocks ATX activity. B) Plot of the initial rate of the reaction (slope of the red line in A) over the fold concentration of the conditioned medium assayed. Under the conditions medium was collected from MDA-MB-435S cells, a fold concentration of less than 10 should be used to assay media, otherwise the true ATX activity in the sample would be underestimated. However, for the conditions used in the Hs578Bst medium collection, higher fold concentrations can be assayed.

2.6 Measurement of mRNA levels

2.6.1 mRNA isolation and reverse transcription

mRNA from cell culture experiments was isolated using the RNAqueous® kit or from Trizol®, both from Invitrogen Life Technologies (Carlsbad, CA, USA). Using the RNAqueous® kit, cells on dishes were scraped into 500 μL of lysis/binding buffer, which is a concentrated chaotropic guaidimium salt solution. The buffer was passed through a 26-gauge needle

three times to shear genomic DNA. An equal volume of 64% ethanol was added and mixed by inversion to reduce the viscosity of the mixture. Each sample was then added to a filter cartridge in a collection tube. The filter cartridge contains a silica fibre pad, which binds and retains nucleic acids in the presence of the lysis buffer (304). The bound nucleic acids were washed with the kit buffers and eluted in 100 µL with a low ionic strength elution buffer that was pre-heated to 80°C to facilitate elution.

Trizol® is a monophasic solution containing phenol and guanidine isothocyanate, which can also be used to isolate mRNA from tissues (305, 306). Tissue pieces 20-40 mg were homogenized in 1 mL of Trizol® as described previously (Section 2.4.2), whereas cells on dishes were scraped directly into 1 mL of Trizol®. If necessary, samples were centrifuged to remove insoluble debris. The samples were then incubated for 10 min at room temperature to permit complete dissociation of the nucleoprotein complex. Next, 200 µL of chloroform was added and the tubes were capped, shaken vigorously by hand for 15 s and incubated for 5 min at room temperature. This caused the sample to dissociate into an upper aqueous layer where RNA will be present and a lower organic phase. The tubes were centrifuged at 13,000 rpm for 15 min at 4°C. The aqueous phase was removed into a fresh tube by angling the tube at 45° and pipetting the solution out, being careful to avoid drawing any of the interphase or organic layer. The collected aqueous layers were then re-extracted with 200 µL of

cholorform to ensure removal of any traces of phenol, which can artificially suppress the $A_{260/280}$ ratio for RNA. RNA was then precipitated by adding 500 µL of 100% isopropanol and incubating at -20°C for 1 h. The tubes were then centrifuged at 13,000 rpm for 15 min at 4°C and supernatant was then discarded. The pellet was washed twice with 1 mL of 75% ethanol, vortexed briefly, and centrifuged for 5 min at 4°C. The RNA pellet was then air-dried for 10 min, making sure to not let it dry out completely since this could decrease solubility upon suspension. The RNA pellet was resuspended in 50 µL by passing the solution up and down several times in a pipet followed by heating at 60°C for 15 min.

Once RNA was isolated from either method, genomic DNA was removed using the DNA-free™ kit (Life Technolgies). Samples were incubated with 2 U recombinant DNAse I for 30 min at 37°C in 10 mM Tris-HCl pH 7.5, 2.5 mM $MgCl_2$ and 0.5 mM $CaCl_2$, followed by a second incubation with an additional 2 U recombinant DNAse I. One U of DNAse I activity is defined in the kit as an increase in the absorbance of a high molecular weight DNA substrate at a rate of 0.001 absorbance units (A_{260})/min per mL at 25°C. After the two incubations, DNAse Inactivation Reagent was added to block the DNAse I activity and chelate the Mg^{2+} and Ca^{2+} cations. After DNA digestion, the $A_{260/280}$ ratio was measured using the Nanodrop spectrophotometer ND-1000 (Thermo Scientific). mRNA samples had A260/280 ratios of ≥1.95.

The mRNA (100-500 ng) was then reverse-transcribed to complementary DNA (cDNA) using qScript™ cDNA Supermix from Quanta Biosciences (Gaitherburg, MD, USA). The supermix contained optimized concentrations of $MgCl_2$, RNAse inhibitor protein, dNTPs, qScript reverse transcriptase random primers and oligo deoxythymidine primers. The mixture was incubated at 25°C for 10 min, followed by sequential incubation at 42°C for 60 min and 95°C for 5 min, then cooled to 4°C in a Mastercycler® gradient (Eppendorf AG, Hamburg, Germany). Samples were kept at 4°C for immediate processing or -20°C for long-term storage.

2.6.2 Quantitative real-time PCR

cDNA samples were assayed with RT2 SYBR® Green qPCR Mastermix, Low ROX (SABiosciences, Fredrick, MD), and 10 μM forward and reverse primers (Table 2.2). Primer design was optimized using Primer-Blast (National Center for Biotechnology Information, NIH, Bethesda, MD, USA). The reaction mix was assayed using the Applied Biosystems 7500 real-time PCR System (Life Technologies). The thermocycling protocol starts with 1 cycle at 50°C for 2 min followed by 1 cycle at 95°C for 10 min. The transcripts were then amplified during 40 cycles at 95°C for 15 s and 60°C for 1 min. Quantification of fluorescent SYBER Green bound to double-stranded DNA was performed at the end of each cycle at 60°C. Gene expression was normalized to the housekeeping genes hypoxanthine-guanine

phosphoribosyltransferase (*HPRT*), peptidylprolyl isomerase A (*PPIA*; cyclophilin A) or glyceraldehyde phosphate dehydrogenase (*GAPDH*). Relative changes in expression of ATX mRNA were essentially the same with both reference mRNAs and results are routinely expressed relative to *GAPDH* mRNA.

The specificity of the amplicon was confirmed by melting curve analysis of the amplicon dissociation performed by the Applied Biosystems 7500 software immediately after amplification. This protocol consisted of 1 cycle at 95°C for 15 s followed by 1 cycle at 60°C for 1 min and a final cycle at 95°C for 15 s. The instrument measured the decease in SYBR Green fluorescence when the double-stranded amplicons dissociated as the thermocycler was ramped up to the final temperature of 95°C. The results were displayed as a plot showing the first derivative of the rate of change in fluorescence as a function of temperature, such that any non-specific products or primer dimers would be detectable in the dissociation curve as separate peaks.

Gene	Species	Primers
CSF2	Human	F: 5'-ATG ATG GCC AGC CAC TAC AA-3' R: 5'-CTG GCT CCC AGC AGT CAA AG-3'
CXCL10	Human	F: 5'-AGC AGA GGA ACC TCC AGT CT-3' R: 5'-ATG CAG GTA CAG CGT ACA GT-3'
ENPP2 (ATX)	Human	F: 5'-ACA ACG AGG AGA GCT GCA AT-3' R: 3'-AGA AGT CCA GGC TGG TGA GA-3'
ENPP2 (ATX)	Mouse	F: 5'-GAA AGC AGA GCA TTC AGG GC-3' R: 5'-GGA TAT TAC CTG GTA TGA CCC GAA A-3'
ENPP2 (ATX)	Human/ Mouse	F: 5'-CAT TTA TTG GTG GAA CGC AGA-3' R: 5'-ACT TTG TCA AGC TCA TTT CC-3'
HPRT	Human	F: 5'-CGA CGA GCC CTC AGG CGA AC-3' R: 5'-CGG GTC GCC ATA ACG GAG CC-3'
HPRT	Human/ Mouse	F: 5'-AGA TCC ATT CCT ATG ACT GT-3' R: 5'-AAT CAA GAC ATT CTT TCC AG-3'
GAPDH	Human/ Mouse	F: 5'-ACT TTG TCA AGC TCA TTT CC-3' R: 5'-TCT TAC TCC TTG GAG GCC AT-3'
IL1A	Human	F: 5'-CTT CTG GGA AAC TCA CGG CA-3' R: 5'-AGC ACA CCC AGT AGT CTT GC-3'
IL1B	Human	F: 5'-AAC AGG CTG CTC TGG GAT TC-3' R: 5'-AGT CAT CCT CAT TGC CAC TGT-3'
IL6	Human	F: 5'-AGT TCC TGC AGA AAA AGG CAA AG-3' R: 5'-AAA GCT GCG CAG AAT GAG ATG-3'
IL8	Human	F: 5'-CCA CCG GAA GGA ACC ATC TC-3' R: 5'-CTC CTT GGC AAA ACT GCA CC-3'
PDGFA	Human	F: 5'-AAG CAG CCA ACC AGA TGT GA-3' R: 5'-GGA GGA GAA CAA AGA CCG CA-3'
PDGFB	Human	F: 5'-CTT CCT GTC TCT CTG CTG CTA-3' R: 5'-CAT CTT CCT CTC CGG GGT C-3'
PPIA	Human	F: 5'-CCA CCG CCG AGG AAA ACC GT-3' R: 5'-AAA GGA GAC GCG GCC CAA GG-3'
PPIA	Human/ Mouse	F: 5'-GAT GAG AAC TTC ATC CTA AA-3' R: 5'-TCA GTC TTG GCA GTG CAG AT-3'
TNFA	Human	F: 5'-CCC ATG TTG TAG CAA ACC CTC-3' R: 5'-CCC ATG TTG TAG CAA ACC CTC-3'

Table 2.2. Primer sequences of genes probed in qRT-PCR assays. Abbreviations used: *CSF2*: Colony stimulating factor 2 (GM-CSF: granulocyte-macrophage colony stimulating factor); *CXCL10*: C-X-C motif chemokine 10; *ENPP2* (ATX): ecto-nucleotide pyrophosphatase/phosphodiesterase family member 2; *HPRT*: hypoxanthine-guanine phosphoribosyltransferase; *GAPDH*: glyceraldehyde phosphate dehydrogenase; *IL*: interleukin; *PDGFA* or *B*: platelet derived growth factor A or B; *PPIA*: peptidylprolyl isomerase A (cyclophilin A); *TNFA*: tumor necrosis factor alpha.

2.7 ATX mRNA expression in human mammary tissue and breast cancer tumors

mRNA expression for ATX in human breast cancer tumors was compared to levels in normal mammary tissue from a patient de-identified database obtained from Dr. John Mackey, Department of Oncology, University of Alberta (307, 308). In this study, total RNA was isolated from the samples using Trizol® and purified using Qiagen RNAeasy® columns according to the manufacturer's recommended protocols. The RNA was then quantified using a NanoDrop 1000 Spectrophotometer (NanoDrop Technologies, Wilmington, DE, USA) and its integrity evaluated using a Bioanalyzer 2100 (Agilent Technologies, Santa Clara, CA, USA) according to the manufacturer's protocols. Only RNA samples with RNA Integrity Numbers (RIN) greater than 5.0 were used.

The RNA was subjected to linear amplification and Cy3 labeling and Hybridization to Agilent Whole Human Genome Arrays using Agilent kits (One Color Low RNA Input Linear Amplification Kit Plus, RNA Spike-In Kit and Gene Expression Hybridization Kit) according to the manufacturer's recommended protocols. The arrays were scanned using an Agilent Scanner, the results were quantified using Feature Extraction Software 9.5 (Agilent). Data was analyzed using GeneSpring 10.0.2 (Agilent). The data were transformed and normalized using GeneSpring default settings; the data were adjusted to a minimum threshold of 1.0 to eliminate unreasonably low values,

transformed to Log2, normalized per array using a shift to the 75 percentile, and finally normalized per gene using a baseline transformation to the median value per gene over all samples.

2.8 Sodium dodcecyl sulphate-polyacrylamide (SDS-PAGE) gel electrophoresis, western blotting and immunohistochemistry

2.8.1 SDS-PAGE gel electrophoresis and western blotting

SDS-PAGE gel electrophoresis (309) and western blots were performed on plasma for ATX. Four μL of plasma were diluted in 4x sample loading buffer (250 mM Tris-HCl pH 6.8, 4% SDS, 30% glycerol, 0.003% bromphenol blue and 10% 2-mercaptoethanol added freshly), and then boiled for 15 min. The treated samples were loaded in 10- or 15-well SDS-PAGE gels along with 10 μL of Precision Plus® All-Blue Protein Standards (Bio-Rad) consisting of 250, 150, 100, 75, 50, 37, 25, 20, 15 and 10 kDa protein standards. The stacking gels were comprised of 125 mM Tris-HCl pH 6.8, 0.1% SDS, 3.9% acrylamide and 0.1% bisacrylamide, and the separating gels contained 375 mM Tris-HCl pH 8.8, 0.1% SDS, 10% acrylamide and 0.28% bisacrylamide. Proteins were separated at 130 V for 2.5 h in Laemmli electrophoresis buffer (25 mM Tris base pH 8.3, 192 mM glycine, 0.1 % SDS) using a Mini-Protean II protein electrophoresis apparatus (Bio-Rad).

The proteins were then transferred onto 0.45-μm Transblot nitrocellulose membranes (Bio-Rad) for 4 h at 400 mAmps at 4°C in Tris-glycine buffer (25 mM Tris base, 192 mM glycine) containing 20% methanol and 0.05% SDS. Blots were then blocked in 5% milk powder for 1 h at room temperature. ATX primary antibody, a gift from Dr. T Clair (National Cancer Institute, Bethesda, MA, USA) (53), (1:1000 dilution) was incubated overnight at 4°C in blocking solution containing 5% milk powder in TBS-Tween 0.1% (TBST). The blots were then washed 4 times in (TBST), and incubated with goat anti-rabbit immunoglobulin G (IgG) secondary antibody conjugated with horseradish peroxidase (1:2000 dilution) (Santa Cruz Biotechnology Inc, Santa Cruz, CA, USA) for 1 h in blocking solution at room temperature. Membranes were washed three times in TBST and immunocomplexes were detected using the Immun-Star™ WesternC™ ECL kit (Biorad) by exposure to autoradiography film (Kodak, Rochester, NY, USA). Developed films were scanned and densitometric analysis was performed using ImageJ software (NIH, Bethesda, MD, USA).

2.8.2 Immunohistochemistry

Immunohistochemistry was performed on 5-μm paraffin-embedded tumor sections attached to positively-charged coated glass slides and dried for 4 h at 60°C. Slides were dewaxed by soaking in three changes of xylene for 10 min. Slides were then dipped 20 times in three changes of 100%

ethanol, and one change each of 80% and 50% ethanol, before being rinsed in running distilled water for 5 min. Antigen retrieval was performed by microwaving hydrated slides in a plastic pressure cooker for 20 min in 10 mM citric acid pH 6.0, and the pressure cooker was cooled in a water bath at room temperature for an additional 20 min. Slides were washed under distilled water for 5 min. Next, endogenous peroxidase activity was blocked by submerging slides in 9:1 methanol: 30% hydrogen peroxide for 10 min. Slides were then soaked for 10 min in PBS. Sections were outlined with a wax pen (Dako, Burlington, ON) and blocked with Dako Antibody Diluent with background reducing reagents (S3022) for 30 min at room temperature in a humidified chamber. The solution was then shaken off the slides and Antibody Diluent with primary rabbit antibodies (Table 2.3) was added and the slides were incubated at 4°C overnight.

The slides were washed on the second day with two changes of PBS with 0.1% Tween-20 (PBST) for 5 min. Samples were then covered with Dako Envision™+ Rabbit secondary antibody conjugated to horseradish peroxdiase (K4002) at room temperature for 30 min, and washed in PBST. Samples were then developed with Dako Liquid DAB+ (diaminobenzidine) Substrate Chromogen System (K3468) for 0.5-5 min. DAB forms a very stable brown end-product at the site of the target secondary antibody. The reaction was quenched in PBS, and the slides were washed in running distilled water for 5 min. The slides were next soaked in a 1% copper sulphate aqueous solution

for 3 min for chromogenic enhancement, and then rinsed again in water. The slides were counterstained in Harris Modified Method hematoxylin (Fisher Scientific) for 3 min, and then washed under warm tap water until clear. Slides were then dehydrated with increasing ethanol concentrations (50%, 80% and 100%) and three changes xylene, and glass coverslips were mounted with xylene-based mounting medium (Fisher Scientific).

Primary Antibody	Company	Catalog #	Concentration (mg/mL)	Dilution
ATX	Dr. Tim Clair (53)	ATX-102	1.0	1:1000
CD-31	Abcam (Toronto, ON)	ab28364	0.2	1:50
CD-45	Abcam	Ab10558	1.0	1:1600
cleaved caspase 3	Cell Signaling (Danvers, MA, USA)	D175	0.1	1:75
fibroblast activation protein	Abcam	ab53066	1.0	1:500
firefly luciferase (goat antibody with biotin link)	Abcam	ab634	10	1:8000
IgG control	Bioss (Woburn, MA, USA)	bs-0295P	1.0	1:1000
Ki67	Cell Signaling	D3B5	0.1	1:200

Table 2.3. Primary rabbit antibodies used in immunohistochemistry.

Images were acquired from at least 3 random fields per specimen at 5X, 20X, 40X or 100X using a Zeiss Axioskop 2 imaging system (Carl Zeiss Canada, Ltd., Toronto, ON). For thyroid cancer tissue microarrays, two different pathologists reviewed and quantified the level of antibody staining from 0 (minimal), 1+, 2+, to 3+ (strong) without knowledge of the clinical outcome of the patients. At least two of three tissue array cores needed to be

intact for analysis and cores that were fragmented or incomplete were not scored. Staining was assessed for each case, in triplicate.

2.9 Measurement of plasma ONO-8430506 concentrations

Twenty volumes of acetonitrile/ethanol (7/3) containing ONO-8410506 (ONO Pharmaceuticals Ltd.), an internal reference with a similar structure to ONO-8430506, was added to each sample. The mixture was transferred into a 96-well filter plate (Multiscreen Solvinert®, 0.45-μm pore-size, low-binding hydrophilic PTFE, EMD Millipore), which was centrifuged at 4˚C and 1,600 rpm for 5 min. The same volume of distilled water was added to the filtrate in each well and then assayed by liquid chromatography/mass spectrometry. The concentration of ONO-8430506 in each sample was calculated from its relative peak area compared to the internal reference. Ono Pharmaceuticals in Japan performed all measurements on plasma samples, which we shipped on dry ice.

2.10 Measurements of lysophospholipid concentrations

2.10.1 Sample preparation

Blood plasma was treated with internal standards C17:0-LPA (5 ng) and isotope labeled [$^{13}C_2D_2$] S1P (20 ng) in 12x75 mm glass tubes, and 400 μL of 50 mM acetic acid aqueous solution, pH 4.0 was added. Lipid phosphates were then extracted by vigorous vortexing into 1 mL of water-

saturated butanol followed by centrifugation at 2800 x *g* for 30 min (310, 311). Next, 600 μL of the butanol phase was transferred to fresh tube and dried under nitrogen. Then samples were then resuspended in 100 μL of 2:1 methanol:chroloform. Similarly, 15-40 mg of tumor was homogenized in 500 μL of 50 mM acetic acid pH 4.0 as described in Section 2.4.2 and 400 μL of the homogenate was likewise extracted into butanol along with internal standards.

Solutions at six concentrations (0, 18, 60, 120, 300 and 600 nM) for S1P and SA1P and (0, 4.5, 15, 30, 75 and 150 nM) C16:0-LPA, C18:0-LPA, C18:1-LPA and C20:4-LPA were prepared and calibration curves were constructed using peak area ratios of standard to internal standard response versus the analyte concentrations. The absolute amounts of S1P, SA1P, C16:0-LPA, C18:0-LPA, C18:1-LPA and C20:4-LPA were determined from the calibration curves; all other LPA species were estimated based on the analyte to C17:0-LPA internal standard peak area ratio.

2.10.2 Liquid chromatography and mass spectrometry

Lysophospholipids were measured by LC/MS using electrospray ionization in the negative mode using an Agilent 1200 series LC system coupled to a 3200 QTRAP mass spectrometer (AB SCIEX, Concord, ON). The LC separation was on an Acclaim® 150 mm × 2.1 mm HILIC-10 column, 3-μm particle size (Thermo Fisher Scientific) maintained at 25°C. The mobile

phase was: A, 92/8 acetonitrile/125 mM ammonium formate in water adjusted with formic acid to pH 3.0; and B, 50 mM ammonium formate with 0.2% formic acid in water. The gradient was: 0-0.1 min, 10% B; 0.1-4 min, 10% to 45% B; step to 80% B at 4.1 min; 4.1-5 min, 80% B; 5.1 min back to 0% B with 5 min hold for column re-equilibrium. The mobile phase flow rate was 350 µL/min from 4.1 min to 8 min and 400 µL/min for all other periods. The injection volume was 10 µL and the cycle time was 10 min/injection. The LC effluent was diverted to waste outside of the 0.8 to 5 min retention time window to minimize contamination of the mass spectrometer. Mass spectrometric analysis was performed using multiple reaction monitoring (MRM). Nitrogen was used as the curtain gas, nebulizing gas and drying gas. The source-dependent parameters used are as follows: curtain gas at 20 arbitrary units; gas 1 at 55; gas 2 at 60; ionspray voltage at -4500 V and source temperature at 400°C. The declustering potential (DP) and entrance potential (EP) were -60 V and -5 V respectively for all experiments. The collision energy (CE) and cell exit potential (CXP) were set to -60 V and -1 V for S1P transitions and to -30 V a -1 V for LPA transitions.

The MRM transitions monitored were: S1P *m/z* 378→79; SA1P *m/z* 380→79; S1P/$^{13}C_2D_2$ *m/z* 383→79; C16:0-LPA *m/z* 409→153; C16:1-LPA *m/z* 407→153; C18:0-LPA *m/z* 437→153; C18:1-LPA *m/z* 435→153; C18:2-LPA *m/z* 433→153; C18:3-LPA *m/z* 431→153; C20:4-LPA *m/z* 457→153; C20:5-LPA *m/z* 455→153; C22:6-LPA *m/z* 481→153; C17:0-LPA *m/z*

423→153. Dr. Yuan Zhao and Dr. Jonathan Curtis, Faculty of Agriculture, Food and Nutritional Science, University of Alberta, performed all lysophospholipid mass spectrometry measurements.

2.11 Enzyme-linked immunosorbent assay (ELISA)

2.11.1 ATX sandwich ELISA

ATX protein concentration was quantified from 100 µL of centrifuged cell culture conditioned medium (total of 1 mL medium from a 12-well cell culture plate) using the ATX sandwich ELISA Kit (K-5600) from Echelon. An eight-point standard curve was created using recombinant ATX (0, 1.5625, 3.125, 6.25, 12.5, 25, 50 and 100 ng/mL). Samples were incubated on the ATX detection plate for 1 h at room temperature with gentle shaking. The samples were then discarded from the plate, and washed three times for 5 min on a shaker with 200 µL per well of PBST (PBS with 0.1% Tween 20). The anti-ATX antibody solution (100 µL per well) was incubated on the plate for 1 h at room temperature with gentle shaking, and the plate was washed again with PBST three times. This was repeated with the secondary detector. TMB solution was added (100 µL per well) for 30 min and the plate was protected from light, and 50 µL of 1N H_2SO_4 was added to stop the reaction. Absorbance was read on a spectrophotometer at 450 nm. ATX protein concentrations interpolated from the standard curve were then normalized to

both the incubation volume of conditioned medium and protein content from cell lysates by the BCA assay (Thermo Scientific).

2.11.2 Multiplex cytokine/chemokine arrays

Sixty-four human cytokines, chemokines and growth factors were analyzed by Eve Technologies Corp. (Calgary, AB) using a MILLIPLEX Human Cytokine/Chemokine 41-plex kit and a MILLIPLEX Human Cytokine/Chemokine 23-plex kit (Millipore, St. Charles, MO, USA), according to the manufacturer's protocol on a Luminex 100 system (Luminex, Austin, TX, USA) (analytes listed in Table 2.4). For mouse specimens, a 32-plex kit was used (Table 2.4).

Tissues specimens (5-10 mg) were homogenized in 200 µL of 20 mM Tris HCl (pH 7.5) buffer with 0.5% Tween 20, 150 mM NaCl and protease inhibitor, then centrifuged for 10 min at 4°C and the supernatant transferred to a fresh tube. Protein content was measured using the BCA protein assay (Fisher Scientific) and adjusted to 2-5 µg/µL. For supernatant analysis, cancer cells were seeded in 12 well plates, grown to ~70% confluence and then washed and pre-incubated for 6 h in 1 mL phenol-free RPMI 1640 medium containing 1% FBSC. The media were then changed with or without addition of 5 µM oleoyl-LPA and incubated for 24 h, then centrifuged. Measurements were normalized to both volume of medium and cell protein. Plasma samples were diluted 1:1 with PBS prior to analysis.

Analyte	Species	Full name [Alternate Names]
CCL1	Human	Chemokine (C-C motif) ligand 1 [I-309, P500, TCA3, SCYA1]
CCL2	Human/Mouse	Chemokine (C-C motif) ligand 2 [monocyte chemotactic protein-1 (MCP-1), small inducible cytokine A2]
CCL3	Human/Mouse	Chemokine (C-C motif) ligand 3 [macrophage inflammatory protein 1-alpha (MIP-1α)]
CCL4	Human/Mouse	Chemokine (C-C motif) ligand 4 [macrophage inflammatory protein 1-beta (MIP-1β)]
CCL5	Human/Mouse	Chemokine (C-C motif) ligand 5 [RANTES]
CCL7	Human	Chemokine (C-C motif) ligand 7 [monocyte chemotactic protein-3 (MCP-3), FIC, MARC, NC28]
CCL8	Human	Chemokine (C-C motif) ligand 8 [monocyte chemotactic protein-2 (MCP-2), HC14]
CCL11	Human/Mouse	Chemokine (C-C motif) ligand 11 [Eotaxin-1, SCYA11]
CCL13	Human	Chemokine (C-C motif) ligand 13 [monocyte chemotactic protein-4 (MCP-4)]
CCL15	Human	Chemokine (C-C motif) ligand 15 [macrophage inflammatory protein 1-d (MIP-1d), leukotactin-1, MIP5, HCC-2]
CCL17	Human	Chemokine (C-C motif) ligand 17 [TARC]
CCL21	Human	Chemokine (C-C motif) ligrand 21 [6CKine, Exodus-2, SLC, TCA-4 CKβ9]
CCL22	Human	Chemokine (C-C motif) ligand 22 [macrophage derived chemokine (MDC)]
CCL24	Human	Chemokine (C-C motif) ligand 24 [Eotaxin-2, myeloid progenitor inhibitory factor 2 (MPIF-2)]
CCL26	Human	Chemokine (C-C motif) ligand 26 [Eotaxin-3, MIP-4alpha, SCYA26, TSC-1]
CCL27	Human	Chemokine (C-C motif) ligand 27 [IL-11 R-alpha-locus chemokine (ILC), SCYA27, ALP, ILC, CTACK, skinkine, ESkine, PESKY, CTAK]
CD135	Human	Cluster of differentiation antigen 135 [Fms-like tyrosine kinase 3 ligand (Flt-3 ligand)]
CSF1	Mouse	Colony-stimulating factor 1 [macrophage colony-stimulating factor (M-CSF)]
CX3CL1	Human	Chemokine (C-X3-C motif) ligand 1 [Fractalkine]
CXCL1	Human/Mouse	Chemokine (C-X-C motif) ligand 1 [GRO, KC]
CXCL2	Mouse	Chemokine (C-X-C motif) ligand 2 [macrophage inflammatory protein 2 (MIP-2)]
CXCL5	Human/Mouse	Chemokine (C-X-C motif) ligand 5 [Epithelial-Derived Neutrophil- Activating Protein 78 (ENA-78), SCYB5]
CXCL9	Mouse	Chemokine (C-X-C motif) ligand 9 [monokine induced by gamma interferon (MIG)]
CXCL10	Human/Mouse	C-X-C motif chemokine 10 [Interferon gamma-induced protein 10 (IP-10), C7, IFI10, INP10, SCYB10, crg-2, gIP-10, mob-1]
CXCL12	Human	C-X-C motif chemokine 12 [stromal cell-derived factor 1 (SDF 1), IRH, PBSF, TLSF]
CXCL13	Human	C-X-C motif chemokine 13 [BCA-1, BCL, BLR1L, B lymphocyte chemoattractant]

EGF	Human	Epidermal Growth Factor
FGF-2	Human	basic fibroblast growth factor [bFGF, FGF-β]
G-CSF	Human/Mouse	Granulocyte Colony-Stimulating Factor
GM-CSF	Human/Mouse	Granulocyte-Macrophage Colony-Stimulating Factor
IFNα2	Human	Interferon alpha-2
IFNγ	Human/Mouse	Interferon gamma [IFG, IFI]
IL-1α	Human/Mouse	Interleukin 1 alpha
IL-1β	Human/Mouse	Interleukin 1 beta
IL-1Rα	Human	Interleukin-1 alpha receptor antagonist
IL-2	Human/Mouse	Interleukin 2 [T-cell growth factor (TCGF), lymphokine]
IL-3	Human/Mouse	Interleukin 3 [MCGF]
IL-4	Human/Mouse	Interleukin 4 [BCGF-1, BSF-1]
IL-5	Human/Mouse	Interleukin 5 [EDF, TRF]
IL-6	Human/Mouse	Interleukin-6 [HGF, HSF, BSF2, IFNB2]
IL-7	Human/Mouse	Interleukin 7
IL-8	Human	Interleukin 8 [chemokine (C-X-C motif) ligand 8 (CXCL8), GCP-1, LECT, LUCT, NAF, NAP-1]
IL-9	Human/Mouse	Interleukin 9 [HP40]
IL-10	Human/Mouse	Interleukin 10 [cytokine synthesis inhibitory factor (CSIF)]
IL-12p40	Human/Mouse	Interleukin 12 p40 subunit [natural killer cell stimulatory factor 2, cytotoxic lymphocyte maturation factor 2, p40]
IL-12p70	Human/Mouse	Interleukin 12 p70 subunit [p70]
IL-13	Human/Mouse	Interleukin 13
IL-15	Human/Mouse	Interleukin 15
IL-16	Human	Interleukin 16 [LCF, NIL16, PRIL16]
IL-17A	Human/Mouse	Interleukin 17 or Interleukin 17A
IL-20	Human	Interleukin 20 [IL10D, ZCYTO10]
IL-21	Human	Interleukin 21
IL-23	Human	Interleukin 23 [IL-23A, IL23P19]
IL-28A	Human	Interleukin 28A [IFNL2]
IL-33	Human	Interleukin 33 [NF-HEV mature, IL1F11, DVS27]
LIF	Human/Mouse	Leukemia Inhibitory Factor
PDGF-AA	Human	Platelet Derived Growth Factor-AA
PDGF-BB	Human	Platelet Derived Growth Factor-BB
sCD40L	Human	Soluble cluster of differentiation antigen 40 ligand [CD154]
SCF	Human	Stem Cell Factor
TGF-α	Human	Tumor Growth Factor-alpha
TNF-α	Human/Mouse	Tumor Necrosis Factor-alpha
TNF-β	Human	Tumor Necrosis Factor-beta
TPO	Human	Thrombopoietin
TRAIL	Human	TNF-related apoptosis-inducing ligand [TNFSF10,CD253]
TSLP	Human	Thymic stromal lymphopoietin
VEGF	Human/Mouse	Vascular endothelial growth factor A

Table 2.4. Analytes quantified by multiplex ELISA. Systematic abbreviations are given in the left column and the full name and/or other common names for each analyte are in the right column.

2.12 Statistics

Results are expressed as means ± standard error of mean (SEM), or standard deviation (SD), as indicated. The two-tailed student's t-test for two unpaired groups, the paired t-test for two paired groups, and the one-way ANOVA for three or more groups were used to test for significance ($p < 0.05$). Correlations for immunohistochemical staining were assessed using Fisher's exact test for tables and the Spearman rank correlation for continuous tables. Statistics were calculated and results plotted using Origin Pro 8.5 or 9.1 (OriginLab Corporation, Northampton, MA, USA).

CHAPTER 3

REGULATION OF AUTOTAXIN EXPRESSION BY LYSOPHOSPHOLIPIDS AND EVALUATION OF ONO-8430506 EFFICACY

3.1 Introduction

Studies of ATX biology *in vivo* are limited because knocking out ATX is embryonically lethal (5, 6). Conditional tissue knockout models may be ineffective because ATX is a secreted enzyme and is present abundantly in plasma. Hence, any local tissue deficiency could be replenished in the extracellular space by circulating ATX from other unaffected tissues. Therefore, for studies looking at the effects of ATX *in vivo*, potent inhibitors are required. Also, ATX inhibitors have great therapeutic potential for many pathological conditions implicated by aberrant LPA signaling. Most ATX inhibitors are LPA and S1P analogs, since early studies into the regulation of ATX had shown that LPA and S1P are potent competitive inhibitors of ATX activity (261, 271-273). However, this work was performed in assays with low μM concentrations of fluorescent LPC analogs and the inhibition was competitive. This means that the observed inhibition probably has no physiological relevance since physiological plasma concentrations of LPC are >200 μM and this would overcome the inhibition. Significantly, these ATX inhibitors have little potency *in vivo* (64, 181, 244). Hence, most lysophospholipid derivatives may be poor ATX competitive inhibitors under physiological conditions. Also, the direct physiological feedback of LPA and S1P on ATX activity through product inhibition probably does not occur.

Consequently, it is important to understand how ATX expression and activity are regulated by lysophospholipids, and the results of these studies

are presented here. In addition, we evaluated a novel non-lipid oral ATX inhibitor ONO-8430506 in mice, under development by ONO Pharmaceuticals Ltd. (285). This work establishes the suitability of ONO-8430506 for *in vivo* therapeutic studies of ATX inhibition in cancer.

3.2 Effects of LPA and S1P on ATX activity

The hypotheses that LPA and S1P exert feedback regulation on ATX activity was developed mainly by using Fluorescent Substrate-3 (FS-3), which is an analog of LPC that yields a fluorescent product when cleaved by ATX (261, 273). This compound is relatively expensive and assays are normally performed at low μM concentrations of FS-3. We used 5 μM FS-3 in the assay with recombinant ATX and confirmed that the reaction was inhibited by increasing LPA and S1P concentrations from 50 nM to 10 μM (Figure 3.1A). At a fixed LPA or S1P concentration of 1 μM which suppresses at least 60% of the ATX activity at 5 μM FS-3, these inhibitions were progressively and significantly decreased when the concentration of FS-3 was increased to 15 and 50 μM (Figure 3.1B). This finding was expected from the competitive nature of the inhibition, and we predict that there would be virtually no inhibition of ATX activity at a physiologically relevant concentration of 200 μM FS-3. However, performing this experiment would be cost prohibitive. Instead, we used the choline-release ATX assay where we incubated 200 μM LPC with ATX and measured the total choline produced by the lysoPLD

activity of ATX. In these studies, increasing LPA and S1P concentrations up to 10 μM had only marginal inhibitory effects on ATX activity (Figure 3.1A).

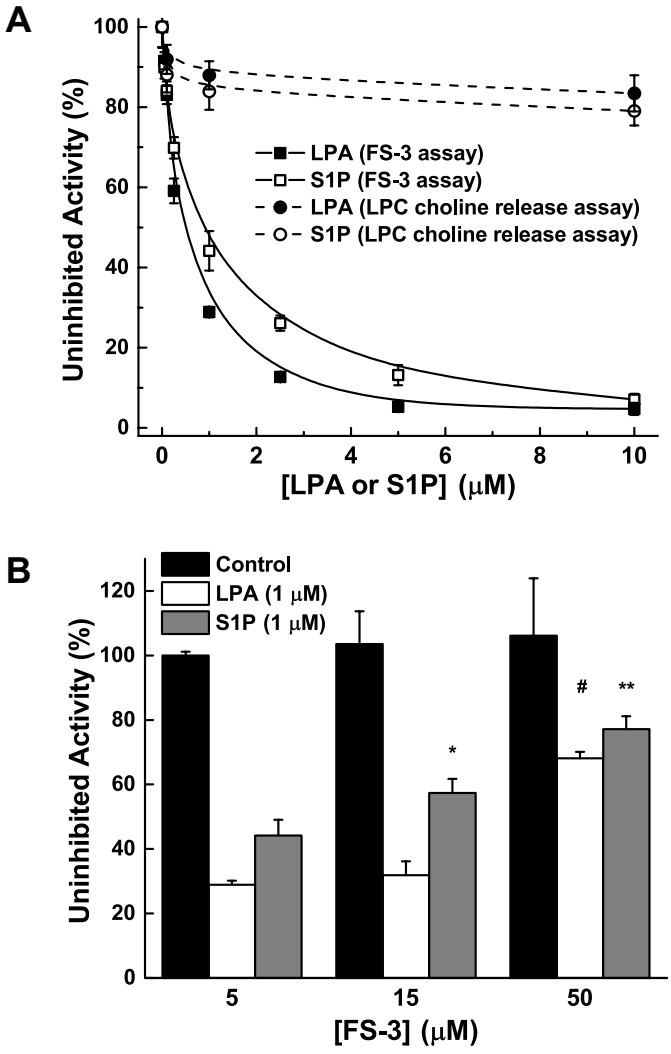

Figure 3.1. LPA and S1P are poor inhibitors of ATX activity at physiological concentrations of substrate. A) LPA and S1P potently inhibit ATX activity (ATX at 100 ng/mL concentration) when incubated with 5 μM FS-3 in the fluorogenic assay. However, this inhibition does not occur in the presence of 200 μM LPC in the choline-release assay (ATX at 1000 ng/mL concentration). B) Increasing the FS-3 concentration decreases the inhibition effect of 1 μM LPA or S1P on ATX activity. *, indicates a significant increase ($p<0.05$) in activity in the presence of S1P with 15 μM FS-3 compared to 5 μM FS-3; **, indicates a significant increase ($p<0.05$) in activity in the presence of S1P at 50 μM FS-3 compared to 5 or 15 μM FS-3; #, indicates a significant increase ($p<0.05$) in activity in the presence of LPA at 50 μM FS-3 compared to 5 or 10 μM FS-3.

3.3 LPA and S1P feedback regulation on ATX in cultured cells

3.3.1 LPA and S1P inhibit ATX mRNA production in a dose-dependent manner

Our routine approach for studies of the effects of lysophospholipids in cell culture is to use delipidated fetal bovine serum (FBSC) and then titrate in the desired concentrations of lysophospholipids (17, 217). We have observed in these types of experiments that cells incubated in FBSC have higher levels of ATX mRNA than cells in FBS, which contain all the lipids naturally found in serum. Hence, we hypothesized that lysophospholipids might exert a feedback regulation on ATX by negatively regulating it synthesis.

To test this hypothesis, we selected two cancer cells lines that express relatively high amounts of ATX: SW-579 thyroid cancer cells and MDA-MB-435S melanoma cells (17, 184). We then added both LPA and S1P to delipidated serum in concentrations from 100 nM to 5 μM and measured a dose-dependent decrease in ATX mRNA expression (Figure 3.2). We also verified this effect of LPA and S1P on ATX protein secretion by ELISA measurements on conditioned media (Figure 3.3). Hence, LPA or S1P decreased both the production and secretion of ATX.

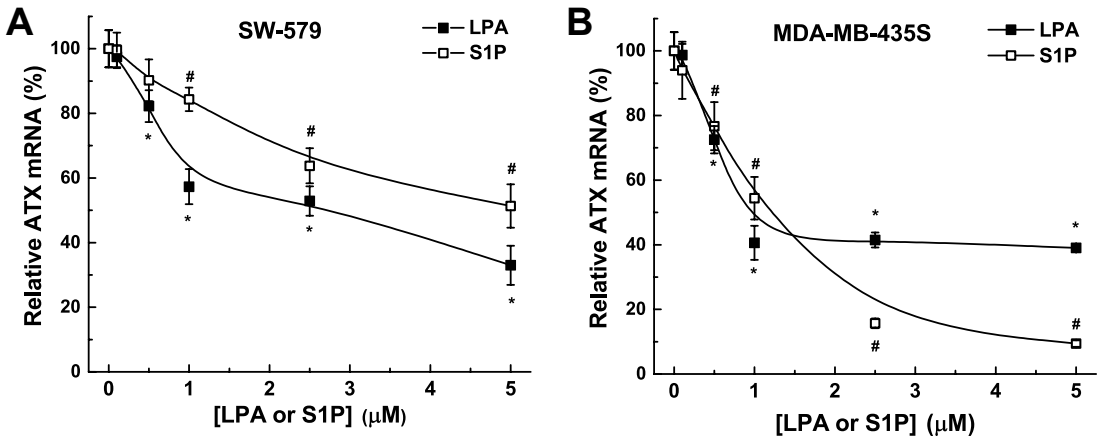

Figure 3.2. LPA and S1P decrease ATX mRNA expression. A) SW-579 B) MDA-MB-435S cells were incubated for 24 h in 10% FBSC medium with increasing concentrations of either LPA or S1P. *, significant reduction with LPA and # with S1P compared to no treatment ($p<0.05$).

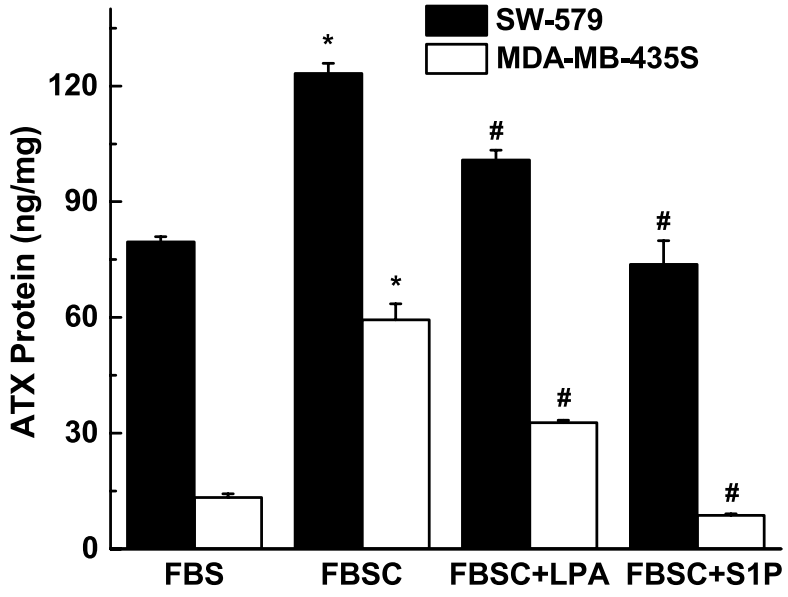

Figure 3.3. LPA and S1P decrease secretion of ATX. SW-579 and MDA-MB-435S cells were incubated for 48 h in medium containing FBS or FBSC with or without 5 μM LPA or S1P. Secreted ATX protein was quantified by ELISA and normalized to both volume of conditioned medium and cell lysate protein content. ATX protein from FBS/FBSC was subtracted from the total ATX protein measured after incubation. *, indicates a significant increase ($p<0.05$) in ATX protein in FBSC medium compared to FBS medium. #, indicates a significant decease ($p<0.05$) in ATX protein following LPA or S1P treatment in FBSC compared to FBSC alone.

3.3.2 LPA and S1P inhibition of ATX expression is receptor-mediated through phosphatidylinositol-3-kinase

Next, we examined the mechanism by which LPA and S1P suppress ATX mRNA transcription. These effects are LPA and S1P receptor-mediated, since the suppressions of ATX mRNA expression were reversed by 1 μM Ki16425, an $LPA_{1/3}$ antagonist (312), and by 1 μM VPC23019, an $S1P_{1/3}$ antagonist (313), respectively (Figure 3.4). Likewise, in cells cultured in FBS, treatment with Ki16425 and VPC23019 increased ATX mRNA levels by blocking signaling by lipids present in FBS (Figure 3.4). Decreases in ATX mRNA expression were also obtained when the delipidated serum (FBSC) was supplemented with 1 μM wls-31 (197, 283), an $LPA_{1/2}$ receptor agonist, or SEW2871, an $S1P_1$ receptor agonist (314, 315) (Figure 3.4).

The effects of LPA and S1P in decreasing ATX mRNA expression were blocked by two inhibitors of phosphatidylinositol 3-kinase, 10 μM LY294002 (316, 317) and 1 μM wortmannin (318, 319) (Figure 3.4). These inhibitors also increased ATX mRNA expression in cells cultured in FBS, but had no effect on their own in cells in delipidated medium (Figure 3.4). Inhibiting ERK activation or protein kinase C with 20 μM PD98059 (320, 321) or 10 μM Gö6983 (322), respectively, had no significant effect on LPA- or S1P-induced decreases in ATX mRNA (results not shown).

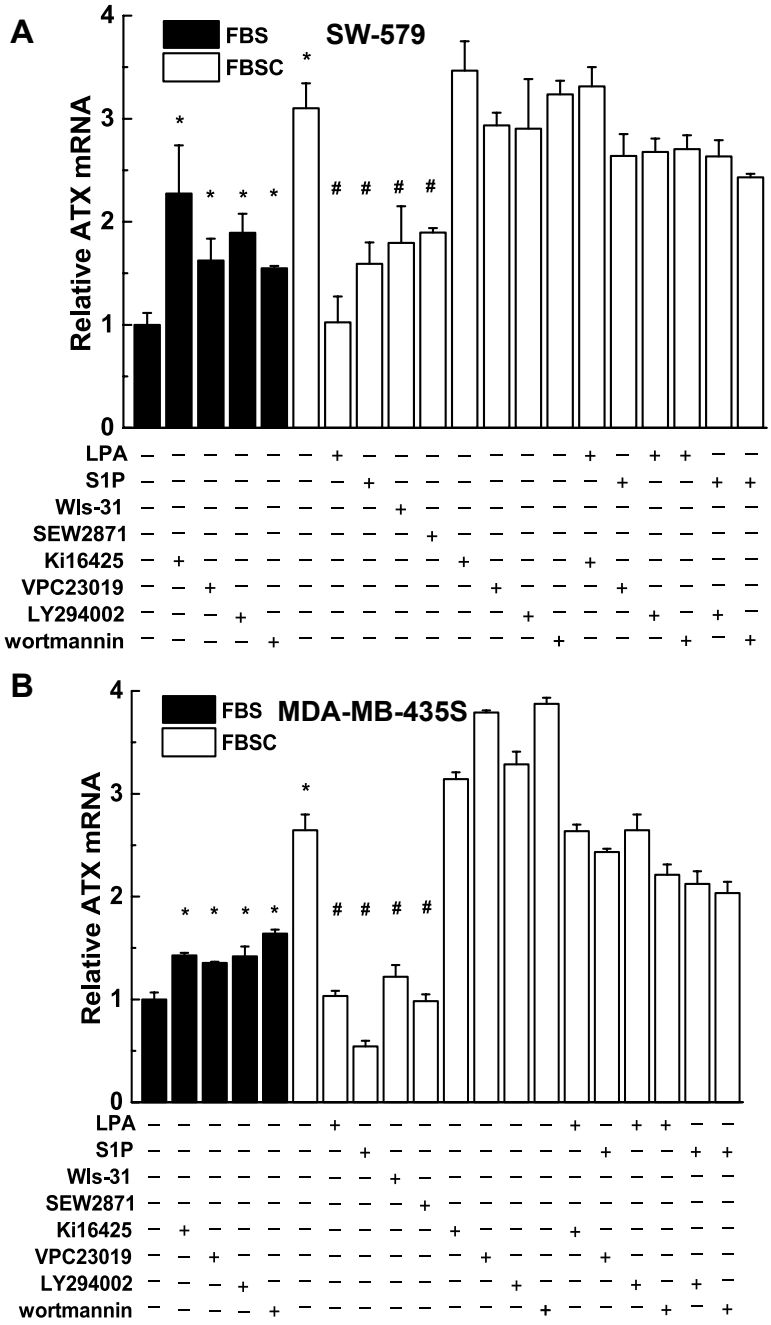

Figure 3.4. LPA and S1P inhibit ATX mRNA expression through LPA and S1P receptor-mediated activation of phosphatidylinositol 3-kinase. A) SW-579 cells and B) MDA-MB-435S were incubated for 24 h in 10% FBS or FBSC in the presence of 5 μM LPA or S1P, agonists (1 μM wls-31 or SEW2871), antagonists (1 μM Ki16425 or VPC23019) and inhibitors (10 μM LY294402 or 1 μM wortmannin) as shown. *, indicates a significant increase ($p<0.05$) in ATX mRNA compared to FBS treatment. #, indicates a significant decrease ($p<0.05$) in ATX mRNA compared to FBSC treatment.

3.3.3 ATX will inhibit its own expression and secretion in the presence of LPC

We also determined if the secretion of ATX by SW-579 thyroid cancer cells and MDA-MB-435S melanoma cells would establish a negative feedback regulatory loop on further ATX production. Cells were incubated in delipidated medium (FBSC) and treated with 100 μM LPC, the substrate for the lysoPLD activity of ATX. This decreased ATX mRNA concentrations, an effect that was reversed by inhibiting ATX activity with either ONO-8430506 or S32826 (Figure 3.5). As controls, we demonstrated that these inhibitors had no significant effects on ATX mRNA levels when added in the absence of LPC, or in the presence of LPA. They were also ineffective when incubated in FBS since FBS contains LPA and S1P (and LPC, although the ATX inhibitors would block additional LPA production) (Figure 3.5). Hence, as predicted, only LPA, or LPA generated from LPC by ATX, but not LPC directly itself, suppresses ATX mRNA expression.

The suppression of ATX mRNA expression by LPA and LPC resulted in decreased secretion of ATX from the cells, as measured by ELISA on conditioned medium (Figure 3.6). Inhibiting ATX activity with ONO-8430506 or S32826 reversed these effects of LPC by blocking the production of LPA (Figure 3.6).

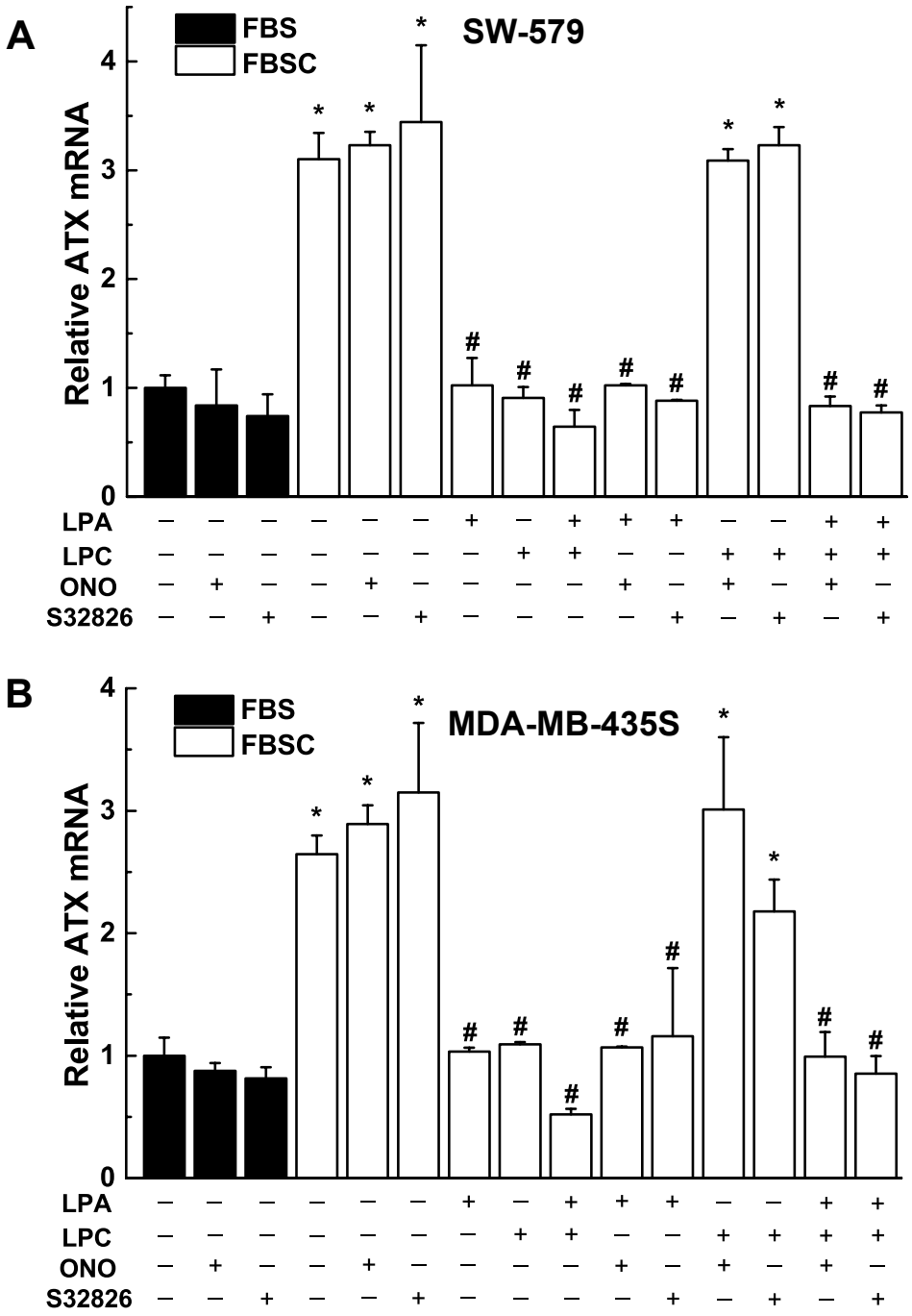

Figure 3.5. LPC-mediated inhibition of ATX mRNA expression is blocked by ATX inhibitors. A) SW-579 cells and B) MDA-MB-435S cells were incubated for 24 h in 10% FBS or FBSC supplemented with 1% BSA in the presence of 5 μM LPA and/or 100 μM LPC with 10 μM of the ATX inhibitors ONO-8430506 or S32826. *, indicates a significant increase ($p<0.05$) compared to FBS treatment. #, indicates a significant decrease ($p<0.05$) compared to FBSC treatment.

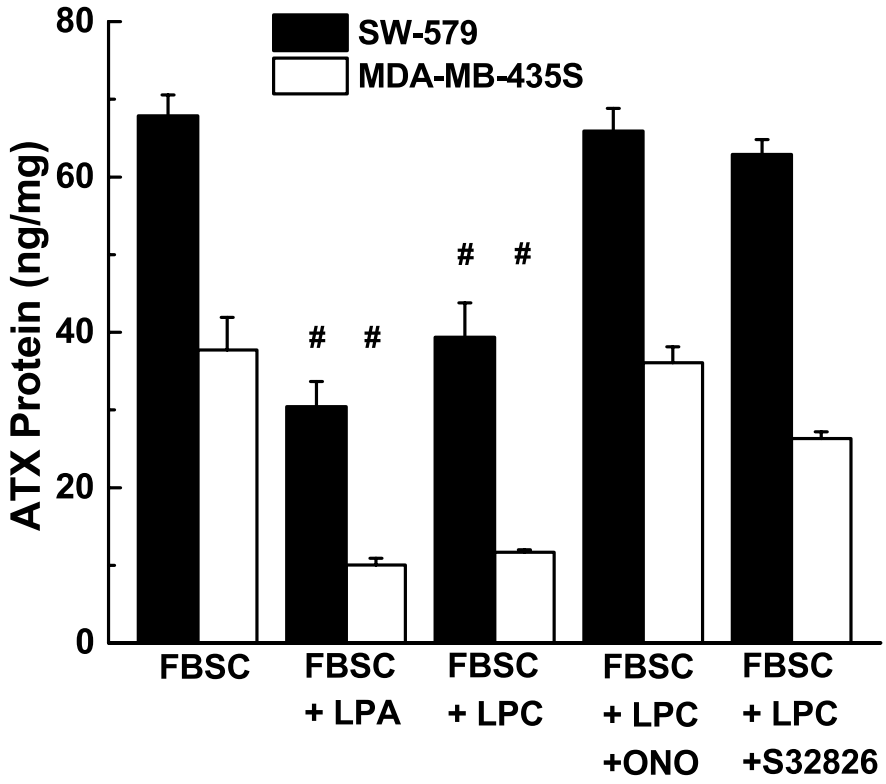

Figure 3.6. LPC-mediated inhibition of ATX protein secretion is blocked by ATX inhibitors. SW-579 and MDA-MB-435S cells were incubated for 48 h in medium containing FBSC with or without 5 μM LPA or S1P and/or 100 μM LPC with 10 μM of the ATX inhibitors ONO-8430506 or S32826. Secreted ATX protein was quantified by ELISA and normalized to both volume of conditioned medium and cell lysate protein content. ATX protein from FBSC was subtracted from the total ATX protein measured after incubation. #, indicates a significant decrease ($p<0.05$) compared to FBSC treatment.

3.4 The effect of ONO-8430506 on plasma ATX activity and lysophospholipid concentrations in mice

Next we wanted to study the relationship between lysophospholipid concentrations and ATX protein *in vivo* by potently inhibiting ATX activity. However, this work would require an ATX inhibitor to be effective for extended periods of time. As discussed in Section 1.7.3, lipid mimetic ATX inhibitors

like S23826 only inhibit ATX activity in circulating plasma on the order of minutes (7). Therefore, we began by first assessing the effectiveness in mice of the non-lipid ATX inhibitor ONO-8430506, a tetrahydrocarboline derivative (285) (Figure 3.7A). This compound was identified by screening an in-house marine library of compounds at Ono Pharmaceuticals Ltd. *Ex vivo*, we determined that ONO-8430506 has subnanomolar IC_{50} for inhibition of ATX activity and an IC_{90} of approximately 100 nM in mouse plasma (Figure 3.7B).

We then demonstrated the biological efficacy of ONO-8430506 in female Balb/c mice, which were gavaged with 10 or 100 mg/kg ONO-8430506 or vehicle (water) for 1 or 4 days, and we collected plasma at both 6 h and 24 h after last treatment. ONO-8430506 concentrations in plasma remained consistently above the IC_{90} after 4 days of treatment, ever 24 h after the last administered dose (Figure 3.7C). Plasma ATX activity was decreased by 50-90% compared to vehicle-treated mice depending on the dose and duration of treatment (Figure 3.7D).

The efficacy of ONO-8430506 in inhibiting ATX activity was also determined by measuring the effects on circulating LPA concentrations. Treatment with either 10 or 100 mg/kg ONO-8430506 for 4 days effectively decreased plasma concentrations of LPA, especially the polyunsaturated species (Figure 3.8). We also demonstrated that ONO-8430506 does not decrease plasma S1P or SA1P concentrations (Figure 3.9).

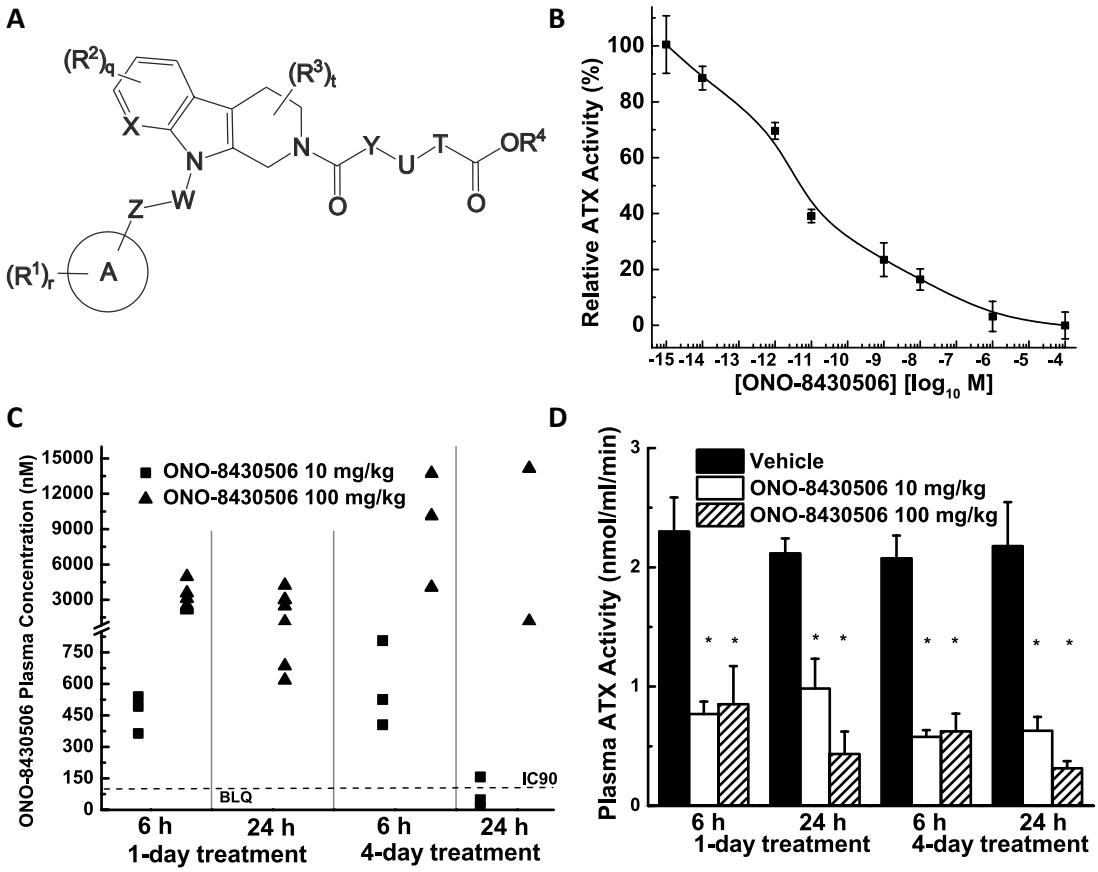

Figure 3.7. ONO-8430506 is a potent ATX inhibitor both *ex vivo* and *in vivo.* A) Generic backbone structure of ONO-8430506 (details available from Patent #WO2012005227). B) Effects of ONO-8430506 on ATX activity in mouse plasma. Results are means ± SEM for plasma from 4 mice. C) Mice were treated with a daily dose of 10 or 100 mg/kg ONO-8430506 for 1 or 4 days and blood plasma was collected at 6 and 24 h after the last dose. Plasma concentrations of ONO-8430506 were measured by mass spectrometry for n = 3-7 mice per group. IC_{90} as determined from (A). BLQ = below level of quantification. D) Mice were treated as in (C) and ATX activity was measured in the blood plasma. Results are means ± SEM for 3 mice per group. *, indicates a significant difference ($p<0.05$) of the ONO-8430506 treatment compared to the corresponding vehicle-treated mice.

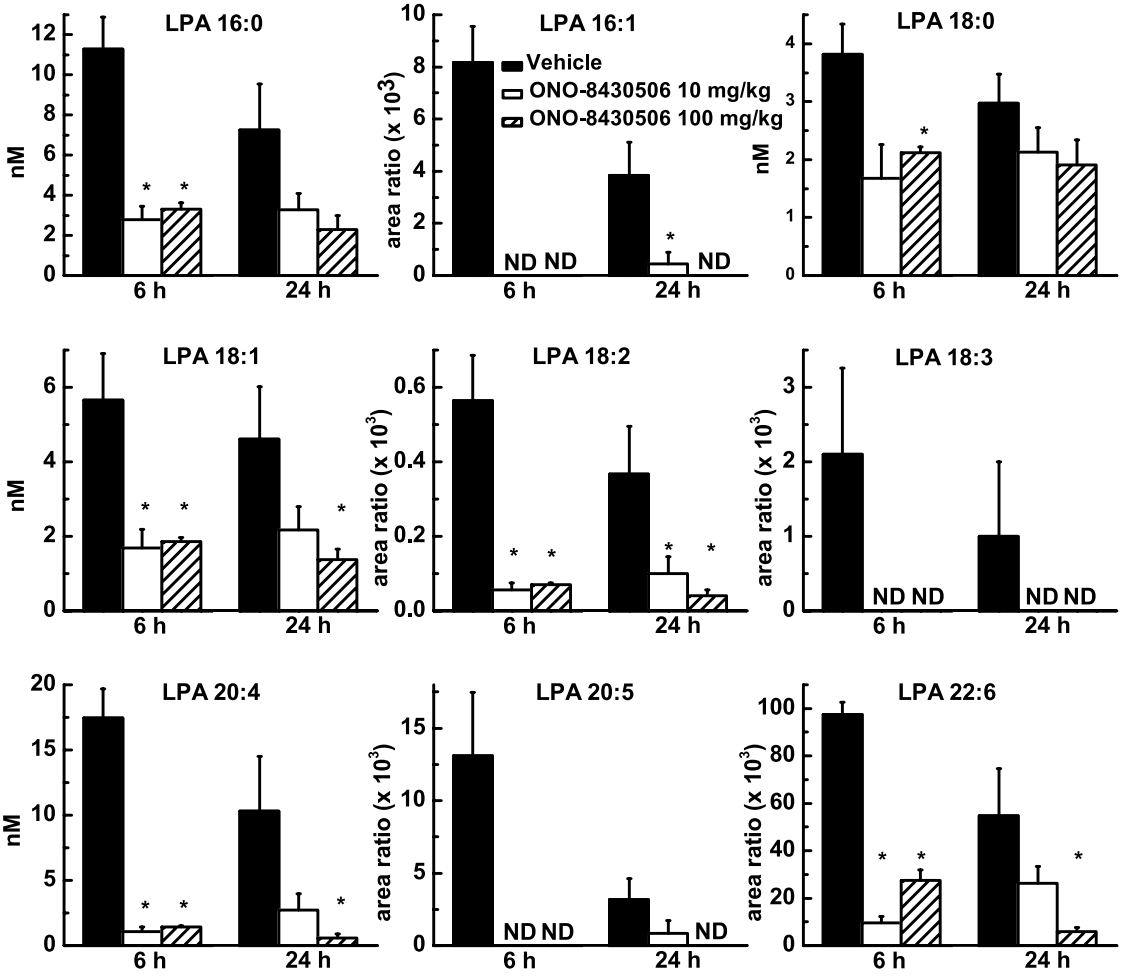

Figure 3.8. Effects of four daily doses of 10 mg/kg ONO-8430506 versus 100 mg/kg ONO-8430506 on plasma molecular species of LPA. Mice were treated daily with 10 or 100 mg/kg ONO-8430506 and blood plasma was collected 6 h and 24 h after last dose. Control mice were gavaged with water. LPA were measured in the blood plasma by comparison to corresponding standards for species 16:0, 18:0, 18:1, and 20:4, or relative to the C17:0-LPA internal standard for the other species. Results are means ± SEM for 3 mice per group. *, indicates a significant difference ($p<0.05$) of the ONO-8430506 treatment compared to the corresponding vehicle-treated mice.

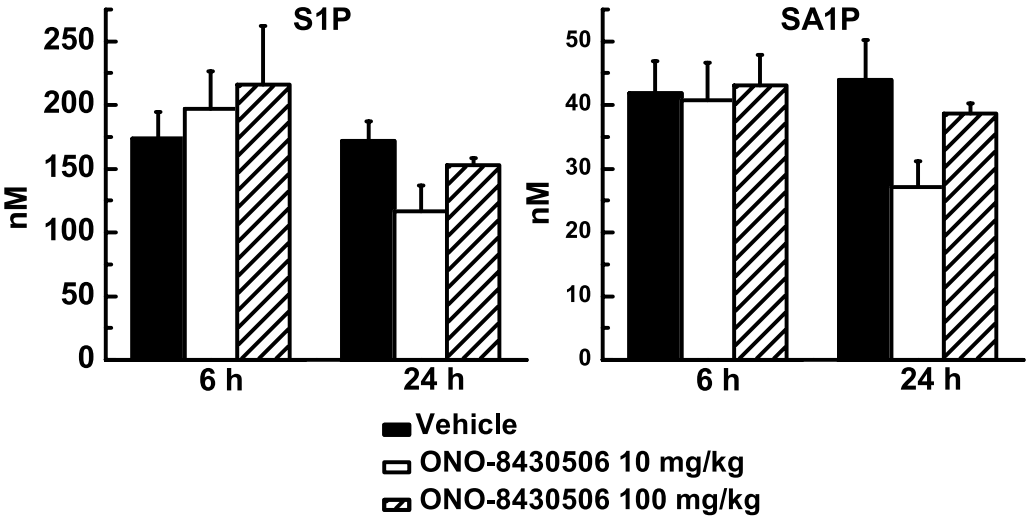

Figure 3.9. ONO-8430506 does not decrease plasma S1P and SA1P concentrations. Mice were treated daily for 4 days with 10 or 100 mg/kg ONO-8430506 and blood plasma was collected 6 h and 24 h after last dose. Control mice were gavaged with water. S1P and SA1P were measured in the blood plasma by comparison to corresponding isotopically-labelled standards. Results are means ± SEM for 3 mice per group. *, indicates a significant difference ($p<0.05$) of the ONO-8430506 treatment compared to the corresponding vehicle-treated mice.

3.5 The effects of ATX inhibition on ATX mRNA expression and protein production *in vivo*

This role of ATX in regulating its own expression was also investigated by treating mice for 4 days with 100 mg/kg ONO-8430506. Adipose tissue is a major source of ATX in the circulation (90, 149, 150, 323), and therefore, we measured the expression of ATX mRNA in the mammary fat pads of the female mice. ATX mRNA were increased by about 5.5-fold in the ONO-8430506-treated mice and this was accompanied by 3-fold increase in the concentration of ATX protein in the plasma (Figure 3.10). We conclude from these results that the expression and secretion of ATX from adipose tissue is suppressed by plasma LPA concentrations. Conversely, decreasing plasma

LPA concentrations increases ATX secretion tissues including adipose tissue, resulting in more ATX in the plasma. However, this ATX is catalytically inhibited (Figure 3.7).

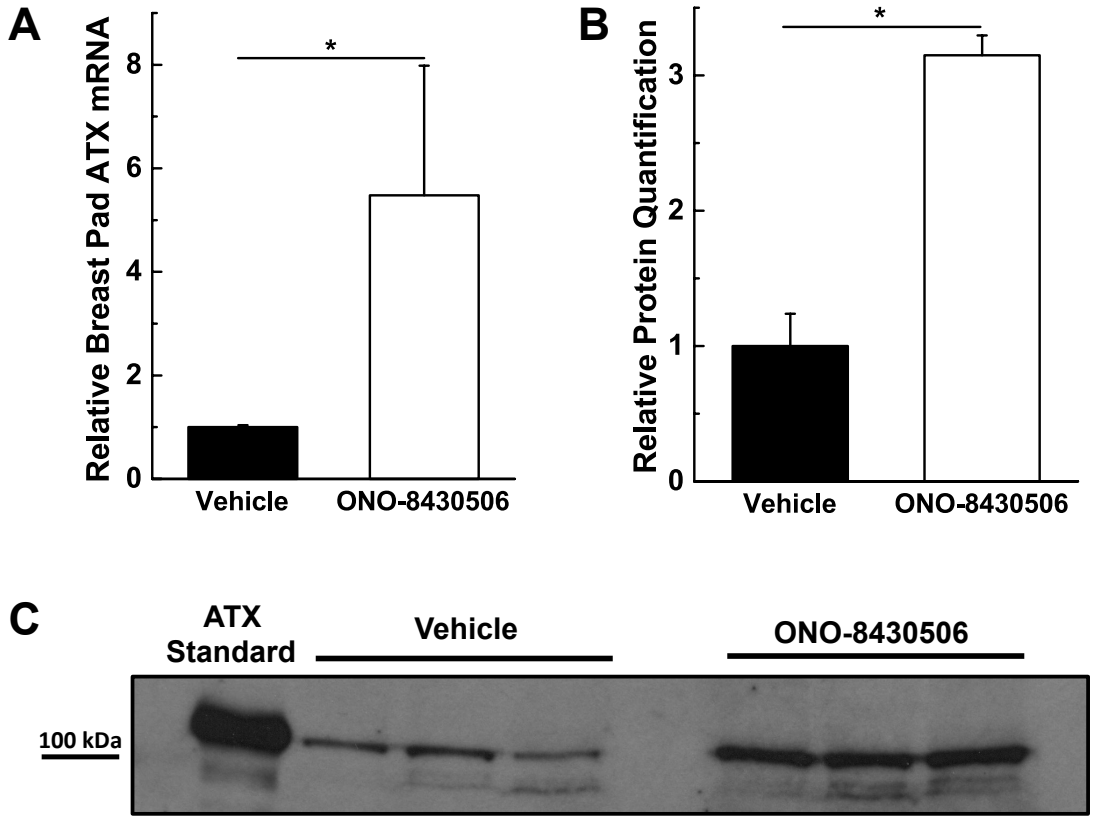

Figure 3.10. Inhibition of ATX activity in mice increases ATX mRNA expression in adipose tissue and ATX protein concentration in plasma. Female mice were treated with 100 mg/kg ONO-8430506 once a day for four days and samples were taken at 6 h after the last treatment. A) ATX mRNA concentrations in breast adipose tissue and (B-C) plasma ATX protein of mice treated with ONO-8430506 compared to vehicle-treated mice. ATX standard is from concentrated MDA-MB-435S conditioned medium. *, indicates a significant change in ONO-8430506-treated mice compared to vehicle-treated mice ($p<0.05$); n=3-5 mice per group.

3.6 Discussion

We conclude from these results that the direct inhibition of ATX activity by LPA and S1P is an artifact caused by using low concentrations of substrate in the activity assay. This type of product inhibition is unlikely to have physiological relevance because of the high availability (200-400 μM) of extracellular LPC. This has implications for ATX inhibitor screening since low concentrations of fluorescent probes are often used to screen libraries of compounds (265, 324). While these probes may be efficient for screening potential compounds, positive hits for ATX inhibition should be verified in the presence of physiological concentrations of LPC before being tested further. We also conclude from our work that activation of phosphatidylinositol-3-kinase through LPA_1 and $S1P_1$ receptors decreases the expression of mRNA for ATX. LPA generated from LPC by ATX suppresses ATX mRNA production and this effect can be blocked by potent ATX activity inhibition. This demonstrates the importance of the secreted ATX producing LPA from LPC in this feedback regulation.

Inhibition of ATX activity *in vivo* and the consequent decrease in plasma LPA increased ATX production in adipose tissue resulting in a higher concentration of ATX protein in the plasma. However, the ATX inhibitor, ONO-8430506 keeps this ATX catalytically inactive as verified by the marked decrease in LPA concentrations. The mechanism by which ATX would normally regulate its own secretion by increasing LPA concentrations is

typical of a physiological feedback loop. It is, therefore, fully expected that a potent ATX inhibitor would increase ATX expression. In fact, such an increase can serve as a surrogate measure of the effectiveness of the inhibitor. In this feedback model, sphingolipid phosphate concentrations were not changed. This is consistent with prior evidence that ATX+/- mice have about half the amount of plasma LPA whereas concentrations of S1P are not affected (5, 6). Overall, this work has established a novel regulation of ATX expression where LPA and S1P can block ATX production and secretion. We will show that this regulation is overcome by inflammatory cytokines in Chapter 4, thus explaining why high LPA levels and high ATX expression can coexist in inflammatory conditions. The work in this Chapter also demonstrates that ONO-8430506 is a potent and highly bioavailable oral ATX inhibitor suitable for therapeutic studies.

CHAPTER 4

INVESTIGATIONS OF AUTOTAXIN INHIBITION ON BREAST TUMOR GROWTH AND INFLAMMATORY-MEDIATED PRODUCTION OF AUTOTAXIN IN MAMMARY ADIPOSE TISSUE

4.1 Introduction

Breast cancer is the most common malignancy among women and about 33% of these women die from metastases (325). Treatments of breast cancer often fail because of the development of resistance to chemotherapy and radiotherapy (326). We propose that LPA contributes to these problems (10, 164). LPA has received little attention compared to our knowledge of the adverse effects of estrogens and epidermal growth factor (EGF) in different types of breast cancer. Currently, there are no cancer therapies targeting LPA signaling and this provides an exciting opportunity for developing novel strategies for improving cancer therapy.

The importance of LPA to breast cancer progression and cancer therapy resistance has been discussed in Section 1.6. Based on that evidence, we hypothesized that inhibiting ATX activity and LPA production should decrease breast tumor growth and metastasis. In these studies, we chose to study the effects of ATX inhibition using ONO-8430506 in a syngeneic mouse model of breast cancer in which there is an intact immune system. Balb/c 4T1 breast cancer is a model for aggressive triple negative (no estrogen receptor, progesterone receptor, or her2/neu) breast cancer (327). Most chemotherapies target at least one of these receptors, meaning their absence reduces treatment options (328). Patients with triple negative breast cancer overall have higher relapse rates and poorer survival outcomes (329). The 4T1 breast cancer system easily metastasizes early in tumor

development (287, 330). Hence this system is also used to model metastatic stage IV breast cancer (287, 331). Overall, this system represents a very aggressive cancer system for which more therapeutic options are required.

Since LPA is also known to induce treatment resistance, we also tested if ATX inhibition would improve the therapeutic efficacy of doxorubicin, a common first-line breast cancer treatment that works in part by intercalating DNA, impairing DNA replication. Finally, we also examined the relationship between LPA and ATX levels in cancer, a pathological inflammatory condition, and compared these results to the physiological situation described in Chapter 3.

4.2 Evaluation of ONO-8430506 ATX inhibition monotherapy and combination therapy with doxorubicin on breast tumor growth and metastasis

In initial monotherapy studies, having shown that both 10 mg/kg and 100 mg/kg dosages were equally effective at blocking ATX activity and decreasing plasma LPA levels (Figures 3.7 & 3.8), we treated mice with 10 mg/kg/day of ONO-8430506 from day 1 after the injection of 4T1-12B or 4T1 cells to determine the effects on tumor growth. ONO-8430506 decreased tumor volume by about 60% up to about day 11 (Figure 4.1A inset). Excised tumors were on average 2.5-times smaller in the ONO-8430506-treated group (Figure 4.1B) and identical results were obtained from mice injected with 4T1-

12B or 4T1 cells (Figure 4.1). Treatment with ONO-8430506 of some mice injected with 4T1 cells was continued until day 21. Tumor growth in ONO-8430506-treated mice caught up to the vehicle group by day 13 and thereafter, primary tumor size was not significantly different from the vehicle-treated mice (Figure 4.1A).

We next tested the ability of ONO-8430506 to enhance the effects of doxorubicin in decreasing tumor progression. We chose a low dose of doxorubicin that had relatively little effect in blocking breast tumor growth (Figure 4.2 inset). However, the effectiveness of both doxorubicin and ONO-8430506 were enhanced significantly when they were combined until about day 20 (Figure 4.2). Towards the end of the experiment, doxorubicin treatments had decreased both the body weights and white blood cell counts of the mice while ONO-8430506 was well tolerated without obvious side effects on body mass or white blood cell counts (Figure 4.3).

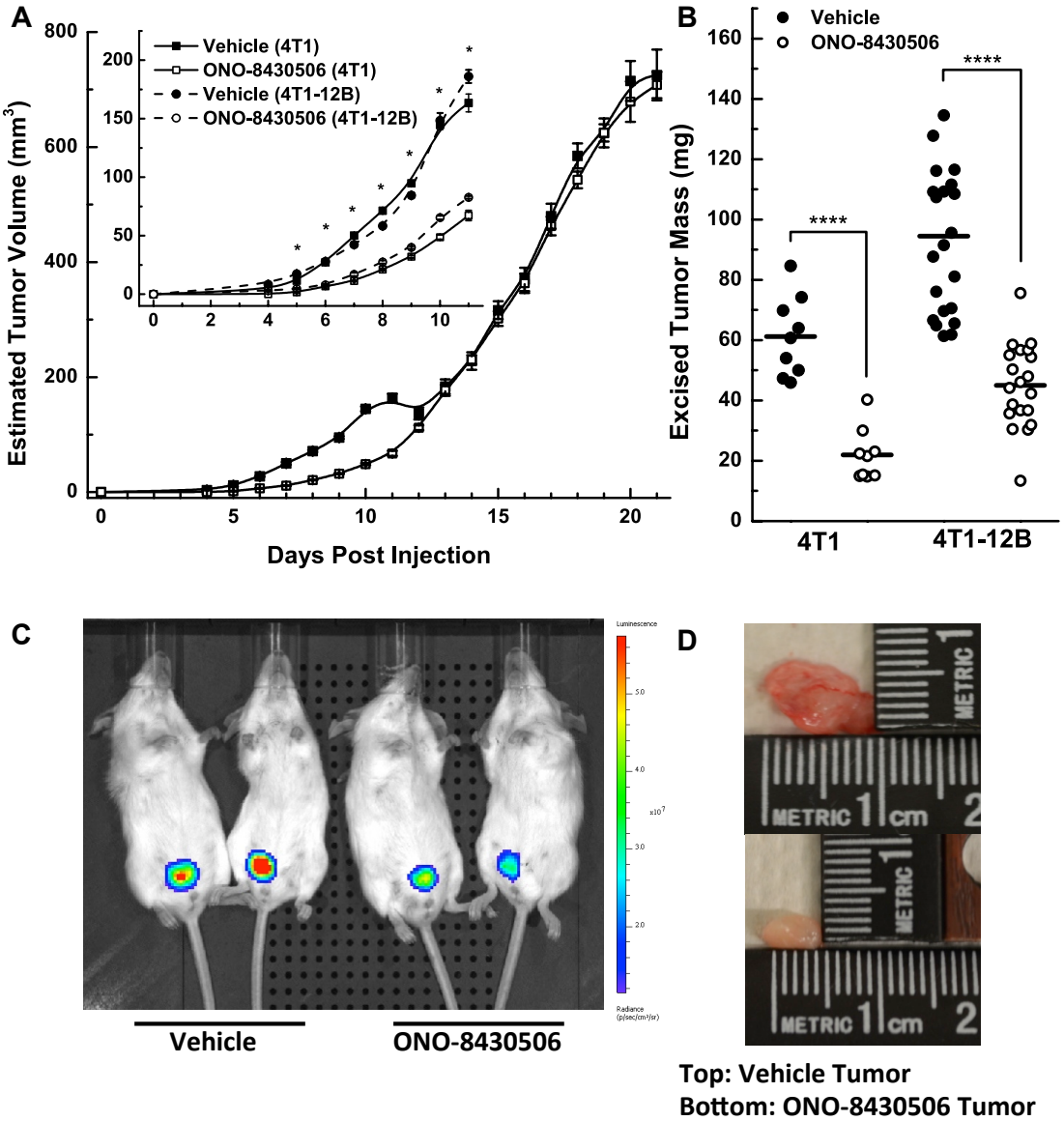

Figure 4.1. ONO-8430506 monotherapy slows the initial growth of 4T1 and 4T1-12B breast tumors. A) Estimated primary tumor size of mice injected with 4T1 (to day 21) and 4T1-12B (to day 11) tumor cells and gavaged daily with either vehicle or ONO-8430506 10 mg/kg. Tumor volume = width^2 x length/2. Results are means ± SEM for 20-26 mice per group pooled from at least two independent experiments for each 4T1 cell type. The insert shows that estimated tumor growth up to day 11. *, indicates a significant difference between vehicle- and ONO-8430506-treated mice ($p<0.05$). B) Masses of primary tumors formed from 4T1 and 4T1-12B at day 11. n = 9-26 per group from at least two independent experiments. Tumors from control mice were about 2.5 times heavier than from ONO-8430506-treated mice (****, $p<10^{-6}$). C) D-luciferin imaging of vehicle- and ONO-8430506-treated mice with 4T1-12B-derived tumors at day 11. D) Representative photographs of day 11-excised tumors.

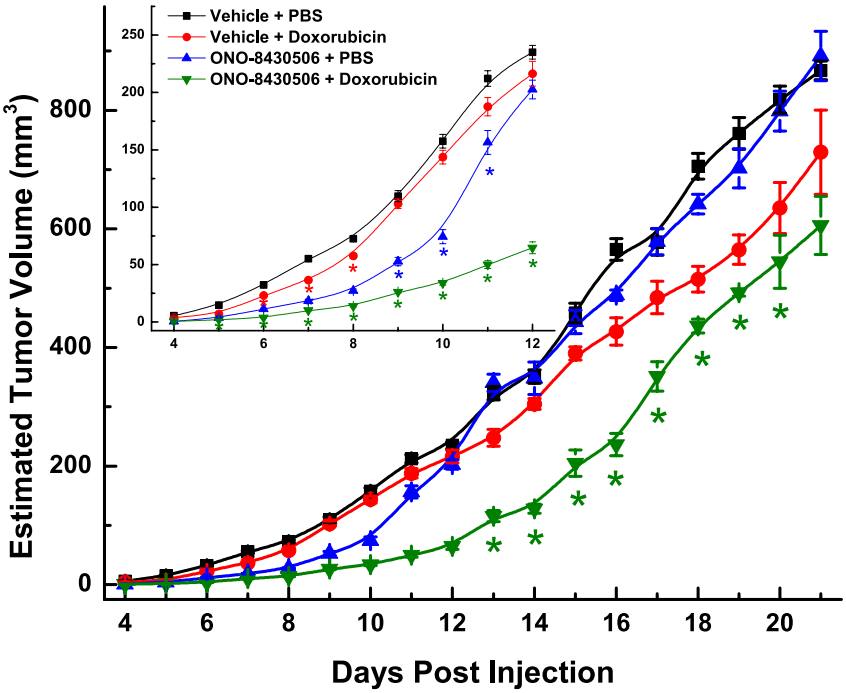

Figure 4.2. Combination of ATX inhibition with doxorubicin treatments produces a synergistic effect in decreasing breast tumors in mice. Mice with 4T1 tumors were gavaged daily with vehicle or 10 mg/kg ONO-8430506. They were injected intraperitoneally with PBS or doxorubicin (4 mg/kg) every third day starting from day 3 after the injection of 4T1 cells. Tumor volumes are shown until day 21 and the inset shows an expanded view up to day 12. Results are means ± SEM for 9 mice per group. *p<0.05 compared to vehicle treatment.

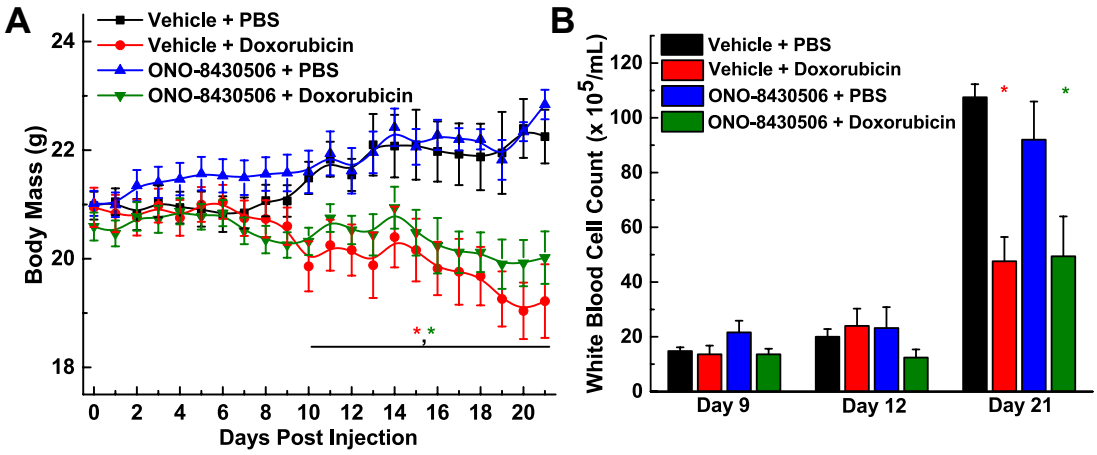

Figure 4.3. ONO-8430506 does not affect mouse body mass (A) or white blood cell count (B). Results are means ± SEM for 9 mice per group. *p<0.05 compared to vehicle treatment.

In initial studies with ONO-8430506 monotherapy, we found that spontaneous lung macrometastasis was decreased by 60% with ATX inhibition (Figure 4.4A). In combination studies, we found that doxorubicin therapy combined with ONO-8430506 further suppressed both spontaneous lung and liver micrometastases compared to either treatment alone (Figure 4.4B). This reduction in metastasis probably follows from the decreased tumor growth as in an experimental metastasis model where 4T1 cells are injected into the tail-vein, only the combination therapy significantly decreased lung metastasis (Figure 4.4C). This demonstrates that ATX inhibition sensitizes cells in both the primary tumor and at metastatic sites to doxorubicin therapy.

Next, we turned our investigations to the primary tumor to study the effects of drug treatment on tumor growth. First, like in the plasma (Figure 3.8), we found that ONO-8430506 also significantly decreased the concentrations of LPA (C16:0, C16:1, C18:1, C18:2 C18:3, C20:4) in the tumor (Figure 4.5A). The decreases in the polyunsaturated species of LPA are consistent with the inhibition of ATX in the tumor rather from an effect because of decreases in the *de novo* synthesis of phospholipids within the tumor. There was a trend towards decreased concentrations of S1P and SA1P, but this did not reach statistical significance (Figure 4.5B).

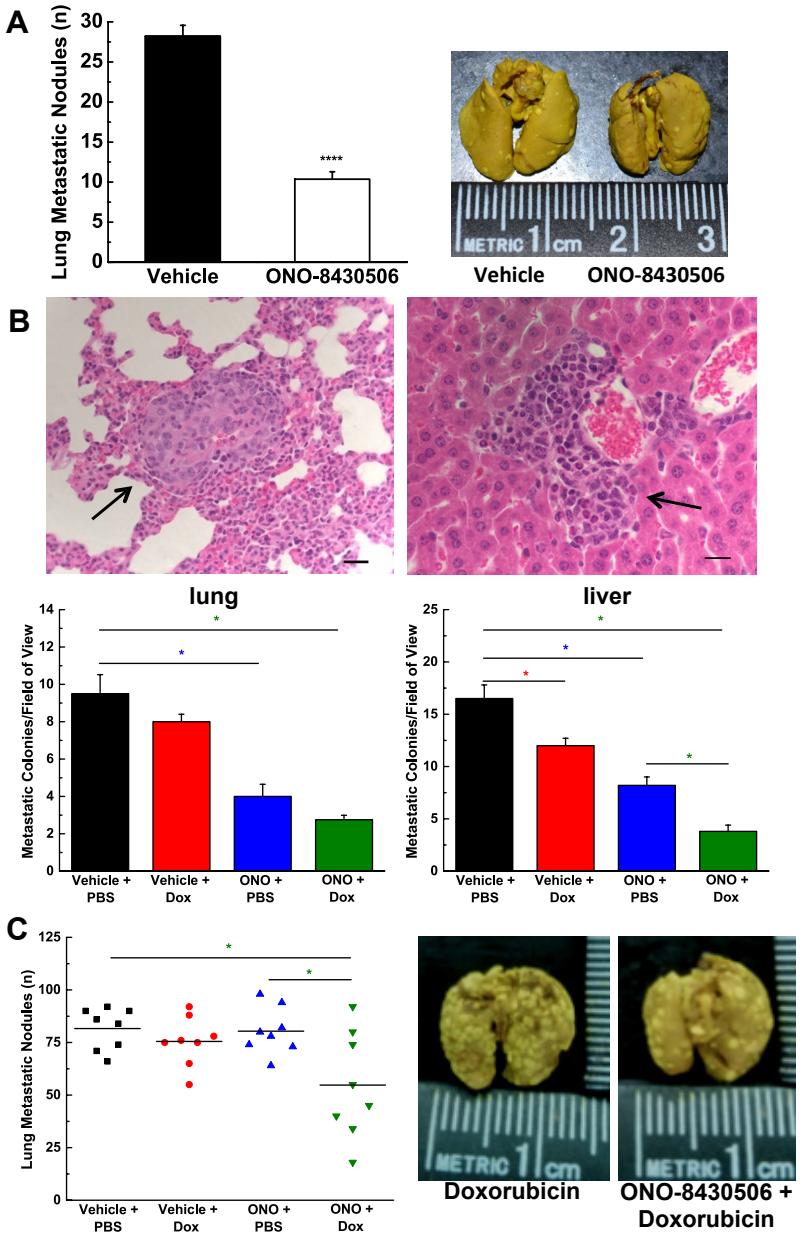

Figure 4.4. ATX inhibition combined with doxorubicin decreases spontaneous and experimental metastasis in mice. A) Numbers of visible lung metastatic nodules in mice with tumors collected at day 21 (means ± SEM for 10 mice/group; ****, $p<10^{-9}$). Representative photograph of lungs stained with Bouin solution. B) Quantification of lung and liver spontaneous micrometastases from hematoylin and eosin-stained sections after 21 days of tumor growth from the experiment in Figure 4.2 (means ± SEM for 4 mice/group). Scale bar = 25 μm. C) Lung metastatic nodule counts from mice 14 days after tail vein injection of 4T1 cells, and representative images of stained lungs. The left lung of 8 mouse lungs from each group was counted for macroscopic nodules (*, $p<0.05$ by ANOVA).

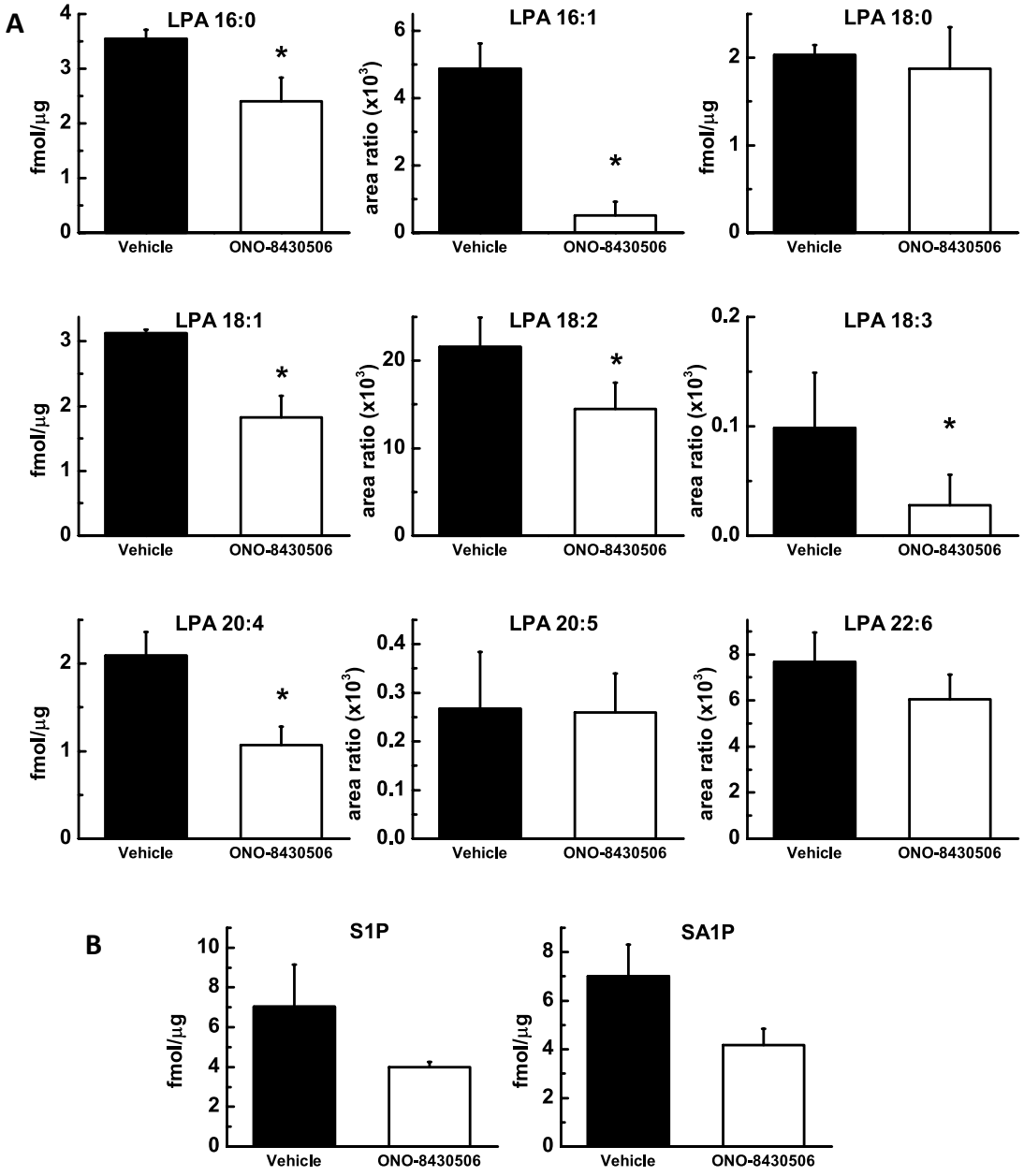

Figure 4.5. Effects of ONO-8430506 on the concentrations of lysophospholipid molecular species in 4T1 breast tumors. LPA molecular species (A), but not S1P and SA1P (B) were suppressed in 4T1 tumors at day 11 treated with ONO-8430506. Mice were treated daily with 10 mg/kg ONO-8430506 and lysophospholipids were analyzed in the tumors 6 h after the last treatment. Lysophospholipid quantities were normalized to protein extracted. Control mice were gavaged with water. Results are means ± SEM for 4-5 mice per group. *, indicates a significant difference ($p<0.05$) of the ONO-8430506 treatment compared to the corresponding vehicle-treated mice.

ONO-8430506-treated tumors showed about a 1.8-fold decrease in staining for Ki67, a marker of cell division, compared to vehicle-treated tumors. Ki67 levels were also decreased by doxorubicin treatment, but there was no additive effect with ONO-8430506 (Figure 4.6A). Combination therapy did significantly increase apoptosis compared to vehicle treatment as assessed by cleaved caspase 3 staining (Figure 4.6B). There was no effect seen on angiogenesis as assessed by staining blood vessel epithelial cells with CD-31 (not shown).

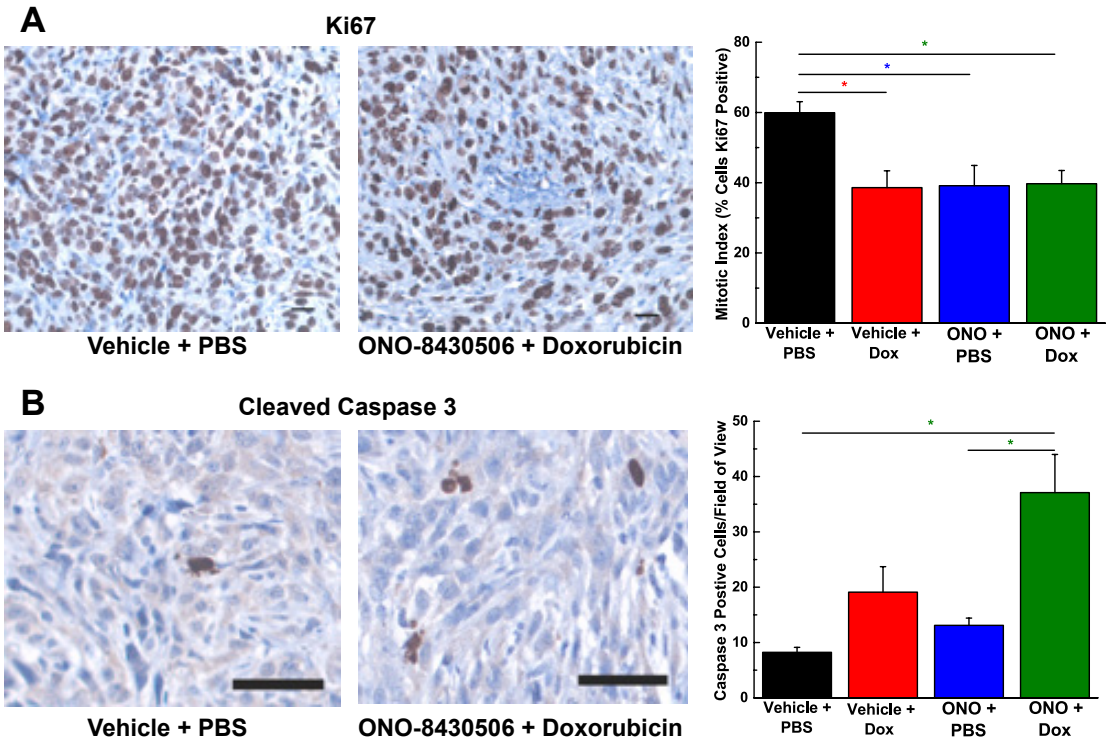

Figure 4.6. Combination of ATX inhibition with doxorubicin reduces the rate of cell division and increases apoptosis in 4T1 tumors. A) Representative images of staining for Ki67, a marker of cell proliferation, and quantification of the number of positive cells (mitotic index). B) Representative images of staining for cleaved caspase 3, a marker of apoptosis, and quantification of the number of positive cells per field of view. Scale bar = 25 μm. Results are means ± SEM from 3-6 mice/group; *, $p<0.05$ by ANOVA.

4.3 ATX expression profiles in breast tumors and mammary adipose tissue

4.3.1 Effects of LPA, LPC and ONO-8430506 on 4T1 cell growth *in vitro*

In the previous section, we demonstrated that ONO-8430506 slows tumor growth *in vivo*. Therefore, in cell culture, we predicted that LPA ought to increase cell growth rates. Incubation of 4T1 breast cancer cells with 5 μM LPA for 24 h increases cell growth rates by 40% compared to no treatment (Figure 4.7). However, incubation with 100 μM LPC does not increase cell growth (Figure 4.7). Our interpretation from this finding is that 4T1 cells do not secrete enough ATX to produce meaningful quantities of LPA from LPC and this will be examined below. Also, incubation with ONO-8430506 does not slow cell growth (Figure 4.7). Therefore, the effects of ONO-8430506 monotherapy on slowing tumor growth *in vivo* appear to be cytostatic rather than cytotoxic through depletion of LPA as a growth factor for the tumor. This is consistent with our immunohistochemistry findings where ONO-8430506 monotherapy deceases Ki67 staining but does not affect cleaved caspase 3 staining (Figure 4.6).

Hence, we conclude that ONO-8430506 slows tumor growth in our 4T1 breast cancer model by inhibiting ATX production by a non-cancer cell source that produces the LPA cancer cells use for tumor progression.

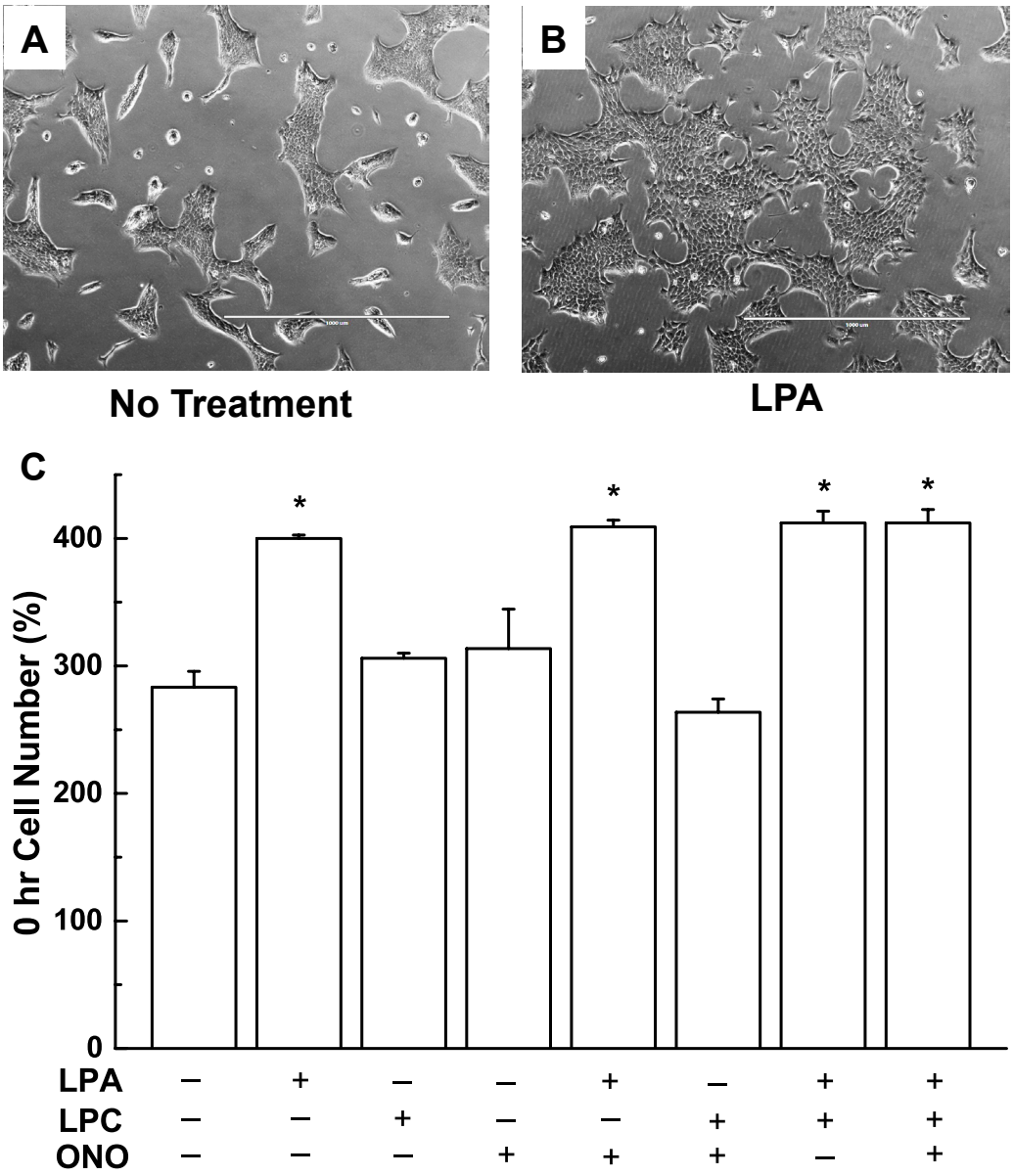

Figure 4.7. LPA, but not LPC, stimulates 4T1 cell growth *in vitro* and ONO-8430506 does not affect this growth. 4T1 cells were grown for 24 h in starvation medium supplemented with 1% BSA with or without 5 μM LPA, 100 μM LPC, and/or 20 μM ONO-8430506. Cells were then trypsinized and counted with a hemocytometer. A) Photographs of control cells and B) cells treated with LPA. Scale bar = 1000 μm. C) Counts of cells at the end of the 24-h treatment. Each sample represents three independent experiments and results are means ± SEM. *, indicates a significant increase in cell number compared to no treatment ($p<0.05$).

4.3.2 ATX expression within the 4T1 breast tumor

We performed immunohistochemistry for ATX on 4T1-12B tumors collected after 11 days of tumor growth, and compared the staining pattern to that of fibroblast activation protein (FAP) to identify the tumor stroma, and for firefly luciferase to identify the 4T1-12B cancer cells exclusively (Figure 4.8A-E). ATX staining was predominately within the stromal components.

To demonstrate that ATX in the tumor was predominately produced by stromal cells in the tumor microenvironment (Figure 4.8F), we digested fresh tumors and sorted them by fluorescence-activated cell sorting (FACS) into cancer cells, leukocytes, endothelial cells and fibroblasts. This was achieved by using cell surface antigen markers whose expressions are highly enriched in each respective cell population (299-301). mRNA measurements for ATX on the sorted populations demonstrated that cancer cells express very low ATX compared to stromal cell populations (Figure 4.8G). ATX mRNA levels are about 100-fold higher in enriched fibroblasts compared to cancer cells. These fibroblasts are derived from the mammary tissue, suggesting that mammary tissue expresses more ATX than do the cancer epithelial cells.

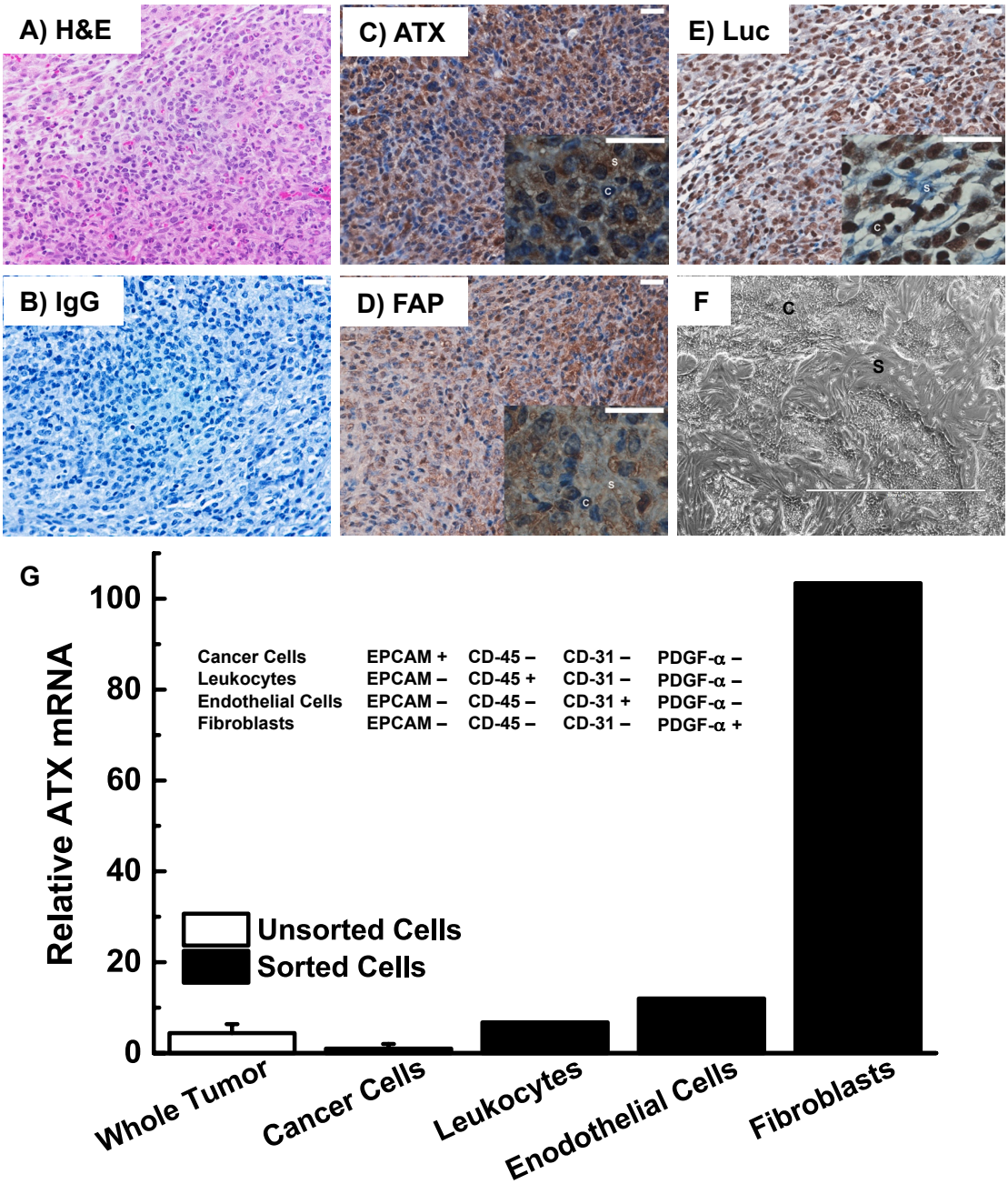

Figure 4.8. ATX production in 4T1 tumors is confined to stromal cell populations. A) Hematoxylin and eosin (H&E) staining of a 4T1-12B tumor. B) IgG isotype control. Representative staining for C) ATX, D) FAP (fibroblast activation protein) and E) firefly luciferase (Luc). "C" is an illustrative 4T1-12B cancer cell as indicated by firefly luciferase staining, and "S" is tumor stroma. Scale bar = 25 μm. F) A digested and plated 4T1 tumor reveal a heterogenous cell population of cancer (C) and stromal cells (S). Scale bar = 1000 μm. G) ATX expression in 4T1 tumors comes predominantly from cancer-associated fibroblasts (preliminary results). Whole 4T1 tumors were enzymatically digested and sorted by FACS for cancer cells (epithelial

cells) using EPCAM (epithelial cell adhesion molecule), leukocytes using CD-45, endothelial cells using CD-31, and cancer-associated fibroblasts (CAFs) using platelet-derived growth factor alpha (PDGFα). ATX mRNA was quantified by qRT-PCR relative to *GAPDH* in whole tumors (unsorted tumor digest) and compared to FACS-sorted populations. n=3 each for whole tumor and cancer cells (means ± SEM), and currently n=1 for the other cell populations.

4.3.3 ATX expression within human breast tumors and the Hs578T/ Hs578Bst system

We next measured ATX mRNA expression in human breast tumors from microarray data and compared their levels to normal mammary adipose tissue obtained from breast reduction surgeries. ATX mRNA levels in tumors were about four-fold lower than from breast tissue (Figure 4.9A). This is consistent with breast cancer cells that make up the majority of cells in the tumor expressing lower ATX levels than the mammary tissue. Consistent with other work, we could not correlate ATX expression in tumors to any clinical outcomes (not shown) (332).

We also characterized ATX mRNA and activity levels in cell cultures of Hs578T triple negative breast cancer cells and Hs578Bst myoepithelial stromal cells, which were derived from normal tissue peripheral to the tumor (333). Despite Hs578T expressing a relatively high amount of ATX (3rd largest expresser out of 58 breast cancer cells lines in the Cancer Cell Line Encyclopedia (Figure 1.9)) (184), Hs578Bst cells express even higher quantities of ATX mRNA, and this expression translates into more secreted ATX into the cell culture medium (Figure 4.9B).

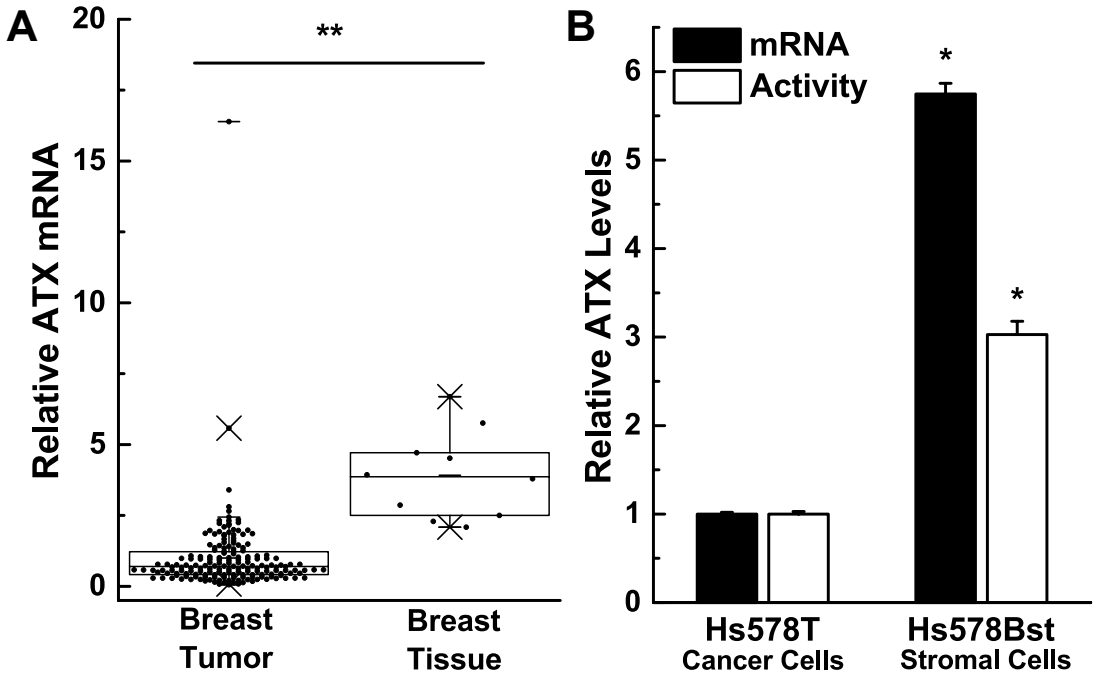

Figure 4.9. Human breast tumors express less ATX mRNA than mammary breast tissue and this pattern is modeled in the Hs578T/Hs578Bst system. A) ATX mRNA in human breast cancer tumors (n=176) is about four-fold lower that in normal breast tissue (n=10); **, $p<0.0001$. Box plots show minimum, mean, and maximum values (-), 25th, 50th, and 75th percentiles (box), and 1st and 99th percentiles (x). B) Both ATX mRNA and activity are significantly higher in Hs578Bst stromal cells compared to patient-matched Hs578T cancer cells. Results are means ± SEM from three independent experiments, *, $p<0.05$.

We also performed immunohistochemistry for ATX on human breast tumors and contiguous normal breast tissue, and found that stromal cells within the tumor stain 2.9 times more intensely than stromal cells in the breast tissue (Figure 4.10). We, therefore, conclude that breast cancer cells express little ATX relative to stromal cells and breast tumors overall express lower ATX quantities than normal mammary tissue. It appears that the proximity of stromal cells to cancer cells is positively associated with high ATX expression. This prediction was tested.

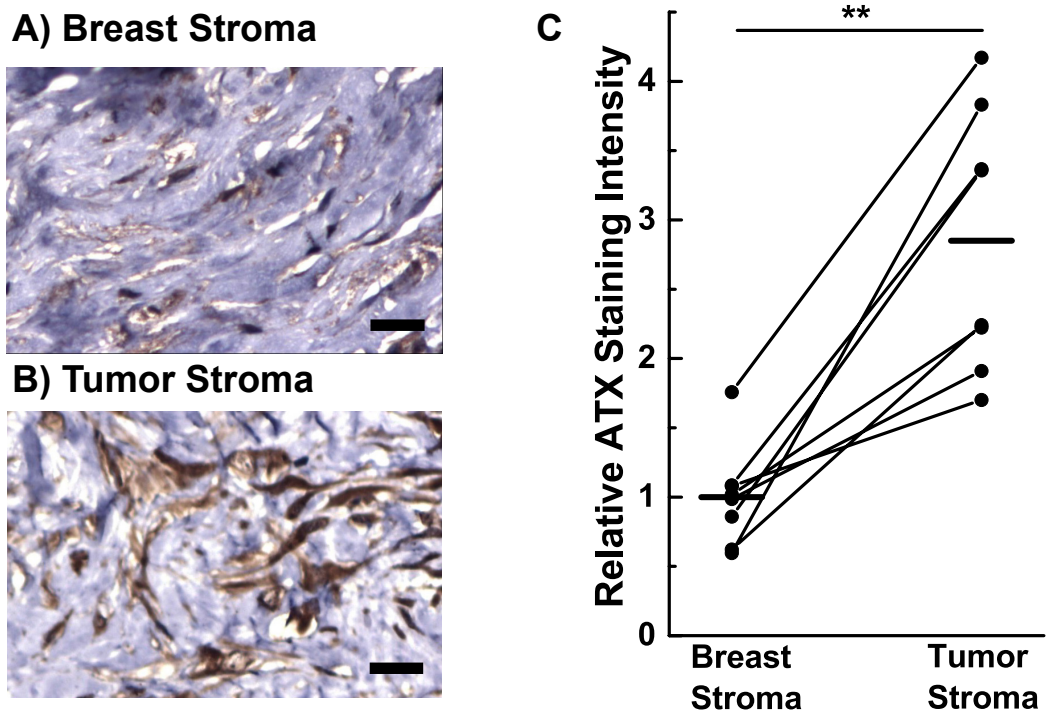

Figure 4.10. Stromal cells within a human breast tumor express more ATX than stromal cells in breast tissue adjacent to a tumor. Slides were prepared from paraffin-embedded tissue containing the tumor and contiguous breast tissue adjacent to the tumor. Representative photographs of ATX immunohistochemistry in A) breast tissue stroma and B) tumor stroma from the same patient on the same slide. Scale bar = 25 μm. C) Quantification of ATX staining intensity by ImageJ analysis for n=8 specimens with the means indicated by horizontal bars. **, $p<0.001$ by paired t-test.

4.4 Effects of 4T1 breast tumor development on ATX production in adjacent mammary adipose tissue and plasma ATX and LPA levels

We measured ATX mRNA in the fat pad surrounding the tumor at days 11, 16, and 21 compared to the contralateral fat pad that did not contain tumor. In all samples, the presence of the tumor increased ATX mRNA expression in the fat pad by up to 3-fold relative to the contralateral pad (Figure 4.11A). As a control, injection of 50% Matrigel into the breast pad

without 4T1 cells did not significantly alter ATX mRNA. Also, ATX mRNA expression in these fat pads from mice that did not have breast tumors was about 3-fold lower than in the contralateral normal fat pad of tumor-bearing mice. Significantly, ATX mRNA in the tumor was >1500 times higher than in the 4T1 cells used for the injection and >30,000 times higher in the breast tissue surrounding the tumor (Figure 4.11A).

mRNA levels for ATX were reflected by ATX activity, which was at least 2-fold higher in the fat pad containing the cancer compared to the contralateral pad. The sham injection with Matrigel had no significant effect on ATX activity (Figure 4.11B).

Plasma ATX activity and protein levels increased in tumor-bearing mice after day 16 (Figure 4.12A,B). Treatment with ONO-8430506 suppressed this increase in ATX activity at 24 h after last gavage and it decreased ATX activity by > 90% at 6 h (Figure 4.12A). Plasma ATX activity did not change during the experiment in littermates that were gavaged with the vehicle and were not injected with cancer cells (Figure 4.12A). This increase in ATX activity correlated to increases in plasma LPA but not S1P levels in mice with day-21 tumors (Figure 4.12C).

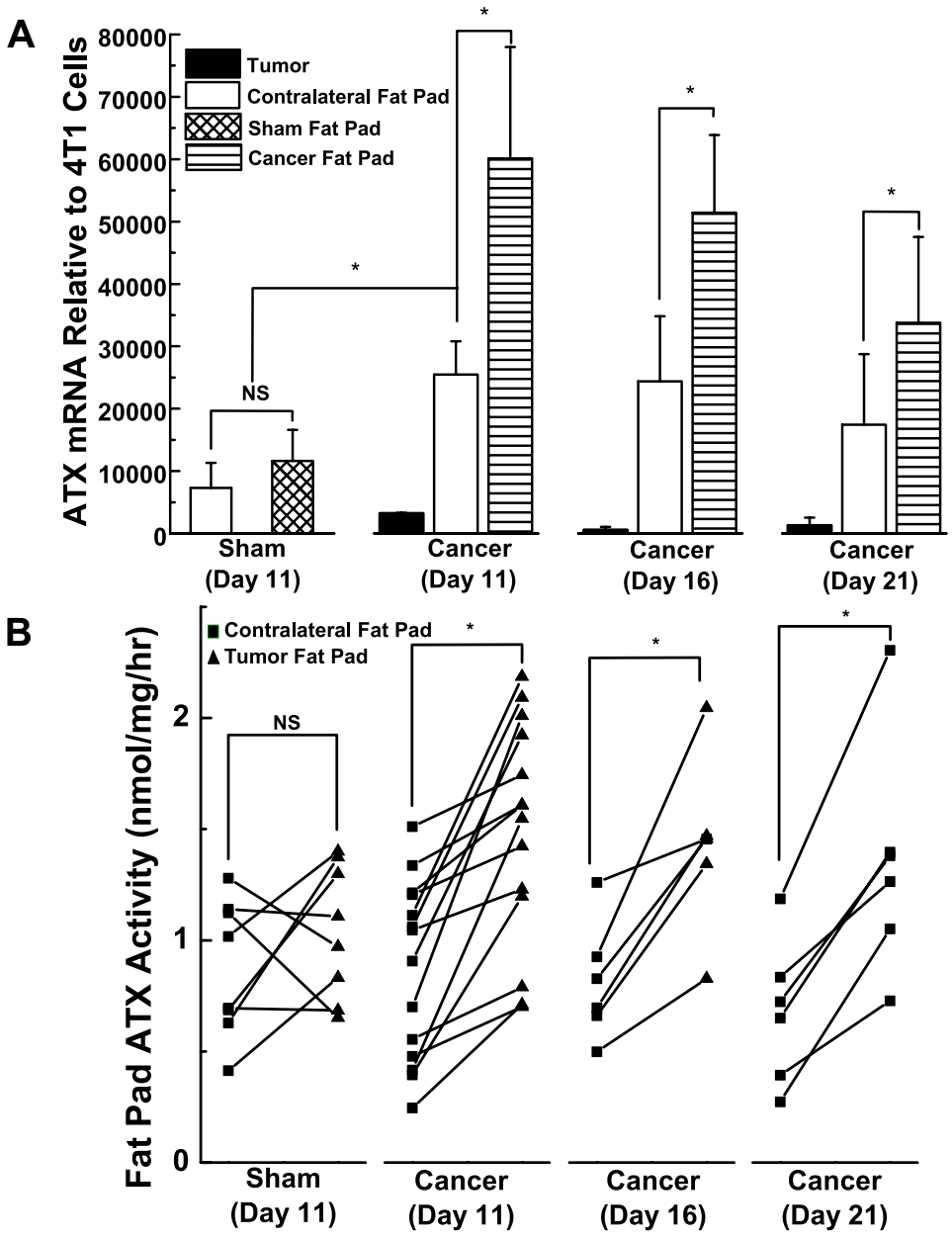

Figure 4.11. ATX expression in the mammary fat pad increases with 4T1 breast tumor growth. A) ATX mRNA levels, relative to that in the 4T1 cells, are shown for the contralateral fat pad versus the sham injection breast pad collected at day 11, and to tumors and paired contralateral breast pads/breast pads surrounding the tumor collected at days 11, 16 and 21. Results are means ± SEM with 6-14 mice per group. *, indicates significant difference ($p < 0.05$) by paired t-test between the two fat pads. NS = not significant. B) ATX activity in homogenates of paired breast fat pads from (A). *, indicates significant difference ($p < 0.05$) by paired t-test.

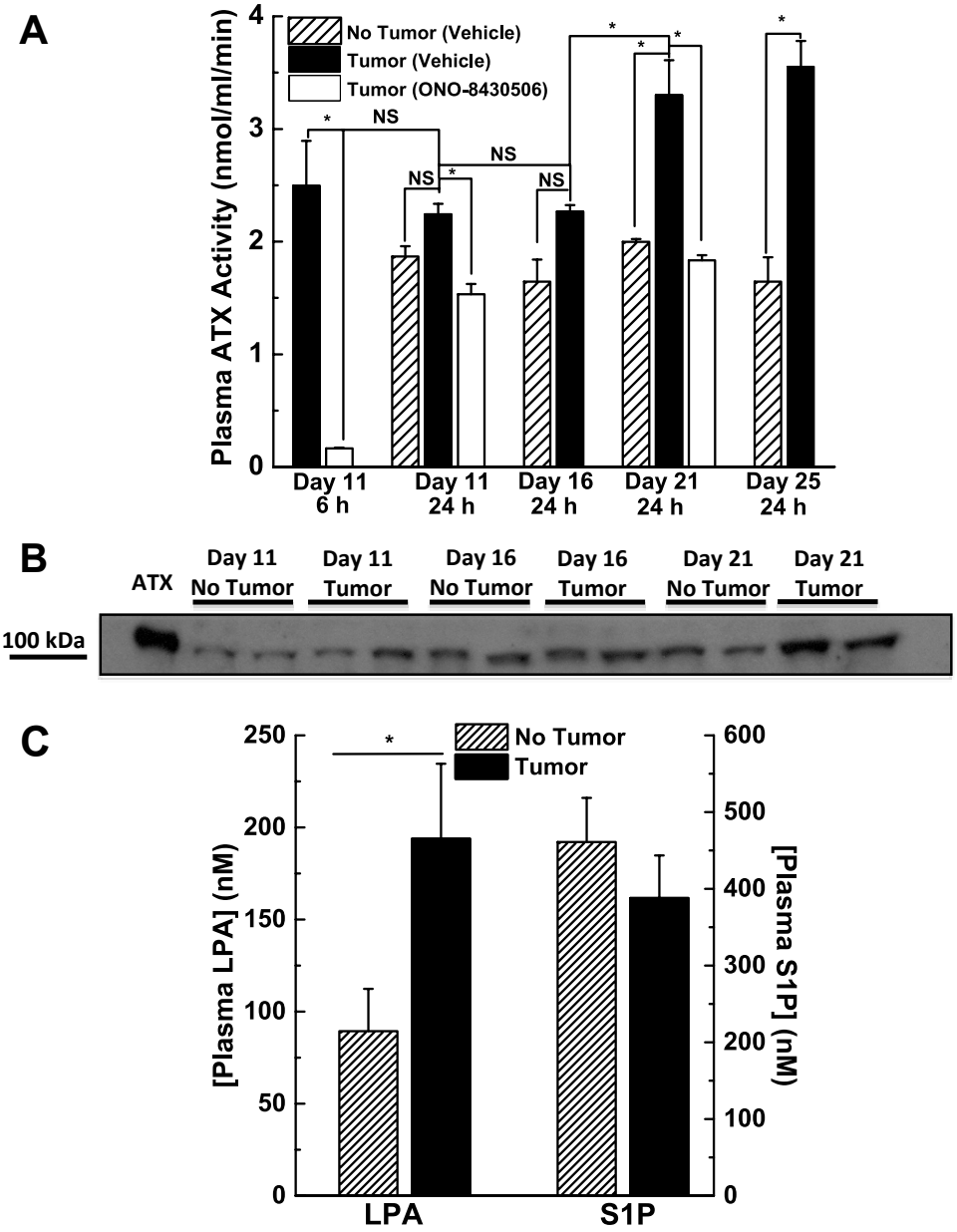

Figure 4.12. Plasma ATX activity and LPA levels increase in mice with advanced 4T1 breast cancer development. A) ATX activity of plasma collected from mice at either 6 or 24 h after last treatment as indicated (vehicle or ONO-8430506). Results are means ± SEM, n=3-26 per group. *, indicates significant difference ($p<0.05$) by ANOVA. B) Plasma (4 µL) from day 11, 16 and 21 mice treated with vehicle with and without tumors was probed for ATX by Western blot. Concentrated medium from MDA-MB-435S cells, which express high ATX activity (17) was used as a positive control. C) Plasma concentrations of LPA (sum of C16:0, C18:0, C18:1 and C20:4 molecular species) and S1P levels in mice with day 21 tumors compared to mice with no tumors. *, indicates a significant increase in mice with tumors compared to mice without tumors; n=5-8 mice per group.

4.5 Influence of ATX inhibition on inflammatory mediator production in mice

Based on the above results, we hypothesized that there was an inflammatory “cross-talk” between the breast tumor and adipose tissue. We used multiplex ELISA provided by Eve Technologies (Calgary, AB) to analyze 32 inflammatory mediators in tissues collected from mice. We observed increases in inflammatory chemokines (CCL family) (Figure 4.13A-C) and cytokines (Figure 4.13D-P) involved with immune cell activation and migration (117) in mammary adipose tissue adjacent to the tumor compared to the contralateral fat pad. No changes in inflammatory mediator expression were seen with sham injection (not shown). The complete list of inflammatory mediators and the levels identified in both 4T1 tumors and mammary adipose tissue both adjacent and contralateral to the tumor are shown in Table 4.1.

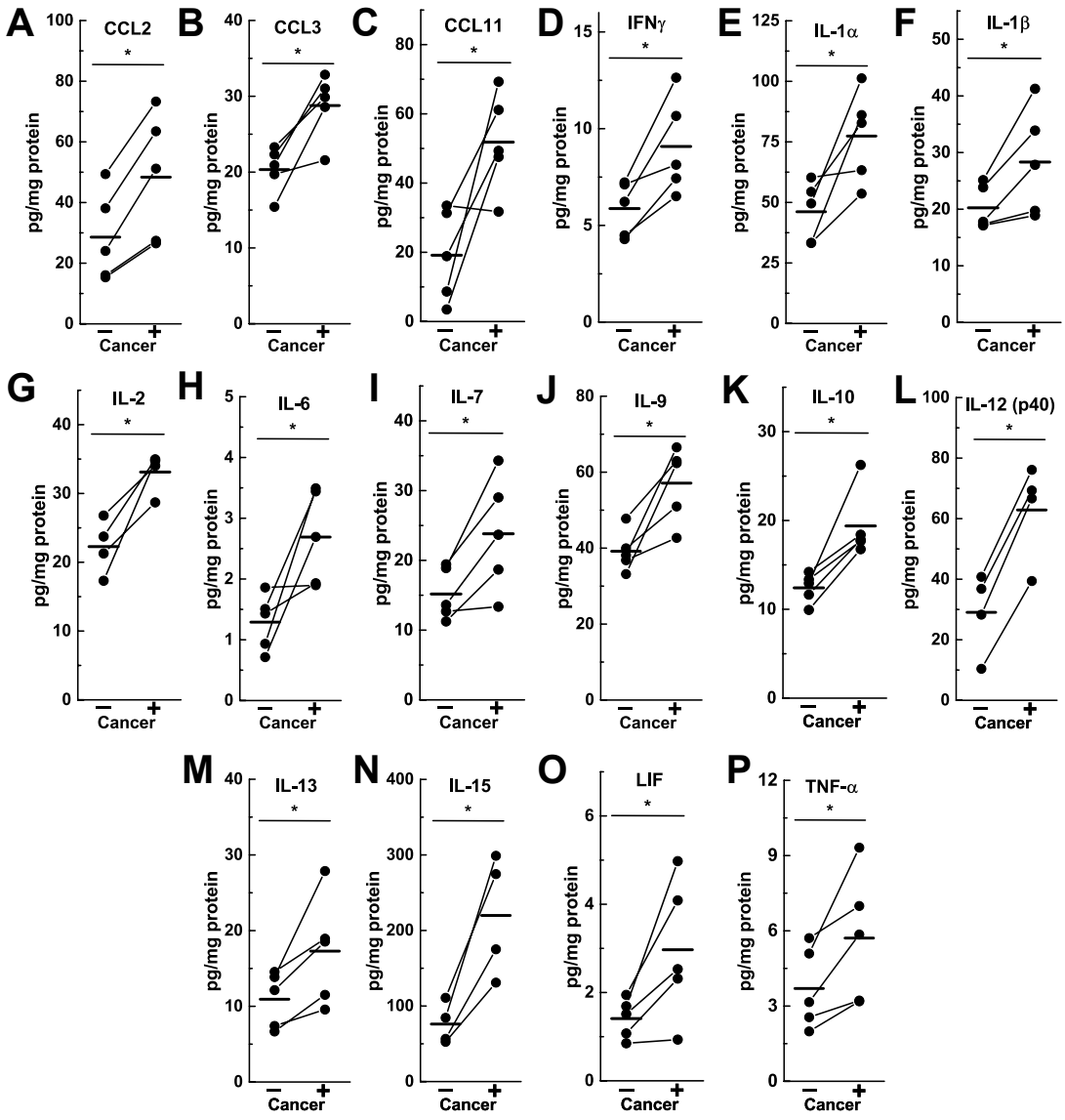

Figure 4.13. 4T1 breast tumors in Balb/c mice significantly increase the expression of inflammatory mediators in adjacent adipose compared to the contralateral mammary fat pad. Mammary adipose tissue was collected after 10 days of tumor growth and inflammatory mediators were measured by multiplex analysis. Results are normalized to total protein content. Results are from 4-5 paired mammary adipose tissues with the means indicated by horizontal bars. *p<0.05 by paired t-test.

	Normal Breast (Contralateral Breast) (pg/mg protein)				Cancer Breast (pg/mg protein)				Tumor (pg/mg protein)				Fold Change (Cancer Breast vs Normal Breast)	p-value (Cancer Breast vs Normal Breast)	Fold Change (Tumor vs Cancer Breast)	p-value (Tumor vs Cancer Breast)
	Mean	SEM	Min	Max	Mean	SEM	Min	Max	Mean	SEM	Min	Max				
CCL2	28.6	6.6	15.3	49.4	48.4	9.4	26.5	73.3	125.5	11.9	96.0	158.9	1.7	0.005	2.6	0.02
CCL3	20.3	1.4	15.4	23.3	28.8	1.9	21.6	32.9	33.4	8.0	20.3	64.6	1.4	0.01	1.2	0.67
CCL4	11.4	3.0	4.0	20.8	18.1	6.3	0.0	36.6	26.1	4.9	18.1	45.1	1.6	0.22	1.4	0.47
CCL5	30.2	13.6	9.4	79.0	30.3	12.0	11.3	76.9	11.8	0.5	10.2	13.3	1.0	0.99	0.4	0.19
CCL11	19.2	6.0	3.5	33.5	51.8	6.4	31.7	69.3	257.8	35.4	154.1	367.3	2.7	0.03	5.0	0.01
CSF1	4.2	1.0	2.4	7.7	9.7	2.8	0.0	16.8	7.4	1.4	4.5	12.5	2.3	0.10	0.8	0.93
CXCL1	34.5	5.2	23.7	52.9	35.5	4.1	24.8	49.4	192.2	60.5	100.0	429.0	1.0	0.87	5.4	0.07
CXCL2	25.1	3.5	13.5	33.9	40.8	12.3	0.0	66.0	103.8	40.4	30.4	255.6	1.6	0.30	2.5	0.20
CXCL5	26.9	4.6	14.7	38.9	53.7	8.1	0.0	72.4	4.0	1.4	0.6	8.2	2.0	0.06	0.1	0.04
CXCL9	104.3	27.3	45.2	169.2	215.9	76.1	69.6	443.6	281.1	32.4	182.8	355.2	2.1	0.18	1.3	0.41
CXCL10	2.3	0.5	1.3	3.8	6.8	2.6	2.6	16.7	37.1	3.4	26.3	46.9	3.0	0.15	5.5	0.001
G-CSF	424.4	121.3	115.1	745.3	365.8	101.6	115.8	603.4	1126.5	110.7	955.8	1558.3	0.9	0.52	3.1	0.003
GM-CSF	7.3	3.6	0.0	17.1	15.7	5.8	0.0	31.4	16.8	1.6	12.4	22.1	2.1	0.06	1.1	0.88
IFNγ	5.9	0.6	4.3	7.2	9.1	1.1	6.5	12.6	1.4	0.3	0.6	2.1	1.5	0.02	0.2	0.004
IL-1α	46.1	5.5	33.2	60.3	77.4	8.5	53.6	101.2	88.6	22.0	51.2	174.3	1.7	0.03	1.1	0.72
IL-1β	20.2	1.8	17.1	25.1	28.3	4.3	18.9	41.3	13.8	1.0	11.1	16.7	1.4	0.04	0.5	0.03
IL-2	22.3	2.0	0.0	26.8	33.1	1.5	0.0	35.0	4.8	0.4	3.8	5.8	1.5	0.02	0.1	0.03
IL-3	1.8	0.5	0.8	3.2	4.3	1.4	1.7	9.1	1.6	0.2	1.2	2.1	2.4	0.09	0.4	0.13
IL-4	0.4	0.0	0.2	0.4	1.7	0.6	0.6	3.7	1.2	0.2	0.8	2.0	4.5	0.07	0.7	0.29
IL-5	1.0	0.1	0.8	1.2	1.7	0.4	0.9	3.0	16.5	3.8	9.5	29.8	1.8	0.07	9.4	0.02
IL-6	1.3	0.2	0.7	1.9	2.7	0.3	1.9	3.5	14.8	2.7	9.6	24.2	2.1	0.04	5.5	0.02
IL-7	15.2	1.7	11.2	19.4	23.8	3.7	13.4	34.3	3.1	0.8	1.3	5.3	1.6	0.02	0.1	0.006
IL-9	39.2	2.4	33.2	47.8	57.1	4.4	42.7	66.6	15.4	0.4	14.2	16.7	1.5	0.02	0.3	0.0007
IL-10	12.4	0.7	9.9	14.2	19.4	1.7	16.8	26.3	7.9	0.2	7.2	8.7	1.6	0.01	0.4	0.004
IL-12p40	27.1	5.6	10.4	40.8	62.9	8.1	39.3	76.1	2.8	0.4	1.6	3.8	2.3	0.0005	0.04	0.03
IL-12p70	15.6	1.6	10.8	19.7	20.7	3.6	10.2	29.5	5.2	0.9	2.3	7.0	1.3	0.13	0.3	0.02
IL-13	10.9	1.6	6.7	14.6	17.3	3.2	9.6	27.9	1.6	0.4	0.9	3.0	1.6	0.04	0.1	0.009
IL-15	72.4	11.2	52.6	110.9	219.9	39.9	0.0	298.9	12.1	1.0	9.7	15.8	3.0	0.02	0.1	0.04
IL-17A	0.8	0.1	0.5	1.2	1.5	0.3	0.0	2.2	0.3	0.0	0.2	0.3	1.9	0.08	0.2	0.07
LIF	1.4	0.2	0.9	1.9	3.0	0.7	0.9	5.0	44.6	0.9	42.6	47.2	2.1	0.05	15.0	0.00001
TNF-α	3.7	0.7	2.0	5.7	5.7	1.2	3.2	9.3	1.7	0.2	1.0	2.2	1.5	0.04	0.3	0.03174
VEGF	3.7	0.8	1.6	6.0	5.7	1.6	2.2	10.8	1.3	0.5	0.5	3.3	1.6	0.27	0.2	0.09

Table 4.1. Quantification of chemokines, cytokines and growth factors assayed by multiplex analysis in mammary adipose tissue and orthotopic 4T1 breast tumors after 10 days of tumor growth. Fold change is presented in red for analytes more than two-fold higher, blue for more than two-fold lower and black for less than two-fold change. n=4-5 per group. $p<0.05$ by paired t-test shown in red.

We next measured the expression of inflammatory mediators in the plasma and tissues of mice after 10 days of tumor growth and treatment with either vehicle or 10 mg/kg/day of the ATX inhibitor ONO-8430506. This treatment was shown previously to severely decrease LPA concentrations in the plasma and breast tumors (Figures 3.8 and 4.5). In the mice, 4T1 tumors were 60% smaller with ONO-8430506 treatment compared to vehicle treatment as expected (Figure 4.1). The pro-inflammatory cytokines TNF-α and G-CSF were significantly elevated in the plasma of mice with tumors compared to sham-treatment mice. ONO-8430506 treatment only decreased the elevated cytokine levels in the plasma of mice with tumors (Figure 4.14).

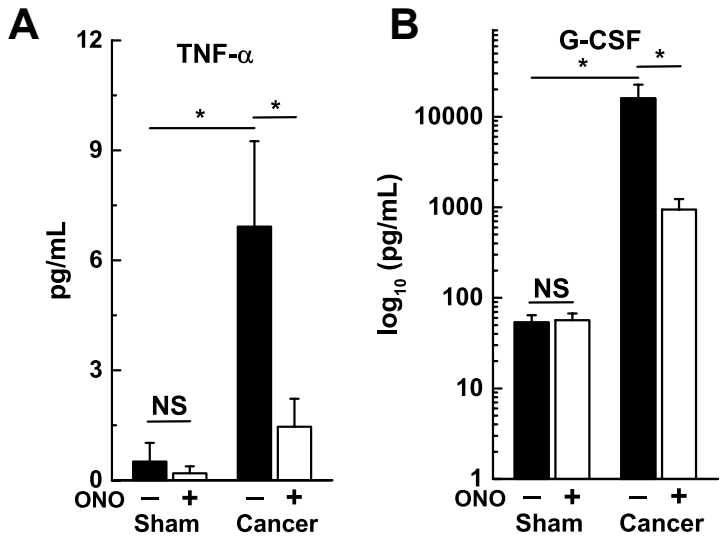

Figure 4.14. TNF-α and G-CSF are highly elevated in the plasma of mice with 4T1 breast cancer tumors compared to sham treatment and can be suppressed by ATX inhibition. Mice were injected in the mammary fat pad with 20,000 mammary tissue cells (Sham) or 4T1 breast cancer cells (Cancer), and gavaged daily for 10 days with either vehicle or 10 mg/kg ONO-8430506. Mice were sacrificed 6 h after last treatment. ONO-8430506 did not suppress TNF-α or G-CSF levels in the sham group. The G-CSF results are plotted on a $\log_{10}$ scale. Results are means ± SEM from 5 mice per group. *$p<0.05$ by ANOVA, NS = not significant.

More substantially, ATX inhibition decreased the expression of 20 inflammatory mediators by 1.5- to 8-fold in mammary adipose tissue adjacent to tumors (Figure 4.15). However, no effect of ATX inhibition on inflammatory mediator levels was seen either in the contralateral fat pad or sham-treated mice. ONO-8430506 also did not affect levels of measured inflammatory mediators within the 4T1 tumors themselves when expressed per mg of tumor. However, since the tumors were 60% smaller, the total production of inflammatory mediators within the tumor would be proportionally less and consequently reduce the total inflammatory mediator load on surrounding adipose tissue. ATX inhibition did suppress leukocyte infiltration as measured by CD-45 staining by >50% in both cancer-affected mammary adipose tissue and tumors, but not normal contralateral adipose tissue (Figure 4.16). We confirmed earlier that ONO-8430506 monotherapy does not affect the total numbers of white blood cells in plasma (Figure 4.3B).

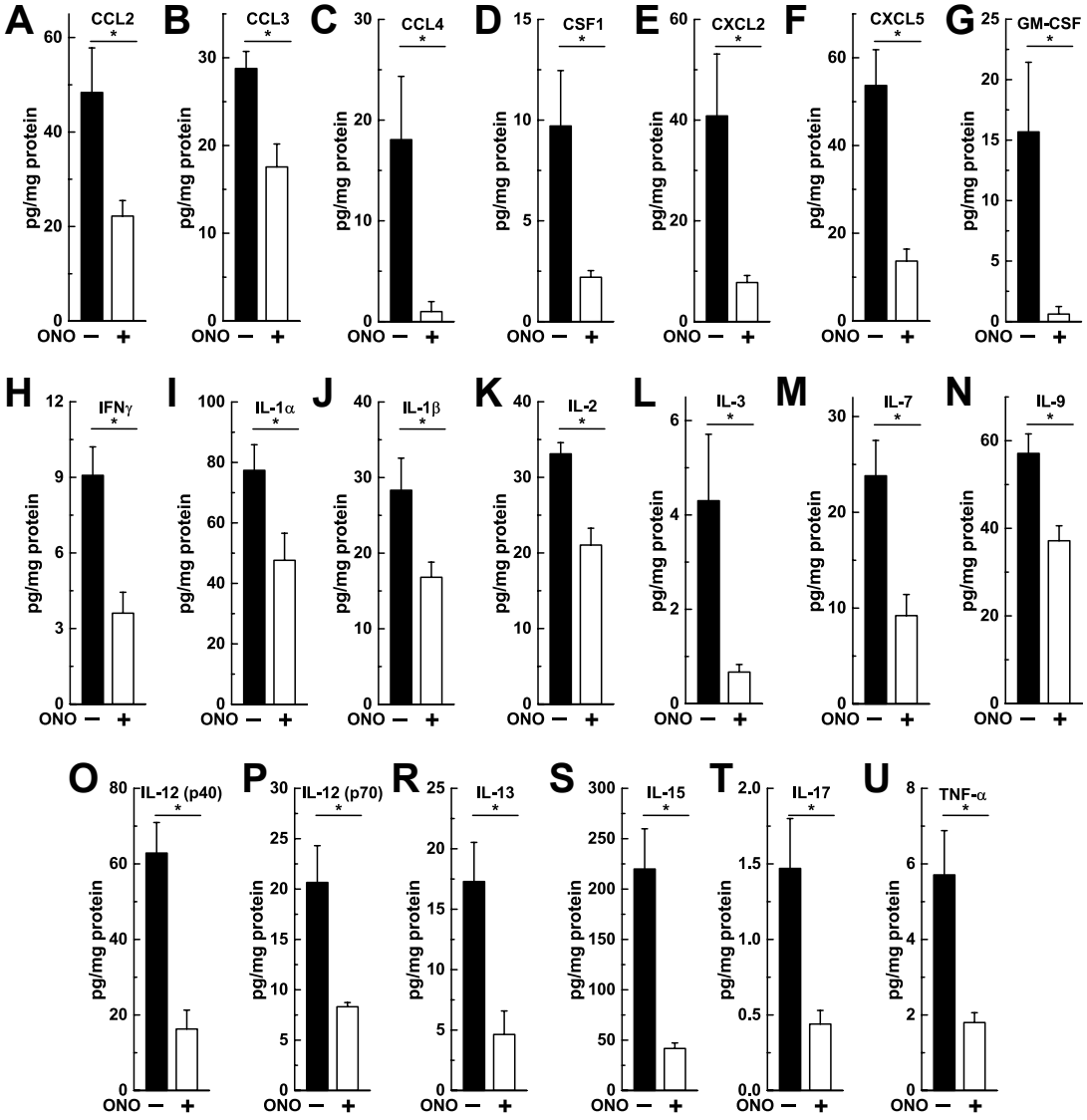

Figure 4.15. Inflammatory mediators are significantly suppressed by ATX inhibition in mammary adipose tissue adjacent to a 4T1 breast cancer tumor. Mice were injected in the mammary fat pad with 20,000 4T1 breast cancer cells, and gavaged daily for 10 days with either vehicle or 10 mg/kg ONO-8430506. Mice were sacrificed 6 h after last treatment. Inflammatory mediators were measured in mammary adipose tissue by multiplex analysis. Results are normalized to total protein content. Results are means ± SEM from 4-5 mice per group. *p<0.05 compared to no treatment.

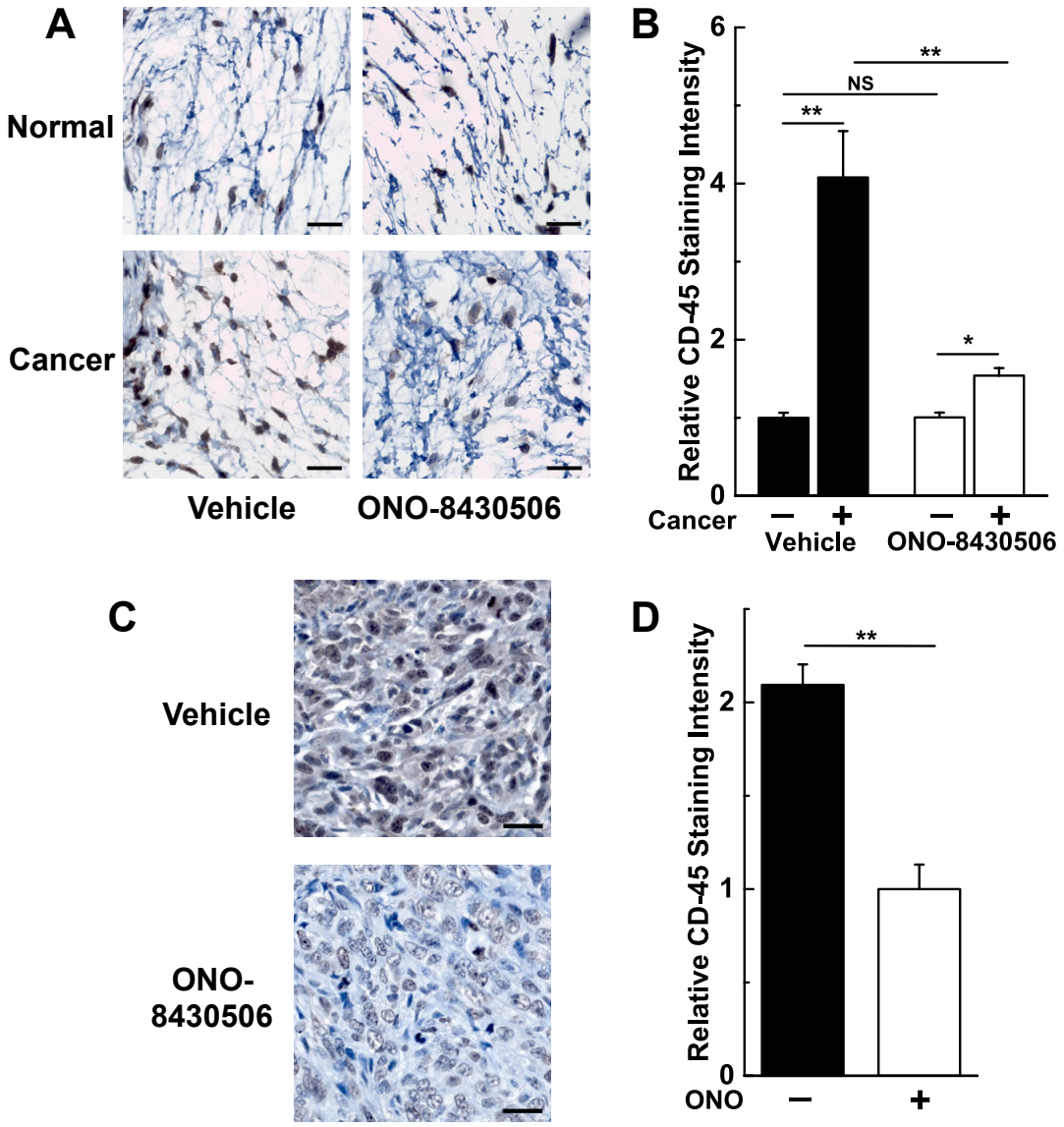

Figure 4.16. ATX inhibition suppresses leukocyte infiltration into mammary adipose tissue adjacent to a 4T1 breast tumor and within 4T1 tumors. A) Representative photographs of mammary adipose tissue opposite to a 4T1 tumor (Normal) and adjacent to a 4T1 tumor (Cancer) treated with vehicle or 10 mg/kg ONO-8430506 for 10 days and stained for CD-45. Mice were sacrificed 6 h after last treatment. B) Quantification of CD-45 staining intensity in mammary adipose tissue. C) Representative photographs of 4T1 tumors stained with CD-45. D) Quantification of CD-45 staining intensity in tumors. Results are means ± SEM from 5 mice per group. *p<0.05, **P<0.001 by ANOVA, NS = not significant. Scale bar = 25 μm.

4.6 Inflammatory mediator secretion in 4T1 cancer cells and adipose tissue is increased by LPA and adipose tissue increases ATX secretion following treatment with inflammatory mediators

We next determined the effects of LPA on the production of inflammatory mediators in cell culture. Treatment of 4T1 cells with 5 μM LPA significantly increased chemokine and cytokine expression for 9 different meditators, including CCL2, CCL5, CSF1, CXCL1, CXCL2, CXCL10, IL-6, IL-15 and LIF (Figure 4.17). We also tested the ability of LPA and 10 inflammatory mediators to increase the growth rates of 4T1 cells. LPA alone increased cell growth rates over 24 h by 30% and all inflammatory mediators tested (CCL2, CCL3, CCL11, CXCL10, G-CSF, GM-CSF, IL-1α, IL-1β, IL-6 and TNF-α) had similar effects (Figure 4.18). For CCL3, CCL11, CXCL10, G-CSF, IL-1B, IL6 and TNF-α, the effects of LPA on cell division were additive (Figure 4.18).

Treatment of adipose tissue with LPA also significantly increased the production of the chemokines and cytokines CCL2, CCL5, CXCL1, CXCL10 and TNF-α (Figure 4.19A-E). Conversely, the cytokines G-CSF and TNF-α significantly increased ATX production and secretion into the culture medium (Figure 4.19F,G).

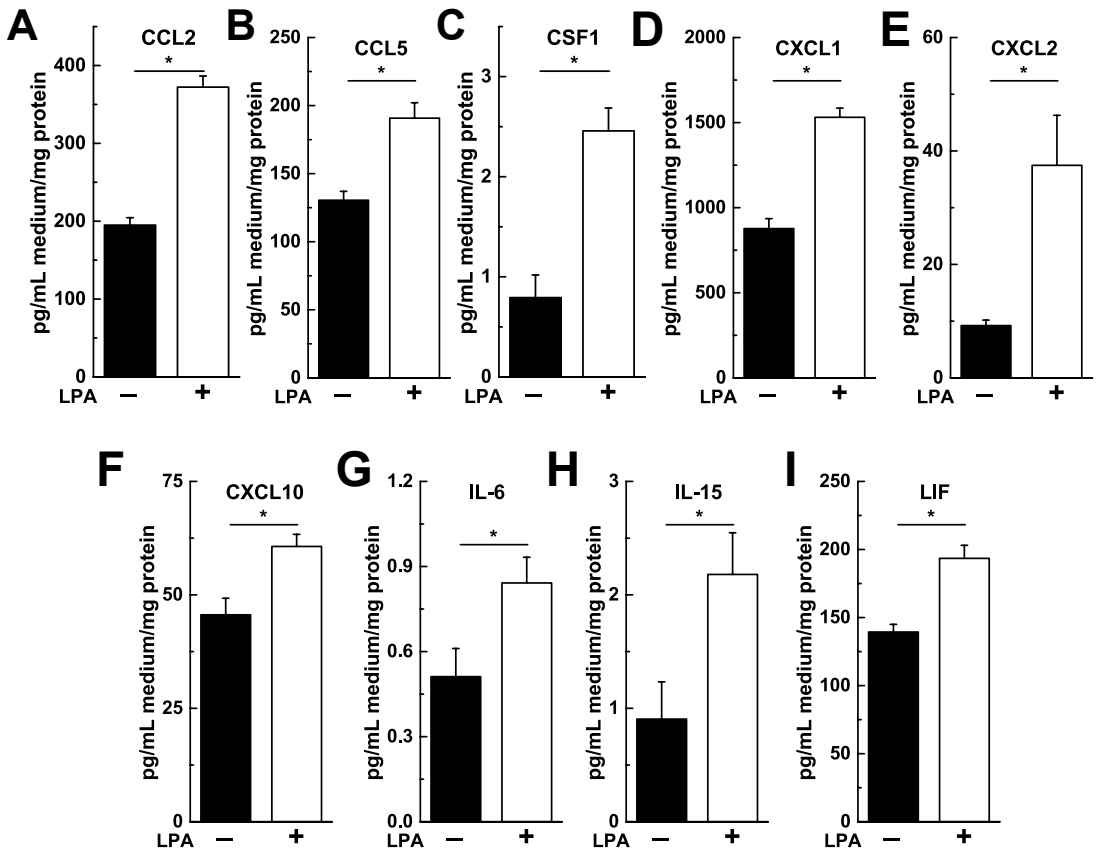

Figure 4.17. Chemokine and cytokine secretion in 4T1 breast cancer cells is significantly increased by LPA treatment. 4T1 cells were treated with 5 μM LPA for 24 h in medium containing 0.1% bovine serum albumin and medium was analyzed by multiplex measurements. Results are normalized to both total volume of medium and cell protein content. Results are means ± SEM from four independent experiments. *p<0.05 compared to no treatment.

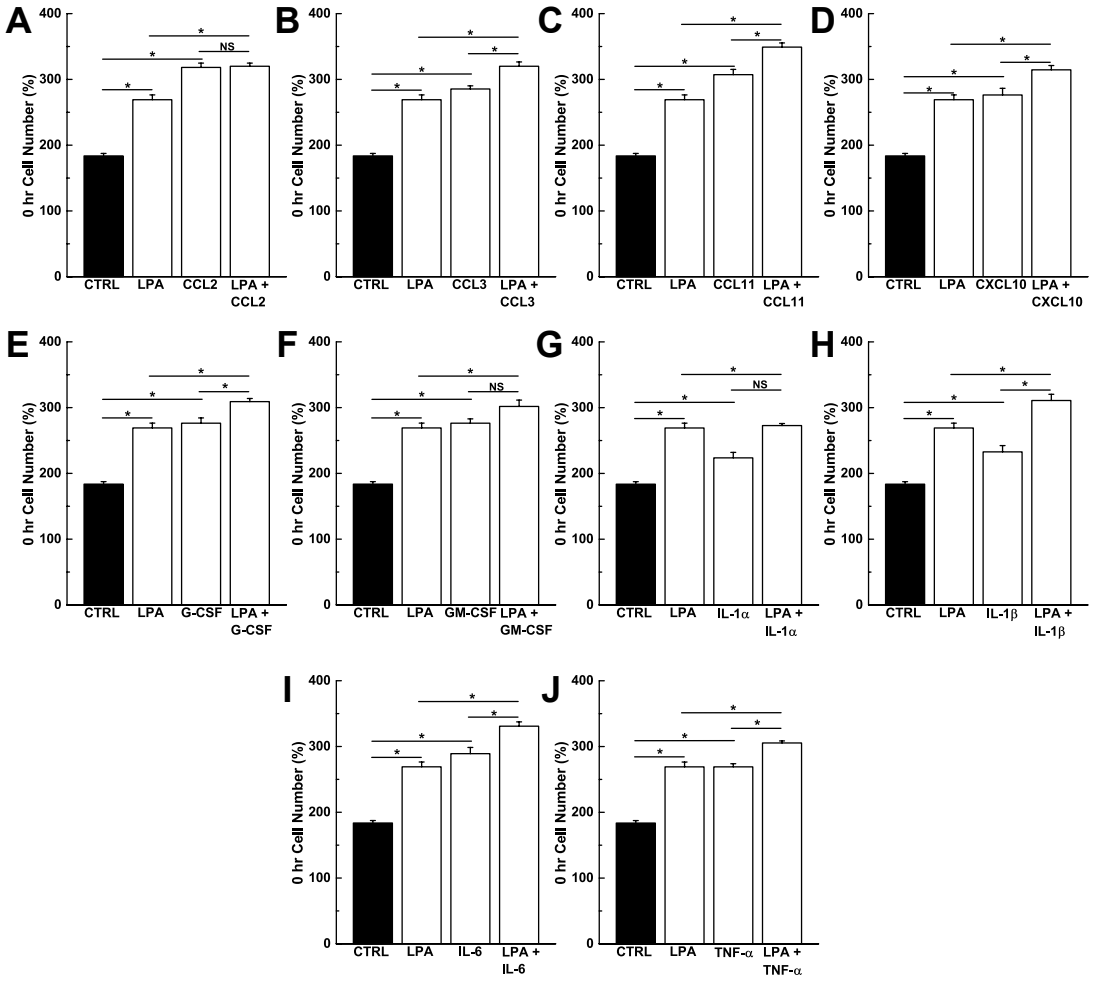

Figure 4.18. Effects of incubating 4T1 breast cancer cells with LPA and chemokines and cytokines. 4T1 cells were grown in serum-free medium supplemented with 0.1% bovine serum albumin for 24 h and treated with or without 5 μM LPA, and/or 10 ng/mL CCL2, CCL3, CCL11, CXCL10, G-CSF, GM-CSF, IL-1α, IL-1β, IL-6 and TNF-α. Cells were then counted at the end of the 24-h treatment. Each sample represents three independent experiments and results are expressed as means ± SEM relative to the cell count at the start of the experiment (0 h). CTRL = no treatment (24-h control). *$p<0.05$ by ANOVA; NS = not significant.

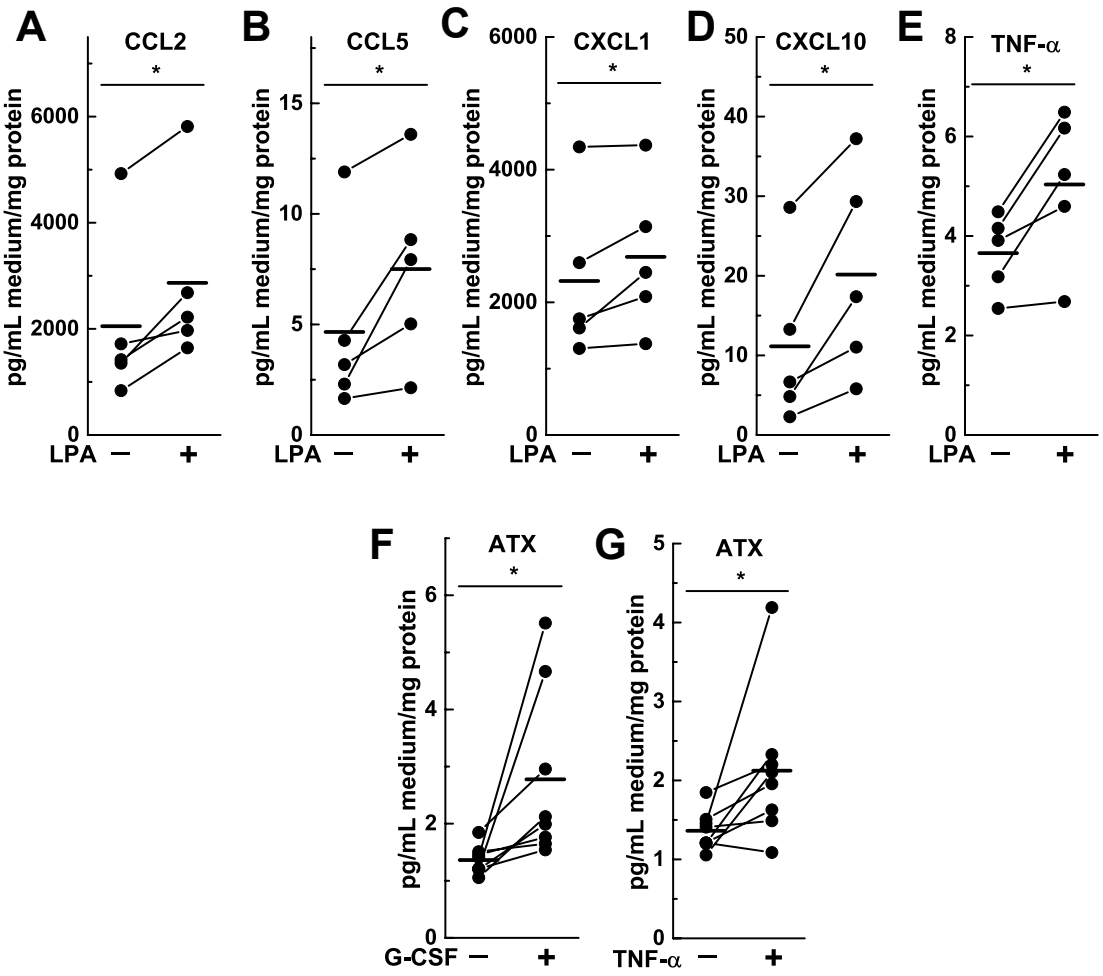

Figure 4.19. Chemokine and cytokine secretion in mammary adipose tissue culture is increased by LPA and cytokines increase ATX secretion from mammary adipose. A-E) Adipose tissue in culture was treated with 5 μM LPA for 24 h in medium containing 0.1% bovine serum albumin and medium was analyzed by multiplex measurements. Results are normalized to both total volume of medium and cell protein content. Results are from 5 paired mammary adipose tissues with the means indicated by horizontal bars. F-G) Mammary adipose tissue was treated with 10 ng/mL G-CSF and TNF-α for 48 h and medium was analyzed for ATX by sandwich ELISA. Results are from 8 paired mammary adipose tissues. *p<0.05 by paired t-test compared to no treatment.

4.7 Relationship between ATX expression and LPA levels in inflammatory conditions

In Chapter 3, we demonstrated that LPA can suppress ATX production, and reducing LPA concentrations in mice with ONO-8430506 resulted in an increase in ATX production. These results imply a negative relationship between LPA and ATX protein concentrations. However, in mice with advanced 4T1 tumors, both LPA and ATX activity are increased (Figure 4.12). These same mice also have systemically higher inflammatory cytokine levels (Figure 4.14).

From all these observations, we proposed that cytokines could mitigate the inhibition of ATX mRNA expression by LPA (and S1P). To test this in cell culture and follow up with our findings in Chapter 3, we stimulated SW-579 cells (which express high levels of ATX) with either or both TNF-α and IL-1β, which increased ATX mRNA compared to no treatment (Figure 4.20). This increase was sufficient to completely overcome the inhibition on ATX mRNA expression by either 1 μM LPA or S1P (Figure 4.20).

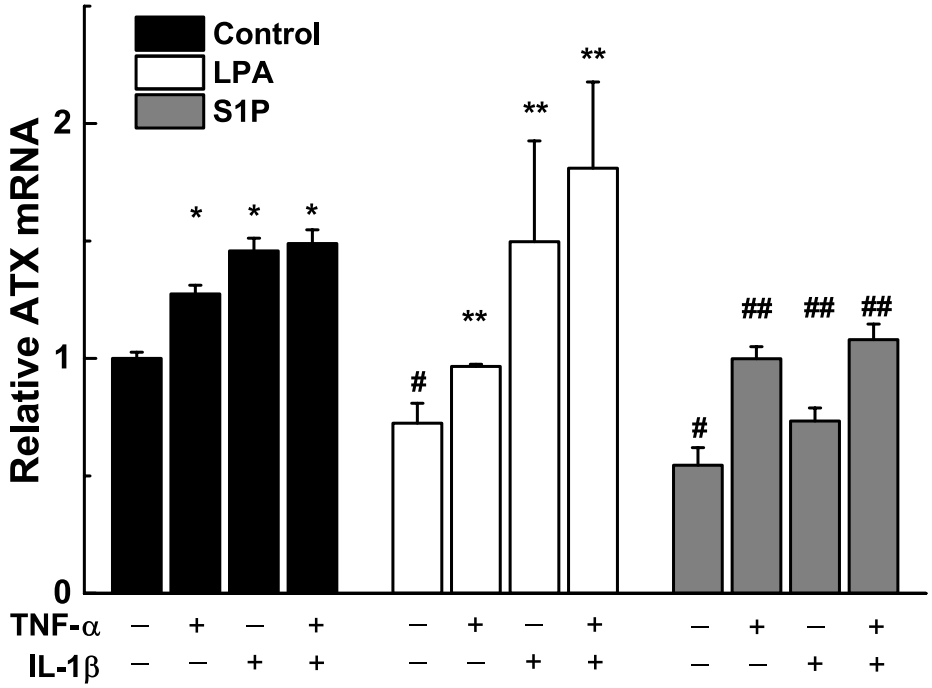

Figure 4.20. Pro-inflammatory cytokines can overcome LPA- and S1P-mediated inhibition of ATX mRNA expression. SW-579 cells were incubated for 24 h in the presence of 1 μM LPA or S1P, and 10 ng/mL of the pro-inflammatory cytokines TNF-α and/or IL-β as indicated. *, indicates a significant increase in ATX mRNA for cells treated with cytokines compared to no treatment; #, indicates that LPA and S1P significant suppress ATX mRNA expression compared to no treatment; **, indicates a significant increase in ATX mRNA for cells treated with both LPA and cytokines compared to LPA treatment alone; ##, indicates a significant increase in ATX mRNA for cells treated with both S1P and cytokines compared to S1P treatment alone.

4.8 Low-dose gamma radiation increases ATX production in stromal cells

We also conducted preliminary experiments to demonstrate that ATX production could be upregulated in response to radiation exposure. We hypothesized that in response to radiation, the tumor induces ATX expression as a survival and repair mechanism, and this could be an important component of radiation therapy resistance. To test this hypothesis, we

exposed patient-matched Hs578Bst stromal cells and Hs578T cancer cells to low dosages of gamma radiation. These dosages are representative to what tissues adjacent to a tumor might receive during radiation treatment (Figure 4.21). Stromal cells increased ATX production by 2.25-fold at 1 Gray radiation, but interestingly, no increases in ATX activity were measured under the same conditions in Hs578T cancer cells (Figure 4.21). The reason for this finding is unclear, however, it may be that breast cancer cells rely on stromal cells and the surrounding mammary adipose tissue to produce ATX in situations of tissue damage. Further work on the role of ATX production in radiotherapy treatment is warranted (Section 6.4).

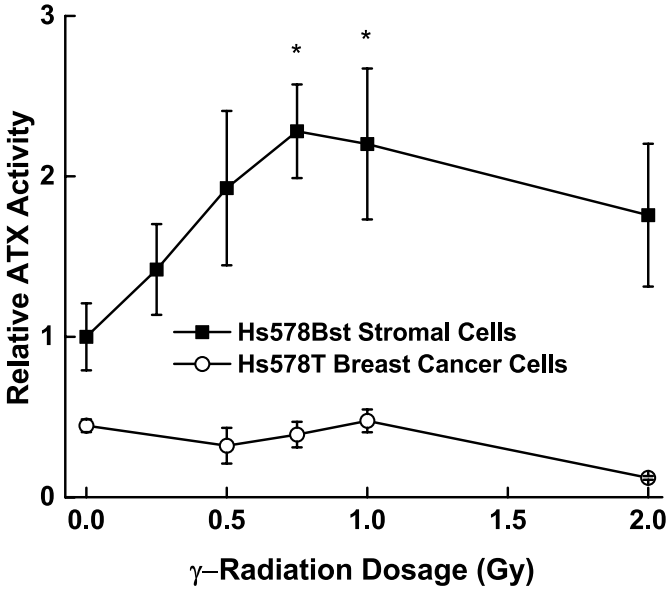

Figure 4.21. Gamma radiation can increase ATX production in HS578Bst stromal cells. Exposure to gamma radiation increases ATX secretion in Hs578Bst stromal cells in a dose-dependent manner. However, no increase occurs in patient-matched Hs578T breast cancer cells. ATX activity measured were performed using the FS-3 assay on concentrated conditioned medium collected 48 h after treatment. Results are means ± SD from three independent experiments. *, indicates a significant difference compared to no treatment ($p<0.05$).

4.9 Discussion

We established for the first time a “proof-of-principle” that inhibiting ATX activity with daily administration of 10 mg/kg ONO-8430506 reduces the initial phase of breast tumor growth by 60-70%. This occurred up to day 11 after injecting 20,000 4T1 or 4T1-12B cells. After 12 days, tumor growth from 4T1 cells in mice treated with ONO-8430506 caught up to that of the control mice. This is when the breast tumors gradually invaded the abdominal musculature. Inhibiting ATX activity had no significant effect on primary tumor growth at this very advanced stage of cancer when factors other than ATX may become more important in driving tumor growth. However, ONO-8430506 did decrease the number of metastatic nodules in the lungs by about 60% at day 21, likely as a result of the delay in tumor growth. The anti-tumor effects were extended and synergistic when combined with doxorubicin.

ATX is a secreted enzyme, which can associate with the surface of cells by binding to surface heparin, heparin sulfate proteoglycans (71), or β_3-integrins (63, 67). This cell surface binding is thought to deliver LPA locally to its receptors. The utility of an ATX inhibitor for treating cancer need not be restricted to those cancer cells that produce ATX as illustrated by our breast cancer model with 4T1 or 4T1-12B cells, which produce very little ATX. However, the cancer cells were injected directly into the mammary fat pad and it is well established that adipose tissue and adipocytes secrete relatively large quantities of ATX (90, 149, 150).

We confirmed this and established that ATX mRNA expression in the mammary fat pad was >30,000-fold higher than in 4T1 and 4T1-12B cells. We propose that mammary adipose is an important component of inflammatory-mediated tumor growth in breast cancer and that ATX is a potent inflammatory mediator. Transgenic mice that overexpress ATX accumulate more fat than wild-type controls when fed a high-fat diet (151). The relationship between obesity and breast cancer incidence has also been established and it is estimated that obesity contributes to at least 20% of cancer deaths by influencing cancer onset (334, 335). Obesity increases the risk of chronic inflammation in adipose tissue, which is a well-recognized risk factor for cancer initiation and progression (336-338). Our results demonstrate that ATX production in adipose tissue can explain at least part of this linkage between adiposity and breast cancer. There appears to be a bidirectional interaction between adipose tissue and the tumor ATX activity, which increases tumor growth as illustrated by the inhibitory action of ONO-8430506 on this process. Also, ATX expression in the mammary fat pad that contains the tumor is increased relative to that in the contralateral fat pad, which did not contain a tumor.

Furthermore, ATX activity within the breast tumors was associated with stromal cells rather than the cancer cells. This finding could explain why using shRNA against ATX in 4T1 cells had no significant effect in slowing primary tumor growth (332). Therefore, we showed that inhibition of ATX activity

associated with non-cancer cells surrounding and within the tumor, rather than the cancer cells themselves, decreases local LPA production and thus the stimulation of breast tumor cell growth, survival and metastasis.

We propose that the tumor establishes an inflammatory environment that increases ATX expression in both tumor stroma and the surrounding mammary adipose tissue (Figure 4.22). This is supported by our results showing that ATX inhibition decreases the production of inflammatory mediators in adipose tissue as the tumor grows. The 60% inhibition of tumor growth, which is produced by ATX inhibition, would also decrease the cytokine load experienced by surrounding adipose tissue. ATX inhibition with ONO-8430506 significantly suppresses inflammatory mediators only in tumor-inflamed breast tissue and does not affect the tonal physiological levels of these mediators in normal adipose tissue.

ATX is part of the defense mechanism used by the body to facilitate wound healing (9, 339). This association between expression of ATX and pro-inflammatory mediators becomes dysfunctional in inflammatory conditions such as in fibrosis (79, 238), rheumatoid arthritis (146) and the inflamed mucosa from Crohn's disease and ulcerative colitis (145, 163). Tumors have been likened to ”wounds that do not heal” (282, 340, 341) and inflammation is one of the hallmarks of cancer (281, 282). Our work demonstrates that ATX is an important part of this inflammatory process in breast cancer.

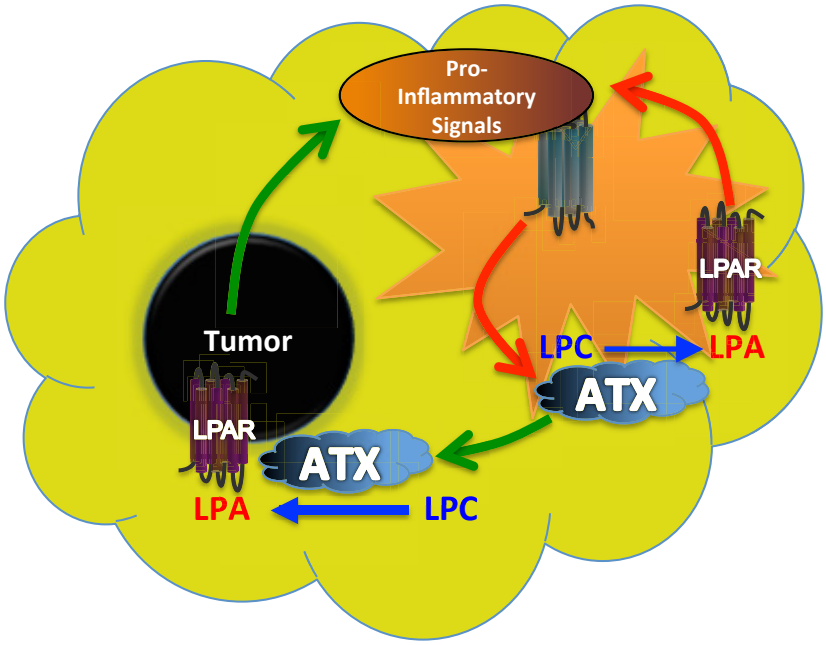

Figure 4.22. Proposed model for ATX production in breast cancers when the cancer cells produce little ATX themselves. In breast cancers, a paracrine model of ATX secretion is possible since adipose tissue secretes high levels of ATX, whereas breast cancer cells normally produce negligible ATX. As the tumor grows, pro-inflammatory signals secreted by the tumor create an inflammatory environment within the surrounding adipose tissue (green arrows). This signaling increases ATX secretion and LPA production, which in turn can establish an autocrine feedback loop of increased pro-inflammatory signaling and ATX production (red arrows) within the adipose tissue. Increased ATX and LPA production can in turn contribute to tumor progression (green arrows). LPAR = LPA receptors.

Numerous studies have assessed the use of plasma/serum ATX levels as a biomarker for human cancers. Serum ATX levels do not predict ovarian cancer (342), but they did have diagnostic potential for follicular lymphoma and pancreatic cancer (343, 344). Plasma ATX levels in our vehicle-treated mice did not increase until after 16 days of tumor growth, which represents a very advanced, metastatic cancer in mice. We conclude from the mouse

model that plasma ATX levels may have little diagnostic utility, but the results do implicate increased ATX expression in late stage metastatic cancer.

In conclusion, we established for the first time that sustained inhibition of ATX and LPA production provides a novel strategy for decreasing the initial phase of breast tumor growth and metastasis in mice. The 4T1 cancer cells that were injected into the orthotopic mammary fat pad express insignificant ATX themselves. This emphasizes the importance of the mammary fat pad as a source of ATX activity, which was a component in the development of the breast tumor. This work also indicates that decreasing LPA production and signaling in tumors could provide novel approaches to decreasing the development of metastasis and resistance to chemotherapy like doxorubicin. A more detailed discussion of our findings and insights into ATX inhibitor combination chemotherapy or radiotherapy treatment regimens is covered in Section 6.4.

CHAPTER 5

AUTOTAXIN AS A BIOMARKER, INFLAMMATORY MEDIATOR AND THERAPEUTIC TAGET IN PAPILLARY THYROID CANCER

5.1 Introduction

Worldwide, the incidence of papillary thyroid cancer has doubled in the past decade (345, 346). This cancer is now the fourth most common malignant disease in women, and although overall survival rates are excellent, thyroid cancer has a very high propensity to metastasize (346, 347) (348-350). Between 25-40% of patients require either surgery and/or radioactive iodine to control the disease (346, 347). Of this group approximately 20% demonstrate metastatic disease that is resistant to radioactive iodine therapy (346, 347). These patients suffer a disproportionate burden because they are often subject to repeated attempts at surgical resection of metastatic disease as well as repeat, high-dose, application of radioactive iodine (347). The application of tyrosine receptor kinase inhibitors in clinical trials has generated mixed results and relatively few patients derive a benefit from these adjuvant treatments (351).

Thyroid malignancy is diagnosed by fine needle biopsy, but ≥25% of biopsies are not definitive and these patients undergo a diagnostic hemi-thyroidectomy. About 80% of these patients do not have cancer. Histology alone cannot predict nodal metastases or the potential for recurrent disease (276, 279, 280, 352). Moreover, there are no clinically utilized markers for metastatic disease and morphologic predictors of papillary thyroid cancer behaviour are imperfect. Molecular diagnostics are now commercially available that enable clinicians to differentiate benign from malignant disease

in previously indeterminate nodules. This often leads to over-treatment of patients with indolent larger tumors, whereas aggressive smaller tumors with high propensity for nodal spread and recurrence are missed. Hence, the clinical ability to predict poor outcomes remains significantly impaired (353). *RET/PTC*, *RAS* and *BRAF* mutations all play a role in tumorigenesis (345, 354), but predicting radioactive iodine resistant and recurrent disease requires a better understanding of the pathways that drive thyroid tumor growth and metastases.

Aggressive disease is driven by a migratory phenotype that shares common pathways with inflammation (281, 355). We propose that ATX and its production of LPA are important components of this inflammatory axis, which contributes significantly to metastasis and resistance to chemotherapy and radiotherapy (10, 165). The role of inflammation has been documented in the development of thyroid cancer and it is a factor that drives locally aggressive disease variants and metastatic disease (354, 356-361). Further, we predicted that ATX could distinguish malignant from benign neoplasms since several reports have shown ATX mRNA to be higher in thyroid cancer tumors than in adenomas (362-365).

5.2 Analysis of ATX in patient specimens

5.2.1 ATX immunohistochemistry

Table 1 summarizes the demographic results for our tissue arrays comprising of thyroid cancer patients with and without metastases. We determined ATX expression in primary tumor specimens with (n=71) and without (n=123) nodal metastases as well as in nodal metastatic sections (n=15), benign follicular adenomas (n=64) and neighboring benign thyroid tissue (n=33). In this cohort, as was the clinical standard, all patients with biopsy proven papillary thyroid cancer had ipsilateral or bilateral level VI lymph node dissections to consistently address the possibility of lymphatic metastases (Figure 5.1).

	Normal (n=33)	Benign Neoplasm (n=64)	PTC (LN-) (n=123)	PTC (LN+) (n=71)	LN (n=15)
Mean age	49.4±13.4	51.9±13.7	48.6±15.3	46.9±16.6	51.2±18.3
Female (%)	85%	59%	72%	70%	73%
Mean tumor size (cm)	-	3.6±1.9	2.3±1.8	2.6±1.5	4.1±1.6

Table 5.1. Patient demographics of immunohistochemistry specimens. PTC, papillary thyroid cancer; LN, metastatic lymph node status. Results shown are means ± SD.

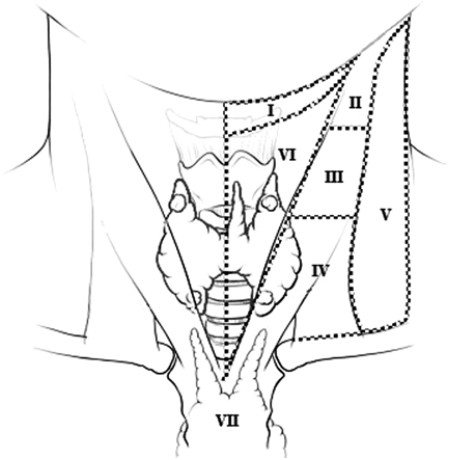

Figure 5.1. Location of cervical lymph nodes in relation to the thyroid gland. Level I, submental and submandibular nodes; level II, upper jugular nodes; level III, midjugular nodes; level IV, lower jugular nodes; level V, posterior triangle and supraclavicular nodes; level VI, pretracheal, prelayngeal, and paratracheal nodes; level VII, nodes within the superior mediastinum. The "butterfly" thyroid gland is depicted over the trachea. Figure adapted from (366).

Representative ATX staining was typically cytoplasmic (Figure 5.2). ATX protein expression was undetectable, or minimally so, in about 90% of the non-neoplastic thyroid tissue. ATX expression was low in benign neoplastic tissue, comprised of follicular adenomas, but a small fraction did stain strongly positive for ATX (Table 5.2). However, we observed neighbouring tissue with incidental microscopic papillary thyroid cancer in 7 of the 12 “benign” cases that did stain strongly positive.

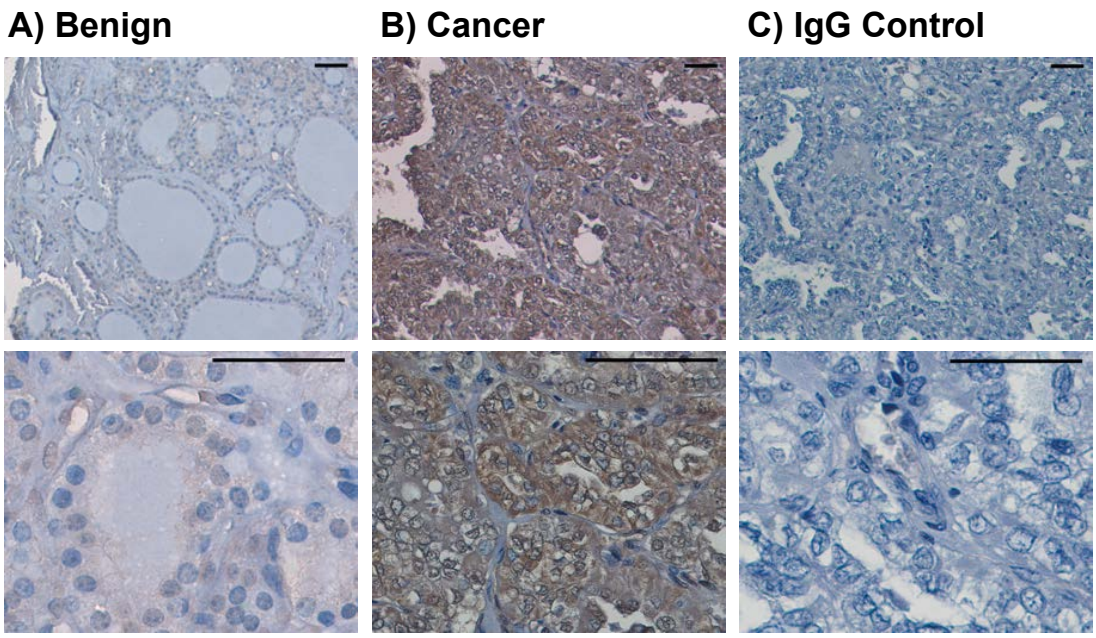

Figure 5.2. Immunohistochemical assessment of ATX in papillary thyroid cancer and benign specimens. ATX is highly expressed in cancer but not benign specimens. A) Representative immunohistochemical stains of ATX at low power (10x) top and high power (40x) bottom in benign thyroid adenomas (n=64) and (B) primary tumors (n=194). C) Rabbit IgG isotype control on primary tumors. Scale bar = 50 μm.

It is clear that the majority (>80%) of primary papillary thyroid tumors exhibited strong ATX staining and this was observed regardless of nodal status. Primary tumors were much more likely to demonstrate moderate or

strong staining compared to normal thyroid tissue ($p<0.0001$) or benign neoplasms ($p<0.0001$). Nodal metastases also showed stronger ATX staining compared to normal thyroid tissue and benign thyroid neoplasms ($p<0.0001$).

Scoring		0 (%)	1+ (%)	2+ (%)	3+ (%)
normal thyroid*	(n=33)	81	8	11	0
benign neoplastic tumors†	(n=64)	26	34	20	18
node-negative primary tumors*†	(n=123)	8	9	30	52
node-positive primary tumors	(n=71)	8	8	31	53
lymph node metastasis	(n=15)	13	27	40	20

*P<0.0001; †P<0.0001

Table 5.2. Percentage (%) of thyroid specimens staining for ATX in normal tissue, benign neoplasms, primary papillary thyroid tumors with and without metastasis, and papillary thyroid cancer metastases in lymph node deposits.

5.2.2 ATX mRNA and LPA levels in thyroid tissues

mRNA levels obtained from snap frozen specimens further outlined the strong preference for ATX expression in malignancy. Primary papillary thyroid tumors, and more so lymph node metastases, exhibited mRNA levels between 3-30-fold higher than normal thyroid tissue or benign tumors (Figure 5.3) ($p<0.05$). Increased ATX mRNA expression in primary tumors compared to normal tissue was also confirmed in matching primary tumors and metastatic specimens from individual patients, and this increase was even greater in metastatic samples compared to matched primary tumors ($p<0.05$) (Figure 5.4). High ATX expression in thyroid tumors also correlated with >2-fold increases in LPA concentrations (C16:0, C18:0, C18:1 and C20:4)

compared to the patients without thyroid cancer (Figure 5.5) ($p<0.05$). We could not detect S1P in these specimens (results not shown).

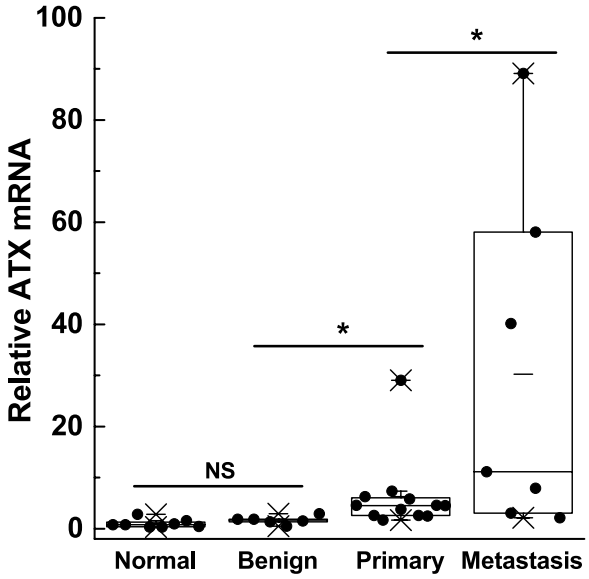

Figure 5.3. ATX mRNA is elevated in cancer specimens compared to benign and normal specimens. No increase in ATX was found in benign specimens compared to normal specimens. ATX mRNA was further increased in specimens from metastatic lymph nodes compared to the primary tumors. ATX mRNA measurements in patient samples normalized to *GAPDH*. n=7-12 per group. *p<0.05 by ANOVA with post hoc test. NS = not significant.

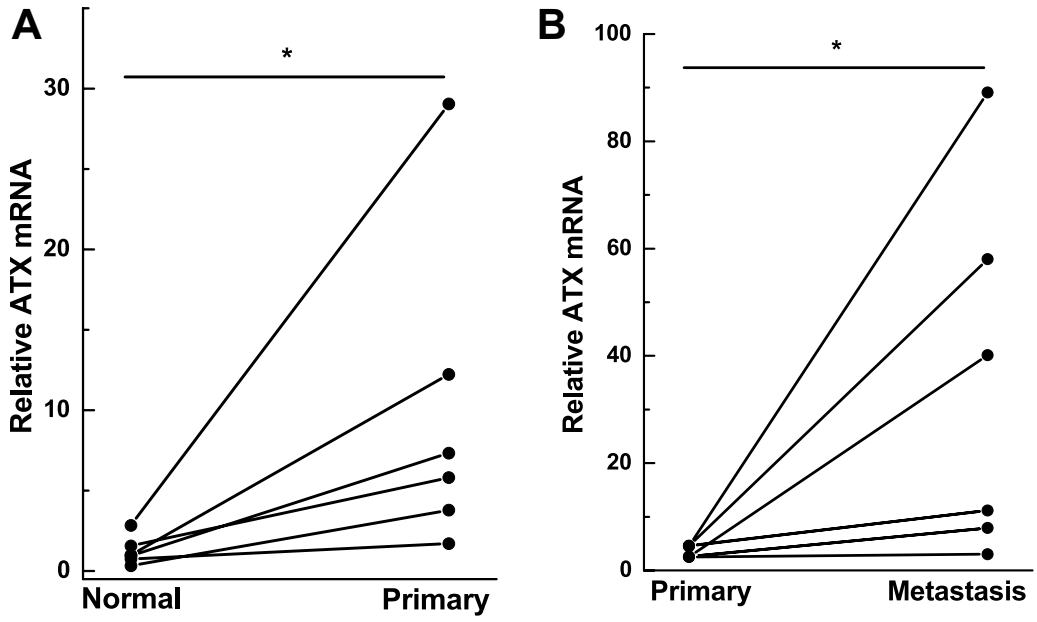

Figure 5.4. ATX mRNA is highly expressed in papillary thyroid cancer specimens and further increased in lymph node metastases. A) ATX mRNA in 6 patient-matched normal and primary tumor specimens. B) ATX mRNA in 6 patient-matched primary tumor and lymph node metastasis specimens. ATX mRNA in expressed relative to *GAPDH*. *p<0.05 by paired t-test.

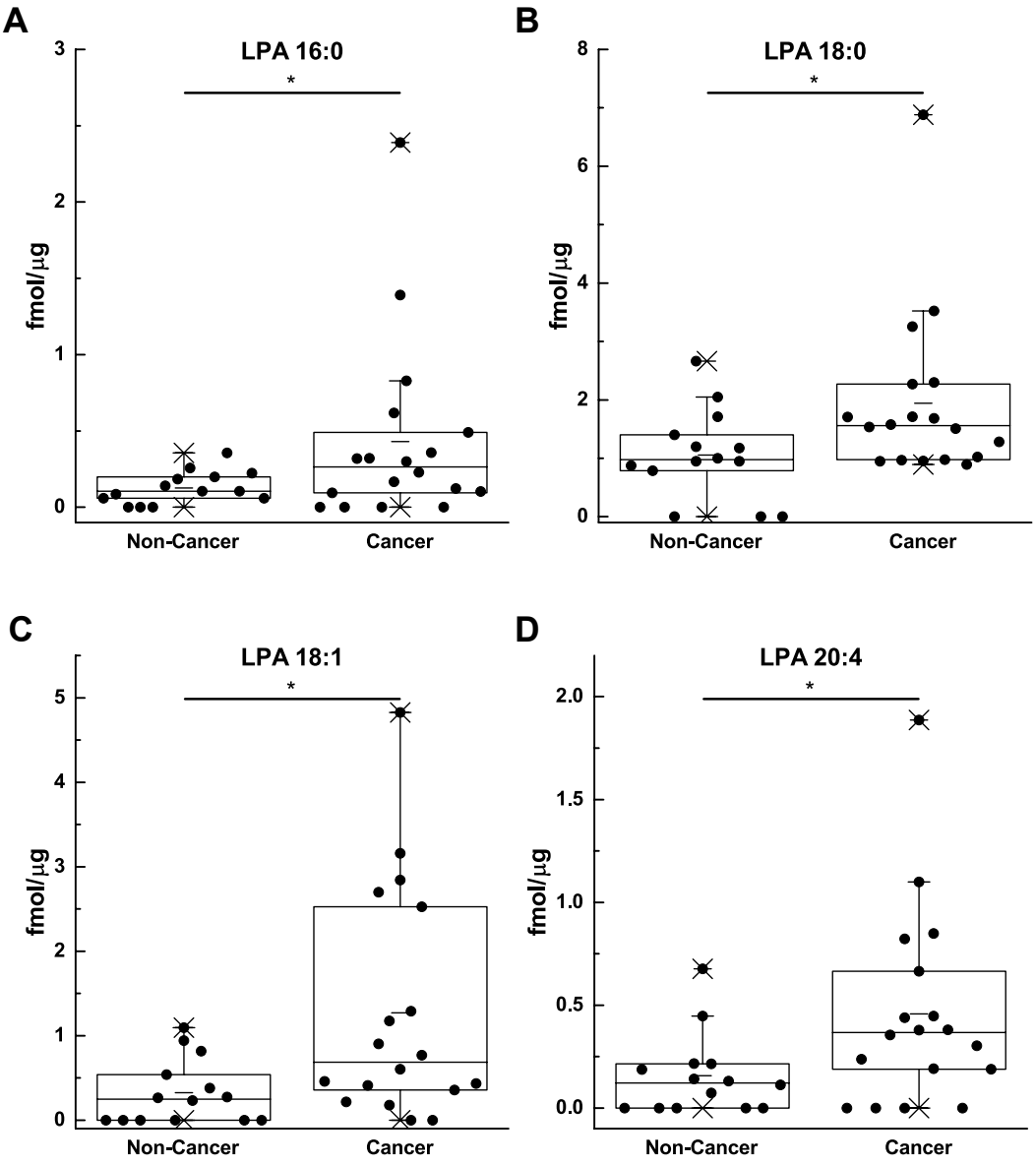

Figure 5.5. LPA molecular species are increased in cancer specimens compared to non-cancer specimens. Non-cancer specimens (normal or benign nodules) have lower LPA levels than cancer (primary or metastasis) specimens. Box plots show minimum, mean, and maximum values (-), 25th, 50th, and 75th percentiles (box), and 1st and 99th percentiles (x). n=14-18 specimens per group, *p<0.05.

5.2.3 ATX mRNA and activity in primary cultures

To quantify the levels of ATX production and exclude other sources of production, we determined ATX expression in purified cells cultured from freshly isolated human tumors and tissues. The expression of ATX mRNA was 10-fold higher in cancer cells from primary tumors and 40-fold higher in cells from metastatic nodules compared to cells from normal or benign thyroid samples (Figure 5.6A). Furthermore, significantly higher levels of secreted ATX activity (Figure 5.6B) were obtained in metastatic specimens compared to primary tumors ($p<0.01$), benign tumors ($p<0.01$), or normal thyroid tissue ($p<0.001$). These results correlated closely with mRNA concentrations identified in corresponding tissues.

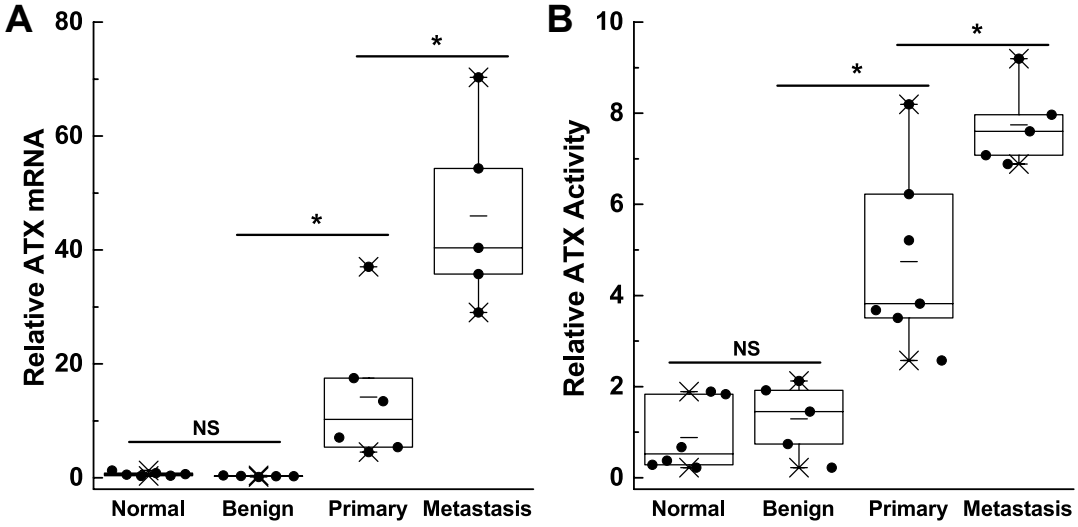

Figure 5.6. ATX mRNA expression and activity are higher in papillary thyroid cancer cell cultures compared to cultures of normal or benign specimens. A) ATX mRNA measurements (normalized to *GAPDH*) and (B) activity measurements in conditioned media from primary cultures established from patient tissues, n=5-7 per group. Box plots show minimum, mean, and maximum values (-), 25th, 50th, and 75th percentiles (box), and 1st and 99th percentiles (x). *$p<0.05$ by ANOVA with post hoc test. NS = not significant.

5.3 Quantification of inflammatory mediators in patient specimens

Having defined a clear role for ATX in primary and metastatic papillary thyroid cancer, we also characterized the inflammatory phenotype using a multiplex analysis (Eve Technologies, Calgary, AB) of inflammatory mediators obtained from the human tissue isolates. We measured 64 analytes encompassing regulators of communication between cells and their extracellular environment (chemokines, cytokines, lymphokines, interferons, colony stimulating factors and growth factors) (see Table 2.4 for list of analytes and abbreviations). Of these, 15 were significantly higher in the metastatic papillary thyroid cancer tumors than in normal thyroid tissue or benign disease (Figure 5.7). None of these mediators were increased in benign neoplasms compared to normal tissue. In the primary cancer tumors, we observed increases in inflammatory chemokines (CCL family and CXCL1) (Figure 5.7A-E) and marked elevation of cytokines (Figure 5.7F-O) involved with the immune cell activation and migration (117). PDGF-AA levels are higher in malignancy indicating probable activation of the PDGFRa cascade and its signaling pathways, which are strongly associated with cellular migration and angiogenesis (280, 367). Conversely, the level of TRAIL ligand (CD253), a central driver of apoptosis (368), was decreased by 75% in primary tumors compared to normal tissue (Figure 5.7P). The levels of all analytes are given in Table 5.3.

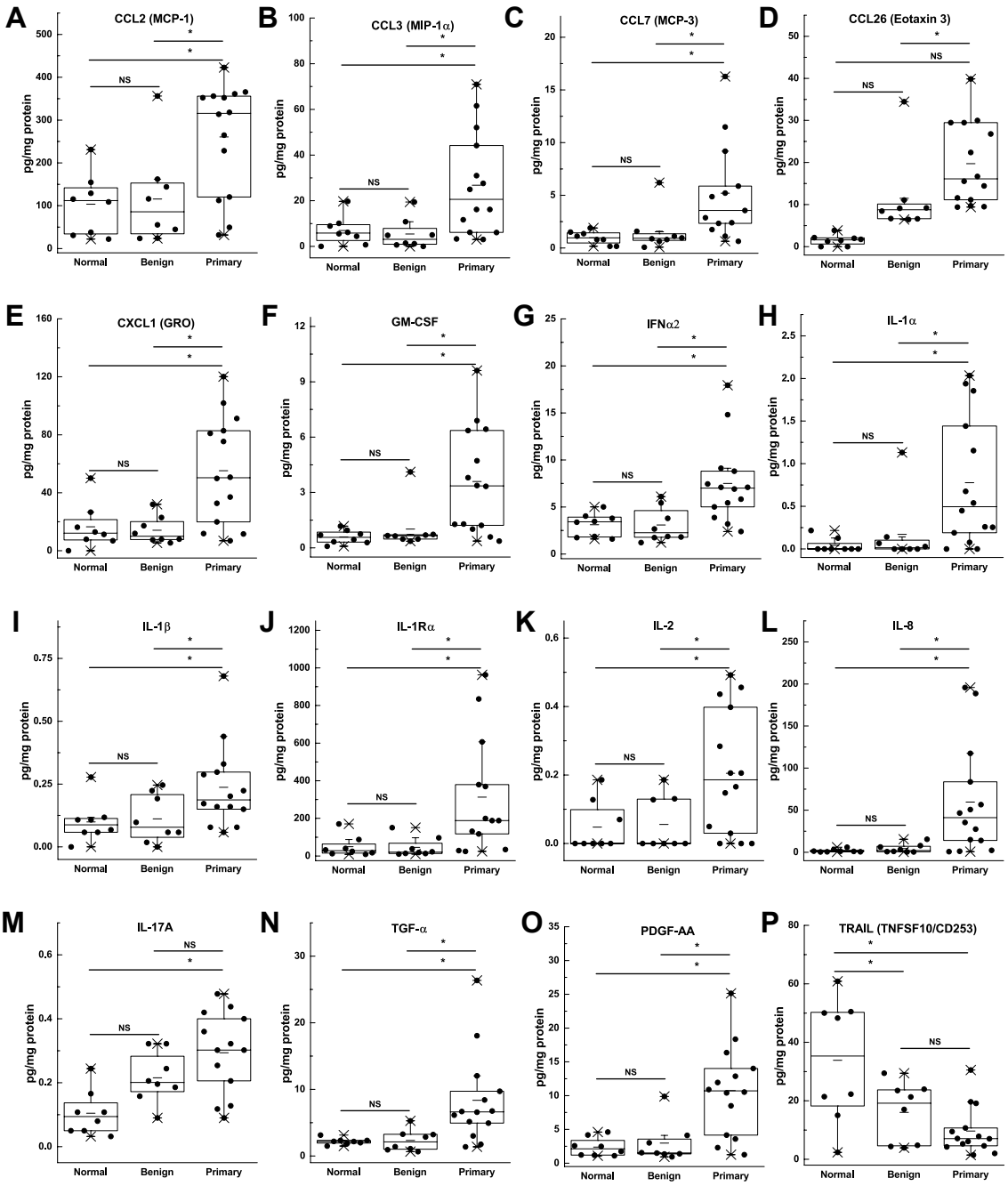

Figure 5.7. Chemokines, cytokines and growth factors are significantly elevated in patient primary thyroid cancer specimens compared to benign nodules and normal thyroid tissue. Multiplex measurement results are normalized to total protein content. Box plots show minimum, mean, and maximum values (-), 25th, 50th, and 75th percentiles (box), and 1st and 99th percentiles (x). n=8-14 specimens per group, *p<0.05 by ANOVA with post hoc test.

	Normal (pg/mg protein)				Benign (pg/mg protein)				Primary (pg/mg protein)							
	Mean	SEM	Min	Max	Mean	SEM	Min	Max	Mean	SEM	Min	Max	Fold Change (Benign vs Normal)	p-value (Benign vs Normal)	Fold Change (Primary vs Benign)	p-value (Primary vs Benign)
CCL1	0.1	0.0	0.1	0.2	0.2	0.1	0.0	1.1	0.8	0.3	0.0	3.1	1.77	0.429	3.41	0.127
CCL2	103.7	25.3	22.1	231.2	115.8	39.2	23.7	356.0	260.6	34.7	31.7	422.8	1.12	0.799	2.25	0.016
CCL3	7.0	2.2	0.0	19.7	5.4	2.4	0.0	19.4	26.8	6.0	3.0	70.9	0.78	0.643	4.94	0.017
CCL4	6.1	2.3	0.3	20.1	3.0	1.1	0.6	9.6	15.8	6.6	1.3	85.5	0.49	0.241	5.19	0.165
CCL5	205.3	57.9	21.6	425.8	103.5	26.6	40.2	253.4	256.4	33.6	95.1	467.9	0.50	0.132	2.48	0.005
CCL7	1.0	0.2	0.2	1.9	1.5	0.7	0.1	6.2	5.2	1.3	0.6	16.3	1.57	0.450	3.39	0.046
CCL8	3.7	0.3	2.8	5.1	3.5	0.4	1.6	5.5	5.3	0.9	2.5	15.6	0.95	0.721	1.54	0.134
CCL11	0.5	0.2	0.0	1.9	1.9	0.8	0.6	6.9	7.2	4.1	0.3	53.1	3.71	0.174	3.83	0.371
CCL13	5.7	0.4	4.3	7.5	5.4	1.0	2.3	10.6	7.9	1.4	2.8	24.8	0.95	0.787	1.46	0.230
CCL15	2.5	0.5	0.0	3.5	3.4	0.3	2.0	4.7	3.6	0.9	0.3	11.5	1.37	0.174	1.08	0.832
CCL17	0.8	0.3	0.1	2.4	0.4	0.1	0.1	0.8	18.7	10.0	0.1	133.2	0.51	0.235	49.12	0.214
CCL21	85.4	34.6	16.1	259.2	20.3	5.0	7.2	52.3	32.5	4.4	13.0	78.7	0.24	0.084	1.60	0.096
CCL22	23.8	7.3	2.9	58.7	40.2	27.0	3.8	228.0	82.2	26.9	13.4	373.1	1.69	0.566	2.05	0.319
CCL24	11.4	2.8	3.2	25.0	16.0	7.9	1.9	69.7	60.4	22.7	3.3	307.2	1.40	0.594	3.78	0.166
CCL26	1.6	0.4	0.0	3.9	11.5	3.3	6.4	34.4	19.7	2.6	9.4	39.9	7.38	0.061	1.71	0.041
CCL27	3.6	0.4	1.7	5.2	3.5	0.6	2.1	6.9	4.0	0.9	0.4	9.2	0.99	0.957	1.13	0.712
CD135	5.8	1.1	3.0	12.1	5.5	0.8	2.3	9.3	5.4	0.7	2.7	10.5	0.94	0.815	0.99	0.970
CXCL1	16.5	5.5	0.0	50.1	14.1	3.3	5.4	32.0	55.2	9.9	7.0	120.1	0.86	0.718	3.91	0.006
CXCL5	3.6	0.6	1.0	5.3	5.2	1.5	2.4	14.9	9.5	2.4	3.2	30.0	1.43	0.356	1.83	0.208
CXCL10	143.5	64.3	2.6	535.6	154.7	127.3	2.7	1042.6	449.5	153.4	7.6	1583.1	1.08	0.938	2.91	0.206
CXCL12	100.7	23.6	20.2	212.2	47.7	14.0	3.4	115.7	76.4	12.5	27.4	185.7	0.47	0.074	1.60	0.160
CXCL13	96.0	54.3	0.4	343.7	5.4	3.5	0.3	28.6	81.6	31.8	1.2	349.7	0.06	0.118	15.09	0.089
CX3CL1	43.4	5.5	18.7	61.4	40.0	6.4	9.9	68.2	174.7	58.3	32.1	725.7	0.92	0.688	4.37	0.100
EGF	17.2	11.3	0.2	94.5	1.5	0.6	0.0	5.3	0.5	0.3	0.0	3.4	0.09	0.187	0.35	0.011
FGF-2	416.2	33.7	192.8	480.2	420.1	35.1	247.9	505.1	467.9	15.1	399.5	610.1	1.01	0.938	1.11	0.309
G-CSF	1.9	0.4	0.8	4.3	2.0	0.2	1.2	2.9	3.5	0.8	1.2	13.0	1.04	0.862	1.79	0.175
GM-CSF	0.6	0.1	0.1	1.2	1.0	0.4	0.4	4.1	3.6	0.8	0.4	9.6	1.73	0.372	3.53	0.026
IFNα2	3.1	0.4	1.6	5.0	3.1	0.7	1.2	6.1	7.5	1.1	2.4	17.9	0.99	0.966	2.44	0.012
IFNγ	0.7	0.2	0.2	1.7	0.6	0.1	0.3	1.3	1.0	0.2	0.5	2.3	0.87	0.714	1.69	0.078
IL-1α	0.0	0.0	0.0	0.2	0.2	0.1	0.0	1.1	0.8	0.2	0.0	2.0	3.97	0.382	4.55	0.049
IL-1β	0.1	0.0	0.0	0.3	0.1	0.0	0.0	0.2	0.2	0.0	0.1	0.7	1.12	0.787	2.12	0.045
IL-1Rα	49.3	19.4	9.2	170.8	45.5	18.1	10.7	150.7	312.8	85.7	24.3	963.1	0.92	0.889	6.87	0.027
IL-2	0.0	0.0	0.0	0.2	0.1	0.0	0.0	0.2	0.2	0.0	0.0	0.5	1.45	0.630	2.94	0.041
IL-3	0.0	0.0	0.0	0.1	0.1	0.0	0.0	0.1	0.1	0.0	0.0	0.2	2.60	0.102	1.40	0.325
IL-4	1.0	0.5	0.0	4.4	0.2	0.1	0.1	0.4	0.4	0.1	0.0	1.2	0.26	0.208	1.71	0.230
IL-5	0.0	0.0	0.0	0.1	0.1	0.0	0.0	0.1	0.1	0.0	0.0	0.1	1.46	0.086	1.08	0.626
IL-6	0.6	0.2	0.1	1.2	0.5	0.2	0.0	2.0	20.8	12.3	0.1	151.4	0.94	0.903	38.96	0.231
IL-7	0.4	0.0	0.3	0.5	0.4	0.0	0.3	0.5	0.4	0.0	0.2	0.5	1.06	0.550	0.95	0.553
IL-8	1.8	0.7	0.4	6.0	4.4	1.9	0.5	15.5	59.7	17.4	0.7	195.8	2.41	0.212	13.45	0.028
IL-9	0.1	0.0	0.1	0.2	0.2	0.0	0.1	0.2	0.2	0.0	0.1	0.2	1.20	0.268	1.04	0.652
IL-10	0.2	0.1	0.1	0.8	0.2	0.0	0.0	0.4	0.3	0.1	0.2	1.3	0.74	0.510	2.00	0.117
IL-12p40	0.4	0.1	0.0	0.9	0.4	0.1	0.0	1.2	2.7	1.0	0.0	10.3	1.00	0.994	7.23	0.094
IL-12p70	0.2	0.1	0.0	0.5	0.2	0.1	0.0	0.8	0.5	0.1	0.0	1.3	1.18	0.809	2.46	0.079
IL-13	0.7	0.2	0.2	2.3	0.7	0.2	0.3	1.8	1.0	0.2	0.3	3.2	0.95	0.903	1.44	0.291
IL-15	1.1	0.3	0.3	2.5	0.6	0.1	0.2	1.1	1.4	0.2	0.5	3.3	0.58	0.161	2.16	0.010
IL-16	334.0	133.7	22.1	960.9	47.8	12.0	14.5	103.7	307.0	90.7	35.5	1184.0	0.14	0.051	6.42	0.066
IL-17A	0.1	0.0	0.0	0.2	0.2	0.0	0.1	0.3	0.3	0.0	0.1	0.5	2.06	0.051	1.36	0.138
IL-20	3.5	0.9	0.6	7.0	2.1	0.6	0.0	4.2	3.3	0.6	0.0	6.7	0.59	0.196	1.59	0.198
IL-21	2.3	0.4	0.4	4.6	2.1	0.7	0.0	6.7	4.2	0.7	0.8	8.6	0.89	0.766	2.01	0.065
IL-23	4.6	1.5	0.0	13.3	1.5	0.7	0.0	5.8	3.5	0.7	0.0	7.5	0.33	0.093	2.29	0.082
IL-28A	0.2	0.1	0.0	1.2	0.0	0.0	0.0	0.2	0.7	0.3	0.0	2.6	0.17	0.300	21.23	0.082
IL-33	58.7	18.9	5.2	165.1	16.4	4.8	2.1	43.8	42.9	13.0	1.0	172.3	0.28	0.052	2.62	0.151
LIF	0.0	0.0	0.0	0.0	5.7	2.0	0.0	17.5	0.4	0.2	0.0	2.0	ND in normal	0.012	0.06	0.002
PDGF-AA	2.4	0.5	1.1	4.6	3.0	1.1	0.9	9.9	10.7	1.8	1.2	25.1	1.24	0.624	3.62	0.006
PDGF-BB	27.1	12.6	4.2	109.6	53.1	38.3	5.0	320.2	33.6	14.4	4.2	217.3	1.96	0.529	0.63	0.577
sCD40L	11.0	4.6	1.5	32.0	3.4	0.5	2.1	5.5	7.0	1.7	1.6	23.8	0.31	0.126	2.05	0.139
SCF	0.6	0.1	0.1	1.1	0.4	0.1	0.3	0.8	0.7	0.1	0.2	1.3	0.69	0.171	1.77	0.062
TGF-α	2.2	0.2	1.5	3.2	2.3	0.6	0.7	5.3	8.4	1.8	1.4	26.4	1.07	0.811	3.57	0.023
TNF-α	0.4	0.2	0.0	1.8	0.2	0.0	0.0	0.4	0.6	0.1	0.1	1.5	0.36	0.344	3.67	0.052
TNF-β	0.2	0.0	0.0	0.4	0.3	0.1	0.1	0.7	0.4	0.1	0.0	1.0	1.63	0.121	1.30	0.376
TPO	2.2	1.1	0.0	7.6	1.8	0.4	0.0	4.0	1.2	0.4	0.0	4.3	0.81	0.743	0.69	0.416
TRAIL	33.9	7.4	2.4	60.8	16.0	3.6	3.9	29.5	9.7	2.2	1.5	30.5	0.47	0.049	0.60	0.122
TSLP	0.1	0.0	0.0	0.2	0.1	0.1	0.0	0.8	0.2	0.1	0.0	0.8	2.09	0.582	2.11	0.331
VEGF	13.0	1.6	4.5	16.4	30.4	16.5	4.2	140.3	74.7	25.4	4.2	341.8	2.33	0.313	2.46	0.234

Table 5.3. Quantification of analytes assayed by multiplex ELISA in patient normal thyroid tissue, benign nodules, and primary cancer tumors. Fold change is presented in red for analytes more than two-fold higher, blue for more than two-fold lower, and black for less than two-fold change. n=8-14 specimens per group. $p<0.05$ shown in red.

The metastatic phenotype was emphasized further by elevation of immune cell recruiters and modulators, CCL21, TNF-α, sCD40L, IL-4, IL-16 and IL-33 in metastatic specimens matched with primary tumors (Figure 5.8). The complete list of inflammatory modulators and the levels identified in primary tumor tissue and metastatic deposits of papillary thyroid cancer are shown in Table 5.4.

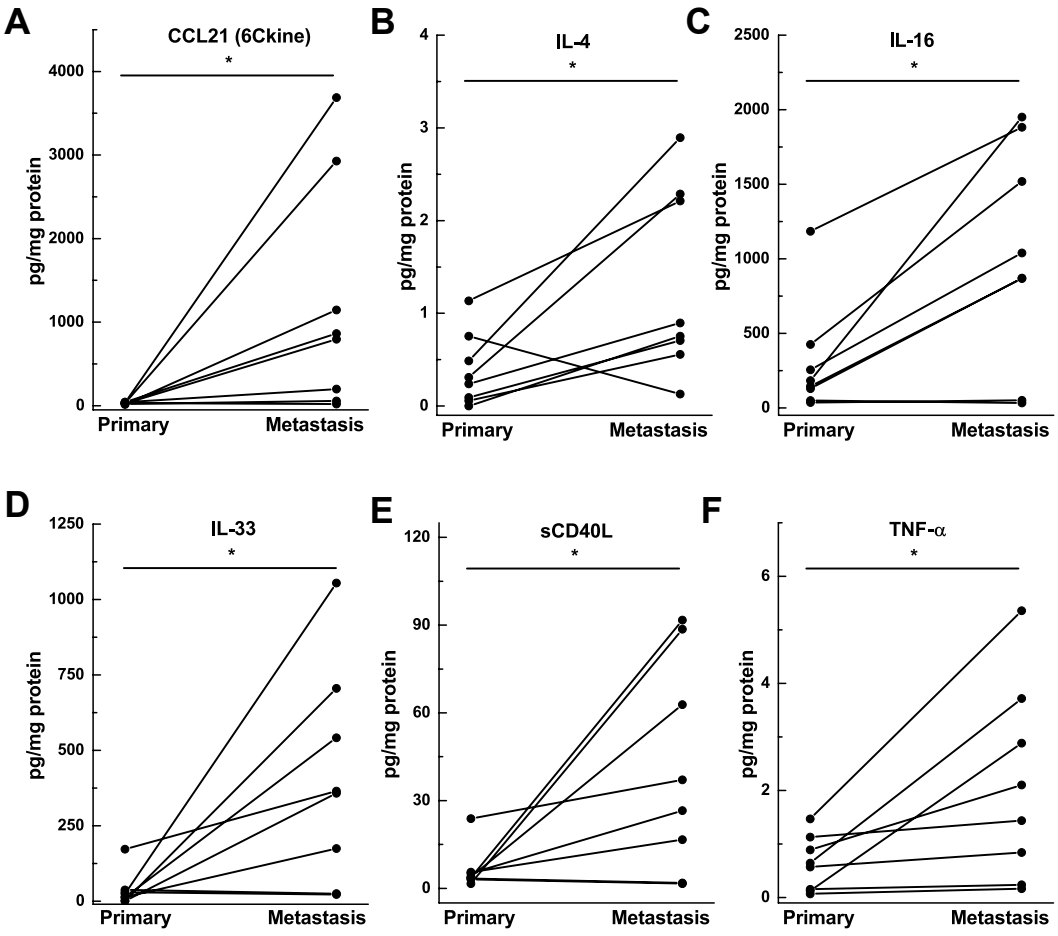

Figure 5.8. Chemokines and cytokines are significantly elevated in patient-matched thyroid metastatic lymph node nodules (metastasis) compared to primary thyroid tumors (primary). Multiplex measurement results are normalized to total protein content. n=8 matched specimens, *p<0.05 by paired t-test.

	Primary (pg/mg protein)				Metastasis (pg/mg protein)					
	Mean	SEM	Min	Max	Mean	SEM	Min	Max	Fold Change (Metastasis vs Primary)	p-value (paired)
CCL1	0.5	1.0	0.0	1.5	0.3	0.3	0.2	0.6	0.67	0.444
CCL2	341.1	93.0	264.7	422.8	246.5	241.8	48.9	377.5	0.72	0.140
CCL3	24.8	39.5	3.0	61.5	67.4	194.0	6.7	331.4	2.72	0.343
CCL4	20.9	57.0	1.3	85.5	13.6	25.2	1.4	46.9	0.65	0.051
CCL5	228.8	258.6	95.1	467.9	357.6	306.0	55.6	458.1	1.56	0.070
CCL7	4.0	5.1	0.0	9.2	4.0	12.1	0.8	20.8	0.98	0.980
CCL8	6.0	7.5	2.5	15.6	4.5	1.4	3.1	5.9	0.76	0.385
CCL11	11.6	34.2	0.3	53.1	1.3	2.5	0.4	4.3	0.11	0.180
CCL13	9.0	12.2	2.8	24.8	6.7	3.4	4.0	10.5	0.75	0.380
CCL15	4.6	7.0	1.0	11.5	3.4	2.6	1.6	6.3	0.75	0.426
CCL17	22.3	80.1	0.1	133.2	15.4	48.9	0.2	82.7	0.69	0.338
CCL21	29.5	16.6	14.5	42.9	1212.1	2424.4	19.3	3689.1	41.05	0.045
CCL22	71.6	122.7	17.7	202.5	108.0	139.2	19.2	268.4	1.51	0.322
CCL24	46.9	98.2	4.5	160.8	102.3	161.0	7.1	252.1	2.18	0.091
CCL26	20.9	20.0	9.4	39.9	16.8	8.0	12.4	24.7	0.80	0.211
CCL27	4.7	6.9	0.4	9.2	2.8	3.9	0.5	6.6	0.60	0.273
CD135	5.9	4.8	3.6	10.5	11.3	13.9	3.5	22.3	1.93	0.155
CX3CL1	142.2	418.6	32.1	725.7	65.9	97.7	15.6	170.0	0.46	0.417
CXCL1	62.1	68.7	11.6	120.1	50.7	44.3	12.0	83.2	0.82	0.378
CXCL5	40.2	156.0	3.5	257.8	23.6	67.7	2.6	113.6	0.59	0.662
CXCL10	640.6	1239.4	7.6	1583.1	195.3	270.0	7.7	498.0	0.30	0.098
CXCL12	77.4	76.4	27.4	165.2	116.0	97.6	62.8	229.9	1.50	0.209
CXCL13	104.0	238.5	1.2	349.7	184.4	250.8	0.4	349.0	1.77	0.196
EGF	0.5	1.7	0.0	2.8	0.2	0.7	0.0	1.2	0.51	0.555
FGF-2	462.2	115.4	399.5	610.1	393.0	125.8	219.9	436.3	0.85	0.052
G-CSF	4.5	6.8	1.2	13.0	2.1	1.5	1.2	4.0	0.48	0.164
GM-CSF	3.1	3.8	0.4	6.9	2.0	1.7	0.6	3.1	0.64	0.124
IFNα2	7.9	7.7	3.9	17.9	9.0	16.4	3.5	31.8	1.15	0.786
IFNγ	1.0	1.1	0.5	2.3	0.9	0.8	0.5	1.9	0.92	0.806
IL-1α	1.0	1.6	0.0	2.0	1.1	1.8	0.0	3.2	1.04	0.933
IL-1β	0.3	0.3	0.1	0.7	0.4	0.7	0.1	1.3	1.59	0.199
IL-1Rα	266.0	473.3	14.7	835.0	358.1	609.0	11.1	834.4	1.35	0.589
IL-2	0.2	0.4	0.0	0.5	0.2	0.3	0.0	0.4	0.68	0.147
IL-3	0.1	0.1	0.1	0.1	0.0	0.1	0.0	0.1	0.55	0.051
IL-4	0.4	0.7	0.0	1.1	1.3	1.8	0.1	2.9	3.40	0.027
IL-5	0.1	0.0	0.0	0.1	0.1	0.0	0.0	0.1	1.03	0.846
IL-6	35.6	101.8	0.1	151.4	6.8	15.2	0.1	24.5	0.19	0.157
IL-7	0.4	0.1	0.2	0.5	0.4	0.3	0.3	0.8	1.04	0.863
IL-8	52.4	62.9	0.7	117.6	53.7	133.7	1.7	231.6	1.03	0.965
IL-9	0.2	0.0	0.2	0.2	0.2	0.2	0.1	0.4	0.93	0.734
IL-10	0.4	0.6	0.2	1.3	1.5	3.2	0.2	5.5	3.89	0.113
IL-12p40	4.9	7.9	0.3	10.3	5.4	6.7	0.3	8.8	1.11	0.427
IL-12p70	0.5	0.7	0.0	1.0	0.8	1.1	0.5	1.4	1.48	0.333
IL-13	1.3	1.5	0.5	3.2	1.1	2.1	0.3	4.0	0.87	0.784
IL-15	1.1	0.6	0.5	1.4	1.0	1.2	0.3	2.3	0.92	0.724
IL-16	300.7	668.0	35.5	1184.0	1026.5	1305.3	33.4	1950.5	3.41	0.009
IL-17A	0.5	1.2	0.1	2.2	0.5	0.9	0.1	1.7	0.86	0.266
IL-20	3.6	4.4	0.0	6.7	4.8	7.5	1.2	14.7	1.33	0.387
IL-21	3.9	4.3	1.5	8.6	4.5	5.9	1.3	12.0	1.17	0.704
IL-23	3.5	4.8	0.0	7.5	2.7	3.9	0.0	6.6	0.77	0.409
IL-28A	0.5	1.4	0.0	2.0	0.9	1.6	0.0	2.4	1.97	0.366
IL-33	36.6	99.6	1.0	172.3	406.0	626.3	22.5	1054.7	11.09	0.024
LIF	0.4	1.4	0.0	2.0	0.1	0.6	0.0	0.9	0.27	0.377
PDGF-AA	9.9	9.7	1.2	18.4	7.7	9.6	4.1	19.7	0.78	0.449
PDGF-BB	17.6	24.6	4.2	40.8	22.1	29.1	4.3	50.4	1.26	0.564
sCD40L	6.2	12.7	1.6	23.8	40.8	64.2	1.6	91.7	6.55	0.036
SCF	0.7	0.8	0.2	1.3	0.8	0.4	0.4	1.2	1.16	0.453
TGF-α	4.5	3.8	1.4	6.8	8.6	13.4	3.2	24.2	1.91	0.158
TNF-α	0.6	0.9	0.1	1.5	2.1	3.2	0.2	5.4	3.31	0.032
TNF-β	0.5	0.5	0.2	1.0	0.3	0.3	0.0	0.5	0.62	0.103
TPO	1.1	2.8	0.0	3.3	2.6	3.8	0.6	6.1	2.25	0.145
TRAIL	10.7	17.5	1.5	30.5	14.9	29.1	1.5	50.3	1.40	0.573
TSLP	0.2	0.4	0.0	0.6	0.5	1.0	0.0	1.7	2.34	0.287
VEGF	85.2	220.1	5.1	341.8	38.6	98.5	3.1	167.3	0.45	0.199

Table 5.4. Quantification of analytes assayed by multiplex ELISA in patient-matched thyroid cancer primary and metastatic lymph node tumors. Fold change is presented in red for analytes more than two-fold higher in metastasis, blue for more than two-fold lower in metastasis, and black for less than two-fold change. n=8 patient matched specimens. $p<0.05$ by paired t-test are shown in red.

Of all the inflammatory mediators studied, only leukemia inhibitory factor (LIF) was significantly elevated in the benign nodules whereas it is not detectable in normal tissue (Figure 5.9). LIF is an interleukin 6-class cytokine that inhibits cell differentiation, and is important for maintaining the pluripotency of stem cells (369). It is also implicated as a migratory signal that promotes stromal fibroblast infiltration into cancerous tumors (370). Interestingly, the levels of LIF in tumors are similar to those in normal tissue, and are nearly 20 times lower compared to benign specimens (Figure 5.9).

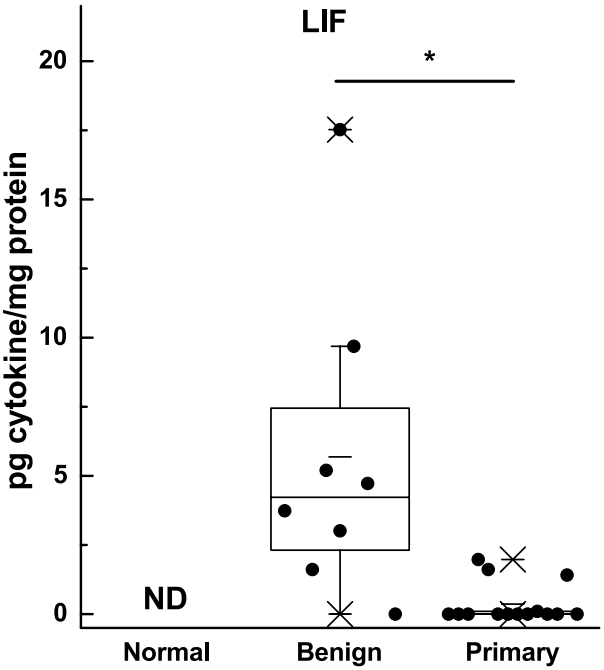

Figure 5.9. Leukemia inhibitory factor (LIF) is elevated in benign neoplastic specimens compared to cancer primary tumors. LIF was not detected (ND) in any samples from normal thyroid tissue. Box plots show minimum, mean, and maximum values (-), 25th, 50th, and 75th percentiles (box), and 1st and 99th percentiles (x). n = 8-14 per group, *P<0.05 by ANOVA with post hoc test.

5.4 Regulation of ATX and inflammatory mediators in human thyroid cancer cell culture and their effects on cell growth

We next explored the mechanistic relationship between elevated LPA concentrations and the expression of migratory and immune-cell recruiting mediators using 8305C and SW-579 thyroid cancer cells. Incubation with LPA for 24 h increased the secretion of 16 chemokines, cytokines and growth factors with the exception of CCL2 and 1L-1α in 8305C cells (Figure 5.10). These changes in inflammatory mediators were accompanied by increased concentrations of mRNA (Figure 5.11). Conversely, incubating these cells with 10 inflammatory chemokines and cytokines and the growth factors PDGF-AA and BB increased ATX mRNA expression and secretion (Figures 5.12, 5.13). These results establish the importance of ATX in mediating a broad activation in the inflammatory cycle.

We also demonstrated that LPA generated by ATX secreted from thyroid cancer cells increases cell growth. The division of thyroid cancer cells that was stimulated by LPC is dependent on the catalytic activity of ATX since the ATX inhibitor ONO-8430506 completely blocked the LPC effect. As controls, we demonstrate that ONO-8430506 itself does not block LPA-induced cell division (Figure 5.14). The effects of LPC on cell division were additive with those of CCL2, IL-1β, IL-6, IL-8, G-CSF, PDGF-AA, sCD40L and TNF-α. ONO-8430506 inhibited only the LPC-dependent component of this growth (Figure 5.15).

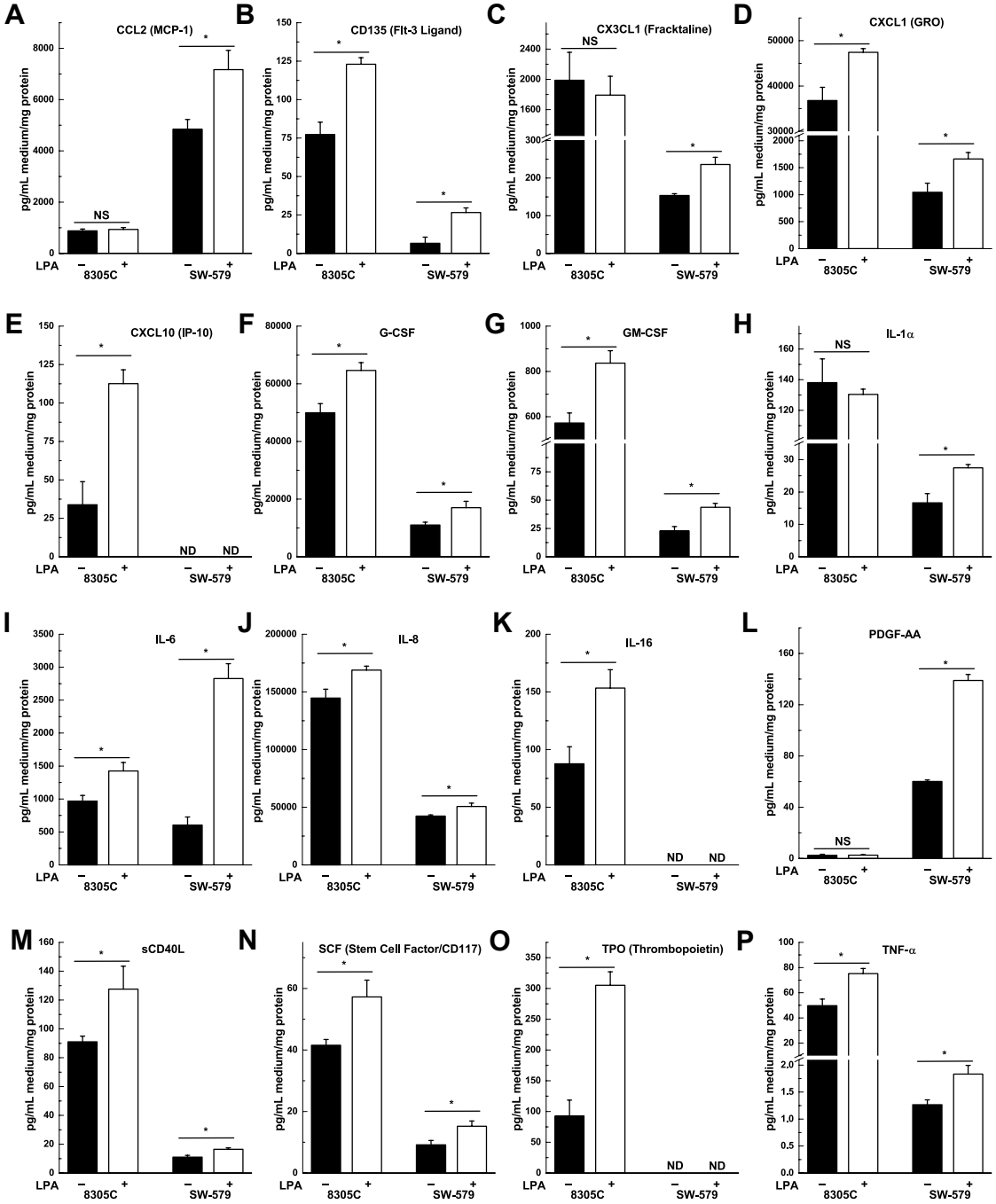

Figure 5.10. Chemokine, cytokine and growth factor secretion in 8305C and SW-579 thyroid cancer cells is significantly increased by LPA treatment. 8305C and SW-579 cancer cells were treated with 5 μM LPA for 24 h in 1% FBSC medium and medium was analyzed by multiplex measurements. Results are normalized to both total volume of medium and cell protein content. Results are means ± SEM from four independent experiments, *p<0.05 compared to no treatment, NS = not significant, ND = not detectable.

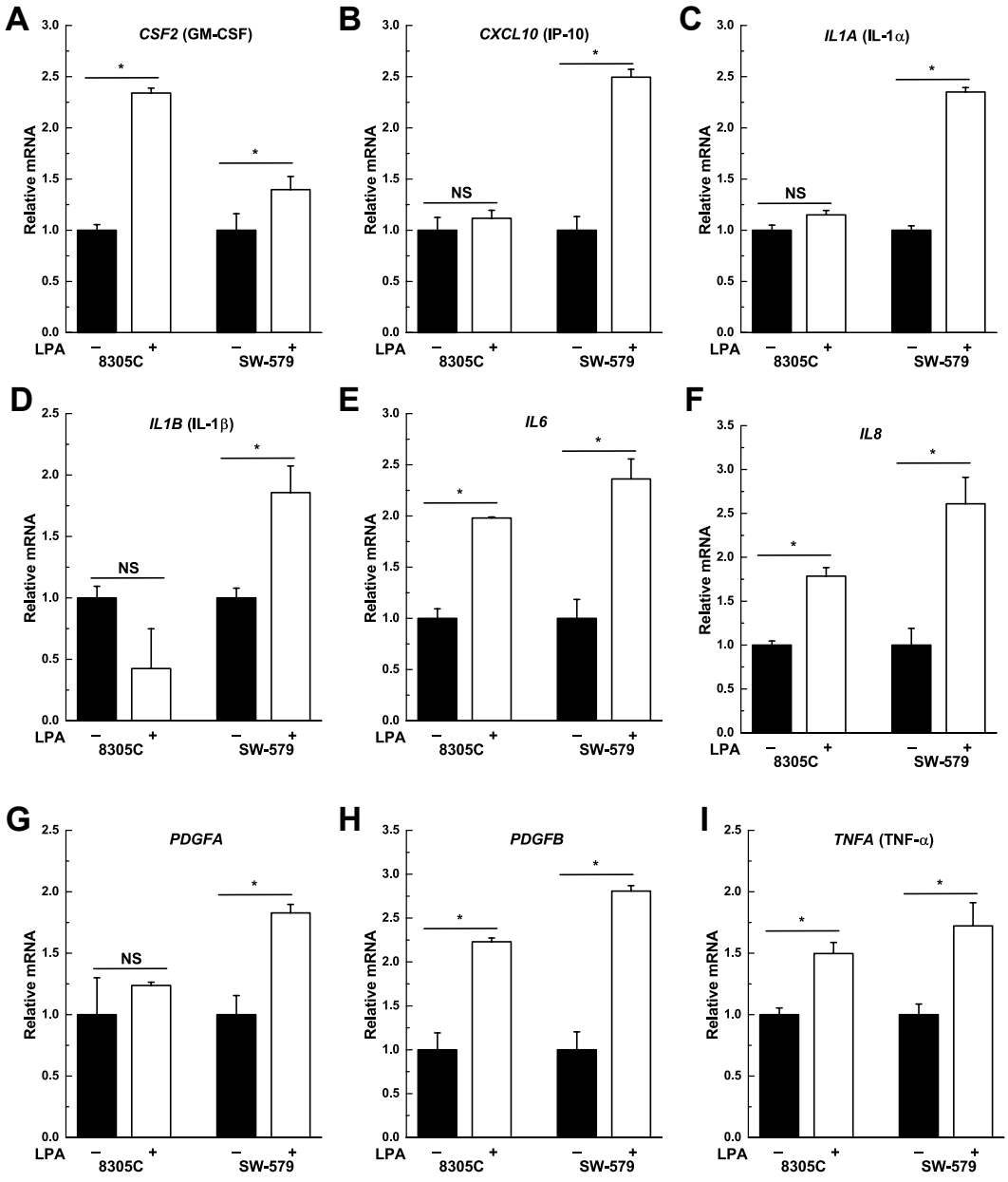

Figure 5.11. LPA increases the expression of chemokines, cytokines and growth factors in thyroid cancer cells. 8305C and SW-579 cancer cells were treated with 5 μM LPA for 12 h in 1% FBSC medium and mRNA levels were measured relative to *GAPDH*. Results are from at least three independent experiments. *p<0.05 compared to no treatment, NS = not significant.

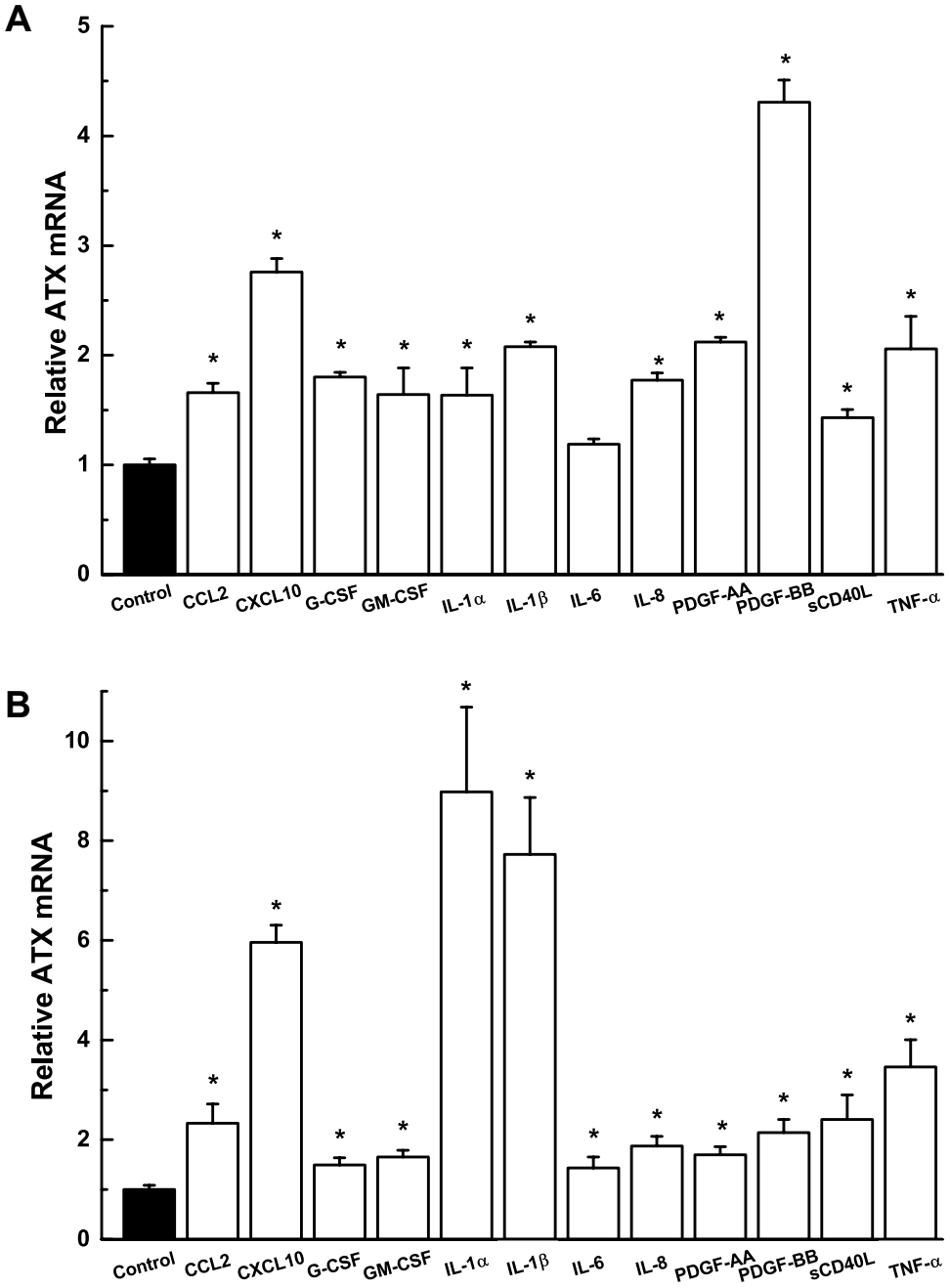

Figure 5.12. ATX mRNA expression is increased following addition of chemokines, cytokines and growth factors to thyroid cancer cells. A) 8305C and (B) SW-579 cancer cells were treated with 10 ng/mL CCL2 (MCP-1), CXCL10 (IP-10), G-CSF, GM-CSF, IL-1α, IL-1β, IL-6, IL-8, sCD40L or TNF-α, or 50 ng/mL PDGF-AA or PGDF-BB for 24 h in 1% FBSC medium and mRNA levels were measured relative to *GAPDH*. Results are from at least three independent experiments. *p<0.05 compared to no treatment control.

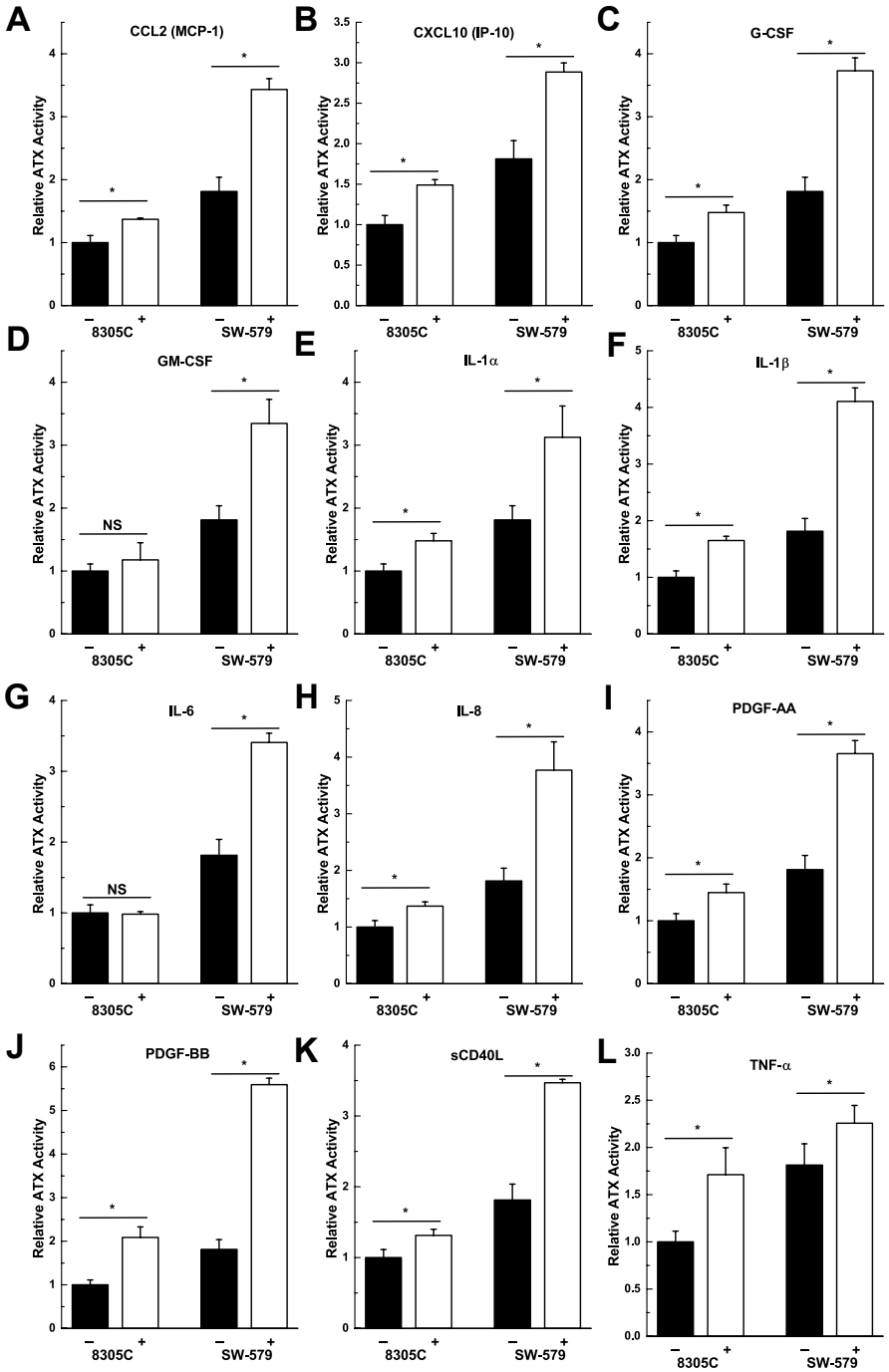

Figure 5.13. Chemokines, cytokines and growth factors increase ATX secretion from thyroid cancer cells. 8305C and SW-579 cancer cells were treated with 10 ng/mL CCL2 (MCP-1), CXCL10 (IP-10), G-CSF, GM-CSF, IL-1α, IL-1β, IL-6, IL-8, sCD40L or TNF-α, or 50 ng/mL PDGF-AA or PGDF-BB for 48 h in 1% FBSC. ATX activity in concentrated conditioned medium was normalized to cell protein content. Results are from at least three independent experiments. *P<0.05 compared to no treatment, NS = not significant.

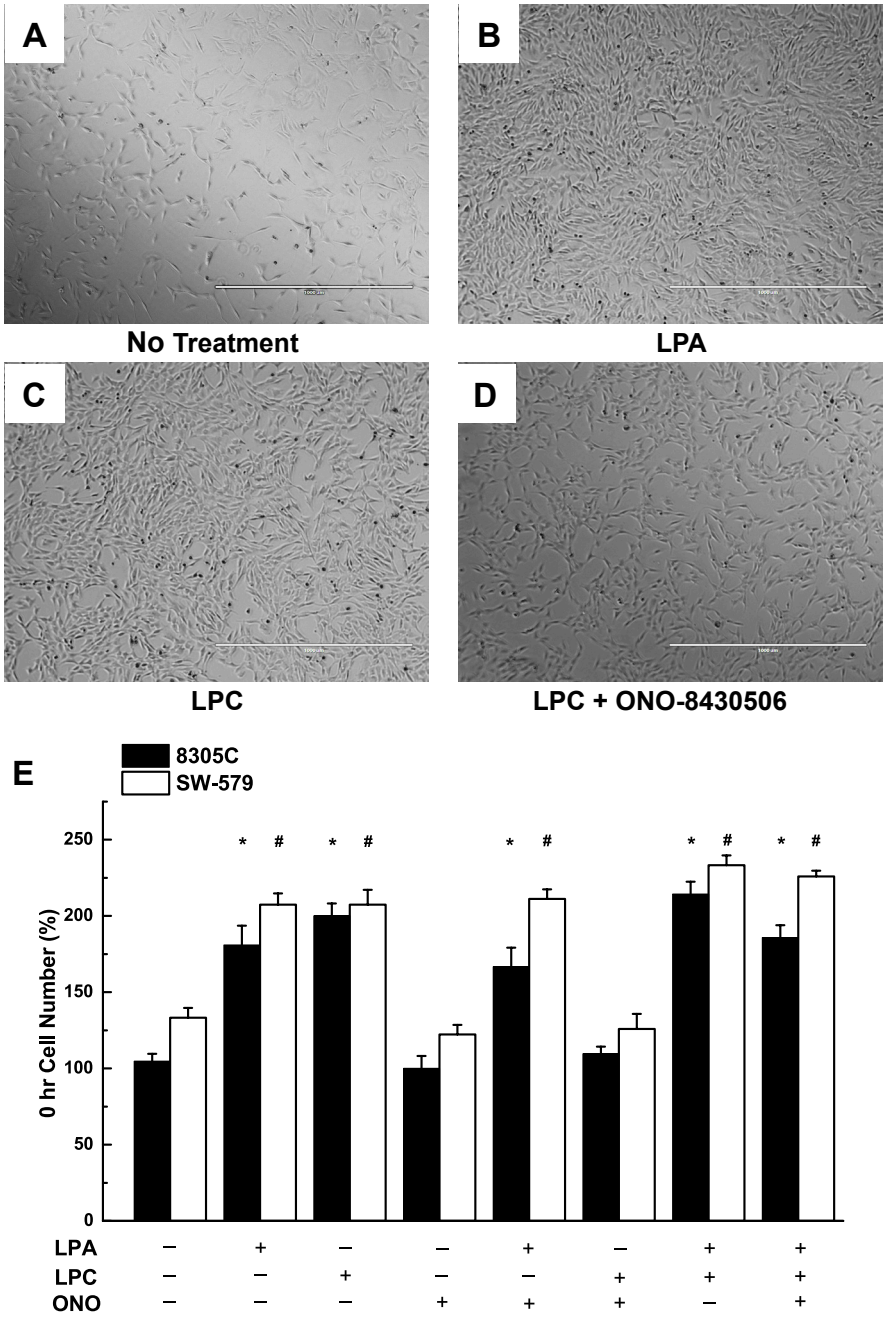

Figure 5.14. LPA increases the growth rate of thyroid cancer cells and ATX inhibition blocks LPC-mediated cell growth. 8305C and SW-579 cells were grown in serum-free medium supplemented with 1% bovine serum albuimin for 36 h and treated with or without 5 μM LPA, 100 μM LPC or 10 μM of the ATX inhibitor ONO-8430506. A-D) Representatives photographs of SW-579 cells after 36 h treatment. Scale bar = 1000 μm. E) Counts of cells at the end of the 36-h treatment. Each sample represents three independent experiments and results are expressed as means ± SEM. *$p<0.05$ compared to no treatment for 8305C cells and $^{\#}p<0.05$ compared to no treatment for SW-579 cells.

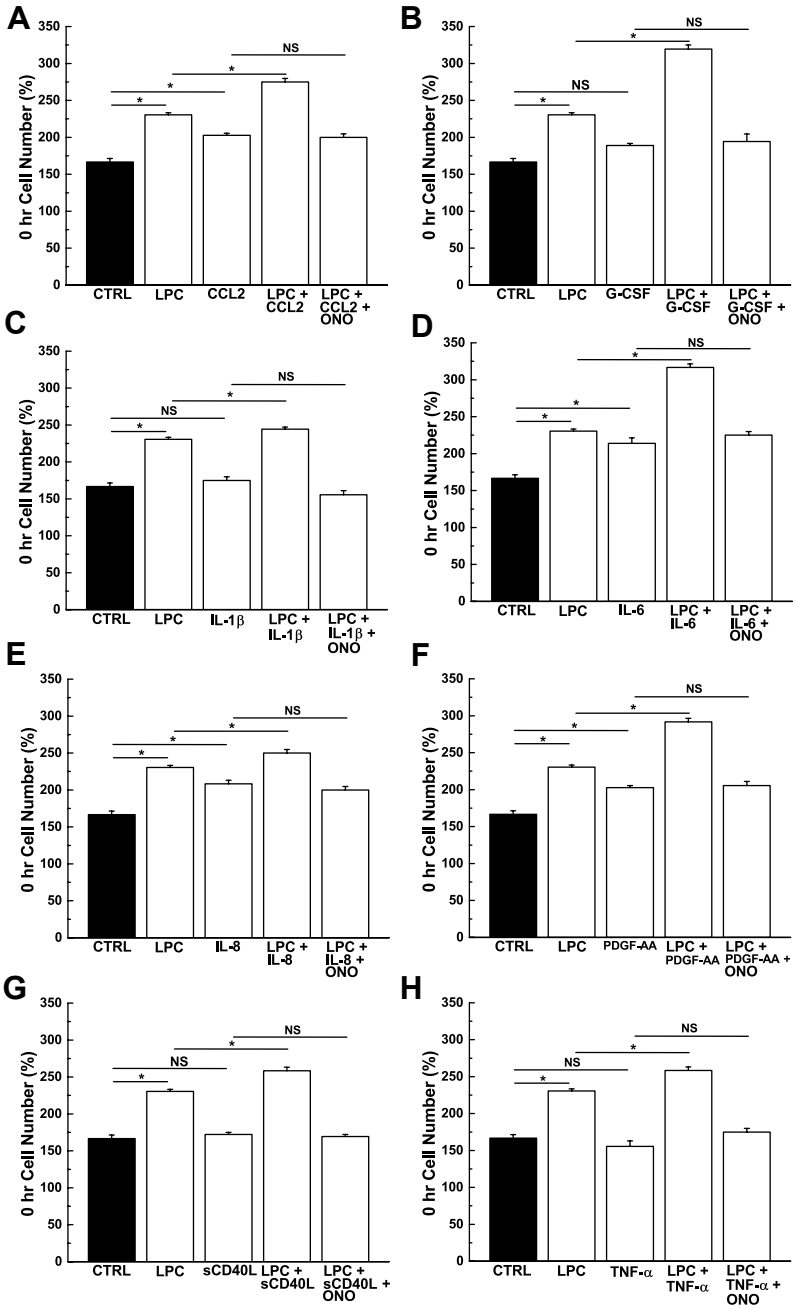

Figure 5.15. Effects of incubating SW-579 thyroid cancer cells with LPC and chemokines, cytokines or growth factors. SW-579 cells were grown in serum-free medium supplemented with 1% bovine serum albumin for 36 h and treated with or without 100 μM LPC, 10 ng/mL CCL2, G-CSF, IL-1β, IL-6, IL-8, scD40L or TNF-α, or 50 ng/mL PDGF-AA and 10 μM of the ATX inhibitor ONO-8430506. Cells were then counted at the end of the 36-h treatment. ONO-8430506 blocked LPC-dependent cell growth. Each sample represents three independent experiments and results are expressed as means ± SEM. CTRL = no treatment (control). *$p<0.05$; NS = not significant.

5.5 Effects of ATX inhibition on tumor growth and inflammatory signaling mediators in thyroid cancer xenograft mouse models

We hypothesized from the results described above that blocking LPA signaling would have two effects in thyroid tumor growth: it would attenuate both the direct effects of LPA and the indirect actions that are mediated through production of inflammatory mediators. This hypothesis was tested using a SCID mouse model with the human thyroid cancer cell lines 8305C and SW-579. Both cell lines are highly tumorigenic. Daily dosing the mice with 20mg/kg of the ATX inhibitor ONO-8430506 at 7 days after the establishment of tumors resulted in a decrease of tumor growth of 50-60% (Figure 5.16). Effective ATX blockade with ONO-8430506 was demonstrated by reduced plasma ATX activity (>90%) and LPA concentrations (>70%) (Figure 5.17A-F). As predicted, plasma S1P and SA1P concentrations were not affected (Figure 5.17G,H).

Overall, this decrease in tumor growth was associated with a decreased mitotic rate and vascularity as quantified by Ki67 (Figure 5.18A,B) and CD-31 staining (Figure 5.18C,D), respectively. We also assessed ONO-8430506-induced apoptosis by staining for cleaved caspase-3. Both 8305C and SW-579 tumors treated with the ATX inhibitor had 2-fold higher levels, but this trend did not reach statistical significance (Figure 5.19).

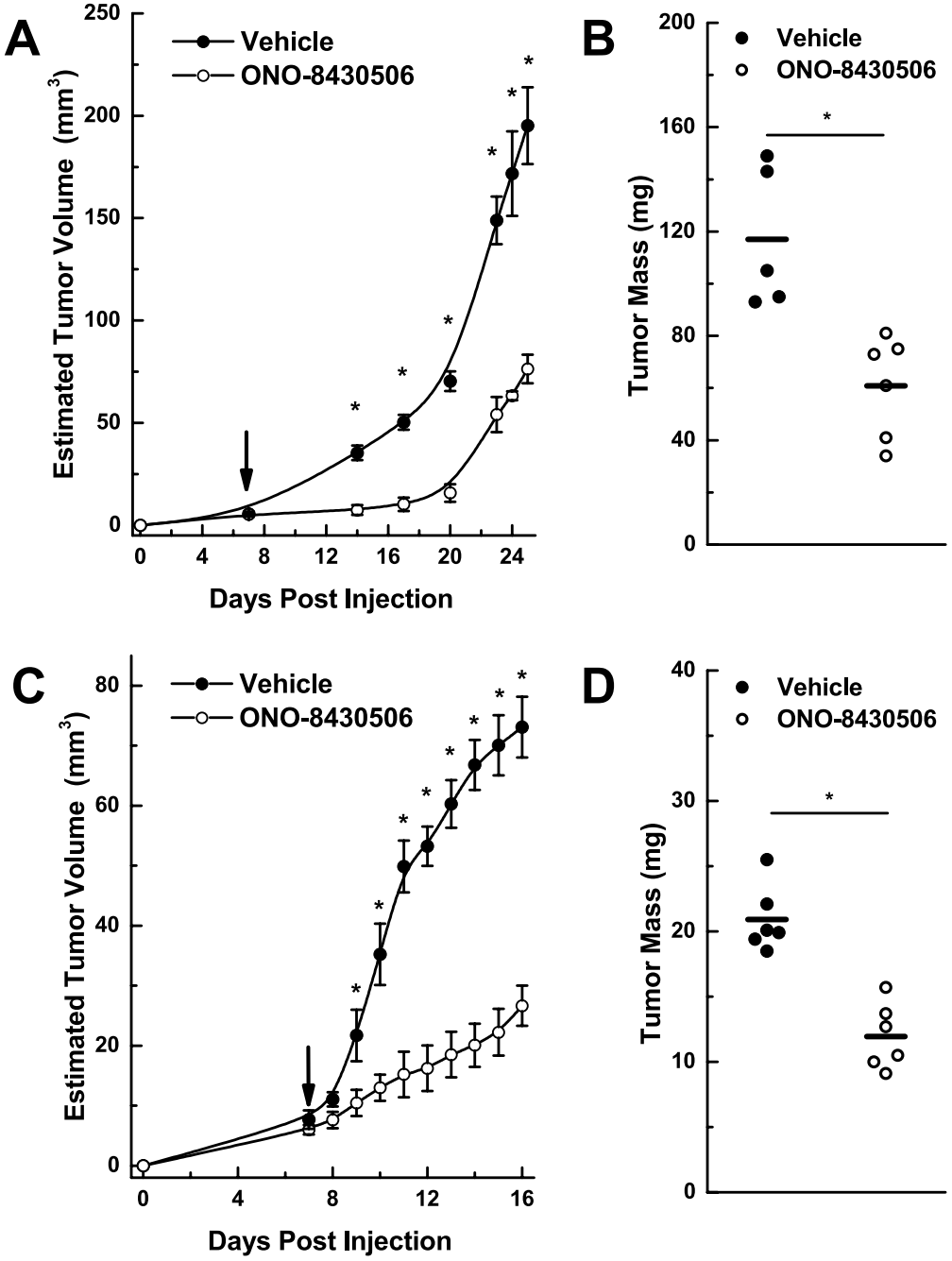

Figure 5.16. ATX inhibition with ONO-8430506 slows the growth of xenograft thyroid tumors in SCID mice. A) Estimated tumor size and (B) excised tumor mass from mice injected with 8305C cancer cells. n=5-6 per group. C) Estimated tumor size and (D) excised tumor mass from mice injected with SW-579 cancer cells. n=6 per group. In both experiments mice were gavaged daily with either vehicle or 20 mg/kg ONO-8430506 after 7 days of tumor growth.

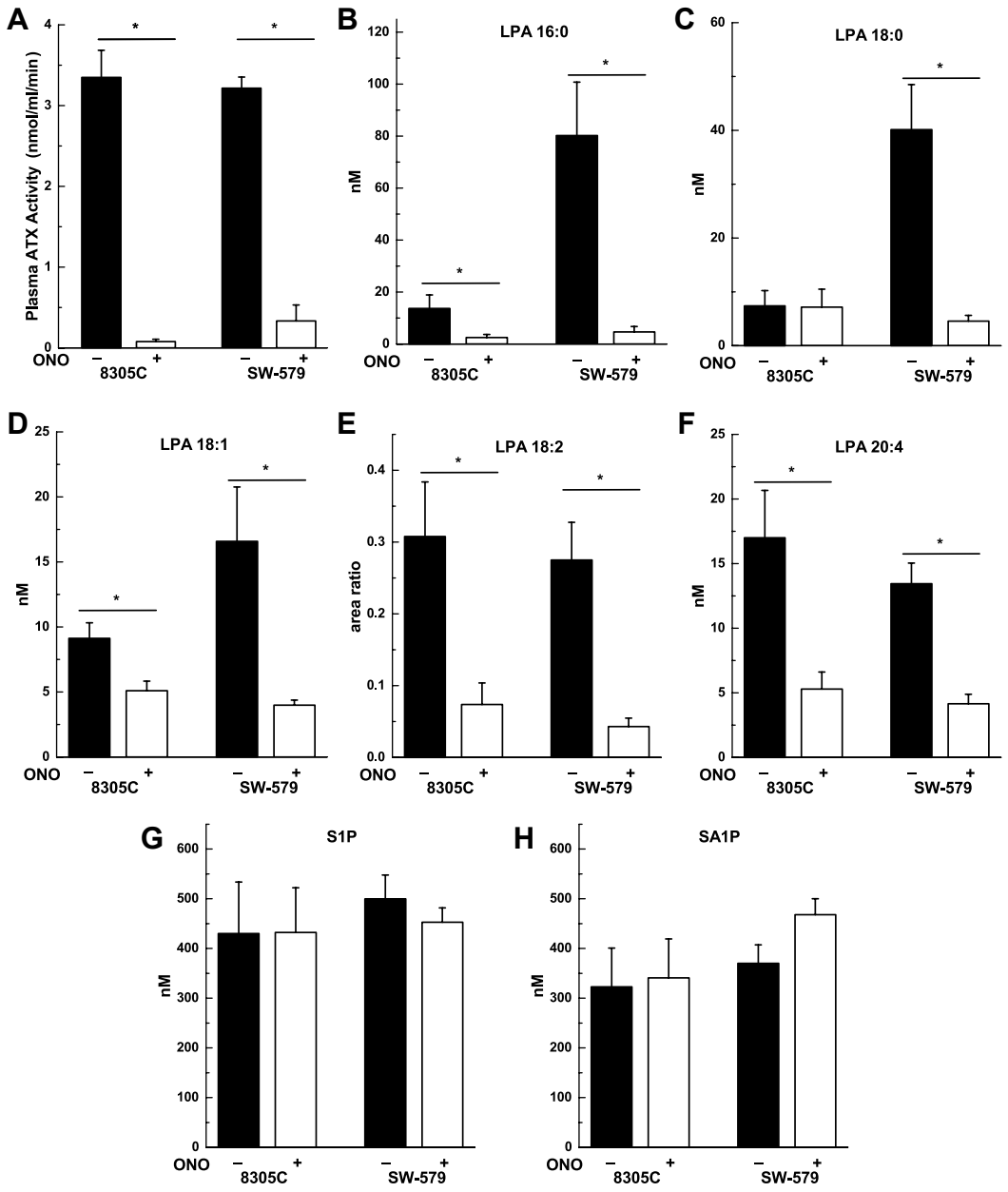

Figure 5.17. Effects of ONO-8430506 on plasma ATX activity (A) and lysophospholipid species (B-H). Mice were treated daily with 20 mg/kg ONO-8430506, and blood plasma was collected 6 h after last dose. Control mice were gavaged with water. ATX activity was measured by the choline-release ATX assay after 4 h incubation at 37°C with 3 mM C14:0-LPC. Lysophospholipid concentrations were measured in blood plasma by comparison to corresponding standards or relative to the C17:0-LPA internal standard. Results are means ± SEM for 5 mice/group. *p<0.05 compared to vehicle treatment.

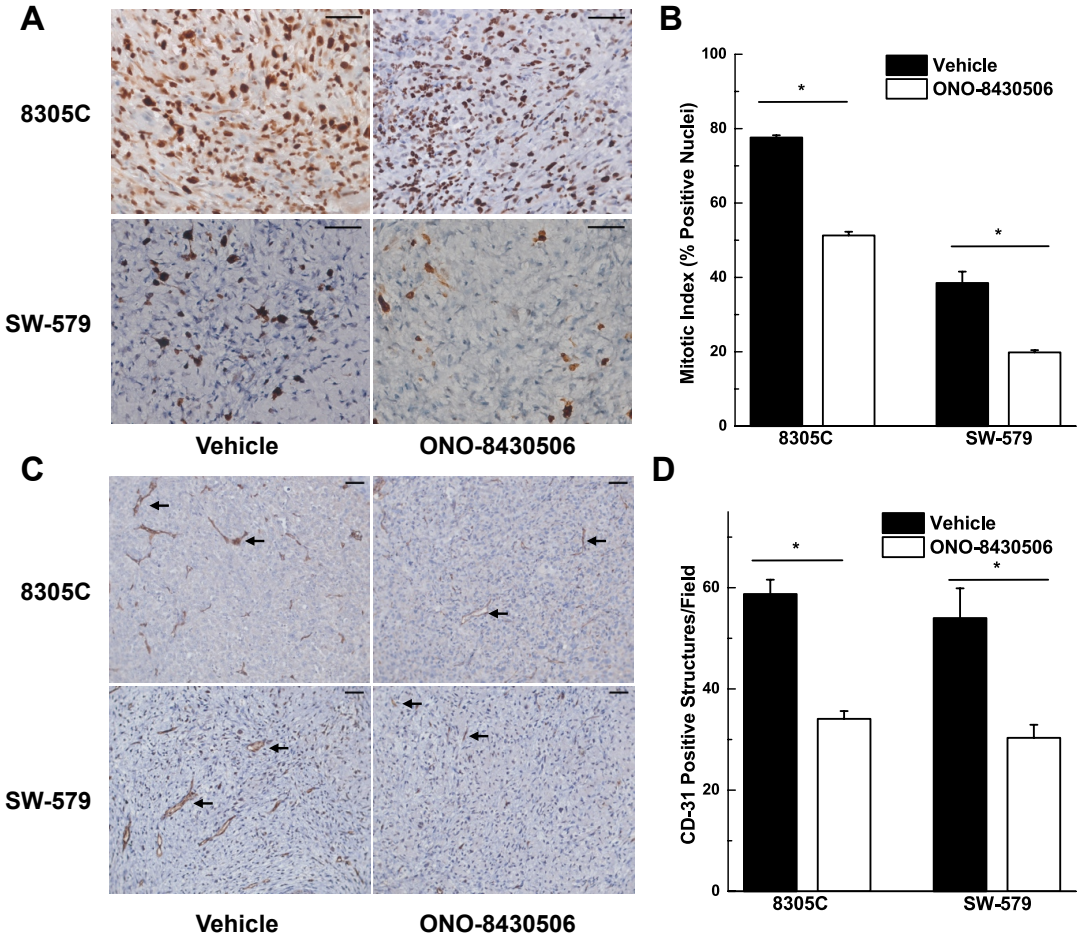

Figure 5.18. ATX inhibition with ONO-8430506 reduces Ki67 and CD-31 levels in xenograft thyroid tumors. A) Representative photographs and (B) quantification of nuclear Ki67 staining. C) Representative photographs and (D) quantification of CD-31 positive structures. Arrows point to representative structures. Mice were treated daily with 20 mg/kg ONO-8430506, and vehicle mice were gavaged with water. Tumors were collected 6 h after last treatment. Scale bar = 50 μm. n=3-4 per group, *p<0.05 compared to vehicle treatment.

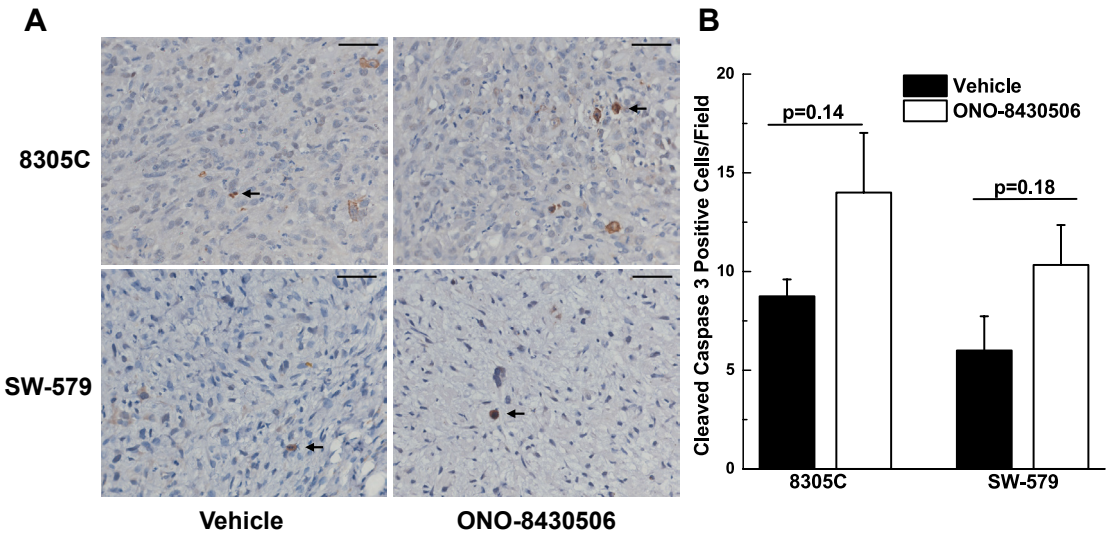

Figure 5.19. Immunohistochemical assessment of apoptosis in excised xenograft tumors. A) Representative photographs and (B) quantification of cleaved caspase 3-positive cells per field of view. Arrows point to representative staining. Mice were treated daily with 20 mg/kg ONO-8430506, and vehicle mice were gavaged with water. Tumors were collected 6 h after last treatment. Scale bar = 50 μm. n=3-4 per group. Results did not reach statistical significance.

Inhibition of ATX did markedly and broadly decrease the concentrations of 14 inflammatory chemokines and cytokines within the tumors (Figure 5.20A-N). The effects on angiogenesis seen in Figure 5.18 are compatible with the decreased PDGF-AA and VEGF concentrations caused by ONO-8430506 (Figure 5.20O,P). Staining for the inhibited ATX in tumors showed that it was confined to the cancer cells, consistent with cancer cells being the predominant producer of ATX in thyroid tumors (Figure 5.21).

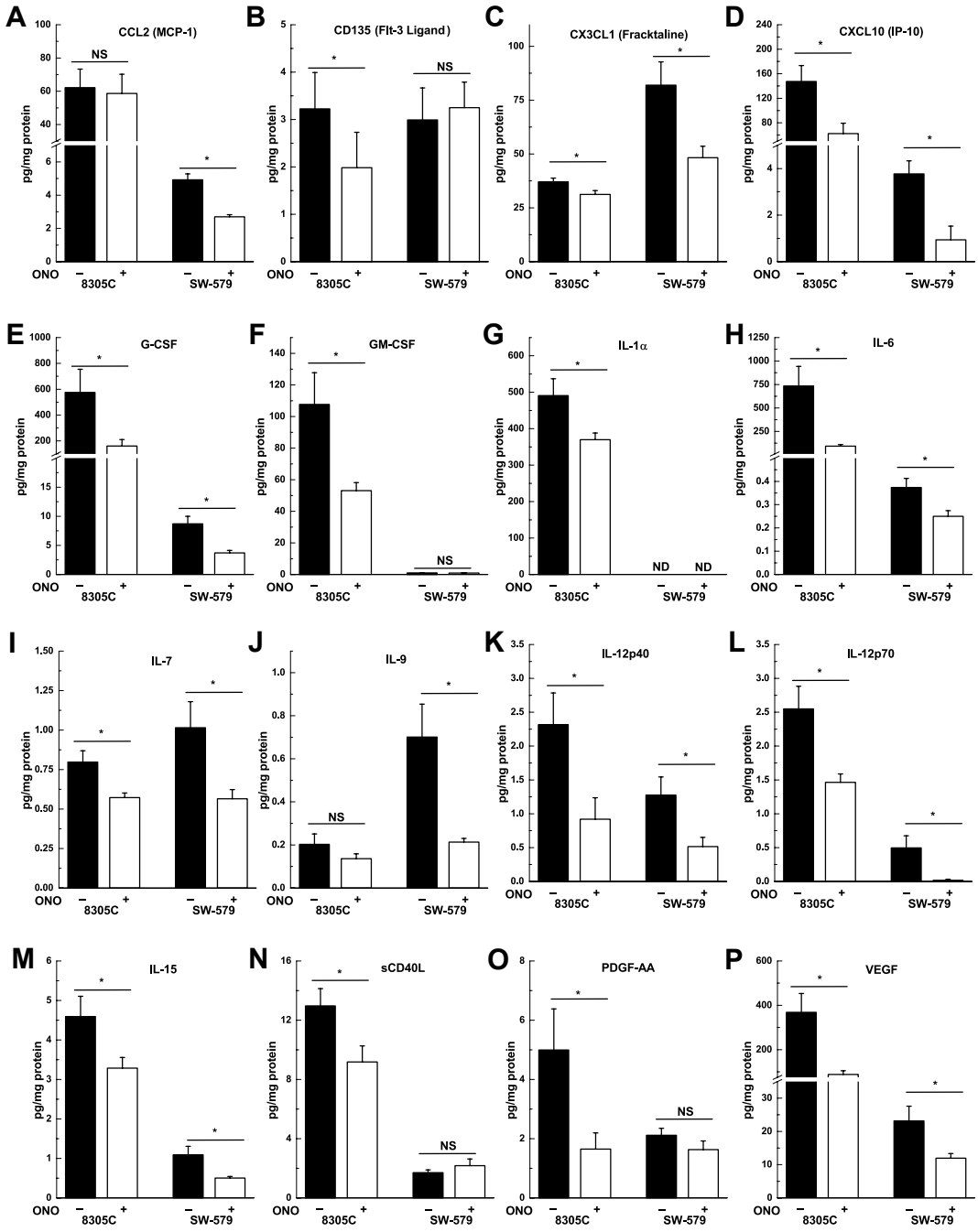

Figure 5.20. Chemokines, cytokines and growth factors in 8305C and SW-579 xenograft thyroid tumors are significantly suppressed by ONO-8430506 treatment compared to vehicle treatment. Mice were treated daily with 20 mg/kg ONO-8430506, and vehicle mice were gavaged with water. Tumors were collected 6 h after last treatment. Multiplex measurement results are normalized to total protein content. Results are means ± SEM for 4-6 mice per group, *p<0.05 compared to vehicle treatment, NS = not significant, ND = not detectable.

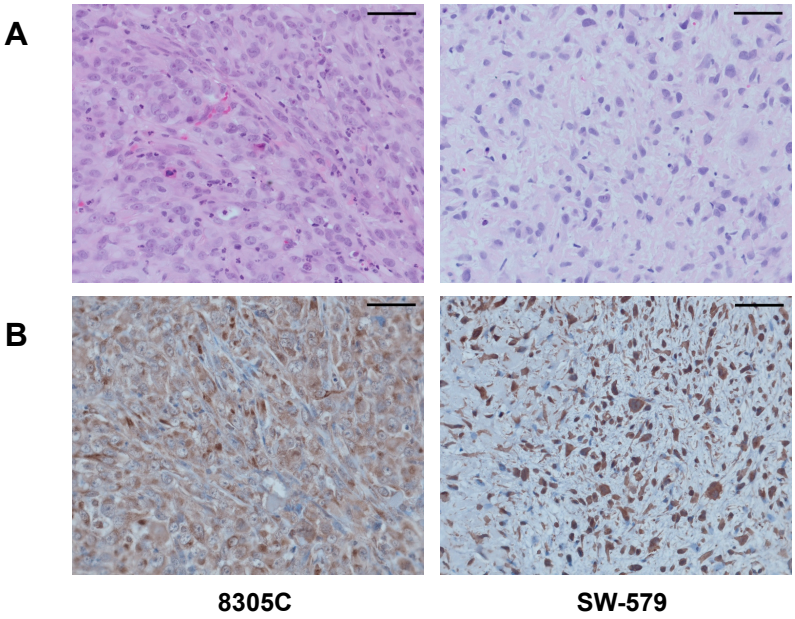

Figure 5.21. (A) Hematoxylin and eosin and (B) representative ATX immunohistochemical staining in 8305C and SW-579 xenograft thyroid tumors. No differences in hematoxylin and eosin or ATX staining were seen between vehicle- or ONO-8430506-treated tumors. ATX staining was confined to the cancer cells. Scale bar = 50 μm.

5.6 Discussion

The present studies provide a new paradigm for understanding the role of inflammation in papillary thyroid cancers. High ATX expression and the resulting elevation in LPA concentrations is associated with increased expression of inflammatory chemokines, cytokines and growth factors and this phenotype can distinguish malignant nodules from benign disease. Second, we document that the progressive inflammatory response persists in metastatic tissue where similar or even higher levels of inflammatory mediators are observed compared to primary tumors. The qualitative and quantitative effects of the inflammatory response are larger tumors with

increased mitotic rate and vascularity. This is similar to what is observed in aggressive disease where tumor size, mitotic rate and vascularity are linked with decreased survival (371). Third, it is clear that selective inhibition of autotaxin with ONO-8430506 is sufficient to decrease the level of ATX activity by more than 90% as well as significantly decrease the concentrations of inflammatory modulators in our mouse models of thyroid cancer. These effects in turn led to a significant decrease in tumor growth potential and limited the proliferative index and vascularity of these tumors. We propose that ONO-8430506, as a selective agent disrupting ATX activity, represents a new option for therapy for aggressive, metastatic papillary thyroid cancer. Hence, ATX blockade could block the production of inflammatory drivers found in other tumors that not only promote tumorigenesis, but also immune evasion and treatment resistance (10, 372-374).

Our work with cultured thyroid cancer cells explains the relationship between ATX/LPA and inflammatory mediators. ATX activity and LPA formation stimulate the production of inflammatory mediators, which result in a vicious cycle of more ATX secretion (Figure 5.22). This inflammatory phenotype increases the division of thyroid cancer cells and the component that depends on LPC could be blocked by ATX inhibition. We also know that ATX and LPA increase cancer cell migration, metastasis (17, 18) and survival during chemotherapy and radiotherapy (10, 18).

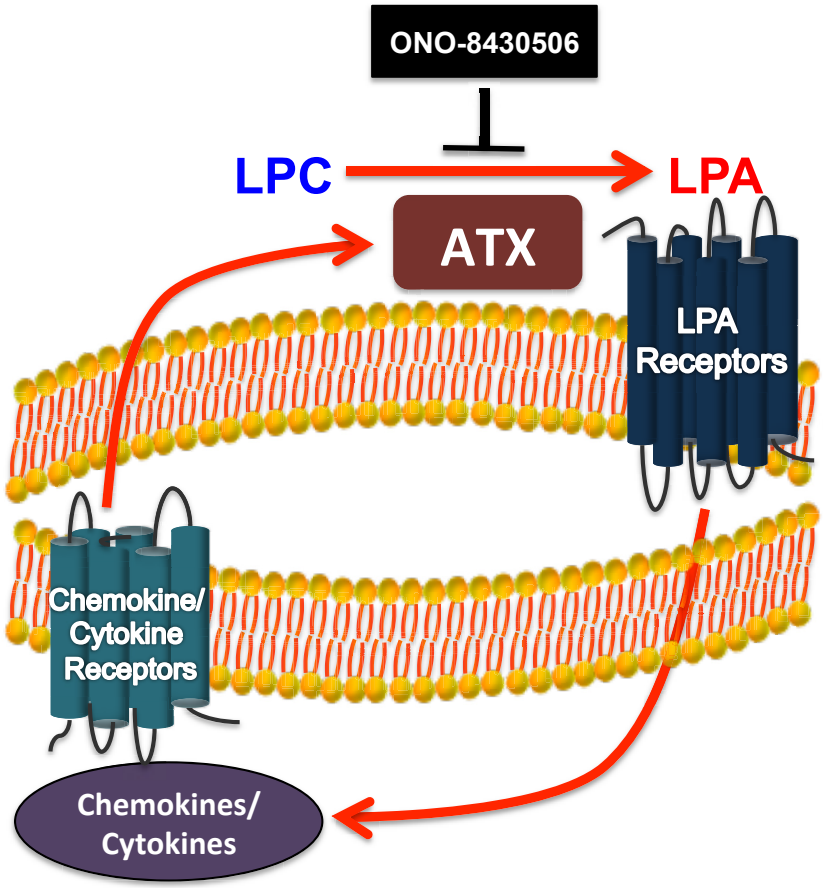

Figure 5.22. Model of the relationship between ATX/LPA and inflammatory chemokine and cytokine production and signaling in thyroid cancer cells. ATX produces LPA by hydrolyzing the choline headgroup from LPC. LPA signaling through its receptors leads to an increase in chemokine and cytokine production. These inflammatory mediators signal through their own receptors to further induce ATX production, establishing a vicious cycle that drives thyroid cancer progression. This cycle can be broken by inhibiting ATX catalytic activity with ONO-8430506, which in turns reduces both LPA and chemokine/cytokine concentrations and ultimately slows thyroid tumor growth.

We used two SCID mouse models with human thyroid cancer cells to demonstrate the existence of the ATX-LPA-inflammatory cycle *in vivo*. These mice have severe decreases in T and B lymphocyte expression, which prevents immune rejection of heterologous cancer cells. However, we could

still determine the effects of the ATX inhibitor, ONO-8430506, on the production of inflammatory mediators by the cancer cells themselves. ONO-8430506 had a long acting effect in decreasing ATX activity and LPA production. As a result it effectively broke the inflammatory cycle and decreased the concentrations of inflammatory cytokines in the thyroid tumors resulting in decreased tumor growth. Our mouse models of thyroid cancer, which employ flank injections of cancer cells, do not lead to metastasis. However, inhibiting ATX activity and LPA signaling decreased metastasis in other mouse models (253, 255) and in our breast cancer studies (Chapter 4).

Our work with cultured thyroid cancer cells explains the connection between LPA signaling and inflammation in thyroid cancer that was inferred by previous studies (363-365, 375). ATX activity and LPA formation stimulate the production of inflammatory mediators, which result in a vicious cycle of more ATX secretion (Figure 5.22). This inflammatory phenotype increases the division of thyroid cancer cells and the component that depends directly on LPA formation could be blocked by ATX inhibition. LPA also has an indirect effect on tumor growth through stimulating the production of inflammatory mediators which themselves can promote growth. The interesting concept that follows is that ATX may provide a singular focus for initiating the global inflammatory response in tumors although the particular inflammatory mediators most important to particular cancer types may vary, for example, IL-1α, IL-6 and IL-17 in pancreatic, gastric and colorectal cancers,

respectively (372-374). In general, ATX/LPA signaling and the subsequently upregulated inflammatory programs drive tumor growth, immune evasion, metastasis and resistance to chemotherapy and radiotherapy in virtually all the major cancers, including melanoma, neuroblastoma, glioblastoma multiforme and breast, lung, colon, ovarian, renal cell and hepatic cancers (10, 17, 18, 163).

Tumors have been likened to ”wounds that do not heal” (282, 340, 341) and ATX is part of the defense mechanism used by the body to facilitate wound healing (9, 339). We show that increased expression of ATX, LPA and inflammatory mediators is characteristic of malignant thyroid disease and thus ATX is an integral component of tumorigenesis in thyroid follicular cells. This includes driving tumor growth and promoting markers of more aggressive tumor histology including proliferation and vascularity, metastasis, immune evasion and treatment resistance (10, 376-378). The inflammatory process mediated by ATX in thyroid cells is an autocrine cycle. This paradigm probably extends to other cancers such as glioblastomas and melanomas where ATX is secreted by the cancer cells (379, 380). In contrast, as shown in Chapter 4, breast cancer cells do not normally make significant quantities of ATX. Instead the inflammatory milieu produced by the breast tumor stimulates ATX secretion by adjacent adipose tissue (Figure 4.22). In both scenarios, breaking the inflammatory cycle with a long acting ATX inhibitor decreases tumor growth in mice. Therefore, regardless of where the ATX is

produced, an ATX inhibitor is effective at depriving cancer cells of LPA and thus attenuating the activation of all LPA receptors. ATX inhibition in thyroid cancer also decreases the secretion of a large variety of inflammatory chemokines and cytokines, which consequently mitigates cancer progression. Our results support the use of ATX inhibition as a potentially new strategy for counteracting the ATX-LPA axis and the role of inflammation in driving the progression of thyroid and other cancers.

CHAPTER 6

GENERAL DISCUSSION AND FUTURE DIRECTIONS

6.1 Introduction

In this section, we will present considerations for effective pharmacological inhibition of ATX/LPA signaling and highlight both major concerns and expectations for the introduction of inhibitors into clinical practice. We will also summarize our new insights into ATX production in cancers consistent with the roles of ATX in other inflammatory diseases. Finally, we will discuss the role non-cancer cell populations play in the production of ATX that fuels cancer progression, and suggest future directions for research.

6.2 Considerations for the inhibition of ATX/LPA signaling

Designing antagonistic ligands against cell-signaling receptors is especially tricky since such ligands may be partial agonists in secondary tissues or have agonistic properties through redundant and/or related receptors. This problem is best highlighted by the use of tamoxifen. Tamoxifen, a selective estrogen receptor-α modulator (SERM), is used as an antagonist to block (pre)cancerous cell division in breast tissue as part of the treatment regimen for both early and advanced estrogen-receptor-α positive breast cancers. Unfortunately, tamoxifen has partial agonist activity in the endometrium, which in turn increases the risk of endometrial cancer (381). Consequently, tamoxifen is not used in patients for greater than five years unless they have already undergone a hysterectomy (382). This agonist

activity in endometrium can be mediated through the G-protein-coupled estrogen receptor GPR30 (383). By comparison, the potential for disparate pharmacology of LPA receptor antagonists may be even greater than for drugs like tamoxifen. There are at least six LPA receptors that have evolved from different ancestral genes with LPA_{1-3} belonging to the Edg receptor family. LPA_{4-6} are more closely related to the purinergic GPCRs (83). The complexity, heterogeneity and redundancy in these receptors present considerable difficulties compared to those of tamoxifen for designing effective LPA receptor antagonists devoid of unintended side effects, including partial agonist activity (Figure 1.3).

As discussed earlier, ATX KO mice die *in utero* and the phenotype can be partially reversed by exogenous addition of LPA to explant embryos (84). This emphasizes the critical role of LPA-mediated signaling, presumably through LPA receptors. To study this, KO mice for all the LPA receptors have been generated and yet all models are viable with no or minimal phenotypes. Even more strange, most LPA signaling is mediated through LPA_{1-3}, and yet despite creating all the double KO combinations of these receptors as well as the triple KO, these mice are viable (9, 32, 33). These findings underscore the incredible redundancy of LPA-receptor signaling pathways (Figure 1.3) and also suggest there may be other receptors that can mediate LPA signaling.

Likewise, ATX inhibitors may be a more effective and safer means of targeting LPA signaling than LPA receptor antagonists since ATX produces virtually all of the extracellular LPA. With ATX, there is only one target for inhibition versus multiple LPA receptors. With effective ATX inhibition, plasma LPA levels rapidly fall and remain inhibited with sustained therapeutic dosing (8). Most disease conditions correlated with ATX/LPA signaling rely on sustained elevated LPA levels brought about by increased ATX protein production. LPA levels in physiological processes seem not to be as high as levels in cancer and other inflammatory-mediated diseases. This suggests that ATX inhibition is more likely to have therapeutic effects by lowering LPA levels below that required for pathogenesis, but still leave for sufficient LPA production to meet physiological requirements. Also, we have presented evidence in Chapter 4 that ATX inhibition may selectively decrease the production of multiple inflammatory mediators induced in pathological conditions like cancer, whereas the levels of tonal inflammatory mediators in normal mice were unaffected. This argues also that ATX inhibition may have little side effects on physiological processes modulated by inflammatory-mediated signaling.

Currently, ATX inhibitors are still in the pre-clinical phase of development. Most of the latest inhibitors are non-LPA-mimics, which have improved bioavailability profiles and no partial-agonist/antagonist reactivity with LPA receptors. We predict that these inhibitors will have great potential,

either on their own or as adjuvant therapy, for treating inflammatory diseases including cancer. We also predict that ATX inhibition could be synergistic with conventional anti-inflammatory therapy given that ATX inhibitors have been shown to be equally effective as NSAIDs in reducing inflammation in animal models (8). In fact, adding an ATX inhibitor might lower dosage requirements for NSAIDs, or a chemotherapeutic agent. This is seen in our own work where ATX inhibition improved the anti-tumor effects of a dosage of doxorubicin in mice that otherwise had virtually no effect on its own (Chapter 4). This could provide benefits by improving the tolerance of patients to the treatment.

6.3 ATX as an inflammatory-dependent, tumor microenvironment promoter of cancer progression and therapy resistance in cancer

As described earlier, ATX is elevated in many different tumors, implicating ATX as a promoter of cancer progression. These results, coupled with the initial identification of ATX as a secreted enzyme in melanoma cell cultures, has given rise to the impression that ATX is generally produced in cancer by an autocrine mechanism (175). Evidence for this model of ATX production is well supported in melanoma (384), gliomas (379, 385), and in thyroid cancer as previously presented (Chapter 5). However, this may not necessarily always be the case as we demonstrated in breast cancer (Chapter 4). Even though high levels of ATX are often found in primary carcinomas and metastatic tumors compared to normal or benign specimens,

this does not mean that the cancer cells themselves produce ATX. When discussing tumors, the terms “tumor cells” and “cancer cells” are often used interchangeably, ignoring the heterogeneous cell populations that comprise tumors. Tumors are composed of not just cancer cells but also of stroma, which include fibroblasts, endothelial cells and leukocytes. All of these cells are surrounded by a host of signaling molecules, which facilitate communication between different cell populations (386, 387). This model of interaction between different cell populations is termed the tumor microenvironment and its importance in understanding cancer biology is rapidly gaining momentum (386-388).

In the Introduction, we illustrated that ATX production by fibroblasts and endothelial cells promotes chronic inflammation-driven diseases like rheumatoid arthritis and atherosclerosis (146, 156). Because cancer is also a chronic inflammatory condition, it is plausible that cancer progression and cancer therapy resistance can be fueled by ATX from non-cancer cell sources, such as the tumor stroma or surrounding tissue. This was illustrated earlier by ATX from endothelial cells promoting resistance of renal cell carcinoma to treatment with sunitinib (223). Our results from the analysis of both human breast tumors and the Balb/c mouse 4T1 breast cancer model also support a non-cancer-cell source for ATX in promoting breast tumor growth and subsequent metastasis (Chapter 4). These cancer cells produce insignificant quantities of ATX compared to breast fibroblasts and breast

adipose tissue. Adipose tissue produces high levels of ATX (150, 151) (Figure 1.6). As mentioned in Chapter 4, we found that 4T1 breast cancer cells express thousands of fold less ATX mRNA and hundreds of fold less ATX protein than the mammary fat pads of Balb/c mice. In fact, in the Broad Institute's Cancer Cell Line Encyclopedia (184), breast cancer cell lines are amongst the lowest expressers of ATX mRNA (Figure 1.9). However, in light of high ATX expression in surrounding breast adipose tissue (Figure 1.6), breast cancers can easily acquire ATX to stimulate LPA production from breast tissue stroma-derived circulating ATX. In fact, cancer cells may be able to recruit ATX to their cell surfaces through integrin binding to the SMB domains of ATX (68). In such a situation, cancer cells can create an artificial pool of ATX adjacent to their LPA receptors, resulting in a microenvironment concentration of LPA many fold higher than in the surrounding extracellular space. The growing tumor containing 4T1 cancer cells in our mouse model further induces the production of ATX mRNA and protein in the surrounding mammary fat pad through the secretion of inflammatory mediators. A paracrine model of ATX production in our mouse model (Figure 4.22) explains why the growth and viability of the 4T1 cancer cells were not affected *in vitro* when treated with the ATX inhibitor ONO-8430506. However, when 4T1 cells were injected into mice, ONO-8430506 decreased both tumor growth and metastasis. Introducing ATX shRNA in 4T1 cells has no significant effect in slowing primary tumor growth (332), consistent with the cancer cells making

an insignificant amount of ATX. Instead, potent ATX inhibition and subsequent depletion of LPA significantly impedes the 4T1 tumor phenotype in our mouse experiments by blocking LPA production from non-cancer sources of ATX that the cancer cells in the tumor relied upon. Hence, the utility of an ATX inhibitor for treating cancer need not be restricted to those cancer cells that produce ATX themselves.

Ultimately, when trying to understand the pathological role of a signaling process across a varied disease spectrum like cancer, it is important to first identify the general phenomenology of that signaling. Then, these commonalities need to be compared to signaling in the physiological context, since pathology is in simplest terms an aberration of a normal process. The knowledge gained from a study of physiology in turn can explain the pathology. In the case of ATX/LPA signaling, LPA receptors are ubiquitous to all cells (37). Consequently, the initiation of a signaling cascade from activation of these receptors depends largely on the availability of LPA. All studies with LPA and cancer cells demonstrate LPA to be a tumorigenic signal in some fashion (for example, proliferation, migration, angiogenesis and survival against cytotoxic stresses) (10, 174). Therefore, a tumor dependent on LPA signaling will create conditions that will lead to sustained generation of the signal. This means then a tumor will create an environment conductive to the upregulation of ATX expression.

Generally speaking, in the post-natal organism, ATX upregulation is physiologically linked to wound healing and tissue remodeling processes. In response to an injury or insult, increased ATX/LPA signaling promotes platelet activation and stimulates the growth and migration of fibroblasts, vascular smooth muscle cells, endothelial cells and keratinocytes (91). Such repair processes are under the purview of acute inflammatory responses, where rapid host responses establish a complex chemotactic signaling network that recruits all the necessary mediators to eliminate the offending agents (389). Once repairs or remodeling is complete after addressing of the insulting stimulus, the acute inflammatory responses self-resolve (113, 114) (Figure 1.7). As one of these resolving responses, ATX/LPA concentrations at the site of injury also return to basal levels (92).

Until now, the relationship between ATX expression and LPA concentration under basal conditions has not been studied extensively. We have now demonstrated that LPA, as a product of ATX activity, negatively regulates ATX mRNA expression and subsequent protein translation (Chapter 3). This feedback regulation ensures that ATX expression is at a level to maintain a steady-state LPA concentration. We can artificially deplete our model system of LPA by removing it from cell culture or block ATX activity in mice. These treatments allow LPA to be turned over without replenishment so that ATX secretion increases significantly. Restoration of LPA concentrations reestablishes homeostasis, and ATX production falls again. Such a feedback

loop allows for adjustments of LPA concentrations to suit the changing needs of the organism. This negative regulatory relationship between LPA and ATX is diminished in the presence of inflammation, and physiologically, inflammation is vital to the wound healing response. In response to inflammatory cytokines like TNF-α, ATX expression is no longer readily suppressed by LPA. Instead, this inflamed system allows for the accumulation of supra-physiological levels of LPA to mediate repair. Once repairs are complete and inflammation resolves, the absence of pro-inflammatory signals ends the upregulation of ATX expression and no longer opposes LPA-mediated suppression of ATX transcription. Therefore, in pathological conditions mediated by chronic inflammation (meaning consistently elevated levels of inflammatory factors) we can now explain how both ATX protein and LPA concentrations are increased to levels that drive diseases like asthma, fibrosis, rheumatoid arthritis, atherosclerosis, bowel disorders, multiple sclerosis and cancer (10, 37, 117, 137, 156, 163, 238, 390).

Cancer, perhaps the most complex and heterogeneous disease, is described in the context of eight broad hallmarks: sustained proliferative signaling, replicative immortality, induced angiogenesis, evasion of growth suppressors, deregulated cellular energetics, activation of invasion and metastasis, resistance to cell death and avoidance of immune destruction (282). These hallmarks are enabled by two characteristics: genomic instability and mutation, and tumor-promoting inflammation (282). LPA signaling is a

known direct contributor to all of the hallmarks. As well as being a wound that does not heal, cancer is essentially a state of chronic inflammation (111, 281, 341). As we have shown, inflammatory signaling by cancer cells induces the expression of ATX, either by the cancer cells in an autocrine fashion like thyroid cancer, or through a paracrine mechanism in mammary tissue in breast cancer. Regardless of its source, the tumor (both cancer and stromal cells) becomes a tissue of sustained ATX/LPA signaling. This signaling is then further reinforced as the cancer progresses because the pro-inflammatory milieu is intensified by the tumor growth.

Similarly, conventional chemotherapy and radiotherapy that have a therapeutic effect by damaging cancer cells and inducing apoptosis also provoke tissue damage and a wound-healing reaction. Here, as part of survival response, the tumor increases the secretion of pro-inflammatory chemokines, cytokines and growth factors to further induce ATX production and secretion. This vicious cycle, which produces LPA, ultimately promotes cancer cell survival and induces treatment resistance. Hence, blocking this vicious cycle by inhibiting ATX activity and LPA signaling breaks this inflammatory-mediated cross-talk between all the different cell populations in the tumor microenvironment and thus cancer progression. Therefore, blocking the effects of inflammation, both resultant and causative from the production of LPA by ATX, should provide a novel treatment for cancers by decreasing

tumor growth, metastasis and the development of resistance to other cancer treatments.

6.4 Future Directions

The ability to potently inhibit ATX *in vivo* for extended periods of time opens an incredibly large area for investigation into therapeutic applications of targeting ATX/LPA signaling. Particularly, in addition to cancer, the ability of ATX inhibition to limit the production of a large spectrum of inflammatory mediators makes drugs like ONO-8430506 novel candidates for treating diseases defined by chronic inflammation. We have preliminary findings to suggest that ATX inhibition reduces both the morbidity and mortality of inflammatory bowel disease in mice induced by dextran sodium sulphate (211). Other prime disease candidates include rheumatoid arthritis, where previous work has shown genetic ablation of ATX in synovial fibroblasts reduces disease progression in mouse models (145, 391). Research with the ATX inhibitor PF-8380 showed that ATX inhibition was just as effective as naproxen in reducing inflammatory hyperalgesia in rat air pouch models (8). This suggests that ATX/LPA signaling may induce expression of COX-2 and/or otherwise influence prostaglandin metabolism. The relationship between ATX/LPA and COX-2 has never been well studied, however, the transcription factor nuclear factor of activated T cells (NFAT) induces the synthesis of both ATX and COX-2 in cancers (392). In animal models, COX-2

production can be quantified in real time using radiotracers (393). Therefore, one possible set of experiments using such probes would be to take our cancer models or other suitable inflammatory systems and treat with ONO-8430506 to determine if ATX inhibition decreases COX-2 levels.

Given the physiological importance of ATX to processes like smooth muscle contraction, platelet aggression and wound healing, we do not know if potent ATX inhibition adversely affects tissue repair and remodeling. So far, all our studies with ONO-8430506 in animals have shown no obvious side effects, but studies using existing wound healing models are warranted (394). While ATX inhibition is effective at reducing particularly unsaturated and polyunsaturated LPA species, saturated species are not adversely affected since their production is probably largely mediated by PLA_2 activity (10, 395). Hence, LPA generation by minor sources like PLA_2 may be sufficient to maintain physiological processes, whereas higher LPA concentrations from induced ATX expression drive pathology. Answers to questions like these are required to determine if ATX inhibitors are contra-indicated in patients with pre-existing wound healing problems, for example, in cases of diabetic neuropathy and autoimmune diseases (396).

In addition to ATX inhibition studies that are now possible with drugs like ONO-8430506, there are still many unanswered fundamental questions regarding ATX biology. One of the most interesting and possibly understudied of these is the role of the ATX SMB2 integrin-binding domain. While the

SMB2 domain does not contribute to ATX activity, it is proposed that binding of this domain particularly to β3 integrins localizes LPA production to the cell surface and thus aids in LPA delivery to LPA receptors (62, 64, 67, 68). If this is indeed true, it is not known if cancer cells or perhaps inflamed tissues express an integrin population that will preferentially recruit ATX. Further, integrins themselves mediate signaling processes (397), and it has been demonstrated that integrin α6β4 promotes ATX expression in MDA-MB-435S melanoma cells through NFAT-mediated transcription (398). One possibility is that ATX binding to integrins induces translocation of transcription factors to the nucleus that in turn increase ATX transcription, establishing a positive-feedback loop.

ATX/LPA research has always been closely tied to the development of cancer therapy resistance. A popular model for cancer therapy resistance is the cancer stem cell model whereby radiotherapy and chemotherapy kill differentiated, fast growing cancer cells but are unable to affect the quiescent undifferentiated cancer stem cells (399). These cells are then able to repopulate a tumor and because of their mesenchymal properties, they are very pro-metastatic (400). LPA signaling is known to induce a migratory phenotype in many different cell populations (401, 402). This migratory phenotype is well characterized by the epithelial-mesenchymal transition (EMT) (403), and LPA is emerging as a potent inducer of the gene signatures that define EMT (404). Though contentious, it may be that cancer stem cells

arise from extreme cases of EMT (405, 406). Regardless, there is much evidence to support that both the EMT phenotype and cancer stem cells arise from and are maintained by chronic inflammation (407, 408). As a promoter of chronic inflammation leading to cancer development and treatment resistance, it may be possible to target cancer stem cell biology through ATX/LPA signaling inhibition.

Recently, our group showed for the first time that activation of LPA_1 increases the stabilization of the transcription factor Nrf2 and induces its nuclear translocation (409). Nrf2 increases the expression of anti-oxidant genes (for example, NADPH-quinone oxidoreductase-1 and hemoxygenase-1), which protects cancer cells against oxidative damage caused by chemotherapy (410). Also, LPA-induced Nrf2 stability increases the expression of the multi-drug resistant transporters, ABCC1, ABCG2, ABCC2 and ABCC3, which export toxic oxidation products and many chemotherapeutic drugs (409). These responses protect against cell death during chemotherapy. In our 4T1 breast cancer model, we showed that ATX inhibition by ONO-8430506 decreased Nrf2 levels and the expression of anti-oxidant genes and multi-drug resistant transporters (409). This explains why the doxorubicin treatment was more effective in mice that were simultaneously treated with an ATX inhibitor. Also, our findings prompt the need for further investigations into combination therapy with other common chemotherapies like paclitaxel, as well as with radiotherapy. We predict that

ATX inhibition should improve the effectiveness of targeted radiation by blocking the initiation of self-repair mechanisms dependent on LPA signaling. Also, as discussed in Chapter 5, radioiodine therapy is a mainstay of thyroid cancer treatment, and resistance to uptake leads to poor patient outcomes. Based on the importance of ATX to thyroid cancer progression, we plan to study if ATX inhibition might mitigate this resistance.

As we demonstrated with our breast cancer work, cancer cells that express negligible ATX can induce ATX expression in neighboring stromal cells and the surrounding mammary adipose through inflammatory processes, and use this induced ATX as their source for LPA. This finding highlights the need for future research into ATX production in cancers to take into account of how the tumor stroma and the surrounding tissue influence tumor development and metastasis. For example, work in colon cancer has shown that TGF-β in stromal cells is important for both tumor initiation and metastasis. In these studies, STAT3 signaling in cancer cells upregulates TGF-β in distant organs through an IL-11 response signature, which in turn creates a favorable microenvironment for cancer cell seeding (299, 411). Similarly, the pro-inflammatory milieu of cancer cells may induce ATX in distant organs to facilitate the development of metastasis. Because of the incredible heterogeneity of cell populations in both tumors and tissues, studying these processes and the effects of ATX inhibition may require the separation of both tumors and tissues into different cell populations. These

isolates can then be analyzed on gene and protein microarrays to tease out critical pathways and mechanisms affected by ATX/LPA signaling.

Finally, to better model the human patient scenario, the role of surgery needs to be incorporated into future work. Usually, upon the discovery of a solid tumor, the mass and adjacent lymph nodes are surgically removed, and then the patient is started on chemotherapy and/or radiotherapy to kill any remaining cells or cells that have begun to metastasize. In some cancers like breast cancer, the patient may be started on chemotherapy and/or radiotherapy to shrink the tumor before the surgery (neoadjuvant therapy) (412). This improves the odds of the surgical margins being free of cancer cells that could either repopulate the tumor and/or initiate metastasis. However, despite best surgical and other therapeutic intentions, many cancer deaths still occur from metastasis. Blocking this metastasis with better treatment regimens should improve treatment outcomes. The situation of no survival benefit despite surgical excision of the primary tumor can be modeled in the Balb/c/4T1 system. Rashid *et al.* demonstrated that excision of 4T1-luc2 (a luciferase expressing 4T1 cell line – see Section 2.3) primary tumors in Balb/c mice after 10 days of tumor growth does not improve survival (330). Despite the tumor being quite small at this stage, the aggressive 4T1 cell line begins to metastasize very early in tumor development (330, 331). Without addressing the metastatic potential of the 4T1 cancer cells early in tumor development, surgery alone is unlikely to improve survival times. We can

conduct monotherapy or combination therapy studies with ONO-8430506, either as neoadjuvant therapy and/or following surgery, to study effects on survival times in mice. This work would model the real world situation where a breast cancer patient discovers a primary mass and the tumor is excised and the patient is treated with chemotherapy and/or radiotherapy afterwards with the intention to cure or increase survival time.

In conclusion, it is worth appreciating the exponentially increasing interest in ATX, and how rapidly progress is being made in understanding this important enzyme to both physiology and pathology. Although first identified in 1992, over half of the entire literature on ATX has been published in just the last four years. One quarter of the total body of knowledge is less than 18 months old. On average, at least one new paper is published weekly. With this kind of attention, the ATX/LPA field is rapidly being transformed and applied to virtually every area of medicine. Now, with the recent development of potent ATX inhibitors, we hope that the basic, translational and medical research realms will quickly move them into clinical trials and eventual clinical practice ahead of the silver anniversary of the discovery of ATX.

BIBLIOGRAPHY

1. Eichholtz, T., K. Jalink, I. Fahrenfort, and W. H. Moolenaar. 1993. The bioactive phospholipid lysophosphatidic acid is released from activated platelets. *Biochem. J.* **291 (Pt 3)**: 677-680.

2. Tigyi, G., and R. Miledi. 1992. Lysophosphatidates bound to serum albumin activate membrane currents in Xenopus oocytes and neurite retraction in PC12 pheochromocytoma cells. *J. Biol. Chem.* **267**: 21360-21367.

3. Baker, D. L., P. Morrison, B. Miller, C. A. Riely, B. Tolley, A. M. Westermann, J. M. Bonfrer, E. Bais, W. H. Moolenaar, and G. Tigyi. 2002. Plasma lysophosphatidic acid concentration and ovarian cancer. *JAMA* **287**: 3081-3082.

4. Sevastou, I., E. Kaffe, M. A. Mouratis, and V. Aidinis. 2013. Lysoglycerophospholipids in chronic inflammatory disorders: the PLA(2)/LPC and ATX/LPA axes. *Biochim. Biophys. Acta* **1831**: 42-60.

5. van Meeteren, L. A., P. Ruurs, C. Stortelers, P. Bouwman, M. A. van Rooijen, J. P. Pradere, T. R. Pettit, M. J. Wakelam, J. S. Saulnier-Blache, C. L. Mummery, W. H. Moolenaar, and J. Jonkers. 2006. Autotaxin, a secreted lysophospholipase D, is essential for blood vessel formation during development. *Mol. Cell. Biol.* **26**: 5015-5022.

6. Tanaka, M., S. Okudaira, Y. Kishi, R. Ohkawa, S. Iseki, M. Ota, S. Noji, Y. Yatomi, J. Aoki, and H. Arai. 2006. Autotaxin stabilizes blood vessels and is required for embryonic vasculature by producing lysophosphatidic acid. *J. Biol. Chem.* **281**: 25822-25830.

7. Ferry, G., N. Moulharat, J. P. Pradere, P. Desos, A. Try, A. Genton, A. Giganti, M. Beucher-Gaudin, M. Lonchampt, M. Bertrand, J. S. Saulnier-Blache, G. C. Tucker, A. Cordi, and J. A. Boutin. 2008. S32826, a nanomolar inhibitor of autotaxin: discovery, synthesis and applications as a pharmacological tool. *J. Pharmacol. Exp. Ther.* **327**: 809-819.

8. Gierse, J., A. Thorarensen, K. Beltey, E. Bradshaw-Pierce, L. Cortes-Burgos, T. Hall, A. Johnston, M. Murphy, O. Nemirovskiy, S. Ogawa, L. Pegg, M. Pelc, M. Prinsen, M. Schnute, J. Wendling, S. Wene, R. Weinberg, A. Wittwer, B. Zweifel, and J. Masferrer. 2010. A novel autotaxin inhibitor reduces lysophosphatidic acid levels in plasma and the site of inflammation. *J. Pharmacol. Exp. Ther.* **334**: 310-317.

9. Nakanaga, K., K. Hama, and J. Aoki. 2010. Autotaxin--an LPA producing enzyme with diverse functions. *J Biochem* **148**: 13-24.

10. Brindley, D. N., F. T. Lin, and G. J. Tigyi. 2013. Role of the autotaxin-lysophosphatidate axis in cancer resistance to chemotherapy and radiotherapy. *Biochim. Biophys. Acta* **1831**: 74-85.

11. Croset, M., N. Brossard, A. Polette, and M. Lagarde. 2000. Characterization of plasma unsaturated lysophosphatidylcholines in human and rat. *Biochem. J.* **345 Pt 1**: 61-67.

12. Wiesner, P., K. Leidl, A. Boettcher, G. Schmitz, and G. Liebisch. 2009. Lipid profiling of FPLC-separated lipoprotein fractions by electrospray ionization tandem mass spectrometry. *J. Lipid Res.* **50**: 574-585.

13. Brindley, D. N. 1993. Hepatic secretion of lysphosphatidylcholine: a novel transport system for polyunsaturated fatty acids and choline. *J. Nutr. Biochem.* **4**: 442-449.

14. Ojala, P. J., T. E. Hirvonen, M. Hermansson, P. Somerharju, and J. Parkkinen. 2007. Acyl chain-dependent effect of lysophosphatidylcholine on human neutrophils. *J. Leukoc. Biol.* **82**: 1501-1509.

15. Funk, C. D. 2001. Prostaglandins and leukotrienes: advances in eicosanoid biology. *Science* **294**: 1871-1875.

16. Aoki, J., A. Taira, Y. Takanezawa, Y. Kishi, K. Hama, T. Kishimoto, K. Mizuno, K. Saku, R. Taguchi, and H. Arai. 2002. Serum lysophosphatidic acid is produced through diverse phospholipase pathways. *J. Biol. Chem.* **277**: 48737-48744.

17. Gaetano, C. G., N. Samadi, J. L. Tomsig, T. L. Macdonald, K. R. Lynch, and D. N. Brindley. 2009. Inhibition of autotaxin production or activity blocks lysophosphatidylcholine-induced migration of human breast cancer and melanoma cells. *Mol. Carcinog.* **48**: 801-809.

18. Samadi, N., C. Gaetano, I. S. Goping, and D. N. Brindley. 2009. Autotaxin protects MCF-7 breast cancer and MDA-MB-435 melanoma cells against Taxol-induced apoptosis. *Oncogene* **28**: 1028-1039.

19. Nishimasu, H., S. Okudaira, K. Hama, E. Mihara, N. Dohmae, A. Inoue, R. Ishitani, J. Takagi, J. Aoki, and O. Nureki. 2011. Crystal structure of autotaxin and insight into GPCR activation by lipid mediators. *Nat Struct Mol Biol* **18**: 205-212.

20. Fourcade, O., M. F. Simon, C. Viode, N. Rugani, F. Leballe, A. Ragab, B. Fournie, L. Sarda, and H. Chap. 1995. Secretory phospholipase A2 generates the novel lipid mediator lysophosphatidic acid in membrane microvesicles shed from activated cells. *Cell* **80**: 919-927.

21. Li, H., Z. Zhao, G. Wei, L. Yan, D. Wang, H. Zhang, G. E. Sandusky, J. Turk, and Y. Xu. 2010. Group VIA phospholipase A2 in both host and tumor cells is involved in ovarian cancer development. *FASEB J.* **24**: 4103-4116.

22. Zhao, X., D. Wang, Z. Zhao, Y. Xiao, S. Sengupta, R. Zhang, K. Lauber, S. Wesselborg, L. Feng, T. M. Rose, Y. Shen, J. Zhang, G. Prestwich, and Y. Xu. 2006. Caspase-3-dependent activation of calcium-independent phospholipase A2 enhances cell migration in non-apoptotic ovarian cancer cells. *J. Biol. Chem.* **281**: 29357-29368.

23. Smart, H. C., F. D. Mast, M. F. Chilije, M. Tavassoli, J. B. Dacks, and V. Zaremberg. 2014. Phylogenetic analysis of glycerol 3-phosphate acyltransferases in opisthokonts reveals unexpected ancestral complexity and novel modern biosynthetic components. *PLoS One* **9**: e110684.

24. Chun, J., T. Hla, K. R. Lynch, S. Spiegel, and W. H. Moolenaar. 2010. International Union of Basic and Clinical Pharmacology. LXXVIII. Lysophospholipid receptor nomenclature. *Pharmacol. Rev.* **62**: 579-587.

25. Brady, A. E., and L. E. Limbird. 2002. G protein-coupled receptor interacting proteins: emerging roles in localization and signal transduction. *Cell. Signal.* **14**: 297-309.

26. Lundstrom, K. 2009. An overview on GPCRs and drug discovery: structure-based drug design and structural biology on GPCRs. *Methods Mol. Biol.* **552**: 51-66.

27. Roth, B. L., and F. H. Marshall. 2012. NOBEL 2012 Chemistry: Studies of a ubiquitous receptor family. *Nature* **492**: 57-57.

28. Hecht, J. H., J. A. Weiner, S. R. Post, and J. Chun. 1996. Ventricular zone gene-1 (vzg-1) encodes a lysophosphatidic acid receptor expressed in neurogenic regions of the developing cerebral cortex. *J. Cell Biol.* **135**: 1071-1083.

29. An, S., T. Bleu, W. Huang, O. G. Hallmark, S. R. Coughlin, and E. J. Goetzl. 1997. Identification of cDNAs encoding two G protein-coupled receptors for lysosphingolipids. *FEBS Lett.* **417**: 279-282.

30. An, S., T. Bleu, O. G. Hallmark, and E. J. Goetzl. 1998. Characterization of a novel subtype of human G protein-coupled receptor for lysophosphatidic acid. *J. Biol. Chem.* **273**: 7906-7910.

31. Bandoh, K., J. Aoki, H. Hosono, S. Kobayashi, T. Kobayashi, K. Murakami-Murofushi, M. Tsujimoto, H. Arai, and K. Inoue. 1999. Molecular cloning and characterization of a novel human G-protein-coupled receptor, EDG7, for lysophosphatidic acid. *J. Biol. Chem.* **274**: 27776-27785.

32. Ye, X., M. K. Skinner, G. Kennedy, and J. Chun. 2008. Age-Dependent Loss of Sperm Production in Mice via Impaired Lysophosphatidic Acid Signaling. *Biol. Reprod.* **79**: 328-336.

33. Contos, J. J. A., I. Ishii, N. Fukushima, M. A. Kingsbury, X. Ye, S. Kawamura, J. H. Brown, and J. Chun. 2002. Characterization of lpa2 (Edg4) and lpa1/lpa2 (Edg2/Edg4) Lysophosphatidic Acid Receptor Knockout Mice: Signaling Deficits without Obvious Phenotypic Abnormality Attributable to lpa2. *Mol. Cell. Biol.* **22**: 6921-6929.

34. Contos, J. J., N. Fukushima, J. A. Weiner, D. Kaushal, and J. Chun. 2000. Requirement for the lpA1 lysophosphatidic acid receptor gene in normal suckling behavior. *Proc. Natl. Acad. Sci. U. S. A.* **97**: 13384-13389.

35. Ye, X., K. Hama, J. J. Contos, B. Anliker, A. Inoue, M. K. Skinner, H. Suzuki, T. Amano, G. Kennedy, H. Arai, J. Aoki, and J. Chun. 2005. LPA3-mediated lysophosphatidic acid signalling in embryo implantation and spacing. *Nature* **435**: 104-108.

36. Contos, J. J., I. Ishii, N. Fukushima, M. A. Kingsbury, X. Ye, S. Kawamura, J. H. Brown, and J. Chun. 2002. Characterization of lpa(2) (Edg4) and lpa(1)/lpa(2) (Edg2/Edg4) lysophosphatidic acid receptor knockout mice: signaling deficits without obvious phenotypic abnormality attributable to lpa(2). *Mol. Cell. Biol.* **22**: 6921-6929.

37. Yung, Y. C., N. C. Stoddard, and J. Chun. 2014. LPA receptor signaling: pharmacology, physiology, and pathophysiology. *J. Lipid Res.* **55**: 1192-1214.

38. Ohuchi, H., A. Hamada, H. Matsuda, A. Takagi, M. Tanaka, J. Aoki, H. Arai, and S. Noji. 2008. Expression patterns of the lysophospholipid receptor genes during mouse early development. *Dev. Dyn.* **237**: 3280-3294.

39. Choi, J. W., D. R. Herr, K. Noguchi, Y. C. Yung, C. W. Lee, T. Mutoh, M. E. Lin, S. T. Teo, K. E. Park, A. N. Mosley, and J. Chun. 2010. LPA

receptors: subtypes and biological actions. *Annu. Rev. Pharmacol. Toxicol.* **50**: 157-186.

40. Meyer zu Heringdorf, D., and K. H. Jakobs. 2007. Lysophospholipid receptors: signalling, pharmacology and regulation by lysophospholipid metabolism. *Biochim. Biophys. Acta* **1768**: 923-940.

41. Lundequist, A., and J. A. Boyce. 2011. LPA5 is abundantly expressed by human mast cells and important for lysophosphatidic acid induced MIP-1beta release. *PLoS One* **6**: e18192.

42. Lee, Z., C. T. Cheng, H. Zhang, M. A. Subler, J. Wu, A. Mukherjee, J. J. Windle, C. K. Chen, and X. Fang. 2008. Role of LPA4/p2y9/GPR23 in negative regulation of cell motility. *Mol. Biol. Cell* **19**: 5435-5445.

43. Lin, M. E., R. R. Rivera, and J. Chun. 2012. Targeted deletion of LPA5 identifies novel roles for lysophosphatidic acid signaling in development of neuropathic pain. *J. Biol. Chem.* **287**: 17608-17617.

44. Pasternack, S. M., I. von Kugelgen, K. Al Aboud, Y. A. Lee, F. Ruschendorf, K. Voss, A. M. Hillmer, G. J. Molderings, T. Franz, A. Ramirez, P. Nurnberg, M. M. Nothen, and R. C. Betz. 2008. G protein-coupled receptor P2Y5 and its ligand LPA are involved in maintenance of human hair growth. *Nat. Genet.* **40**: 329-334.

45. Lee, M., S. Choi, G. Hallden, S. J. Yo, D. Schichnes, and G. W. Aponte. 2009. P2Y5 is a G(alpha)i, G(alpha)12/13 G protein-coupled receptor activated by lysophosphatidic acid that reduces intestinal cell adhesion. *Am J Physiol Gastrointest Liver Physiol* **297**: G641-654.

46. Kok, B. P., G. Venkatraman, D. Capatos, and D. N. Brindley. 2012. Unlike two peas in a pod: lipid phosphate phosphatases and phosphatidate phosphatases. *Chem. Rev.* **112**: 5121-5146.

47. Jasinska, R., Q. X. Zhang, C. Pilquil, I. Singh, J. Xu, J. Dewald, D. A. Dillon, L. G. Berthiaume, G. M. Carman, D. W. Waggoner, and D. N. Brindley. 1999. Lipid phosphate phosphohydrolase-1 degrades exogenous glycerolipid and sphingolipid phosphate esters. *Biochem. J.* **340 (Pt 3)**: 677-686.

48. Tomsig, J. L., A. H. Snyder, E. V. Berdyshev, A. Skobeleva, C. Mataya, V. Natarajan, D. N. Brindley, and K. R. Lynch. 2009. Lipid phosphate phosphohydrolase type 1 (LPP1) degrades extracellular lysophosphatidic acid in vivo. *Biochem. J.* **419**: 611-618.

49. Aaltonen, N., M. Lehtonen, K. Varonen, G. A. Goterris, and J. T. Laitinen. 2012. Lipid phosphate phosphatase inhibitors locally amplify lysophosphatidic acid LPA1 receptor signalling in rat brain cryosections without affecting global LPA degradation. *BMC Pharmacol* **12**: 7.

50. Salous, A. K., M. Panchatcharam, M. Sunkara, P. Mueller, A. Dong, Y. Wang, G. A. Graf, S. S. Smyth, and A. J. Morris. 2013. Mechanism of rapid elimination of lysophosphatidic acid and related lipids from the circulation of mice. *J. Lipid Res.* **54**: 2775-2784.

51. Akira, T., H. Kengo, F. Kenji, and T. Hiroaki. 1986. Involvement of lysophospholipase D in the production of lysophosphatidic acid in rat plasma. *Biochim. Biophys. Acta* **875**: 31-38.

52. Stracke, M. L., H. C. Krutzsch, E. J. Unsworth, A. Arestad, V. Cioce, E. Schiffmann, and L. A. Liotta. 1992. Identification, purification, and partial sequence analysis of autotaxin, a novel motility-stimulating protein. *J. Biol. Chem.* **267**: 2524-2529.

53. Murata, J., H. Y. Lee, T. Clair, H. C. Krutzsch, A. A. Arestad, M. E. Sobel, L. A. Liotta, and M. L. Stracke. 1994. cDNA cloning of the human tumor motility-stimulating protein, autotaxin, reveals a homology with phosphodiesterases. *J. Biol. Chem.* **269**: 30479-30484.

54. Buckley, M. F., K. A. Loveland, W. J. McKinstry, O. M. Garson, and J. W. Goding. 1990. Plasma cell membrane glycoprotein PC-1. cDNA cloning of the human molecule, amino acid sequence, and chromosomal location. *J. Biol. Chem.* **265**: 17506-17511.

55. Funakoshi, I., H. Kato, K. Horie, T. Yano, Y. Hori, H. Kobayashi, T. Inoue, H. Suzuki, S. Fukui, M. Tsukahara, and et al. 1992. Molecular cloning of cDNAs for human fibroblast nucleotide pyrophosphatase. *Arch. Biochem. Biophys.* **295**: 180-187.

56. Kawagoe, H., O. Soma, J. Goji, N. Nishimura, M. Narita, J. Inazawa, H. Nakamura, and K. Sano. 1995. Molecular cloning and chromosomal assignment of the human brain-type phosphodiesterase I/nucleotide pyrophosphatase gene (PDNP2). *Genomics* **30**: 380-384.

57. Umezu-Goto, M., Y. Kishi, A. Taira, K. Hama, N. Dohmae, K. Takio, T. Yamori, G. B. Mills, K. Inoue, J. Aoki, and H. Arai. 2002. Autotaxin has lysophospholipase D activity leading to tumor cell growth and motility by lysophosphatidic acid production. *J. Cell Biol.* **158**: 227-233.

58. Tokumura, A., E. Majima, Y. Kariya, K. Tominaga, K. Kogure, K. Yasuda, and K. Fukuzawa. 2002. Identification of human plasma lysophospholipase D, a lysophosphatidic acid-producing enzyme, as autotaxin, a multifunctional phosphodiesterase. *J. Biol. Chem.* **277**: 39436-39442.

59. Moolenaar, W. H. 2002. Lysophospholipids in the limelight: autotaxin takes center stage. *J. Cell Biol.* **158**: 197-199.

60. Hama, K., J. Aoki, M. Fukaya, Y. Kishi, T. Sakai, R. Suzuki, H. Ohta, T. Yamori, M. Watanabe, J. Chun, and H. Arai. 2004. Lysophosphatidic acid and autotaxin stimulate cell motility of neoplastic and non-neoplastic cells through LPA1. *J. Biol. Chem.* **279**: 17634-17639.

61. Hausmann, J., A. Perrakis, and W. H. Moolenaar. 2013. Structure-function relationships of autotaxin, a secreted lysophospholipase D. *Adv Biol Regul* **53**: 112-117.

62. Perrakis, A., and W. H. Moolenaar. 2014. Autotaxin: structure-function and signaling. *J. Lipid Res.* **55**: 1010-1018.

63. Hausmann, J., S. Kamtekar, E. Christodoulou, J. E. Day, T. Wu, Z. Fulkerson, H. M. Albers, L. A. van Meeteren, A. J. Houben, L. van Zeijl, S. Jansen, M. Andries, T. Hall, L. E. Pegg, T. E. Benson, M. Kasiem, K. Harlos, C. W. Kooi, S. S. Smyth, H. Ovaa, M. Bollen, A. J. Morris, W. H. Moolenaar, and A. Perrakis. 2011. Structural basis of substrate discrimination and integrin binding by autotaxin. *Nat Struct Mol Biol* **18**: 198-204.

64. Moolenaar, W. H., and A. Perrakis. 2011. Insights into autotaxin: how to produce and present a lipid mediator. *Nat Rev Mol Cell Biol* **12**: 674-679.

65. Kanda, H., R. Newton, R. Klein, Y. Morita, M. D. Gunn, and S. D. Rosen. 2008. Autotaxin, an ectoenzyme that produces lysophosphatidic acid, promotes the entry of lymphocytes into secondary lymphoid organs. *Nat Immunol* **9**: 415-423.

66. Pamuklar, Z., L. Federico, S. Liu, M. Umezu-Goto, A. Dong, M. Panchatcharam, Z. Fulkerson, E. Berdyshev, V. Natarajan, X. Fang, L. A. van Meeteren, W. H. Moolenaar, G. B. Mills, A. J. Morris, and S. S. Smyth. 2009. Autotaxin/lysopholipase D and lysophosphatidic acid regulate murine hemostasis and thrombosis. *J. Biol. Chem.* **284**: 7385-7394.

67. Fulkerson, Z., T. Wu, M. Sunkara, C. V. Kooi, A. J. Morris, and S. S. Smyth. 2011. Binding of autotaxin to integrins localizes lysophosphatidic acid

production to platelets and mammalian cells. *J. Biol. Chem.* **286**: 34654-34663.

68. Wu, T., C. V. Kooi, P. Shah, R. Charnigo, C. Huang, S. S. Smyth, and A. J. Morris. 2014. Integrin-mediated cell surface recruitment of autotaxin promotes persistent directional cell migration. *FASEB J.* **28**: 861-870.

69. Hashimoto, T., S. Okudaira, K. Igarashi, K. Hama, Y. Yatomi, and J. Aoki. 2012. Identification and biochemical characterization of a novel autotaxin isoform, ATXdelta, with a four-amino acid deletion. *J Biochem* **151**: 89-97.

70. Boutin, J. A., and G. Ferry. 2009. Autotaxin. *Cell. Mol. Life Sci.* **66**: 3009-3021.

71. Houben, A. J., X. M. van Wijk, L. A. van Meeteren, L. van Zeijl, E. M. van de Westerlo, J. Hausmann, A. Fish, A. Perrakis, T. H. van Kuppevelt, and W. H. Moolenaar. 2013. The polybasic insertion in autotaxin alpha confers specific binding to heparin and cell surface heparan sulfate proteoglycans. *J. Biol. Chem.* **288**: 510-519.

72. Giganti, A., M. Rodriguez, B. Fould, N. Moulharat, F. Coge, P. Chomarat, J. P. Galizzi, P. Valet, J. S. Saulnier-Blache, J. A. Boutin, and G. Ferry. 2008. Murine and human autotaxin alpha, beta, and gamma isoforms: gene organization, tissue distribution, and biochemical characterization. *J. Biol. Chem.* **283**: 7776-7789.

73. Jansen, S., C. Stefan, J. W. Creemers, E. Waelkens, A. Van Eynde, W. Stalmans, and M. Bollen. 2005. Proteolytic maturation and activation of autotaxin (NPP2), a secreted metastasis-enhancing lysophospholipase D. *J. Cell Sci.* **118**: 3081-3089.

74. Koike, S., K. Keino-Masu, T. Ohto, and M. Masu. 2006. The N-terminal hydrophobic sequence of autotaxin (ENPP2) functions as a signal peptide. *Genes Cells* **11**: 133-142.

75. Pradere, J. P., E. Tarnus, S. Gres, P. Valet, and J. S. Saulnier-Blache. 2007. Secretion and lysophospholipase D activity of autotaxin by adipocytes are controlled by N-glycosylation and signal peptidase. *Biochim. Biophys. Acta* **1771**: 93-102.

76. Stracke, M. L., A. Arestad, M. Levine, H. C. Krutzsch, and L. A. Liotta. 1995. Autotaxin is an N-linked glycoprotein but the sugar moieties are not needed for its stimulation of cellular motility. *Melanoma Res.* **5**: 203-209.

77. Jansen, S., N. Callewaert, I. Dewerte, M. Andries, H. Ceulemans, and M. Bollen. 2007. An essential oligomannosidic glycan chain in the catalytic domain of autotaxin, a secreted lysophospholipase-D. *J. Biol. Chem.* **282**: 11084-11091.

78. Jansen, S., M. Andries, K. Vekemans, H. Vanbilloen, A. Verbruggen, and M. Bollen. 2009. Rapid clearance of the circulating metastatic factor autotaxin by the scavenger receptors of liver sinusoidal endothelial cells. *Cancer Lett.* **284**: 216-221.

79. Ikeda, H., and Y. Yatomi. 2012. Autotaxin in liver fibrosis. *Clin. Chim. Acta* **413**: 1817-1821.

80. Koike, S., K. Keino-Masu, and M. Masu. 2010. Deficiency of autotaxin/lysophospholipase D results in head cavity formation in mouse embryos through the LPA receptor-Rho-ROCK pathway. *Biochem. Biophys. Res. Commun.* **400**: 66-71.

81. Koike, S., K. Keino-Masu, T. Ohto, F. Sugiyama, S. Takahashi, and M. Masu. 2009. Autotaxin/lysophospholipase D-mediated lysophosphatidic acid signaling is required to form distinctive large lysosomes in the visceral endoderm cells of the mouse yolk sac. *J. Biol. Chem.* **284**: 33561-33570.

82. Koike, S., Y. Yutoh, K. Keino-Masu, S. Noji, M. Masu, and H. Ohuchi. 2011. Autotaxin is required for the cranial neural tube closure and establishment of the midbrain-hindbrain boundary during mouse development. *Dev. Dyn.* **240**: 413-421.

83. Moolenaar, W. H., A. J. Houben, S. J. Lee, and L. A. van Meeteren. 2013. Autotaxin in embryonic development. *Biochim. Biophys. Acta* **1831**: 13-19.

84. Fotopoulou, S., N. Oikonomou, E. Grigorieva, I. Nikitopoulou, T. Paparountas, A. Thanassopoulou, Z. Zhao, Y. Xu, D. L. Kontoyiannis, E. Remboutsika, and V. Aidinis. 2010. ATX expression and LPA signalling are vital for the development of the nervous system. *Dev. Biol.* **339**: 451-464.

85. Yukiura, H., K. Hama, K. Nakanaga, M. Tanaka, Y. Asaoka, S. Okudaira, N. Arima, A. Inoue, T. Hashimoto, H. Arai, A. Kawahara, H. Nishina, and J. Aoki. 2011. Autotaxin regulates vascular development via multiple lysophosphatidic acid (LPA) receptors in zebrafish. *J. Biol. Chem.* **286**: 43972-43983.

86. Yuelling, L. W., C. T. Waggener, F. S. Afshari, J. A. Lister, and B. Fuss. 2012. Autotaxin/ENPP2 regulates oligodendrocyte differentiation in vivo in the developing zebrafish hindbrain. *Glia* **60**: 1605-1618.

87. Lai, S. L., W. L. Yao, K. C. Tsao, A. J. Houben, H. M. Albers, H. Ovaa, W. H. Moolenaar, and S. J. Lee. 2012. Autotaxin/Lpar3 signaling regulates Kupffer's vesicle formation and left-right asymmetry in zebrafish. *Development* **139**: 4439-4448.

88. Cheng, H. Y., A. Dong, M. Panchatcharam, P. Mueller, F. Yang, Z. Li, G. Mills, J. Chun, A. J. Morris, and S. S. Smyth. 2012. Lysophosphatidic acid signaling protects pulmonary vasculature from hypoxia-induced remodeling. *Arterioscler Thromb Vasc Biol* **32**: 24-32.

89. Lonsdale, J., J. Thomas, M. Salvatore, R. Phillips, E. Lo, S. Shad, R. Hasz, G. Walters, F. Garcia, N. Young, B. Foster, M. Moser, E. Karasik, B. Gillard, K. Ramsey, S. Sullivan, J. Bridge, H. Magazine, J. Syron, J. Fleming, L. Siminoff, H. Traino, M. Mosavel, L. Barker, S. Jewell, D. Rohrer, D. Maxim, D. Filkins, P. Harbach, E. Cortadillo, B. Berghuis, L. Turner, E. Hudson, K. Feenstra, L. Sobin, J. Robb, P. Branton, G. Korzeniewski, C. Shive, D. Tabor, L. Qi, K. Groch, S. Nampally, S. Buia, A. Zimmerman, A. Smith, R. Burges, K. Robinson, K. Valentino, D. Bradbury, M. Cosentino, N. Diaz-Mayoral, M. Kennedy, T. Engel, P. Williams, K. Erickson, K. Ardlie, W. Winckler, G. Getz, D. DeLuca, D. MacArthur, M. Kellis, A. Thomson, T. Young, E. Gelfand, M. Donovan, Y. Meng, G. Grant, D. Mash, Y. Marcus, M. Basile, J. Liu, J. Zhu, Z. Tu, N. J. Cox, D. L. Nicolae, E. R. Gamazon, H. K. Im, A. Konkashbaev, J. Pritchard, M. Stevens, T. Flutre, X. Wen, E. T. Dermitzakis, T. Lappalainen, R. Guigo, J. Monlong, M. Sammeth, D. Koller, A. Battle, S. Mostafavi, M. McCarthy, M. Rivas, J. Maller, I. Rusyn, A. Nobel, F. Wright, A. Shabalin, M. Feolo, N. Sharopova, A. Sturcke, J. Paschal, J. M. Anderson, E. L. Wilder, L. K. Derr, E. D. Green, J. P. Struewing, G. Temple, S. Volpi, J. T. Boyer, E. J. Thomson, M. S. Guyer, C. Ng, A. Abdallah, D. Colantuoni, T. R. Insel, S. E. Koester, A. R. Little, P. K. Bender, T. Lehner, Y. Yao, C. C. Compton, J. B. Vaught, S. Sawyer, N. C. Lockhart, J. Demchok, and H. F. Moore. 2013. The Genotype-Tissue Expression (GTEx) project. *Nat. Genet.* **45**: 580-585.

90. Dusaulcy, R., C. Rancoule, S. Gres, E. Wanecq, A. Colom, C. Guigne, L. A. van Meeteren, W. H. Moolenaar, P. Valet, and J. S. Saulnier-Blache. 2011. Adipose-specific disruption of autotaxin enhances nutritional fattening and reduces plasma lysophosphatidic acid. *J. Lipid Res.* **52**: 1247-1255.

91. Brindley, D. N. 2004. Lipid phosphate phosphatases and related proteins: signaling functions in development, cell division, and cancer. *J. Cell. Biochem.* **92**: 900-912.

92. Mazereeuw-Hautier, J., S. Gres, M. Fanguin, C. Cariven, J. Fauvel, B. Perret, H. Chap, J. P. Salles, and J. S. Saulnier-Blache. 2005. Production of lysophosphatidic acid in blister fluid: involvement of a lysophospholipase D activity. *J. Invest. Dermatol.* **125**: 421-427.

93. Tokumura, A., S. Taira, M. Kikuchi, T. Tsutsumi, Y. Shimizu, and M. A. Watsky. 2012. Lysophospholipids and lysophospholipase D in rabbit aqueous humor following corneal injury. *Prostaglandins Other Lipid Mediat.* **97**: 83-89.

94. Grisanti, L., A. Rezza, C. Clavel, R. Sennett, and M. Rendl. 2013. Enpp2/Autotaxin in dermal papilla precursors is dispensable for hair follicle morphogenesis. *J. Invest. Dermatol.* **133**: 2332-2339.

95. Mebarek, S., A. Abousalham, D. Magne, D. Do le, J. Bandorowicz-Pikula, S. Pikula, and R. Buchet. 2013. Phospholipases of mineralization competent cells and matrix vesicles: roles in physiological and pathological mineralizations. *Int J Mol Sci* **14**: 5036-5129.

96. Evseenko, D., B. Latour, W. Richardson, M. Corselli, A. Sahaghian, S. Cardinal, Y. Zhu, R. Chan, B. Dunn, and G. M. Crooks. 2013. Lysophosphatidic acid mediates myeloid differentiation within the human bone marrow microenvironment. *PLoS One* **8**: e63718.

97. Masuda, K., S. Haruta, K. Orino, M. Kawaminami, and S. Kurusu. 2013. Autotaxin as a novel, tissue-remodeling-related factor in regressing corpora lutea of cycling rats. *FEBS J* **280**: 6600-6612.

98. Awada, R., P. Rondeau, S. Gres, J. S. Saulnier-Blache, C. Lefebvre d'Hellencourt, and E. Bourdon. 2012. Autotaxin protects microglial cells against oxidative stress. *Free Radic. Biol. Med.* **52**: 516-526.

99. Awada, R., J. S. Saulnier-Blache, S. Gres, E. Bourdon, P. Rondeau, A. Parimisetty, R. Orihuela, G. J. Harry, and C. L. d'Hellencourt. 2014. Autotaxin downregulates LPS-induced microglia activation and pro-inflammatory cytokines production. *J. Cell. Biochem.* **115**: 2123-2132.

100. Umemoto, E., H. Hayasaka, Z. Bai, L. Cai, S. Yonekura, X. Peng, A. Takeda, K. Tohya, and M. Miyasaka. 2011. Novel regulators of lymphocyte trafficking across high endothelial venules. *Crit. Rev. Immunol.* **31**: 147-169.

101. Bai, Z., L. Cai, E. Umemoto, A. Takeda, K. Tohya, Y. Komai, P. T. Veeraveedu, E. Hata, Y. Sugiura, A. Kubo, M. Suematsu, H. Hayasaka, S. Okudaira, J. Aoki, T. Tanaka, H. M. Albers, H. Ovaa, and M. Miyasaka. 2013. Constitutive lymphocyte transmigration across the basal lamina of high

endothelial venules is regulated by the autotaxin/lysophosphatidic acid axis. *J. Immunol.* **190**: 2036-2048.

102. Zhang, Y., Y. C. Chen, M. F. Krummel, and S. D. Rosen. 2012. Autotaxin through lysophosphatidic acid stimulates polarization, motility, and transendothelial migration of naive T cells. *J. Immunol.* **189**: 3914-3924.

103. Knowlden, S., and S. N. Georas. 2014. The autotaxin-LPA axis emerges as a novel regulator of lymphocyte homing and inflammation. *J. Immunol.* **192**: 851-857.

104. Nakasaki, T., T. Tanaka, S. Okudaira, M. Hirosawa, E. Umemoto, K. Otani, S. Jin, Z. Bai, H. Hayasaka, Y. Fukui, K. Aozasa, N. Fujita, T. Tsuruo, K. Ozono, J. Aoki, and M. Miyasaka. 2008. Involvement of the lysophosphatidic acid-generating enzyme autotaxin in lymphocyte-endothelial cell interactions. *Am. J. Pathol.* **173**: 1566-1576.

105. van Meeteren, L. A., and W. H. Moolenaar. 2007. Regulation and biological activities of the autotaxin-LPA axis. *Prog. Lipid Res.* **46**: 145-160.

106. Budd, D. C., and Y. Qian. 2013. Development of lysophosphatidic acid pathway modulators as therapies for fibrosis. *Future Med Chem* **5**: 1935-1952.

107. Weissman, G. 1992. Inflammation: historical perspectives. *In* Inflammation: Basic Principles and Clinical Correlates. J. Gallin, editor. Raven Press, New York. 5-13.

108. Krishnamoorthy, S., and K. V. Honn. 2006. Inflammation and disease progression. *Cancer Metastasis Rev.* **25**: 481-491.

109. Muller, W. A. 2002. Leukocyte-endothelial cell interactions in the inflammatory response. *Lab. Invest.* **82**: 521-533.

110. Johnston, B., and E. C. Butcher. 2002. Chemokines in rapid leukocyte adhesion triggering and migration. *Semin. Immunol.* **14**: 83-92.

111. Majno, G. 1998. Chronic inflammation: links with angiogenesis and wound healing. *Am. J. Pathol.* **153**: 1035-1039.

112. Lawrence, T., and D. W. Gilroy. 2007. Chronic inflammation: a failure of resolution? *Int. J. Exp. Pathol.* **88**: 85-94.

113. Serhan, C. N., N. Chiang, and T. E. Van Dyke. 2008. Resolving inflammation: dual anti-inflammatory and pro-resolution lipid mediators. *Nat Rev Immunol* **8**: 349-361.

114. Serhan, C. N., and J. Savill. 2005. Resolution of inflammation: the beginning programs the end. *Nat Immunol* **6**: 1191-1197.

115. Cohen, S., P. E. Bigazzi, and T. Yoshida. 1974. Commentary. Similarities of T cell function in cell-mediated immunity and antibody production. *Cell. Immunol.* **12**: 150-159.

116. Kristensen, F., A. L. Weck, and M. Landy. 1980. Biochemical characterization of lymphokines: proceedings of the second International Lymphokine Workshop Academic Press, New York.

117. Turner, M. D., B. Nedjai, T. Hurst, and D. J. Pennington. 2014. Cytokines and chemokines: At the crossroads of cell signalling and inflammatory disease. *Biochim. Biophys. Acta* **1843**: 2563-2582.

118. de Weerd, N. A., S. A. Samarajiwa, and P. J. Hertzog. 2007. Type I interferon receptors: biochemistry and biological functions. *J. Biol. Chem.* **282**: 20053-20057.

119. Mhaskar, R., O. A. Clark, G. Lyman, T. Engel Ayer Botrel, L. Morganti Paladini, and B. Djulbegovic. 2014. Colony-stimulating factors for chemotherapy-induced febrile neutropenia. *Cochrane Database Syst Rev* **10**: Cd003039.

120. Ho, A. S., and K. W. Moore. 1994. Interleukin-10 and its receptor. *Ther. Immunol.* **1**: 173-185.

121. Ono, S. J., T. Nakamura, D. Miyazaki, M. Ohbayashi, M. Dawson, and M. Toda. 2003. Chemokines: roles in leukocyte development, trafficking, and effector function. *J. Allergy Clin. Immunol.* **111**: 1185-1199.

122. Graham, G. J., and M. Locati. 2013. Regulation of the immune and inflammatory responses by the 'atypical' chemokine receptor D6. *The Journal of Pathology* **229**: 168-175.

123. Gruss, H. J., and S. K. Dower. 1995. The TNF ligand superfamily and its relevance for human diseases. *Cytokines Mol. Ther.* **1**: 75-105.

124. Mantovani, A., S. Sozzani, and M. Introna. 1997. Endothelial activation by cytokines. *Ann. N. Y. Acad. Sci.* **832**: 93-116.

125. Martinon, F., and J. Tschopp. 2007. Inflammatory caspases and inflammasomes: master switches of inflammation. *Cell Death Differ.* **14**: 10-22.

126. Gadient, R. A., and P. H. Patterson. 1999. Leukemia inhibitory factor, Interleukin 6, and other cytokines using the GP130 transducing receptor: roles in inflammation and injury. *Stem Cells* **17**: 127-137.

127. Nishimoto, N., and T. Kishimoto. 2006. Interleukin 6: from bench to bedside. *Nat Clin Pract Rheumatol* **2**: 619-626.

128. Kunkel, S. L., T. Standiford, K. Kasahara, and R. M. Strieter. 1991. Interleukin-8 (IL-8): the major neutrophil chemotactic factor in the lung. *Exp. Lung Res.* **17**: 17-23.

129. Vlahopoulos, S., I. Boldogh, A. Casola, and A. R. Brasier. 1999. Nuclear factor-kappaB-dependent induction of interleukin-8 gene expression by tumor necrosis factor alpha: evidence for an antioxidant sensitive activating pathway distinct from nuclear translocation. *Blood* **94**: 1878-1889.

130. Minty, A., P. Chalon, J. M. Derocq, X. Dumont, J. C. Guillemot, M. Kaghad, C. Labit, P. Leplatois, P. Liauzun, B. Miloux, and et al. 1993. Interleukin-13 is a new human lymphokine regulating inflammatory and immune responses. *Nature* **362**: 248-250.

131. Mosmann, T. R., and S. Sad. 1996. The expanding universe of T-cell subsets: Th1, Th2 and more. *Immunol. Today* **17**: 138-146.

132. Nelms, K., A. D. Keegan, J. Zamorano, J. J. Ryan, and W. E. Paul. 1999. The IL-4 receptor: signaling mechanisms and biologic functions. *Annu. Rev. Immunol.* **17**: 701-738.

133. Fanta, C. H. 2009. Asthma. *N. Engl. J. Med.* **360**: 1002-1014.

134. Barnes, P. J. 2001. Th2 cytokines and asthma: an introduction. *Respir Res* **2**: 64-65.

135. Wang, L., E. Knudsen, Y. Jin, S. Gessani, and A. A. Maghazachi. 2004. Lysophospholipids and chemokines activate distinct signal transduction pathways in T helper 1 and T helper 2 cells. *Cell. Signal.* **16**: 991-1000.

136. Rubenfeld, J., J. Guo, N. Sookrung, R. Chen, W. Chaicumpa, V. Casolaro, Y. Zhao, V. Natarajan, and S. Georas. 2006. Lysophosphatidic acid enhances interleukin-13 gene expression and promoter activity in T cells. *Am J Physiol Lung Cell Mol Physiol* **290**: L66-74.

137. Park, G. Y., Y. G. Lee, E. Berdyshev, S. Nyenhuis, J. Du, P. Fu, I. A. Gorshkova, Y. Li, S. Chung, M. Karpurapu, J. Deng, R. Ranjan, L. Xiao, H. A. Jaffe, S. J. Corbridge, E. A. Kelly, N. N. Jarjour, J. Chun, G. D. Prestwich, E. Kaffe, I. Ninou, V. Aidinis, A. J. Morris, S. S. Smyth, S. J. Ackerman, V. Natarajan, and J. W. Christman. 2013. Autotaxin production of lysophosphatidic Acid mediates allergic asthmatic inflammation. *Am. J. Respir. Crit. Care Med.* **188**: 928-940.

138. Tager, A. M., P. LaCamera, B. S. Shea, G. S. Campanella, M. Selman, Z. Zhao, V. Polosukhin, J. Wain, B. A. Karimi-Shah, N. D. Kim, W. K. Hart, A. Pardo, T. S. Blackwell, Y. Xu, J. Chun, and A. D. Luster. 2008. The lysophosphatidic acid receptor LPA1 links pulmonary fibrosis to lung injury by mediating fibroblast recruitment and vascular leak. *Nat. Med.* **14**: 45-54.

139. Swaney, J. S., C. Chapman, L. D. Correa, K. J. Stebbins, R. A. Bundey, P. C. Prodanovich, P. Fagan, C. S. Baccei, A. M. Santini, J. H. Hutchinson, T. J. Seiders, T. A. Parr, P. Prasit, J. F. Evans, and D. S. Lorrain. 2010. A novel, orally active LPA(1) receptor antagonist inhibits lung fibrosis in the mouse bleomycin model. *Br. J. Pharmacol.* **160**: 1699-1713.

140. Oikonomou, N., M. A. Mouratis, A. Tzouvelekis, E. Kaffe, C. Valavanis, G. Vilaras, A. Karameris, G. D. Prestwich, D. Bouros, and V. Aidinis. 2012. Pulmonary autotaxin expression contributes to the pathogenesis of pulmonary fibrosis. *Am. J. Respir. Cell Mol. Biol.* **47**: 566-574.

141. JohnClancy, and HeatherHasthorpe. 2011. Pathophysiology of rheumatoid arthritis: nature or nurture? *Primary Health Care* **21**: 29-36.

142. McInnes, I. B., and G. Schett. 2007. Cytokines in the pathogenesis of rheumatoid arthritis. *Nat Rev Immunol* **7**: 429-442.

143. Nochi, H., H. Tomura, M. Tobo, N. Tanaka, K. Sato, T. Shinozaki, T. Kobayashi, K. Takagishi, H. Ohta, F. Okajima, and K. Tamoto. 2008. Stimulatory role of lysophosphatidic acid in cyclooxygenase-2 induction by synovial fluid of patients with rheumatoid arthritis in fibroblast-like synovial cells. *J. Immunol.* **181**: 5111-5119.

144. Zhao, C., M. J. Fernandes, G. D. Prestwich, M. Turgeon, J. Di Battista, T. Clair, P. E. Poubelle, and S. G. Bourgoin. 2008. Regulation of lysophosphatidic acid receptor expression and function in human synoviocytes: implications for rheumatoid arthritis? *Mol. Pharmacol.* **73**: 587-600.

145. Nikitopoulou, I., N. Oikonomou, E. Karouzakis, I. Sevastou, N. Nikolaidou-Katsaridou, Z. Zhao, V. Mersinias, M. Armaka, Y. Xu, M. Masu, G.

B. Mills, S. Gay, G. Kollias, and V. Aidinis. 2012. Autotaxin expression from synovial fibroblasts is essential for the pathogenesis of modeled arthritis. *J. Exp. Med.* **209**: 925-933.

146. Bourgoin, S. G., and C. Zhao. 2010. Autotaxin and lysophospholipids in rheumatoid arthritis. *Curr Opin Investig Drugs* **11**: 515-526.

147. Mabey, T., P. Taleongpong, W. Udomsinprasert, N. Jirathanathornnukul, and S. Honsawek. 2015. Plasma and synovial fluid autotaxin correlate with severity in knee osteoarthritis. *Clin. Chim. Acta*: doi: 10.1016/j.cca.2015.1001.1032.

148. Gregor, M. F., and G. k. S. Hotamisligil. 2011. Inflammatory Mechanisms in Obesity. *Annu. Rev. Immunol.* **29**: 415-445.

149. Ferry, G., E. Tellier, A. Try, S. Gres, I. Naime, M. F. Simon, M. Rodriguez, J. Boucher, I. Tack, S. Gesta, P. Chomarat, M. Dieu, M. Raes, J. P. Galizzi, P. Valet, J. A. Boutin, and J. S. Saulnier-Blache. 2003. Autotaxin is released from adipocytes, catalyzes lysophosphatidic acid synthesis, and activates preadipocyte proliferation. Up-regulated expression with adipocyte differentiation and obesity. *J. Biol. Chem.* **278**: 18162-18169.

150. Boucher, J., D. Quilliot, J. P. Praderes, M. F. Simon, S. Gres, C. Guigne, D. Prevot, G. Ferry, J. A. Boutin, C. Carpene, P. Valet, and J. S. Saulnier-Blache. 2005. Potential involvement of adipocyte insulin resistance in obesity-associated up-regulation of adipocyte lysophospholipase D/autotaxin expression. *Diabetologia* **48**: 569-577.

151. Federico, L., H. Ren, P. A. Mueller, T. Wu, S. Liu, J. Popovic, E. M. Blalock, M. Sunkara, H. Ovaa, H. M. Albers, G. B. Mills, A. J. Morris, and S. S. Smyth. 2012. Autotaxin and its product lysophosphatidic acid suppress brown adipose differentiation and promote diet-induced obesity in mice. *Mol. Endocrinol.* **26**: 786-797.

152. Rancoule, C., R. Dusaulcy, K. Treguer, S. Gres, C. Attane, and J. S. Saulnier-Blache. 2014. Involvement of autotaxin/lysophosphatidic acid signaling in obesity and impaired glucose homeostasis. *Biochimie* **96**: 140-143.

153. Hansson, G. K., A. K. Robertson, and C. Soderberg-Naucler. 2006. Inflammation and atherosclerosis. *Annu Rev Pathol* **1**: 297-329.

154. Zhou, Z., P. Subramanian, G. Sevilmis, B. Globke, O. Soehnlein, E. Karshovska, R. Megens, K. Heyll, J. Chun, J. S. Saulnier-Blache, M. Reinholz, M. van Zandvoort, C. Weber, and A. Schober. 2011. Lipoprotein-

derived lysophosphatidic acid promotes atherosclerosis by releasing CXCL1 from the endothelium. *Cell Metab* **13**: 592-600.

155. Dohi, T., K. Miyauchi, R. Ohkawa, K. Nakamura, T. Kishimoto, T. Miyazaki, A. Nishino, N. Nakajima, K. Yaginuma, H. Tamura, T. Kojima, K. Yokoyama, T. Kurata, K. Shimada, Y. Yatomi, and H. Daida. 2012. Increased circulating plasma lysophosphatidic acid in patients with acute coronary syndrome. *Clin. Chim. Acta* **413**: 207-212.

156. Dohi, T., K. Miyauchi, R. Ohkawa, K. Nakamura, M. Kurano, T. Kishimoto, N. Yanagisawa, M. Ogita, T. Miyazaki, A. Nishino, K. Yaginuma, H. Tamura, T. Kojima, K. Yokoyama, T. Kurata, K. Shimada, H. Daida, and Y. Yatomi. 2013. Increased lysophosphatidic acid levels in culprit coronary arteries of patients with acute coronary syndrome. *Atherosclerosis* **229**: 192-197.

157. Kurano, M., A. Suzuki, A. Inoue, Y. Tokuhara, K. Kano, H. Matsumoto, K. Igarashi, R. Ohkawa, K. Nakamura, T. Dohi, K. Miyauchi, H. Daida, K. Tsukamoto, H. Ikeda, J. Aoki, and Y. Yatomi. 2015. Possible involvement of minor lysophospholipids in the increase in plasma lysophosphatidic Acid in acute coronary syndrome. *Arterioscler Thromb Vasc Biol* **35**: 463-470.

158. Watanabe, N., H. Ikeda, K. Nakamura, R. Ohkawa, Y. Kume, J. Aoki, K. Hama, S. Okudaira, M. Tanaka, T. Tomiya, M. Yanase, K. Tejima, T. Nishikawa, M. Arai, H. Arai, M. Omata, K. Fujiwara, and Y. Yatomi. 2007. Both plasma lysophosphatidic acid and serum autotaxin levels are increased in chronic hepatitis C. *J. Clin. Gastroenterol.* **41**: 616-623.

159. Watanabe, N., H. Ikeda, K. Nakamura, R. Ohkawa, Y. Kume, T. Tomiya, K. Tejima, T. Nishikawa, M. Arai, M. Yanase, J. Aoki, H. Arai, M. Omata, K. Fujiwara, and Y. Yatomi. 2007. Plasma lysophosphatidic acid level and serum autotaxin activity are increased in liver injury in rats in relation to its severity. *Life Sci.* **81**: 1009-1015.

160. Nakagawa, H., H. Ikeda, K. Nakamura, R. Ohkawa, R. Masuzaki, R. Tateishi, H. Yoshida, N. Watanabe, K. Tejima, Y. Kume, T. Iwai, A. Suzuki, T. Tomiya, Y. Inoue, T. Nishikawa, N. Ohtomo, Y. Tanoue, M. Omata, K. Igarashi, J. Aoki, K. Koike, and Y. Yatomi. 2011. Autotaxin as a novel serum marker of liver fibrosis. *Clin. Chim. Acta* **412**: 1201-1206.

161. Kremer, A. E., J. J. Martens, W. Kulik, F. Rueff, E. M. Kuiper, H. R. van Buuren, K. J. van Erpecum, J. Kondrackiene, J. Prieto, C. Rust, V. L. Geenes, C. Williamson, W. H. Moolenaar, U. Beuers, and R. P. Oude Elferink. 2010. Lysophosphatidic acid is a potential mediator of cholestatic pruritus. *Gastroenterology* **139**: 1008-1018.

162. Folci, M., F. Meda, M. E. Gershwin, and C. Selmi. 2012. Cutting-edge issues in primary biliary cirrhosis. *Clin. Rev. Allergy Immunol.* **42**: 342-354.

163. Hozumi, H., R. Hokari, C. Kurihara, K. Narimatsu, H. Sato, S. Sato, T. Ueda, M. Higashiyama, Y. Okada, C. Watanabe, S. Komoto, K. Tomita, A. Kawaguchi, S. Nagao, and S. Miura. 2013. Involvement of autotaxin/lysophospholipase D expression in intestinal vessels in aggravation of intestinal damage through lymphocyte migration. *Lab. Invest.* **93**: 508-519.

164. Bekele, R., and D. N. Brindley. 2012. Role of autotaxin and lysophosphatidate in cancer progression and resistance to chemotherapy and radiotherapy. *Clin Lipidol* **7**: 313-328.

165. Samadi, N., R. Bekele, D. Capatos, G. Venkatraman, M. Sariahmetoglu, and D. N. Brindley. 2011. Regulation of lysophosphatidate signaling by autotaxin and lipid phosphate phosphatases with respect to tumor progression, angiogenesis, metastasis and chemo-resistance. *Biochimie* **93**: 61-70.

166. Panchatcharam, M., A. K. Salous, J. Brandon, S. Miriyala, J. Wheeler, P. Patil, M. Sunkara, A. J. Morris, D. Escalante-Alcalde, and S. S. Smyth. 2014. Mice with targeted inactivation of ppap2b in endothelial and hematopoietic cells display enhanced vascular inflammation and permeability. *Arterioscler Thromb Vasc Biol* **34**: 837-845.

167. Smyth, S. S., P. Mueller, F. Yang, J. A. Brandon, and A. J. Morris. 2014. Arguing the case for the autotaxin-lysophosphatidic acid-lipid phosphate phosphatase 3-signaling nexus in the development and complications of atherosclerosis. *Arterioscler Thromb Vasc Biol* **34**: 479-486.

168. Bollen, M., R. Gijsbers, H. Ceulemans, W. Stalmans, and C. Stefan. 2000. Nucleotide pyrophosphatases/phosphodiesterases on the move. *Crit. Rev. Biochem. Mol. Biol.* **35**: 393-432.

169. Debies, M. T., and D. R. Welch. 2001. Genetic basis of human breast cancer metastasis. *J. Mammary Gland Biol. Neoplasia* **6**: 441-451.

170. Moolenaar, W. H., L. A. van Meeteren, and B. N. Giepmans. 2004. The ins and outs of lysophosphatidic acid signaling. *Bioessays* **26**: 870-881.

171. Gendaszewska-Darmach, E. 2008. Lysophosphatidic acids, cyclic phosphatidic acids and autotaxin as promising targets in therapies of cancer and other diseases. *Acta Biochim. Pol.* **55**: 227-240.

172. Liu, S., M. Murph, N. Panupinthu, and G. B. Mills. 2009. ATX-LPA receptor axis in inflammation and cancer. *Cell Cycle* **8**: 3695-3701.

173. Panupinthu, N., H. Y. Lee, and G. B. Mills. 2010. Lysophosphatidic acid production and action: critical new players in breast cancer initiation and progression. *Br. J. Cancer* **102**: 941-946.

174. Houben, A. J., and W. H. Moolenaar. 2011. Autotaxin and LPA receptor signaling in cancer. *Cancer Metastasis Rev.* **30**: 557-565.

175. Gotoh, M., Y. Fujiwara, J. Yue, J. Liu, S. Lee, J. Fells, A. Uchiyama, K. Murakami-Murofushi, S. Kennel, J. Wall, R. Patil, R. Gupte, L. Balazs, D. D. Miller, and G. J. Tigyi. 2012. Controlling cancer through the autotaxin-lysophosphatidic acid receptor axis. *Biochem. Soc. Trans.* **40**: 31-36.

176. Peyruchaud, O., R. Leblanc, and M. David. 2013. Pleiotropic activity of lysophosphatidic acid in bone metastasis. *Biochim. Biophys. Acta* **1831**: 99-104.

177. So, J., F. Q. Wang, J. Navari, J. Schreher, and D. A. Fishman. 2005. LPA-induced epithelial ovarian cancer (EOC) in vitro invasion and migration are mediated by VEGF receptor-2 (VEGF-R2). *Gynecol. Oncol.* **97**: 870-878.

178. Murph, M. M., J. Hurst-Kennedy, V. Newton, D. N. Brindley, and H. Radhakrishna. 2007. Lysophosphatidic acid decreases the nuclear localization and cellular abundance of the p53 tumor suppressor in A549 lung carcinoma cells. *Mol Cancer Res* **5**: 1201-1211.

179. Liu, S., M. Umezu-Goto, M. Murph, Y. Lu, W. Liu, F. Zhang, S. Yu, L. C. Stephens, X. Cui, G. Murrow, K. Coombes, W. Muller, M. C. Hung, C. M. Perou, A. V. Lee, X. Fang, and G. B. Mills. 2009. Expression of autotaxin and lysophosphatidic acid receptors increases mammary tumorigenesis, invasion, and metastases. *Cancer Cell* **15**: 539-550.

180. Euer, N., M. Schwirzke, V. Evtimova, H. Burtscher, M. Jarsch, D. Tarin, and U. H. Weidle. 2002. Identification of genes associated with metastasis of mammary carcinoma in metastatic versus non-metastatic cell lines. *Anticancer Res.* **22**: 733-740.

181. St-Coeur, P. D., D. Ferguson, P. Morin, Jr., and M. Touaibia. 2013. PF-8380 and closely related analogs: synthesis and structure-activity relationship towards autotaxin inhibition and glioma cell viability. *Arch Pharm* **346**: 91-97.

182. Popnikolov, N. K., B. H. Dalwadi, J. D. Thomas, G. J. Johannes, and W. T. Imagawa. 2012. Association of autotaxin and lysophosphatidic acid

receptor 3 with aggressiveness of human breast carcinoma. *Tumour Biol.* **33**: 2237-2243.

183. Leblanc, R., S. C. Lee, M. David, J. C. Bordet, D. D. Norman, R. Patil, D. Miller, D. Sahay, J. Ribeiro, P. Clezardin, G. J. Tigyi, and O. Peyruchaud. 2014. Interaction of platelet-derived autotaxin with tumor integrin alphaVbeta3 controls metastasis of breast cancer cells to bone. *Blood* **124**: 3141-3150.

184. Barretina, J., G. Caponigro, N. Stransky, K. Venkatesan, A. A. Margolin, S. Kim, C. J. Wilson, J. Lehar, G. V. Kryukov, D. Sonkin, A. Reddy, M. Liu, L. Murray, M. F. Berger, J. E. Monahan, P. Morais, J. Meltzer, A. Korejwa, J. Jane-Valbuena, F. A. Mapa, J. Thibault, E. Bric-Furlong, P. Raman, A. Shipway, I. H. Engels, J. Cheng, G. K. Yu, J. Yu, P. Aspesi, M. de Silva, K. Jagtap, M. D. Jones, L. Wang, C. Hatton, E. Palescandolo, S. Gupta, S. Mahan, C. Sougnez, R. C. Onofrio, T. Liefeld, L. MacConaill, W. Winckler, M. Reich, N. Li, J. P. Mesirov, S. B. Gabriel, G. Getz, K. Ardlie, V. Chan, V. E. Myer, B. L. Weber, J. Porter, M. Warmuth, P. Finan, J. L. Harris, M. Meyerson, T. R. Golub, M. P. Morrissey, W. R. Sellers, R. Schlegel, and L. A. Garraway. 2012. The Cancer Cell Line Encyclopedia enables predictive modelling of anticancer drug sensitivity. *Nature* **483**: 603-307.

185. Braeuer, R. R., M. Zigler, T. Kamiya, A. S. Dobroff, L. Huang, W. Choi, D. J. McConkey, E. Shoshan, A. K. Mobley, R. Song, A. Raz, and M. Bar-Eli. 2012. Galectin-3 contributes to melanoma growth and metastasis via regulation of NFAT1 and autotaxin. *Cancer Res.* **72**: 5757-5766.

186. Conrotto, P., U. Andreasson, V. Kuci, C. A. Borrebaeck, and S. Ek. 2011. Knock-down of SOX11 induces autotaxin-dependent increase in proliferation in vitro and more aggressive tumors in vivo. *Mol Oncol* **5**: 527-537.

187. Azare, J., A. Doane, K. Leslie, Q. Chang, M. Berishaj, J. Nnoli, K. Mark, H. Al-Ahmadie, W. Gerald, M. Hassimi, A. Viale, M. Stracke, D. Lyden, and J. Bromberg. 2011. Stat3 mediates expression of autotaxin in breast cancer. *PLoS One* **6**: e27851.

188. Furui, T., R. LaPushin, M. Mao, H. Khan, S. R. Watt, M. A. Watt, Y. Lu, X. Fang, S. Tsutsui, Z. H. Siddik, R. C. Bast, and G. B. Mills. 1999. Overexpression of edg-2/vzg-1 induces apoptosis and anoikis in ovarian cancer cells in a lysophosphatidic acid-independent manner. *Clin. Cancer Res.* **5**: 4308-4318.

189. Pustilnik, T. B., V. Estrella, J. R. Wiener, M. Mao, A. Eder, M. A. Watt, R. C. Bast, Jr., and G. B. Mills. 1999. Lysophosphatidic acid induces urokinase secretion by ovarian cancer cells. *Clin. Cancer Res.* **5**: 3704-3710.

190. Shida, D., J. Kitayama, H. Yamaguchi, Y. Okaji, N. H. Tsuno, T. Watanabe, Y. Takuwa, and H. Nagawa. 2003. Lysophosphatidic acid (LPA) enhances the metastatic potential of human colon carcinoma DLD1 cells through LPA1. *Cancer Res.* **63**: 1706-1711.

191. Schulte, K. M., A. Beyer, K. Kohrer, S. Oberhauser, and H. D. Roher. 2001. Lysophosphatidic acid, a novel lipid growth factor for human thyroid cells: over-expression of the high-affinity receptor edg4 in differentiated thyroid cancer. *Int. J. Cancer* **92**: 249-256.

192. Kitayama, J., D. Shida, A. Sako, M. Ishikawa, K. Hama, J. Aoki, H. Arai, and H. Nagawa. 2004. Over-expression of lysophosphatidic acid receptor-2 in human invasive ductal carcinoma. *Breast Cancer Res* **6**: R640-646.

193. Shida, D., T. Watanabe, J. Aoki, K. Hama, J. Kitayama, H. Sonoda, Y. Kishi, H. Yamaguchi, S. Sasaki, A. Sako, T. Konishi, H. Arai, and H. Nagawa. 2004. Aberrant expression of lysophosphatidic acid (LPA) receptors in human colorectal cancer. *Lab. Invest.* **84**: 1352-1362.

194. Okabe, K., M. Hayashi, K. Kato, M. Okumura, R. Fukui, K. Honoki, N. Fukushima, and T. Tsujiuchi. 2013. Lysophosphatidic acid receptor-3 increases tumorigenicity and aggressiveness of rat hepatoma RH7777 cells. *Mol. Carcinog.* **52**: 247-254.

195. Okabe, K., M. Hayashi, Y. Yamawaki, M. Teranishi, K. Honoki, T. Mori, N. Fukushima, and T. Tsujiuchi. 2011. Possible involvement of lysophosphatidic acid receptor-5 gene in the acquisition of growth advantage of rat tumor cells. *Mol. Carcinog.* **50**: 635-642.

196. Lee, S. C., Y. Fujiwara, J. Liu, J. Yue, Y. Shimizu, D. D. Norman, Y. Wang, R. Tsukahara, E. Szabo, R. Patil, S. Banerjee, D. D. Miller, L. Balazs, M. C. Ghosh, C. M. Waters, T. Oravecz, and G. J. Tigyi. 2015. Autotaxin and LPA1 and LPA5 Receptors Exert Disparate Functions in Tumor Cells versus the Host Tissue Microenvironment in Melanoma Invasion and Metastasis. *Mol Cancer Res* **13**: 174-185.

197. Tang, X., M. G. Benesch, J. Dewald, Y. Y. Zhao, N. Patwardhan, W. L. Santos, J. M. Curtis, T. P. McMullen, and D. N. Brindley. 2014. Lipid phosphate phosphatase-1 expression in cancer cells attenuates tumor growth and metastasis in mice. *J. Lipid Res.* **55**: 2389-2400.

198. Tanyi, J. L., Y. Hasegawa, R. Lapushin, A. J. Morris, J. K. Wolf, A. Berchuck, K. Lu, D. I. Smith, K. Kalli, L. C. Hartmann, K. McCune, D. Fishman, R. Broaddus, K. W. Cheng, E. N. Atkinson, J. M. Yamal, R. C. Bast,

E. A. Felix, R. A. Newman, and G. B. Mills. 2003. Role of decreased levels of lipid phosphate phosphatase-1 in accumulation of lysophosphatidic acid in ovarian cancer. *Clin. Cancer Res.* **9**: 3534-3545.

199. Tanyi, J. L., A. J. Morris, J. K. Wolf, X. Fang, Y. Hasegawa, R. Lapushin, N. Auersperg, Y. J. Sigal, R. A. Newman, E. A. Felix, E. N. Atkinson, and G. B. Mills. 2003. The human lipid phosphate phosphatase-3 decreases the growth, survival, and tumorigenesis of ovarian cancer cells: validation of the lysophosphatidic acid signaling cascade as a target for therapy in ovarian cancer. *Cancer Res.* **63**: 1073-1082.

200. Chatterjee, I., J. O. Humtsoe, E. E. Kohler, C. Sorio, and K. K. Wary. 2011. Lipid phosphate phosphatase-3 regulates tumor growth via beta-catenin and CYCLIN-D1 signaling. *Mol Cancer* **10**: 51.

201. Morris, K. E., L. M. Schang, and D. N. Brindley. 2006. Lipid phosphate phosphatase-2 activity regulates S-phase entry of the cell cycle in Rat2 fibroblasts. *J. Biol. Chem.* **281**: 9297-9306.

202. Flanagan, J. M., J. M. Funes, S. Henderson, L. Wild, N. Carey, and C. Boshoff. 2009. Genomics screen in transformed stem cells reveals RNASEH2A, PPAP2C, and ADARB1 as putative anticancer drug targets. *Mol Cancer Ther* **8**: 249-260.

203. Saulnier-Blache, J. S. 2004. Lysophosphatidic acid: a "bioactive" phospholipid. *Med Sci* **20**: 799-803.

204. Dennis, J., L. Nogaroli, and B. Fuss. 2005. Phosphodiesterase-Ialpha/autotaxin (PD-Ialpha/ATX): a multifunctional protein involved in central nervous system development and disease. *J. Neurosci. Res.* **82**: 737-742.

205. Aoki, J., A. Inoue, and S. Okudaira. 2008. Two pathways for lysophosphatidic acid production. *Biochim. Biophys. Acta* **1781**: 513-518.

206. Ikeda, H., N. Watanabe, K. Nakamura, Y. Kume, Y. Nakai, M. Fujishiro, M. Omata, K. Igarashi, H. Yokota, and Y. Yatomi. 2009. Significance of serum autotaxin activity in gastrointestinal disease. *Rinsho Byori.* **57**: 445-449.

207. Georas, S. N. 2009. Lysophosphatidic acid and autotaxin: emerging roles in innate and adaptive immunity. *Immunol. Res.* **45**: 229-238.

208. Oude Elferink, R. P., A. E. Kremer, and U. Beuers. 2011. Mediators of pruritus during cholestasis. *Curr Opin Gastroenterol* **27**: 289-293.

209. Raap, U., S. Stander, and M. Metz. 2011. Pathophysiology of itch and new treatments. *Curr Opin Allergy Clin Immunol* **11**: 420-427.

210. Fearon, E. R., and B. Vogelstein. 1990. A genetic model for colorectal tumorigenesis. *Cell* **61**: 759-767.

211. Gordon, M., M. El-Kalla, Y. Zhao, Y. Fiteih, J. Law, N. Volodko, A. Mohamed, A. O. S. El-Kadi, L. Liu, J. Odenbach, A. Thiesen, C. Onyskiw, H. A. Ghazaleh, J. Park, S. B. Lee, V. C. Yu, C. Fernandez-Patron, R. T. Alexander, E. Wine, and S. Baksh. 2013. The Tumor Suppressor Gene, RASSF1A, Is Essential for Protection against Inflammation -Induced Injury. *PLoS One* **8**: e75483.

212. Trinchieri, G. 2012. Cancer and inflammation: an old intuition with rapidly evolving new concepts. *Annu. Rev. Immunol.* **30**: 677-706.

213. Llovet, J. M., A. Burroughs, and J. Bruix. 2003. Hepatocellular carcinoma. *Lancet* **362**: 1907-1917.

214. Alter, M. J. 2007. Epidemiology of hepatitis C virus infection. *World J Gastroenterol* **13**: 2436-2441.

215. Cooper, A. B., J. Wu, D. Lu, and M. A. Maluccio. 2007. Is autotaxin (ENPP2) the link between hepatitis C and hepatocellular cancer? *J. Gastrointest. Surg.* **11**: 1628-1634.

216. Wu, J. M., Y. Xu, N. J. Skill, H. Sheng, Z. Zhao, M. Yu, R. Saxena, and M. A. Maluccio. 2010. Autotaxin expression and its connection with the TNF-alpha-NF-kappaB axis in human hepatocellular carcinoma. *Mol Cancer* **9**: 1476-4598.

217. Samadi, N., R. T. Bekele, I. S. Goping, L. M. Schang, and D. N. Brindley. 2011. Lysophosphatidate induces chemo-resistance by releasing breast cancer cells from taxol-induced mitotic arrest. *PLoS One* **6**: e20608.

218. Zhang, R., J. Wang, S. Ma, Z. Huang, and G. Zhang. 2011. Requirement of Osteopontin in the migration and protection against Taxol-induced apoptosis via the ATX-LPA axis in SGC7901 cells. *BMC Cell Biol* **12**: 1471-2121.

219. Vidot, S., J. Witham, R. Agarwal, S. Greenhough, H. S. Bamrah, G. J. Tigyi, S. B. Kaye, and A. Richardson. 2010. Autotaxin delays apoptosis induced by carboplatin in ovarian cancer cells. *Cell. Signal.* **22**: 926-935.

220. Deng, W., E. Shuyu, R. Tsukahara, W. J. Valentine, G. Durgam, V. Gududuru, L. Balazs, V. Manickam, M. Arsura, L. VanMiddlesworth, L. R. Johnson, A. L. Parrill, D. D. Miller, and G. Tigyi. 2007. The lysophosphatidic acid type 2 receptor is required for protection against radiation-induced intestinal injury. *Gastroenterology* **132**: 1834-1851.

221. Lin, F. T., Y. J. Lai, N. Makarova, G. Tigyi, and W. C. Lin. 2007. The lysophosphatidic acid 2 receptor mediates down-regulation of Siva-1 to promote cell survival. *J. Biol. Chem.* **282**: 37759-37769.

222. E, S., Y. J. Lai, R. Tsukahara, C. S. Chen, Y. Fujiwara, J. Yue, J. H. Yu, H. Guo, A. Kihara, G. Tigyi, and F. T. Lin. 2009. Lysophosphatidic acid 2 receptor-mediated supramolecular complex formation regulates its antiapoptotic effect. *J. Biol. Chem.* **284**: 14558-14571.

223. Su, S. C., X. Hu, P. A. Kenney, M. M. Merrill, K. N. Babaian, X. Y. Zhang, T. Maity, S. F. Yang, X. Lin, and C. G. Wood. 2013. Autotaxin-Lysophosphatidic Acid Signaling Axis Mediates Tumorigenesis and Development of Acquired Resistance to Sunitinib in Renal Cell Carcinoma. *Clin. Cancer Res.* **11**: 11.

224. Kano, K., N. Arima, M. Ohgami, and J. Aoki. 2008. LPA and its analogs-attractive tools for elucidation of LPA biology and drug development. *Curr. Med. Chem.* **15**: 2122-2131.

225. Federico, L., Z. Pamuklar, S. S. Smyth, and A. J. Morris. 2008. Therapeutic potential of autotaxin/lysophospholipase d inhibitors. *Curr Drug Targets* **9**: 698-708.

226. Prestwich, G. D., J. Gajewiak, H. Zhang, X. Xu, G. Yang, and M. Serban. 2008. Phosphatase-resistant analogues of lysophosphatidic acid: agonists promote healing, antagonists and autotaxin inhibitors treat cancer. *Biochim. Biophys. Acta* **1781**: 588-594.

227. Parrill, A. L., and D. L. Baker. 2008. Autotaxin inhibition: challenges and progress toward novel anti-cancer agents. *Anticancer Agents Med Chem* **8**: 917-923.

228. Peyruchaud, O. 2009. Novel implications for lysophospholipids, lysophosphatidic acid and sphingosine 1-phosphate, as drug targets in cancer. *Anticancer Agents Med Chem* **9**: 381-391.

229. Xu, X., G. Yang, H. Zhang, and G. D. Prestwich. 2009. Evaluating dual activity LPA receptor pan-antagonist/autotaxin inhibitors as anti-cancer

agents in vivo using engineered human tumors. *Prostaglandins Other Lipid Mediat.* **89**: 140-146.

230. Imai, A., T. Furui, T. Tamaya, and G. B. Mills. 2000. A gonadotropin-releasing hormone-responsive phosphatase hydrolyses lysophosphatidic acid within the plasma membrane of ovarian cancer cells. *J. Clin. Endocrinol. Metab.* **85**: 3370-3375.

231. Beck, A., T. Wurch, C. Bailly, and N. Corvaia. 2010. Strategies and challenges for the next generation of therapeutic antibodies. *Nat Rev Immunol* **10**: 345-352.

232. Fleming, J. K., J. M. Wojciak, M.-A. Campbell, and T. Huxford. 2011. Biochemical and Structural Characterization of Lysophosphatidic Acid Binding by a Humanized Monoclonal Antibody. *J. Mol. Biol.* **408**: 462-476.

233. Goldshmit, Y., R. Matteo, T. Sztal, F. Ellett, F. Frisca, K. Moreno, D. Crombie, G. J. Lieschke, P. D. Currie, R. A. Sabbadini, and A. Pébay. 2012. Blockage of Lysophosphatidic Acid Signaling Improves Spinal Cord Injury Outcomes. *The American Journal of Pathology* **181**: 978-992.

234. Crack, P. J., M. Zhang, M. C. Morganti-Kossmann, A. J. Morris, J. M. Wojciak, J. K. Fleming, I. Karve, D. Wright, M. Sashindranath, Y. Goldshmit, A. Conquest, M. Daglas, L. A. Johnston, R. L. Medcalf, R. A. Sabbadini, and A. Pebay. 2014. Anti-lysophosphatidic acid antibodies improve traumatic brain injury outcomes. *J Neuroinflammation* **11**: 37.

235. Kihara, Y., H. Mizuno, and J. Chun. 2014. Lysophospholipid receptors in drug discovery. *Exp. Cell Res.*: doi: 10.1016/j.yexcr.2014.1011.1020.

236. Rancoule, C., J. P. Pradere, J. Gonzalez, J. Klein, P. Valet, J. L. Bascands, J. P. Schanstra, and J. S. Saulnier-Blache. 2011. Lysophosphatidic acid-1-receptor targeting agents for fibrosis. *Expert Opin Investig Drugs* **20**: 657-667.

237. Gross, T. J., and G. W. Hunninghake. 2001. Idiopathic Pulmonary Fibrosis. *N. Engl. J. Med.* **345**: 517-525.

238. Tang, N., Y. Zhao, R. Feng, Y. Liu, S. Wang, W. Wei, Q. Ding, M. S. An, J. Wen, and L. Li. 2014. Lysophosphatidic acid accelerates lung fibrosis by inducing differentiation of mesenchymal stem cells into myofibroblasts. *J Cell Mol Med* **18**: 156-169.

239. Pattanaik, D., and A. E. Postlethwaite. 2010. A role for lysophosphatidic acid and sphingosine 1-phosphate in the pathogenesis of systemic sclerosis. *Discov Med* **10**: 161-167.

240. Tokumura, A., L. D. Carbone, Y. Yoshioka, J. Morishige, M. Kikuchi, A. Postlethwaite, and M. A. Watsky. 2009. Elevated serum levels of arachidonoyl-lysophosphatidic acid and sphingosine 1-phosphate in systemic sclerosis. *Int J Med Sci* **6**: 168-176.

241. Castelino, F. V., J. Seiders, G. Bain, S. F. Brooks, C. D. King, J. S. Swaney, D. S. Lorrain, J. Chun, A. D. Luster, and A. M. Tager. 2011. Amelioration of dermal fibrosis by genetic deletion or pharmacologic antagonism of lysophosphatidic acid receptor 1 in a mouse model of scleroderma. *Arthritis Rheum.* **63**: 1405-1415.

242. Pyne, N. J., G. Dubois, and S. Pyne. 2013. Role of sphingosine 1-phosphate and lysophosphatidic acid in fibrosis. *Biochim. Biophys. Acta* **1831**: 228-238.

243. Albers, H. M., and H. Ovaa. 2012. Chemical evolution of autotaxin inhibitors. *Chem. Rev.* **112**: 2593-2603.

244. Barbayianni, E., V. Magrioti, P. Moutevelis-Minakakis, and G. Kokotos. 2013. Autotaxin inhibitors: a patent review. *Expert Opin Ther Pat* **23**: 1123-1132.

245. Clair, T., E. Koh, M. Ptaszynska, R. W. Bandle, L. A. Liotta, E. Schiffmann, and M. L. Stracke. 2005. L-histidine inhibits production of lysophosphatidic acid by the tumor-associated cytokine, autotaxin. *Lipids Health Dis* **4**: 5.

246. El-Batch, M., W. Ibrahim, and S. Said. 2011. Effect of histidine on autotaxin activity in experimentally induced liver fibrosis. *J. Biochem. Mol. Toxicol.* **25**: 143-150.

247. Xia, Q., A. M. Deng, S. S. Wu, and M. Zheng. 2011. Cholera toxin inhibits human hepatocarcinoma cell proliferation in vitro via suppressing ATX/LPA axis. *Acta Pharmacol Sin* **32**: 1055-1062.

248. Kehlen, A., R. Lauterbach, A. N. Santos, K. Thiele, U. Kabisch, E. Weber, D. Riemann, and J. Langner. 2001. IL-1 beta- and IL-4-induced down-regulation of autotaxin mRNA and PC-1 in fibroblast-like synoviocytes of patients with rheumatoid arthritis (RA). *Clin. Exp. Immunol.* **123**: 147-154.

249. Sumida, H., K. Nakamura, K. Yanagida, R. Ohkawa, Y. Asano, T. Kadono, K. Tamaki, K. Igarashi, J. Aoki, S. Sato, S. Ishii, T. Shimizu, and Y. Yatomi. 2013. Decrease in circulating autotaxin by oral administration of prednisolone. *Clin. Chim. Acta* **415**: 74-80.

250. Kremer, A. E., R. van Dijk, P. Leckie, F. G. Schaap, E. M. Kuiper, T. Mettang, K. S. Reiners, U. Raap, H. R. van Buuren, K. J. van Erpecum, N. A. Davies, C. Rust, A. Engert, R. Jalan, R. P. Oude Elferink, and U. Beuers. 2012. Serum autotaxin is increased in pruritus of cholestasis, but not of other origin, and responds to therapeutic interventions. *Hepatology* **56**: 1391-1400.

251. Baker, D. L., Y. Fujiwara, K. R. Pigg, R. Tsukahara, S. Kobayashi, H. Murofushi, A. Uchiyama, K. Murakami-Murofushi, E. Koh, R. W. Bandle, H. S. Byun, R. Bittman, D. Fan, M. Murph, G. B. Mills, and G. Tigyi. 2006. Carba analogs of cyclic phosphatidic acid are selective inhibitors of autotaxin and cancer cell invasion and metastasis. *J. Biol. Chem.* **281**: 22786-22793.

252. Kakiuchi, Y., J. Nagai, M. Gotoh, H. Hotta, H. Murofushi, T. Ogawa, H. Ueda, and K. Murakami-Murofushi. 2011. Antinociceptive effect of cyclic phosphatidic acid and its derivative on animal models of acute and chronic pain. *Mol Pain* **7**: 1744-8069.

253. Zhang, H., X. Xu, J. Gajewiak, R. Tsukahara, Y. Fujiwara, J. Liu, J. I. Fells, D. Perygin, A. L. Parrill, G. Tigyi, and G. D. Prestwich. 2009. Dual activity lysophosphatidic acid receptor pan-antagonist/autotaxin inhibitor reduces breast cancer cell migration in vitro and causes tumor regression in vivo. *Cancer Res.* **69**: 5441-5449.

254. Xu, X., and G. D. Prestwich. 2010. Inhibition of tumor growth and angiogenesis by a lysophosphatidic acid antagonist in an engineered three-dimensional lung cancer xenograft model. *Cancer* **116**: 1739-1750.

255. Schleicher, S. M., D. K. Thotala, A. G. Linkous, R. Hu, K. M. Leahy, E. M. Yazlovitskaya, and D. E. Hallahan. 2011. Autotaxin and LPA receptors represent potential molecular targets for the radiosensitization of murine glioma through effects on tumor vasculature. *PLoS One* **6**: e22182.

256. Nikitopoulou, I., E. Kaffe, I. Sevastou, I. Sirioti, M. Samiotaki, D. Madan, G. D. Prestwich, and V. Aidinis. 2013. A metabolically-stabilized phosphonate analog of lysophosphatidic acid attenuates collagen-induced arthritis. *PLoS One* **8**: e70941.

257. Jiang, G., D. Madan, and G. D. Prestwich. 2011. Aromatic phosphonates inhibit the lysophospholipase D activity of autotaxin. *Bioorg. Med. Chem. Lett.* **21**: 5098-5101.

258. North, E. J., A. L. Howard, I. W. Wanjala, T. C. Pham, D. L. Baker, and A. L. Parrill. 2010. Pharmacophore development and application toward the identification of novel, small-molecule autotaxin inhibitors. *J. Med. Chem.* **53**: 3095-3105.

259. Bhave, S. R., D. Y. Dadey, R. M. Karvas, D. J. Ferraro, R. P. Kotipatruni, J. J. Jaboin, A. N. Hallahan, T. A. Dewees, A. G. Linkous, D. E. Hallahan, and D. Thotala. 2013. Autotaxin Inhibition with PF-8380 Enhances the Radiosensitivity of Human and Murine Glioblastoma Cell Lines. *Front Oncol* **3**: 00236.

260. Saga, H., A. Ohhata, A. Hayashi, M. Katoh, T. Maeda, H. Mizuno, Y. Takada, Y. Komichi, H. Ota, N. Matsumura, M. Shibaya, T. Sugiyama, S. Nakade, and K. Kishikawa. 2014. A novel highly potent autotaxin/ENPP2 inhibitor produces prolonged decreases in plasma lysophosphatidic acid formation in vivo and regulates urethral tension. *PLoS One* **9**: e93230.

261. Ferguson, C. G., C. S. Bigman, R. D. Richardson, L. A. van Meeteren, W. H. Moolenaar, and G. D. Prestwich. 2006. Fluorogenic phospholipid substrate to detect lysophospholipase D/autotaxin activity. *Org Lett* **8**: 2023-2026.

262. Saunders, L. P., A. Ouellette, R. Bandle, W. C. Chang, H. Zhou, R. N. Misra, E. M. De La Cruz, and D. T. Braddock. 2008. Identification of small-molecule inhibitors of autotaxin that inhibit melanoma cell migration and invasion. *Mol Cancer Ther* **7**: 3352-3362.

263. Parrill, A. L., U. Echols, T. Nguyen, T. C. Pham, A. Hoeglund, and D. L. Baker. 2008. Virtual screening approaches for the identification of non-lipid autotaxin inhibitors. *Bioorg. Med. Chem.* **16**: 1784-1795.

264. Mize, C. D., A. M. Abbott, S. B. Gacasan, A. L. Parrill, and D. L. Baker. 2011. Ligand-based autotaxin pharmacophore models reflect structure-based docking results. *J. Mol. Graph. Model.* **31**: 76-86.

265. Kawaguchi, M., T. Okabe, S. Okudaira, H. Nishimasu, R. Ishitani, H. Kojima, O. Nureki, J. Aoki, and T. Nagano. 2013. Screening and X-ray crystal structure-based optimization of autotaxin (ENPP2) inhibitors, using a newly developed fluorescence probe. *ACS Chem Biol* **8**: 1713-1721.

266. Nishimasu, H., R. Ishitani, J. Aoki, and O. Nureki. 2012. A 3D view of autotaxin. *Trends Pharmacol. Sci.* **33**: 138-145.

267. Fells, J. I., S. C. Lee, D. D. Norman, R. Tsukahara, R. J. Kirby, S. Nelson, W. Seibel, R. Papoian, R. Patil, D. D. Miller, A. L. Parrill, T.-C. Pham,

D. L. Baker, R. Bittman, and G. Tigyi. 2013. Targeting the Hydrophobic Pocket of Autotaxin with Virtual Screening of Inhibitors Identifies a Common Aromatic Sulfonamide Structural Motif. *FEBS J.* **281**: 1017-1028.

268. Fells, J. I., S. C. Lee, Y. Fujiwara, D. D. Norman, K. G. Lim, R. Tsukahara, J. Liu, R. Patil, D. D. Miller, R. J. Kirby, S. Nelson, W. Seibel, R. Papoian, A. L. Parrill, D. L. Baker, R. Bittman, and G. Tigyi. 2013. Hits of a high-throughput screen identify the hydrophobic pocket of autotaxin/lysophospholipase D as an inhibitory surface. *Mol. Pharmacol.* **84**: 415-424.

269. Parrill, A. L. 2014. Design of anticancer lysophosphatidic acid agonists and antagonists. *Future Med Chem* **6**: 871-883.

270. Parrill, A. L., and D. L. Baker. 2010. Autotaxin inhibitors: a perspective on initial medicinal chemistry efforts. *Expert Opin Ther Pat* **20**: 1619-1625.

271. van Meeteren, L. A., P. Ruurs, E. Christodoulou, J. W. Goding, H. Takakusa, K. Kikuchi, A. Perrakis, T. Nagano, and W. H. Moolenaar. 2005. Inhibition of autotaxin by lysophosphatidic acid and sphingosine 1-phosphate. *J. Biol. Chem.* **280**: 21155-21161.

272. North, E. J., D. A. Osborne, P. K. Bridson, D. L. Baker, and A. L. Parrill. 2009. Autotaxin structure-activity relationships revealed through lysophosphatidylcholine analogs. *Bioorg. Med. Chem.* **17**: 3433-3442.

273. Saunders, L. P., W. Cao, W. C. Chang, R. A. Albright, D. T. Braddock, and E. M. De La Cruz. 2011. Kinetic analysis of autotaxin reveals substrate-specific catalytic pathways and a mechanism for lysophosphatidic acid distribution. *J. Biol. Chem.* **286**: 30130-30141.

274. Society, C. C. 2013. Canadian Cancer Statistics 2013. *Canadian Cancer Society's Advisory Committee on Cancer Statistics*.

275. Teo, K., and V. G. Brunton. 2014. The role and therapeutic potential of the autotaxin-lysophosphatidate signalling axis in breast cancer. *Biochem. J.* **463**: 157-165.

276. Gharib, H., and J. R. Goellner. 1993. Fine-needle aspiration biopsy of the thyroid: an appraisal. *Ann. Intern. Med.* **118**: 282-289.

277. Tee, Y. Y., A. J. Lowe, C. A. Brand, and R. T. Judson. 2007. Fine-needle aspiration may miss a third of all malignancy in palpable thyroid nodules: a comprehensive literature review. *Ann. Surg.* **246**: 714-720.

278. Berker, D., Y. Aydin, I. Ustun, K. Gul, Y. Tutuncu, S. Isik, T. Delibasi, and S. Guler. 2008. The value of fine-needle aspiration biopsy in subcentimeter thyroid nodules. *Thyroid* **18**: 603-608.

279. Arora, N., T. Scognamiglio, B. Zhu, and T. J. Fahey, 3rd. 2008. Do benign thyroid nodules have malignant potential? An evidence-based review. *World J. Surg.* **32**: 1237-1246.

280. Zhang, J., P. Wang, M. Dykstra, P. Gelebart, D. Williams, R. Ingham, E. E. Adewuyi, R. Lai, and T. McMullen. 2012. Platelet-derived growth factor receptor-alpha promotes lymphatic metastases in papillary thyroid cancer. *J. Pathol.* **228**: 241-250.

281. Colotta, F., P. Allavena, A. Sica, C. Garlanda, and A. Mantovani. 2009. Cancer-related inflammation, the seventh hallmark of cancer: links to genetic instability. *Carcinogenesis* **30**: 1073-1081.

282. Hanahan, D., and R. A. Weinberg. 2011. Hallmarks of cancer: the next generation. *Cell* **144**: 646-674.

283. Hooks, S. B., W. L. Santos, D. S. Im, C. E. Heise, T. L. Macdonald, and K. R. Lynch. 2001. Lysophosphatidic acid-induced mitogenesis is regulated by lipid phosphate phosphatases and is Edg-receptor independent. *J. Biol. Chem.* **276**: 4611-4621.

284. Pilquil, C., J. Dewald, A. Cherney, I. Gorshkova, G. Tigyi, D. English, V. Natarajan, and D. N. Brindley. 2006. Lipid phosphate phosphatase-1 regulates lysophosphatidate-induced fibroblast migration by controlling phospholipase D2-dependent phosphatidate generation. *J. Biol. Chem.* **281**: 38418-38429.

285. Morimoto, T., S. Nakatani, A. Ohhata, and T. Sugiyama, inventors; Ono Pharmaceuticals Co. Ltd., assignee. 2012. Tetrahydrocarboline derivative. World Patent WO2012005227. Japanese.

286. Lim, E., K. D. Modi, and J. Kim. 2009. In vivo bioluminescent imaging of mammary tumors using IVIS spectrum. *J Vis Exp*: e1210.

287. Tao, K., M. Fang, J. Alroy, and G. G. Sahagian. 2008. Imagable 4T1 model for the study of late stage breast cancer. *BMC Cancer* **8**: 228.

288. Uphoff, C. C., S. A. Denkmann, and H. G. Drexler. 2012. Treatment of mycoplasma contamination in cell cultures with Plasmocin. *J Biomed Biotechnol* **2012**: 267678.

289. Ambesi-Impiombato, F. S., L. A. Parks, and H. G. Coon. 1980. Culture of hormone-dependent functional epithelial cells from rat thyroids. *Proc. Natl. Acad. Sci. U. S. A.* **77**: 3455-3459.

290. Carswell, K., M.-J. Lee, and S. Fried. 2012. Culture of Isolated Human Adipocytes and Isolated Adipose Tissue. *In* Human Cell Culture Protocols. R. R. Mitry and R. D. Hughes, editors. Humana Press. 203-214.

291. Alcaraz, C., M. De Diego, M. J. Pastor, and J. M. Escribano. 1990. Comparison of a radioimmunoprecipitation assay to immunoblotting and ELISA for detection of antibody to African swine fever virus. *J. Vet. Diagn. Invest.* **2**: 191-196.

292. Smith, P. K., R. I. Krohn, G. T. Hermanson, A. K. Mallia, F. H. Gartner, M. D. Provenzano, E. K. Fujimoto, N. M. Goeke, B. J. Olson, and D. C. Klenk. 1985. Measurement of protein using bicinchoninic acid. *Anal. Biochem.* **150**: 76-85.

293. Freschauf, G. K., F. Karimi-Busheri, A. Ulaczyk-Lesanko, T. R. Mereniuk, A. Ahrens, J. M. Koshy, A. Rasouli-Nia, P. Pasarj, C. F. Holmes, F. Rininsland, D. G. Hall, and M. Weinfeld. 2009. Identification of a small molecule inhibitor of the human DNA repair enzyme polynucleotide kinase/phosphatase. *Cancer Res.* **69**: 7739-7746.

294. Machholz, E., G. Mulder, C. Ruiz, B. F. Corning, and K. R. Pritchett-Corning. 2012. Manual restraint and common compound administration routes in mice and rats. *J Vis Exp*: e2771.

295. Tomayko, M. M., and C. P. Reynolds. 1989. Determination of subcutaneous tumor size in athymic (nude) mice. *Cancer Chemother. Pharmacol.* **24**: 148-154.

296. Chang, M. H., S. L. Cirillo, and J. D. Cirillo. 2011. Using luciferase to image bacterial infections in mice. *J Vis Exp*: e2547.

297. Jeon, Y. H., Y. Choi, J. H. Kang, C. W. Kim, J. M. Jeong, D. S. Lee, and J. K. Chung. 2007. Immune response to firefly luciferase as a naked DNA. *Cancer Biol Ther* **6**: 781-786.

298. Sass, M. D. 1979. Effect of ammonium chloride on osmotic behavior of red cells in nonelectrolytes. *Am. J. Physiol.* **236**: C238-243.

299. Calon, A., E. Espinet, S. Palomo-Ponce, D. V. Tauriello, M. Iglesias, M. V. Cespedes, M. Sevillano, C. Nadal, P. Jung, X. H. Zhang, D. Byrom, A. Riera, D. Rossell, R. Mangues, J. Massague, E. Sancho, and E. Batlle. 2012.

Dependency of colorectal cancer on a TGF-beta-driven program in stromal cells for metastasis initiation. *Cancer Cell* **22**: 571-584.

300. Sharon, Y., L. Alon, S. Glanz, C. Servais, and N. Erez. 2013. Isolation of normal and cancer-associated fibroblasts from fresh tissues by Fluorescence Activated Cell Sorting (FACS). *J Vis Exp*: e4425.

301. Sugimoto, H., T. M. Mundel, M. W. Kieran, and R. Kalluri. 2006. Identification of fibroblast heterogeneity in the tumor microenvironment. *Cancer Biol Ther* **5**: 1640-1646.

302. Imamura, S., and Y. Horiuti. 1978. Enzymatic determination of phospholipase D activity with choline oxidase. *J. Biochem. (Tokyo).* **83**: 677-680.

303. Nakamura, K., R. Ohkawa, S. Okubo, M. Tozuka, M. Okada, S. Aoki, J. Aoki, H. Arai, H. Ikeda, and Y. Yatomi. 2007. Measurement of lysophospholipase D/autotaxin activity in human serum samples. *Clin. Biochem.* **40**: 274-277.

304. Vogelstein, B., and D. Gillespie. 1979. Preparative and analytical purification of DNA from agarose. *Proc. Natl. Acad. Sci. U. S. A.* **76**: 615-619.

305. Chomczynski, P. 1993. A reagent for the single-step simultaneous isolation of RNA, DNA and proteins from cell and tissue samples. *Biotechniques* **15**: 532-534, 536-537.

306. Chomczynski, P., and N. Sacchi. 1987. Single-step method of RNA isolation by acid guanidinium thiocyanate-phenol-chloroform extraction. *Anal. Biochem.* **162**: 156-159.

307. Germain, D., K. Graham, D. Glubrecht, J. Hugh, J. Mackey, and R. Godbout. 2011. DEAD box 1: a novel and independent prognostic marker for early recurrence in breast cancer. *Breast Cancer Res. Treat.* **127**: 53-63.

308. Dechaphunkul, A., M. Phukaoloun, K. Kanjanapradit, K. Graham, S. Ghosh, C. Santos, and J. R. Mackey. 2012. Prognostic significance of tissue inhibitor of metalloproteinase-1 in breast cancer. *Int J Breast Cancer* **2012**: 290854.

309. Laemmli, U. K. 1970. Cleavage of structural proteins during the assembly of the head of bacteriophage T4. *Nature* **227**: 680-685.

310. Scherer, M., K. Leuthauser-Jaschinski, J. Ecker, G. Schmitz, and G. Liebisch. 2010. A rapid and quantitative LC-MS/MS method to profile sphingolipids. *J of Lipid Res* **51**: 2001-2011.

311. Scherer, M., G. Schmitz, and G. Liebisch. 2009. High-throughput analysis of sphingosine 1-phosphate, sphinganine 1-phosphate, and lysophosphatidic acid in plasma samples by liquid chromatography-tandem mass spectrometry. *Clin. Chem.* **55**: 1218-1222.

312. Ohta, H., K. Sato, N. Murata, A. Damirin, E. Malchinkhuu, J. Kon, T. Kimura, M. Tobo, Y. Yamazaki, T. Watanabe, M. Yagi, M. Sato, R. Suzuki, H. Murooka, T. Sakai, T. Nishitoba, D. S. Im, H. Nochi, K. Tamoto, H. Tomura, and F. Okajima. 2003. Ki16425, a subtype-selective antagonist for EDG-family lysophosphatidic acid receptors. *Mol. Pharmacol.* **64**: 994-1005.

313. Davis, M. D., J. J. Clemens, T. L. Macdonald, and K. R. Lynch. 2005. Sphingosine 1-phosphate analogs as receptor antagonists. *J. Biol. Chem.* **280**: 9833-9841.

314. Bolick, D. T., S. Srinivasan, K. W. Kim, M. E. Hatley, J. J. Clemens, A. Whetzel, N. Ferger, T. L. Macdonald, M. D. Davis, P. S. Tsao, K. R. Lynch, and C. C. Hedrick. 2005. Sphingosine-1-phosphate prevents tumor necrosis factor-{alpha}-mediated monocyte adhesion to aortic endothelium in mice. *Arterioscler Thromb Vasc Biol* **25**: 976-981.

315. Karliner, J. S. 2005. Off the shelf but not mass produced. *Chem. Biol.* **12**: 614-615.

316. Vlahos, C. J., W. F. Matter, K. Y. Hui, and R. F. Brown. 1994. A specific inhibitor of phosphatidylinositol 3-kinase, 2-(4-morpholinyl)-8-phenyl-4H-1-benzopyran-4-one (LY294002). *J. Biol. Chem.* **269**: 5241-5248.

317. Sanchez-Margalet, V., I. D. Goldfine, C. J. Vlahos, and C. K. Sung. 1994. Role of phosphatidylinositol-3-kinase in insulin receptor signaling: studies with inhibitor, LY294002. *Biochem. Biophys. Res. Commun.* **204**: 446-452.

318. Wymann, M. P., G. Bulgarelli-Leva, M. J. Zvelebil, L. Pirola, B. Vanhaesebroeck, M. D. Waterfield, and G. Panayotou. 1996. Wortmannin inactivates phosphoinositide 3-kinase by covalent modification of Lys-802, a residue involved in the phosphate transfer reaction. *Mol. Cell. Biol.* **16**: 1722-1733.

319. Vanhaesebroeck, B., S. J. Leevers, K. Ahmadi, J. Timms, R. Katso, P. C. Driscoll, R. Woscholski, P. J. Parker, and M. D. Waterfield. 2001.

Synthesis and function of 3-phosphorylated inositol lipids. *Annu. Rev. Biochem.* **70**: 535-602.

320. Dudley, D. T., L. Pang, S. J. Decker, A. J. Bridges, and A. R. Saltiel. 1995. A synthetic inhibitor of the mitogen-activated protein kinase cascade. *Proc. Natl. Acad. Sci. U. S. A.* **92**: 7686-7689.

321. Pang, L., T. Sawada, S. J. Decker, and A. R. Saltiel. 1995. Inhibition of MAP kinase kinase blocks the differentiation of PC-12 cells induced by nerve growth factor. *J. Biol. Chem.* **270**: 13585-13588.

322. Gschwendt, M., S. Dieterich, J. Rennecke, W. Kittstein, H. J. Mueller, and F. J. Johannes. 1996. Inhibition of protein kinase C mu by various inhibitors. Differentiation from protein kinase c isoenzymes. *FEBS Lett.* **392**: 77-80.

323. Nishimura, S., M. Nagasaki, S. Okudaira, J. Aoki, T. Ohmori, R. Ohkawa, K. Nakamura, K. Igarashi, H. Yamashita, K. Eto, K. Uno, N. Hayashi, T. Kadowaki, I. Komuro, Y. Yatomi, and R. Nagai. 2014. ENPP2 contributes to adipose tissue expansion and insulin resistance in diet-induced obesity. *Diabetes* **63**: 4154-4164.

324. Cavalli, S., A. J. Houben, H. M. Albers, E. W. van Tilburg, A. de Ru, J. Aoki, P. van Veelen, W. H. Moolenaar, and H. Ovaa. 2010. Development of an activity-based probe for autotaxin. *ChemBioChem* **11**: 2311-2317.

325. Jemal, A., R. Siegel, E. Ward, T. Murray, J. Xu, C. Smigal, and M. J. Thun. 2006. Cancer statistics, 2006. *CA Cancer J Clin* **56**: 106-130.

326. Paridaens, R., L. Biganzoli, P. Bruning, J. G. Klijn, T. Gamucci, S. Houston, R. Coleman, J. Schachter, A. Van Vreckem, R. Sylvester, A. Awada, J. Wildiers, and M. Piccart. 2000. Paclitaxel versus doxorubicin as first-line single-agent chemotherapy for metastatic breast cancer: a European Organization for Research and Treatment of Cancer Randomized Study with cross-over. *J. Clin. Oncol.* **18**: 724-733.

327. Foulkes, W. D., I. E. Smith, and J. S. Reis-Filho. 2010. Triple-Negative Breast Cancer. *N. Engl. J. Med.* **363**: 1938-1948.

328. Hudis, C. A., and L. Gianni. 2011. Triple-Negative Breast Cancer: An Unmet Medical Need. *Oncologist* **16**: 1-11.

329. Morrow, M. 2013. Personalizing extent of breast cancer surgery according to molecular subtypes. *Breast* **22 Suppl 2**: S106-109.

330. Rashid, O. M., M. Nagahashi, S. Ramachandran, L. Graham, A. Yamada, S. Spiegel, H. D. Bear, and K. Takabe. 2013. Resection of the primary tumor improves survival in metastatic breast cancer by reducing overall tumor burden. *Surgery* **153**: 771-778.

331. Pulaski, B. A., and S. Ostrand-Rosenberg. 2001. Mouse 4T1 breast tumor model. *Curr Protoc Immunol* **Chapter 20**: Unit 20.22.

332. David, M., E. Wannecq, F. Descotes, S. Jansen, B. Deux, J. Ribeiro, C. M. Serre, S. Gres, N. Bendriss-Vermare, M. Bollen, S. Saez, J. Aoki, J. S. Saulnier-Blache, P. Clezardin, and O. Peyruchaud. 2010. Cancer cell expression of autotaxin controls bone metastasis formation in mouse through lysophosphatidic acid-dependent activation of osteoclasts. *PLoS One* **5**: e9741.

333. Hackett, A. J., H. S. Smith, E. L. Springer, R. B. Owens, W. A. Nelson-Rees, J. L. Riggs, and M. B. Gardner. 1977. Two syngeneic cell lines from human breast tissue: the aneuploid mammary epithelial (Hs578T) and the diploid myoepithelial (Hs578Bst) cell lines. *J. Natl. Cancer Inst.* **58**: 1795-1806.

334. Sundaram, S., A. R. Johnson, and L. Makowski. 2013. Obesity, metabolism and the microenvironment: Links to cancer. *J Carcinog* **12**: 19.

335. De Pergola, G., and F. Silvestris. 2013. Obesity as a major risk factor for cancer. *J Obes* **2013**: 291546.

336. Brown, K. A. 2014. Impact of obesity on mammary gland inflammation and local estrogen production. *J. Mammary Gland Biol. Neoplasia* **19**: 183-189.

337. Lashinger, L. M., E. L. Rossi, and S. D. Hursting. 2014. Obesity and resistance to cancer chemotherapy: interacting roles of inflammation and metabolic dysregulation. *Clin. Pharmacol. Ther.* **96**: 458-463.

338. Park, J., T. S. Morley, M. Kim, D. J. Clegg, and P. E. Scherer. 2014. Obesity and cancer--mechanisms underlying tumour progression and recurrence. *Nat Rev Endocrinol* **10**: 455-465.

339. Okudaira, S., H. Yukiura, and J. Aoki. 2010. Biological roles of lysophosphatidic acid signaling through its production by autotaxin. *Biochimie* **92**: 698-706.

340. Dvorak, H. F. 1986. Tumors: wounds that do not heal. Similarities between tumor stroma generation and wound healing. *N. Engl. J. Med.* **315**: 1650-1659.

341. Schafer, M., and S. Werner. 2008. Cancer as an overhealing wound: an old hypothesis revisited. *Nat Rev Mol Cell Biol* **9**: 628-638.

342. Nakamura, K., K. Igarashi, R. Ohkawa, H. Yokota, A. Masuda, S. Nakagawa, T. Yano, H. Ikeda, J. Aoki, and Y. Yatomi. 2012. Serum autotaxin is not a useful biomarker for ovarian cancer. *Lipids* **47**: 927-930.

343. Masuda, A., K. Nakamura, K. Izutsu, K. Igarashi, R. Ohkawa, M. Jona, K. Higashi, H. Yokota, S. Okudaira, T. Kishimoto, T. Watanabe, Y. Koike, H. Ikeda, Y. Kozai, M. Kurokawa, J. Aoki, and Y. Yatomi. 2008. Serum autotaxin measurement in haematological malignancies: a promising marker for follicular lymphoma. *Br. J. Haematol.* **143**: 60-70.

344. Nakai, Y., H. Ikeda, K. Nakamura, Y. Kume, M. Fujishiro, N. Sasahira, K. Hirano, H. Isayama, M. Tada, T. Kawabe, Y. Komatsu, M. Omata, J. Aoki, K. Koike, and Y. Yatomi. 2011. Specific increase in serum autotaxin activity in patients with pancreatic cancer. *Clin. Biochem.* **44**: 576-581.

345. Pellegriti, G., F. Frasca, C. Regalbuto, S. Squatrito, and R. Vigneri. 2013. Worldwide increasing incidence of thyroid cancer: update on epidemiology and risk factors. *J Cancer Epidemiol* **2013**: 965212.

346. Jung, C. K., M. P. Little, J. H. Lubin, A. V. Brenner, S. A. Wells, Jr., A. J. Sigurdson, and Y. E. Nikiforov. 2014. The increase in thyroid cancer incidence during the last four decades is accompanied by a high frequency of BRAF mutations and a sharp increase in RAS mutations. *J. Clin. Endocrinol. Metab.* **99**: E276-285.

347. Hughes, D. T., A. M. Laird, B. S. Miller, P. G. Gauger, and G. M. Doherty. 2012. Reoperative lymph node dissection for recurrent papillary thyroid cancer and effect on serum thyroglobulin. *Ann. Surg. Oncol.* **19**: 2951-2957.

348. Cooper, D. S., G. M. Doherty, B. R. Haugen, R. T. Kloos, S. L. Lee, S. J. Mandel, E. L. Mazzaferri, B. McIver, F. Pacini, M. Schlumberger, S. I. Sherman, D. L. Steward, and R. M. Tuttle. 2009. Revised American Thyroid Association management guidelines for patients with thyroid nodules and differentiated thyroid cancer. *Thyroid : official journal of the American Thyroid Association* **19**: 1167-1214.

349. Kent, W. D., S. F. Hall, P. A. Isotalo, R. L. Houlden, R. L. George, and P. A. Groome. 2007. Increased incidence of differentiated thyroid carcinoma and detection of subclinical disease. *CMAJ* **177**: 1357-1361.

350. Olson, M. T., A. D. Tatsas, and S. Z. Ali. 2012. Cytotechnologist-attended on-site adequacy evaluation of thyroid fine-needle aspiration: comparison with cytopathologists and correlation with the final interpretation. *Am. J. Clin. Pathol.* **138**: 90-95.

351. Anderson, R. T., J. E. Linnehan, V. Tongbram, K. Keating, and L. J. Wirth. 2013. Clinical, safety, and economic evidence in radioactive iodine-refractory differentiated thyroid cancer: a systematic literature review. *Thyroid* **23**: 392-407.

352. Serra, S., and S. L. Asa. 2008. Controversies in thyroid pathology: the diagnosis of follicular neoplasms. *Endocr Pathol* **19**: 156-165.

353. Vigneri, R., P. Malandrino, and P. Vigneri. 2015. The changing epidemiology of thyroid cancer: why is incidence increasing? *Curr. Opin. Oncol.* **27**: 1-7.

354. Ehlers, M., and M. Schott. 2014. Hashimoto's thyroiditis and papillary thyroid cancer: are they immunologically linked? *Trends Endocrinol Metab* **25**: 656-664.

355. Mantovani, A. 2010. Molecular pathways linking inflammation and cancer. *Curr Mol Med* **10**: 369-373.

356. Ward, L. S. 2014. Immune response in thyroid cancer: widening the boundaries. *Scientifica (Cairo)* **2014**: 125450.

357. Cunha, L. L., M. A. Marcello, and L. S. Ward. 2014. The role of the inflammatory microenvironment in thyroid carcinogenesis. *Endocr Relat Cancer* **21**: R85-R103.

358. Cunha, L. L., M. A. Marcello, S. Nonogaki, E. C. Morari, F. A. Soares, J. Vassallo, and L. S. Ward. 2014. CD8+ tumour-infiltrating lymphocytes and COX2 expression may predict relapse in differentiated thyroid cancer. *Clin. Endocrinol. (Oxf).* doi: 10.1111/cen.12586.

359. Provatopoulou, X., D. Georgiadou, T. N. Sergentanis, E. Kalogera, J. Spyridakis, A. Gounaris, and G. N. Zografos. 2014. Interleukins as markers of inflammation in malignant and benign thyroid disease. *Inflamm. Res.* **63**: 667-674.

360. Marcello, M. A., L. L. Cunha, F. A. Batista, and L. S. Ward. 2014. Obesity and thyroid cancer. *Endocr Relat Cancer* **21**: T255-271.

361. Tafani, M., E. De Santis, L. Coppola, G. A. Perrone, I. Carnevale, A. Russo, B. Pucci, A. Carpi, M. Bizzarri, and M. A. Russo. 2014. Bridging hypoxia, inflammation and estrogen receptors in thyroid cancer progression. *Biomed. Pharmacother.* **68**: 1-5.

362. Barden, C. B., K. W. Shister, B. Zhu, G. Guiter, D. Y. Greenblatt, M. A. Zeiger, and T. J. Fahey, 3rd. 2003. Classification of follicular thyroid tumors by molecular signature: results of gene profiling. *Clin. Cancer Res.* **9**: 1792-1800.

363. Kehlen, A., N. Englert, A. Seifert, T. Klonisch, H. Dralle, J. Langner, and C. Hoang-Vu. 2004. Expression, regulation and function of autotaxin in thyroid carcinomas. *Int. J. Cancer* **109**: 833-838.

364. Bryson, P. C., C. G. Shores, C. Hart, L. Thorne, M. R. Patel, L. Richey, A. Farag, and A. M. Zanation. 2008. Immunohistochemical distinction of follicular thyroid adenomas and follicular carcinomas. *Arch. Otolaryngol. Head Neck Surg.* **134**: 581-586.

365. Hassan, A. M., M. A. Alm El-Din, H. Nagy, N. Ghoneem, M. A. El-Heniedy, N. Koteb, and S. El-Gohary. 2013. Significance of autotaxin activity and overexpression in comparison to soluble intercellular adhesion molecule in thyroid cancer. *Int. J. Biol. Markers* **28**: 84-91.

366. Yeung, M. J., and J. W. Serpell. 2008. Management of the Solitary Thyroid Nodule. *Oncologist* **13**: 105-112.

367. Xue, Y., S. Lim, Y. Yang, Z. Wang, L. D. E. Jensen, E.-M. Hedlund, P. Andersson, M. Sasahara, O. Larsson, D. Galter, R. Cao, K. Hosaka, and Y. Cao. 2012. PDGF-BB modulates hematopoiesis and tumor angiogenesis by inducing erythropoietin production in stromal cells. *Nat. Med.* **18**: 100-110.

368. Oikonomou, E., and A. Pintzas. 2013. The TRAIL of oncogenes to apoptosis. *Biofactors* **39**: 343-354.

369. Graf, U., E. A. Casanova, and P. Cinelli. 2011. The Role of the Leukemia Inhibitory Factor (LIF) - Pathway in Derivation and Maintenance of Murine Pluripotent Stem Cells. *Genes (Basel)* **2**: 280-297.

370. Albrengues, J., I. Bourget, C. Pons, V. Butet, P. Hofman, S. Tartare-Deckert, C. C. Feral, G. Meneguzzi, and C. Gaggioli. 2014. LIF mediates proinvasive activation of stromal fibroblasts in cancer. *Cell Rep* **7**: 1664-1678.

371. Chou, W. C., J. S. Chen, Y. S. Hung, J. T. Hsu, T. C. Chen, C. F. Sun, C. H. Lu, and T. L. Hwang. 2014. Plasma chromogranin A levels predict survival and tumor response in patients with advanced gastroenteropancreatic neuroendocrine tumors. *Anticancer Res.* **34**: 5661-5669.

372. Li, J., T. Lan, C. Zhang, C. Zeng, J. Hou, Z. Yang, M. Zhang, J. Liu, and B. Liu. 2015. Reciprocal activation between IL-6/STAT3 and NOX4/Akt signalings promotes proliferation and survival of non-small cell lung cancer cells. *Oncotarget* **6**: 1031-1048.

373. Tjomsland, V., L. Bojmar, P. Sandstrom, C. Bratthall, D. Messmer, A. Spangeus, and M. Larsson. 2013. IL-1alpha expression in pancreatic ductal adenocarcinoma affects the tumor cell migration and is regulated by the p38MAPK signaling pathway. *PLoS One* **8**: e70874.

374. Wang, K., M. K. Kim, G. Di Caro, J. Wong, S. Shalapour, J. Wan, W. Zhang, Z. Zhong, E. Sanchez-Lopez, L. W. Wu, K. Taniguchi, Y. Feng, E. Fearon, S. I. Grivennikov, and M. Karin. 2014. Interleukin-17 receptor a signaling in transformed enterocytes promotes early colorectal tumorigenesis. *Immunity* **41**: 1052-1063.

375. Seifert, A., T. Klonisch, J. Wulfaenger, F. Haag, H. Dralle, J. Langner, C. Hoang-Vu, and A. Kehlen. 2008. The cellular localization of autotaxin impacts on its biological functions in human thyroid carcinoma cells. *Oncol. Rep.* **19**: 1485-1491.

376. Britschgi, A., R. Andraos, H. Brinkhaus, I. Klebba, V. Romanet, U. Muller, M. Murakami, T. Radimerski, and M. Bentires-Alj. 2012. JAK2/STAT5 inhibition circumvents resistance to PI3K/mTOR blockade: a rationale for cotargeting these pathways in metastatic breast cancer. *Cancer Cell* **22**: 796-811.

377. Chung, A. S., X. Wu, G. Zhuang, H. Ngu, I. Kasman, J. Zhang, J. M. Vernes, Z. Jiang, Y. G. Meng, F. V. Peale, W. Ouyang, and N. Ferrara. 2013. An interleukin-17-mediated paracrine network promotes tumor resistance to anti-angiogenic therapy. *Nat. Med.* **19**: 1114-1123.

378. Pylayeva-Gupta, Y., K. E. Lee, C. H. Hajdu, G. Miller, and D. Bar-Sagi. 2012. Oncogenic Kras-induced GM-CSF production promotes the development of pancreatic neoplasia. *Cancer Cell* **21**: 836-847.

379. Kishi, Y., S. Okudaira, M. Tanaka, K. Hama, D. Shida, J. Kitayama, T. Yamori, J. Aoki, T. Fujimaki, and H. Arai. 2006. Autotaxin is overexpressed in glioblastoma multiforme and contributes to cell motility of glioblastoma by

converting lysophosphatidylcholine to lysophosphatidic acid. *J. Biol. Chem.* **281**: 17492-17500.

380. Jankowski, M. 2011. Autotaxin: its role in biology of melanoma cells and as a pharmacological target. *Enzyme Res* **8**: 194857.

381. Gottardis, M. M., S. P. Robinson, P. G. Satyaswaroop, and V. C. Jordan. 1988. Contrasting Actions of Tamoxifen on Endometrial and Breast Tumor Growth in the Athymic Mouse. *Cancer Res.* **48**: 812-815.

382. Visvanathan, K., R. T. Chlebowski, P. Hurley, N. F. Col, M. Ropka, D. Collyar, M. Morrow, C. Runowicz, K. I. Pritchard, K. Hagerty, B. Arun, J. Garber, V. G. Vogel, J. L. Wade, P. Brown, J. Cuzick, B. S. Kramer, and S. M. Lippman. 2009. American society of clinical oncology clinical practice guideline update on the use of pharmacologic interventions including tamoxifen, raloxifene, and aromatase inhibition for breast cancer risk reduction. *J. Clin. Oncol.* **27**: 3235-3258.

383. Lin, B. C., M. Suzawa, R. D. Blind, S. C. Tobias, S. E. Bulun, T. S. Scanlan, and H. A. Ingraham. 2009. Stimulating the GPR30 estrogen receptor with a novel tamoxifen analogue activates SF-1 and promotes endometrial cell proliferation. *Cancer Res.* **69**: 5415-5423.

384. Uong, A., and L. I. Zon. 2010. Melanocytes in development and cancer. *J. Cell. Physiol.* **222**: 38-41.

385. Hoelzinger, D. B., M. Nakada, T. Demuth, T. Rosensteel, L. B. Reavie, and M. E. Berens. 2008. Autotaxin: a secreted autocrine/paracrine factor that promotes glioma invasion. *J. Neurooncol.* **86**: 297-309.

386. Nyberg, P., T. Salo, and R. Kalluri. 2008. Tumor Microenvironment and angiogenesis. *Front. Biosci.* **13**: 6537-6553.

387. Finger, E. C., and A. J. Giaccia. 2010. Hypoxia, inflammation, and the tumor microenvironment in metastatic disease. *Cancer Metastasis Rev.* **29**: 285-293.

388. Junttila, M. R., and F. J. de Sauvage. 2013. Influence of tumour micro-environment heterogeneity on therapeutic response. *Nature* **501**: 346-354.

389. Jones, G. E. 2000. Cellular signaling in macrophage migration and chemotaxis. *J. Leukoc. Biol.* **68**: 593-602.

390. Zahednasab, H., M. Balood, M. H. Harirchian, S. A. Mesbah-Namin, N. Rahimian, and B. Siroos. 2014. Increased autotaxin activity in multiple sclerosis. *J. Neuroimmunol.* **273**: 120-123.

391. Leah, E. 2012. Experimental arthritis. Pathogenic role of autotaxin and LPA. *Nat Rev Rheumatol* **8**: 72.

392. Müller, M. R., and A. Rao. 2010. NFAT, immunity and cancer: a transcription factor comes of age. *Nat Rev Immunol* **10**: 645-656.

393. Tietz, O., A. Marshall, M. Wuest, M. Wang, and F. Wuest. 2013. Radiotracers for molecular imaging of cyclooxygenase-2 (COX-2) enzyme. *Curr. Med. Chem.* **20**: 4350-4369.

394. Dunn, L., H. C. Prosser, J. T. Tan, L. Z. Vanags, M. K. Ng, and C. A. Bursill. 2013. Murine model of wound healing. *J Vis Exp*: e50265.

395. Ma, L., H. Uchida, J. Nagai, M. Inoue, J. Aoki, and H. Ueda. 2010. Evidence for de novo synthesis of lysophosphatidic acid in the spinal cord through phospholipase A2 and autotaxin in nerve injury-induced neuropathic pain. *J. Pharmacol. Exp. Ther.* **333**: 540-546.

396. Thomas Hess, C. 2011. Checklist for Factors Affecting Wound Healing. *Advances in Skin & Wound Care* **24**: 192 110.1097/1001.ASW.0000396300.0000304173.ec.

397. Harburger, D. S., and D. A. Calderwood. 2009. Integrin signalling at a glance. *J. Cell Sci.* **122**: 159-163.

398. Chen, M., and K. L. O'Connor. 2005. Integrin alpha6beta4 promotes expression of autotaxin/ENPP2 autocrine motility factor in breast carcinoma cells. *Oncogene* **24**: 5125-5130.

399. Lobo, N. A., Y. Shimono, D. Qian, and M. F. Clarke. 2007. The biology of cancer stem cells. *Annu. Rev. Cell Dev. Biol.* **23**: 675-699.

400. Sampieri, K., and R. Fodde. 2012. Cancer stem cells and metastasis. *Semin. Cancer Biol.* **22**: 187-193.

401. Du, J., C. Sun, Z. Hu, Y. Yang, Y. Zhu, D. Zheng, L. Gu, and X. Lu. 2010. Lysophosphatidic Acid Induces MDA-MB-231 Breast Cancer Cells Migration through Activation of PI3K/PAK1/ERK Signaling. *PLoS ONE* **5**: e15940.

402. Kim, E. K., S. J. Yun, K. H. Do, M. S. Kim, M. Cho, D.-S. Suh, C. D. Kim, J. H. Kim, M. J. Birnbaum, and S. S. Bae. 2008. Lysophosphatidic acid induces cell migration through the selective activation of Akt1. *Exp. Mol. Med.* **40**: 445-452.

403. Tse, J. C., and R. Kalluri. 2007. Mechanisms of metastasis: epithelial-to-mesenchymal transition and contribution of tumor microenvironment. *J. Cell. Biochem.* **101**: 816-829.

404. Jahn, S. C., M. E. Law, P. E. Corsino, N. N. Parker, K. Pham, B. J. Davis, J. Lu, and B. K. Law. 2012. An in vivo model of epithelial to mesenchymal transition reveals a mitogenic switch. *Cancer Lett.* **326**: 183-190.

405. May, C. D., N. Sphyris, K. W. Evans, S. J. Werden, W. Guo, and S. A. Mani. 2011. Epithelial-mesenchymal transition and cancer stem cells: a dangerously dynamic duo in breast cancer progression. *Breast Cancer Res* **13**: 202.

406. Scheel, C., and R. A. Weinberg. 2012. Cancer stem cells and epithelial–mesenchymal transition: Concepts and molecular links. *Semin. Cancer Biol.* **22**: 396-403.

407. Tanno, T., and W. Matsui. 2011. Development and maintenance of cancer stem cells under chronic inflammation. *J Nippon Med Sch* **78**: 138-145.

408. Zhou, C., J. Liu, Y. Tang, and X. Liang. 2012. Inflammation linking EMT and cancer stem cells. *Oral Oncol.* **48**: 1068-1075.

409. Venkatraman, G., M. G. Benesch, X. Tang, J. Dewald, T. P. McMullen, and D. N. Brindley. 2015. Lysophosphatidate signaling stabilizes Nrf2 and increases the expression of genes involved in drug resistance and oxidative stress responses: implications for cancer treatment. *FASEB J.* **29**: 772-785.

410. Wang, X. J., Z. Sun, N. F. Villeneuve, S. Zhang, F. Zhao, Y. Li, W. Chen, X. Yi, W. Zheng, G. T. Wondrak, P. K. Wong, and D. D. Zhang. 2008. Nrf2 enhances resistance of cancer cells to chemotherapeutic drugs, the dark side of Nrf2. *Carcinogenesis* **29**: 1235-1243.

411. Calon, A., D. V. Tauriello, and E. Batlle. 2014. TGF-beta in CAF-mediated tumor growth and metastasis. *Semin. Cancer Biol.* **25**: 15-22.

412. Miller, E., H. J. Lee, A. Lulla, L. Hernandez, P. Gokare, and B. Lim. 2014. Current treatment of early breast cancer: adjuvant and neoadjuvant therapy. *F1000Res* **3**: 198.